~~CONFIDENTIAL~~

NACA RM L57K01

NACA

RESEARCH MEMORANDUM

EFFECTS OF COMPONENTS AND VARIOUS MODIFICATIONS ON THE DRAG AND THE STATIC STABILITY AND CONTROL CHARACTERISTICS OF A 42° SWEPT-WING FIGHTER-AIRPLANE MODEL AT MACH NUMBERS OF 1.60 TO 2.50

By James D. Church

Langley Aeronautical Laboratory
Langley Field, Va.

CLASSIFIED DOCUMENT

NATIONAL ADVISORY COMMITTEE FOR AERONAUTICS

WASHINGTON
November 1957
(Reprinting for nonmilitary distribution, April 15, 1959.)

~~CONFIDENTIAL~~

[redacted]

NATIONAL ADVISORY COMMITTEE FOR AERONAUTICS

RESEARCH MEMORANDUM

EFFECTS OF COMPONENTS AND VARIOUS MODIFICATIONS ON THE DRAG AND THE STATIC STABILITY AND CONTROL CHARACTERISTICS OF A 42° SWEPT-WING FIGHTER-AIRPLANE MODEL AT MACH NUMBERS OF 1.60 TO 2.50*

By James D. Church

SUMMARY

An investigation has been conducted at the Langley Unitary Plan wind tunnel of the drag and the static longitudinal and lateral stability and control characteristics of a 42° swept-wing fighter-airplane model. Data were obtained at Mach numbers of 1.60, 1.90, 2.20, and 2.50 at a Reynolds number of approximately 2.1×10^6 per foot, or 1.4×10^6 based on mean aerodynamic chord. Effectiveness of both longitudinal and lateral controls and the effects of model-component breakdown are presented. Changes in drag at zero lift caused by fixing transition and increasing Reynolds number were almost negligible. The complete model incorporating ventral fins was statically stable both longitudinally and directionally at all Mach numbers for angles of attack up to 19°. The effects on static stability of adding various external stores and a speed brake were relatively minor. Addition or extension of three semi-submerged missiles to the basic configuration progressively decreased the directional stability of the model. Body-mounted strakes improved the model directional stability at moderate and high angles of attack.

INTRODUCTION

As a part of a continuing effort by the National Advisory Committee for Aeronautics to determine supersonic aerodynamic characteristics of various aircraft, an investigation of the drag, static stability, and control characteristics of a 42° swept-wing fighter-airplane model was conducted in the Langley Unitary Plan wind tunnel. The data were

*Title, Unclassified.

[redacted]

obtained at Mach numbers of 1.60, 1.90, 2.20, and 2.50 for angles of attack from -8° to 21° and for angles of sideslip from -6° to 10°.

Included in the basic data are some effects of transition, Reynolds number, model-component breakdown, and model modification. The analysis consists of a brief evaluation of the drag and the longitudinal and lateral stability and control characteristics of the model.

COEFFICIENTS AND SYMBOLS

All data are referred to the stability system of axes illustrated in figure 1. Moment coefficients are taken about an assumed center of gravity located at the 0.25 chord of the mean aerodynamic chord.

b wing span, in.

C_L lift coefficient, F_L/qS

$C_{D,c}$ balance-chamber drag coefficient, $\frac{F_{A_c} \cos \alpha}{qS}$

C_D drag coefficient adjusted to zero chamber drag coefficient, $\frac{F_D' - F_{A_c} \cos \alpha}{qS}$

C_m pitching-moment coefficient, $M_{Y_s}/qS\bar{c}$

C_l rolling-moment coefficient, M_{X_s}/qSb

C_n yawing-moment coefficient, M_{Z_s}/qSb

C_Y side-force coefficient, F_Y/qS

C_{L_α} lift-curve slope, $\left(\partial C_L/\partial \alpha\right)_{\alpha=0^\circ}$

$C_{m_{i_t}}$ stabilizer effectiveness, $\left(\partial C_m/\partial i_t\right)_{C_L=0}$

C_{l_β} effective-dihedral parameter, $\left(\Delta C_l/\Delta \beta\right)_{\beta=\pm 5^\circ}$ unless otherwise noted

C_{n_β} directional-stability parameter, $(\Delta C_n/\Delta\beta)_{\beta=\pm5^\circ}$ unless otherwise noted

C_{Y_β} side-force slope parameter, $(\Delta C_Y/\Delta\beta)_{\beta=\pm5^\circ}$ unless otherwise noted

$C_{l_{\delta_a}}$ aileron effectiveness, $(\partial C_l/\partial\delta_a)_{\alpha=0^\circ}$

$\bar{c}$ wing mean aerodynamic chord, in.

F_L force along Z_s-axis, lb

F_{A_c} balance-chamber axial force, lb

F'_D force along X_s-axis, lb

F_Y force along Y_s-axis, lb

i_w wing incidence referred to fuselage reference line, deg

i_t stabilizer incidence angle referred to fuselage reference line, deg

L/D lift-drag ratio

M free-stream Mach number

M_{Y_s} moment about Y_s-axis, in-lb

M_{X_s} moment about X_s-axis, in-lb

M_{Z_s} moment about Z_s-axis, in-lb

P free-stream stagnation pressure, lb/sq in. abs

q free-stream dynamic pressure, lb/sq ft

R Reynolds number

S wing area including body intercept, sq ft

$x/\bar{c}$ static margin in percent $\bar{c}$, $\left(-\frac{dC_m}{dC_L}\right)_{C_m=0} \times 100$

α angle of attack referred to fuselage reference line, deg

β angle of sideslip referred to fuselage center line, deg

Δ increment

δ_a differential deflection of both ailerons perpendicular to hinge line, deg (positive when right aileron down and left aileron up)

δ_s spoiler deflection perpendicular to hinge line, deg (located on upper right wing only)

Subscripts:

s refers to the stability axis

o denotes value of parameter at zero lift coefficient

MODEL DESIGNATION

Components:

B basic body with indentations for three semisubmerged missiles

S_0, S_1, S_2, S_3 externally mounted missiles

Subscript:	Position of missile:
0	All missiles removed
1	All missiles semisubmerged
2	Right and center missiles extended and left missile semisubmerged (when looking downstream)
3	All missiles extended

W wing with outer-panel leading-edge chord-extensions; $i_w = -1^\circ$

V vertical stabilizer and dorsal fin

H all-movable horizontal stabilizer

F ventral fins

Modifications:

D	notched speed or dive brake
P	three externally mounted packs housing six missiles
R	rocket engine housing
S	body strakes
T	two external fuel tanks

The basic configuration for these tests was BS_1WVHF; hence component breakdown is indicated by the absence of any of these symbols. All modifications are indicated by a plus sign; for example, $BS_1W + S$ denotes wing-body combination with strakes mounted.

MODEL AND APPARATUS

The tests were conducted in the low Mach number test section of the Langley Unitary Plan wind tunnel. This tunnel is of the variable-pressure, return-flow type with a test section measuring 4 feet square and approximately 7 feet in length. Mach number may be varied continuously from approximately 1.5 to 2.9 by means of an asymmetric sliding-block nozzle.

Details of the model are shown in figure 2 and its geometric characteristics are given in table I. Photographs of the basic model and the various model modifications are presented in figure 3. Since the model was too small to incorporate the ducting necessary for internal flow, the fuselage nose was extended to fair over the airplane underslung nose inlet. The fuselage cross section varied from a pear shape near the nose to a rectangle with rounded corners near the wing and ended in an elliptical afterbody. Considered to be a part of the basic fuselage were three semisubmerged missile models having inline cruciform wing and tail arrangements.

A 42° sweptback wing with outboard-panel leading-edge chord-extensions was mounted high on the fuselage ($0.25\bar{c}$ was 1.10 inches above fuselage reference line). This wing had an aspect ratio of 3.55, a taper ratio of 0.227, a dihedral angle of -5°, and incidence of -1°. All the empennage surfaces were swept back 45° and consisted of the following: a conventional vertical tail, a rearward-mounted all-movable horizontal stabilizer located 0.26 inch below the fuselage reference line, and two ventral fins mounted beneath the body at a dihedral angle of -70°.

For purposes of identification only, combinations of the preceding items, including extension of the three missile models, are referred to herein as model-component breakdown. (See section on "Model Designation.") On the other hand, the components described in the following paragraph will be treated as model modifications inasmuch as they were primarily tested as additions to the basic model configuration.

Two of the items in the modification category were the missile packs and the fuel tanks. (See fig. 2(c).) These components were essentially groups of special purpose stores externally mounted on the fuselage. Another special item was the fairing along the upper rearward portion of the fuselage for housing a rocket engine. (See fig. 2(a).) A more conventional modification was the addition of a 60° deflected, notched speed brake underneath the body. The remaining component in the modification category was the addition of strakes to the fuselage as shown in figure 2(a). These devices consisted of thin strips extending along the body from the nose to the wing root chord. The strake plan form was a constant width (10 percent of the maximum equivalent body diameter) except in the immediate vicinity of the nose where it was faired to zero width.

Model controls that were investigated included deflections of the horizontal stabilizer, one inboard trailing-edge aileron, and two simulated (long and short) upper-wing-surface spoilers. (See fig. 2(b).)

Forces and moments for the model were measured by means of a six-component internal strain-gage balance. This balance was attached, by means of a sting, to the tunnel central support system. Included in the model support system was a remotely operated, adjustable angle coupling that permitted tests to be made at various angles of attack simultaneously with variations in the angle of sideslip.

TESTS

Tests were made for all configurations through an angle-of-attack range from approximately -8° to 21° at angles of sideslip of about 0° and ±5°. At angles of attack of approximately 0°, 10°, and 15°, additional tests were conducted on the basic configuration for an angle-of-sideslip range from about -6° to 10° to check linearity (to determine the validity of the increment method of evaluating the static lateral stability characteristics). All basic model tests were made with a zero stabilizer deflection. The tests which were to determine stabilizer effectiveness utilized deflections of approximately -8°, -12°, -19°, and -29°. In addition, the -12° and -29° settings were employed to evaluate the effect of stabilizer deflection on the static lateral stability. Various

combinations of aileron and long- and short-spoiler deflections were tested during the lateral-control studies up to maximum values of $\delta_a = -40^\circ$ and $\delta_s = -45^\circ$.

The test conditions of Mach number, stagnation and dynamic pressure, and Reynolds number are listed in the following table:

M	P, lb/sq in. abs	q, lb/sq ft	R, per ft	R (based on $\bar{c}$)
1.60	8.2	499	2.19×10^6	1.40×10^6
1.90	9.1	496	2.19	1.40
2.20	10.5	477	2.19	1.40
2.50	12.2	448	2.04	1.30

Stagnation temperature was maintained at 125° F for all Mach numbers except 2.50 where it was 155° F.

Several additional tests were made to ascertain the effect of Reynolds number on drag. These tests were conducted near zero lift at a Reynolds number of 5.25×10^6 per foot and also at a higher value of R that was dependent on power limitations (maximum of 9.7×10^6 per foot at $M = 2.20$).

In order to determine the effect of transition on the aerodynamic characteristics, some pitch tests were made with the transition fixed on the model. For this condition, a transition strip was placed around the fuselage 2 inches to the rear of the nose and along the 10-percent-chord line of the wing on the upper and lower surfaces. The strips were 1/4 inch wide and consisted of No. 180 carborundum grains imbedded in shellac with approximately 50 grains per 1/4 inch of the strip.

CORRECTIONS AND ACCURACY

The tunnel, as yet, has not been completely calibrated, and any flow angularity that may exist in the test section has not been determined. Pressure gradients in the region of the model have been determined and are sufficiently small so as not to induce any buoyancy effects on the model.

All angles of attack, sideslip, and stabilizer settings have been corrected for deflection under static load conditions.

The balance-chamber drag of the model is defined herein as that force resulting from the pressure acting over the cavity area at the rear of the model (91 percent of the model base area). Values of this force were obtained for all test points and have been subtracted out of all drag results.

The accuracy of the presented data based on balance calibration, repeatability of the data, and tunnel calibration is estimated to be within the following limits:

M	± 0.015
α, β, and i_t, deg	± 0.1
C_L	± 0.005
C_D	± 0.001
C_m	± 0.005
C_l	± 0.0005
C_n	± 0.002
C_Y	± 0.002

PRESENTATION OF RESULTS

The results of this investigation are presented in the following figures:

	Figure
Typical schlieren photographs	4
Typical variation of balance-chamber drag coefficient with angle of attack; $\beta = 0^\circ$	5
Effect of transition on aerodynamic characteristics in pitch; $\beta = 0^\circ$	6
Effect of Reynolds number on zero-lift drag for natural and fixed transition	7
Pitch tests:	
Effect of model-component breakdown on aerodynamic characteristics in pitch	8
Effect of missiles on aerodynamic characteristics in pitch	9
Effect of horizontal stabilizer incidence on aerodynamic characteristics in pitch; BS_1WVHF; $\beta = 0^\circ$	10

DISCUSSION

The results have been presented in the form of basic and summary data curves. Some pertinent observations regarding these data, especially for the results contained in figures 24 to 29, are presented in this section.

Performance

For evaluation purposes, drag will be treated in three parts, namely, zero-lift drag, drag due to lift, and drag due to trim.

The C_{D_o} level for the basic model of 0.0300 to 0.0320 (fig. 26(b)) is relatively unaffected by fixing transition and increasing Reynolds number to 9.7×10^6 per foot (6.2×10^6 based on $\bar{c}$) since these effects are nearly within balance accuracy (figs. 6 and 7). In addition, it is felt that any changes in this level that would result from incorporating a well-designed nose inlet should be relatively minor. Although lower drag levels have been obtained on some research models, experience with models of complete airplane configurations would indicate that this C_{D_o} level appears reasonable for models of airplanes designed to operate in this speed range.

At $M = 1.47$, a Mach line would become coincident with the leading edge of the plan form investigated. Hence, no leading-edge suction is theoretically available for reducing drag due to lift as the Mach line is swept aft of the wing leading edge at all tested speeds. Some suction appears to exist, however, for the results of figure 26(a) show that the test values of $\Delta C_D/C_L^2$ were slightly lower than the zero-suction curve $1/57.3C_{L_\alpha}$.

The effect of drag due to trim is indicated by the comparison of trimmed and untrimmed ($i_t = 0^\circ$) curves of $(L/D)_{max}$ illustrated in figure 28. The L/D loss due to trim was about 0.7 to 1.0 over the speed range and is of the order frequently encountered when a conventional rearward-mounted all-movable stabilizer is utilized as the trimming device.

Despite the L/D loss due to trim, noteworthy features of the tested geometry were the relatively flat variation of L/D of about 4 with Mach number and the less than 30 percent L/D loss (from the maximum available) incurred by trimming at C_L values as low as 0.10.

Longitudinal Stability

The model exhibited stable static longitudinal characteristics throughout the tested range of lift coefficients and Mach numbers (fig. 8). In fact, the wing-body combination (BS_1W) and the complete model (BS_1WVHF) had minimum values of static margin of 13 and 35 percent $\bar{c}$, respectively, about the assumed center-of-gravity location of $0.25\bar{c}$ (fig. 25(b)). Longitudinal stability changes resulting from most of the various model modifications tested (D, P, R, and T) were relatively small (figs. 11 and 12).

Deflection of the all-movable horizontal stabilizer produced linear increments in pitching moment over a wide range of lift coefficients at all Mach numbers and for deflections up to approximately -20° (fig. 10). Stabilizer effectiveness, although exhibiting the characteristic decrease with Mach number, retained a value of -0.0055 at the maximum speed tested (fig. 27(b)).

Airplane range performance is basically determined by the L/D level available; therefore, any reduction in the drag due to trim will benefit the configuration. Inasmuch as the stabilizer had sufficient effectiveness, and since the complete configuration has sufficient static margin, an improvement in supersonic trim $(L/D)_{max}$ can be obtained by a rearward movement of the center of gravity. Data available from tests in the Langley 8-foot transonic tunnel (ref. 1) on the same model indicated the feasibility of such a change, in that the smallest value of static margin encountered was 16 percent for Mach numbers as low as 0.8.

Lateral Stability

All static lateral stability data except those shown in figure 19 were obtained by computing the coefficient increment between angle-of-attack runs made at $\beta = \pm 5^\circ$. The correlation between the slope (from fig. 17) and increment method of determining the stability parameters

is indicated by the favorable comparison of the curves and symbols shown in figure 19.

Figure 29 illustrates the effect of model-component breakdown on the variation of the directional-stability parameter C_{n_β} with Mach number for $\alpha = 0^\circ$ and 15°. The body-alone results had the customary unstable variation with angle of attack. Addition of the wing to the body, although having little effect at $\alpha = 0^\circ$, resulted in an even more unstable configuration at high angles of attack. This effect can be associated with wings mounted high on the fuselage. (See, for example, ref. 2.)

At 0° angle of attack, the vertical tail with its large area contributed a substantial stability increment to the wing-body results and, in addition, exhibited the characteristic decrease with Mach number. However, the directional stability contributed by the vertical tail at $\alpha = 15^\circ$ was only about one-half of the ΔC_{n_β} produced at $\alpha = 0^\circ$. Changes in C_{n_β} of the wing-body-tail combination due to addition of the horizontal stabilizer at either angle of attack were quite small as might have been anticipated.

In order to examine the powerful effect of the ventral fins, it is only necessary to note that the complete model minus ventrals was unstable even at 0° angle of attack for all Mach numbers larger than 1.90. On the other hand, the basic model incorporating the ventral fins was directionally stable at all tested Mach numbers for angles of attack as large as 19° (fig. 19(a)).

The body alone had a negligible amount of effective dihedral that was little affected by variations in either angle of attack or Mach number (fig. 19). Addition of the wing and vertical tail resulted in progressive increases in $-C_{l_\beta}$ at all Mach numbers and for most angles of attack. The effect of adding the horizontal stabilizer was a small decrease in the effective dihedral parameter for angles of attack of less than 12°. Addition of the ventral fins not only substantially reduced the value of $-C_{l_\beta}$ for the body—wing—vertical-stabilizer combination, but also resulted in a basic configuration variation that was essentially independent of angle of attack and Mach number.

Most model modifications (D, P, R, and T) had little influence on the value of C_{n_β} or C_{l_β} for the basic model. The tests involving missile removal or extension (fig. 20), however, indicated that the addition of three semisubmerged missiles and their subsequent extension, progressively decreased the directional stability of the basic model at lower angles of attack. It is of interest, therefore, that the addition of missile packs at the same location on the model as the externally

mounted missiles had little effect on the value of C_{n_β} at any angle of attack (fig. 22).

Strakes

The last topic to be discussed is the effect of body strakes on the aerodynamic characteristics of the model. These tests were incorporated into the present program as a result of recent interest (refs. 2 and 3) in this type of device for improving directional stability at high angles of attack.

Figure 24 illustrates the improvement in C_{n_β} variations produced by the strakes at angles of attack larger than 8° or 9° for both the wing-body combination and the complete or basic model. Approximately 50 to 80 percent of the increase in basic model stability was caused by the effect of the strakes on the C_{n_β} level of the wing-body combination, the remainder apparently resulting from a strake improvement of the contribution of the vertical tail.

In order to determine the utility of this type of device, the effect of strakes on the longitudinal stability must next be examined. Figure 13 indicates that the changes caused by strakes were similar to the effects produced by a canard, that is, the static stability was slightly decreased by the strakes at all Mach numbers. At higher lift coefficients, small additional losses in stability occurred which increased with lift. The effect on lift-curve slope, minimum drag, and drag due to lift was small. Thus, the incidental effects of the strakes on the model pitch characteristics were not extensive enough to preclude the use of this device to improve C_{n_β} at moderate and high angles of attack.

CONCLUSIONS

An investigation has been conducted in the Langley Unitary Plan wind tunnel of the drag and the static longitudinal and lateral stability and control characteristics of a 42° sweptback-wing fighter-airplane model with no internal flow. Data were obtained at Mach numbers of 1.60, 1.90, 2.20, and 2.50 at a Reynolds number of approximately 2.1×10^6 per foot (1.4×10^6 based on mean aerodynamic chord) with the following results:

1. The basic model exhibited stable static longitudinal characteristics throughout the tested range of lift coefficients and Mach numbers.

2. The complete model incorporating ventral fins was statically stable directionally at all Mach numbers for angles of attack up to 19°.

3. Changes in the longitudinal and lateral stability characteristics of the complete model resulting from the addition of missile packs, speed brake, rocket-engine housing, or external fuel tanks were relatively minor.

4. Fixing transition and increasing Reynolds number to 9.7×10^6 per foot did not have a significant effect on the value of drag at zero lift which was about 0.0300 to 0.0320 over the Mach number range tested.

5. The value of trim maximum lift-drag ratio of approximately 4 was relatively invariant with Mach number for the configuration.

6. Addition or extension of three semisubmerged missiles to the basic configuration progressively decreased the directional stability of the model.

7. Body-mounted strakes improved the directional stability of the complete model at moderate and high angles of attack without severely altering the basic pitch characteristics.

Langley Aeronautical Laboratory,
National Advisory Committee for Aeronautics,
Langley Field, Va., October 14, 1957.

REFERENCES

1. Pierpont, P. Kenneth: Transonic Wind-Tunnel Investigation of Static Longitudinal and Lateral Stability and Control Characteristics and Drag Rise of a Representative Fighter Airplane. NASA MEMO 12-14-58L, 1959.

2. Spearman, M. Leroy: Some Factors Affecting the Static Longitudinal and Directional Stability Characteristics of Supersonic Aircraft Configurations. NACA RM L57E24a, 1957.

3. Sleeman, William C., Jr.: Investigation at High Subsonic Speeds of the Effects of Various Horizontal Fuselage Forebody Fins on the Directional and Longitudinal Stability of a Complete Model Having a 45° Sweptback Wing. NACA RM L56J25, 1957.

TABLE I

GEOMETRIC CHARACTERISTICS OF THE 42° SWEPTBACK-WING FIGHTER-AIRPLANE MODEL

FS - fuselage station, where FS 0.00 is 1.06 inches forward of nose
WL - water line, where WL 5.00 is model reference
WS - wing station measured outboard in plane of wing
BL - body line measured outboard and perpendicular to plane of symmetry

Note: WS 0.00 and BL 0.00 are plane of symmetry

Center-of-gravity location:	
Longitudinal (L.E. of $\bar{c}$), percent $\bar{c}$	25.0
Vertical, in.	WL 5.00
Fuselage:	
Length, in.	36.05
Maximum width, in.	3.64
Maximum depth, in.	4.30
Maximum equivalent diameter, in.	4.09
Frontal area, sq ft	0.0912
Overall fineness ratio	8.81
Side area, sq ft	0.8915
Volume, cu ft	0.1978
Base annulus area, sq ft	0.0040
Cavity area, sq ft	0.0390
Wing:	
Loading, lb/sq ft:	
Take-off	83.3
Combat	68.0
Landing	58.2
Projected area (excluding L.E. chord-extensions), sq ft:	
Exposed	0.9750
Theoretical	1.1250
Projected span, in.	23.97
Root chord (WS and BL 0.00):	
Length, in.	11.02
Location (L.E.), in.:	
Longitudinal	FS 15.54
Vertical	WL 6.39
Tip chord (WS 12.04 or BL 11.98), in.	2.50
Mean aerodynamic chord (excluding L.E. chord-extensions):	
Length, in.	7.65
Location (L.E.), in.:	
Longitudinal	FS 20.64
Vertical	WL 6.06
Lateral	WS 4.73
Aspect ratio	3.55
Taper ratio	0.227
Sweepback of quarter-chord line, deg	42
Dihedral, deg	-5
Incidence, deg	-1
Geometric twist, deg	0
Airfoil (parallel to plane of symmetry):	
Root	NACA 65A005
Tip	NACA 65A004
Chord-extension (portion ahead of basic wing plan form):	
Type	Double angled, leading edge
Projected area, sq ft	0.0154
Projected span, sq ft	4.52
Location:	
Lateral, in.:	
Inboard edge	WS 7.50
Outboard edge	WS 12.04
Chord, in.:	
Inboard edge (0.12c)	0.68
Outboard edge (0.12c)	0.30
Aileron (each):	
Type	Plain, sealed
Area, sq ft	0.0571
Span, in.	4.61
Sweepback of hinge line, deg	25.4
Deflection, deg	±20
Location:	
Longitudinal hinge center line, percent chord:	
Inboard edge	76.1
Outboard edge	74.3
Lateral, in.:	
Inboard edge	WS 2.95
Outboard edge	WS 7.56
Chord, in.:	
Inboard edge	2.03
Outboard edge	1.54

TABLE I.- Concluded

GEOMETRIC CHARACTERISTICS OF THE 42° SWEPTBACK-WING FIGHTER-AIRPLANE MODEL

	Long	Short
Spoilers:		
Type	Hinged Plate	
Area, sq ft	0.0219	0.0128
Span, in.	4.47	2.68
Sweepback of hinge line, deg	25.4	
Deflection, deg	0 to 45	
Location:		
Longitudinal hinge center line, percent chord:		
Inboard edge	64.2	60.3
Outboard edge	54.4	54.4
Lateral, in.:		
Inboard edge	WS 2.95	WS 4.74
Outboard edge	WS 7.42	WS 7.42
Chord, in.:		
Inboard edge	0.77	0.72
Outboard edge	0.64	0.64
Horizontal stabilizer (all movable):		
Area, sq ft:		
Exposed (C_r at HL 1.65)	0.1918	
Theoretical	0.3250	
Span, in.	12.80	
Root chord (HL 0.00):		
Length, in.	6.36	
Location (L.E.), in.:		
Longitudinal	FS 29.15	
Vertical	WL 4.74	
Tip chord (HL 6.40), in.	0.95	
Mean aerodynamic chord:		
Length, in.	4.32	
Location (L.E.), in.:		
Longitudinal	FS 32.07	
Vertical	WL 4.74	
Lateral	BL 2.41	
Aspect ratio	3.50	
Taper ratio	0.15	
Sweepback of quarter-chord line, deg	45	
Dihedral, deg	0	
Geometric twist, deg	0	
Airfoil:		
Root	NACA 65A004	
Tip	NACA 65A004	
Tail length ($0.25\bar{c}_{wing}$ to $0.25\bar{c}_{horz.\ stab.}$), in.	10.60	
Hinge line, percent $\bar{c}$	42.5	
Vertical tail:		
Area, sq ft:		
Exposed (C_r at WL 6.65)	0.1627	
Theoretical	0.2725	
Span, in.	7.51	
Root chord (BL 0.00):		
Length, in.	8.18	
Location (L.E.), in.:		
Longitudinal	FS 26.57	
Vertical	WL 4.74	
Tip chord (WL 12.25), in.	2.28	
Mean aerodynamic chord:		
Length, in.	5.78	
Location (L.E.), in.:		
Longitudinal	FS 30.22	
Vertical	WL 7.79	
Aspect ratio	1.44	
Taper ratio	0.278	
Sweepback of quarter-chord line, deg	45	
Airfoil:		
Root	NACA 66A005	
Tip	NACA 66A004	
Tail length ($0.25\bar{c}_{wing}$ to $0.25\bar{c}_{tail}$), in.	9.11	
Ventral fin:		
Area (exposed), sq ft	0.0615	
Span, in.	3.41	
Root chord:		
Length, in.	3.92	
Location (L.E.), in.:		
Longitudinal	FS 27.81	
Vertical	WL 3.09	
Tip chord, in.	1.28	
Mean aerodynamic chord:		
Length, in.	2.82	
Location (L.E.), in.:		
Longitudinal	FS 29.27	
Vertical	WL 1.75	
Lateral	BL 1.50	
Aspect ratio	1.31	
Taper ratio	0.327	
Sweepback of quarter-chord line, deg	45	
Dihedral, deg	-70	
Incidence, deg	0	
Airfoil:		
Root	NACA 66A004.4	
Tip	NACA 66A003	
Tail length ($0.25\bar{c}_{wing}$ to $0.25\bar{c}_{vent.\ fin}$), in.	7.42	

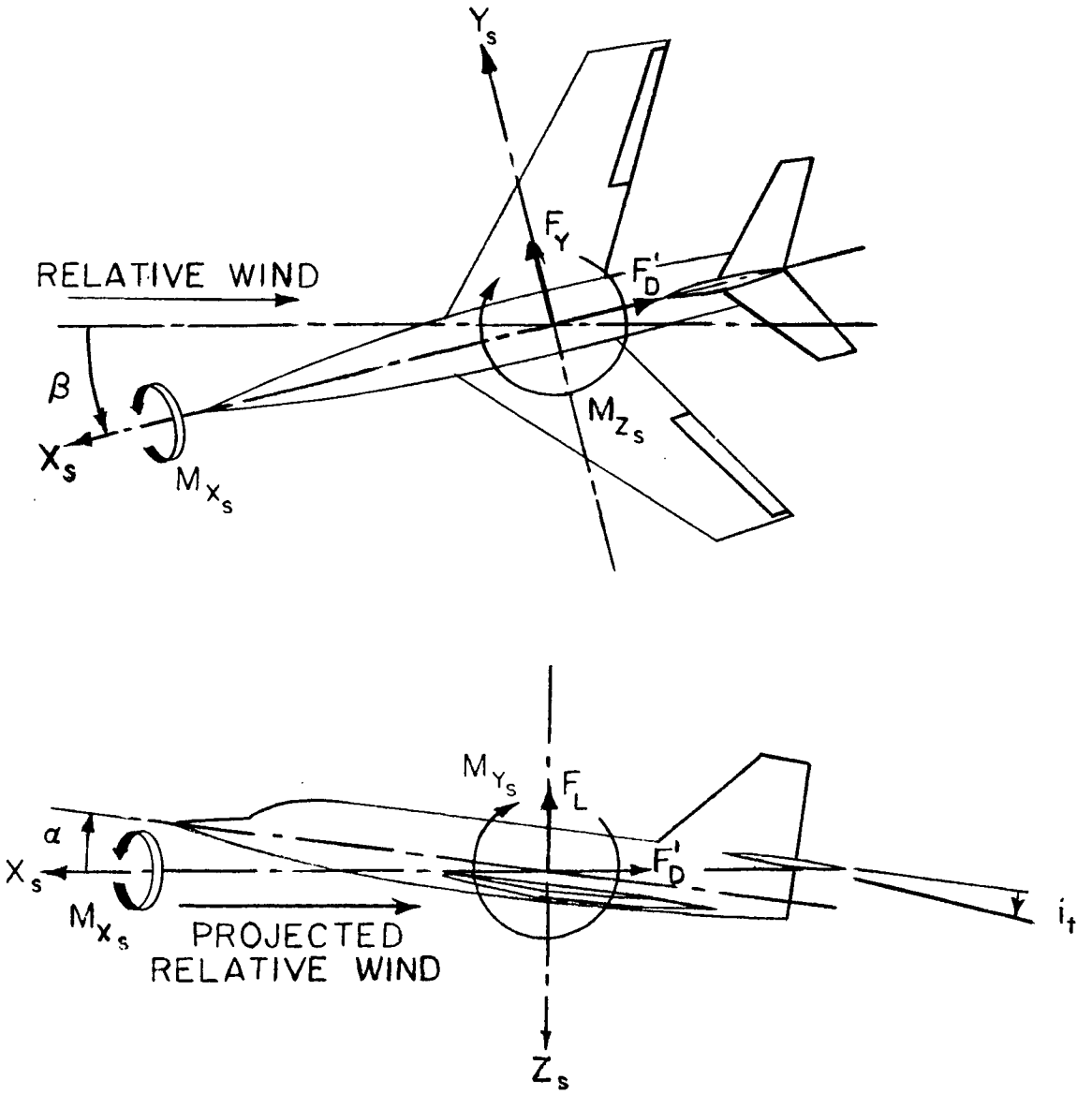

Figure 1.- Stability system of axes. Arrows indicate direction of positive forces, moments, and angles.

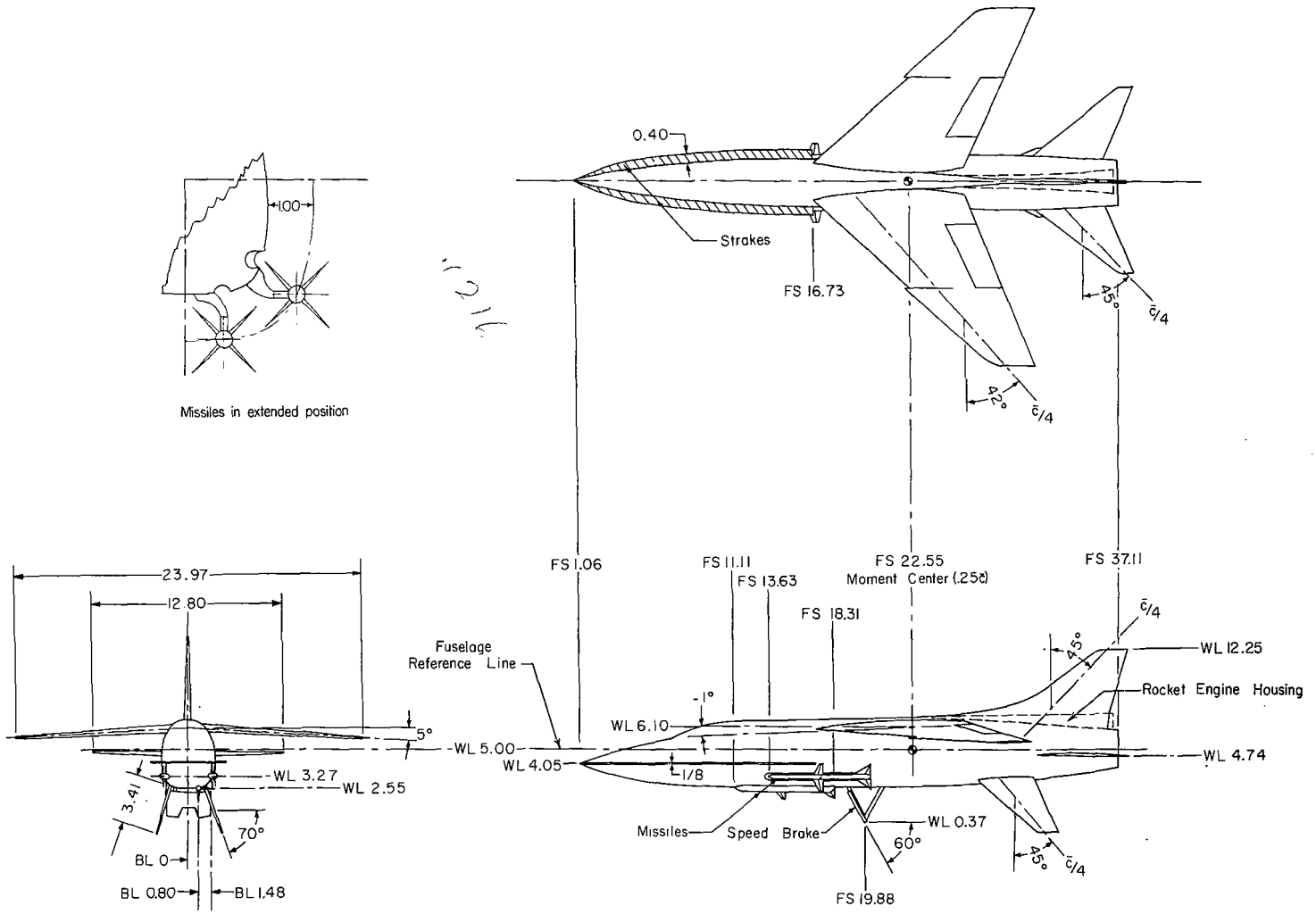

(a) Three-view drawing.

Figure 2.- Sketches of 42° sweptback-wing fighter-airplane model. All dimensions are in inches.

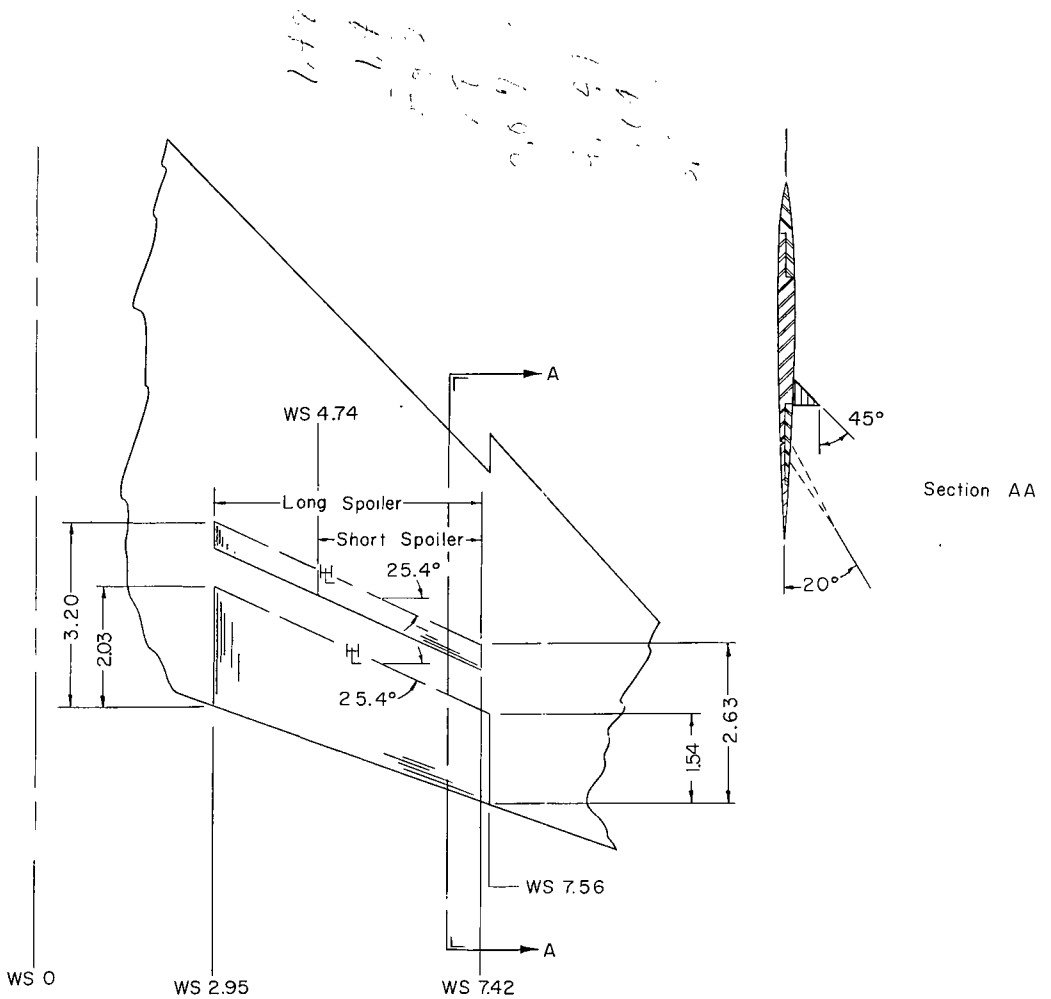

(b) Aileron and spoilers.

Figure 2.- Continued.

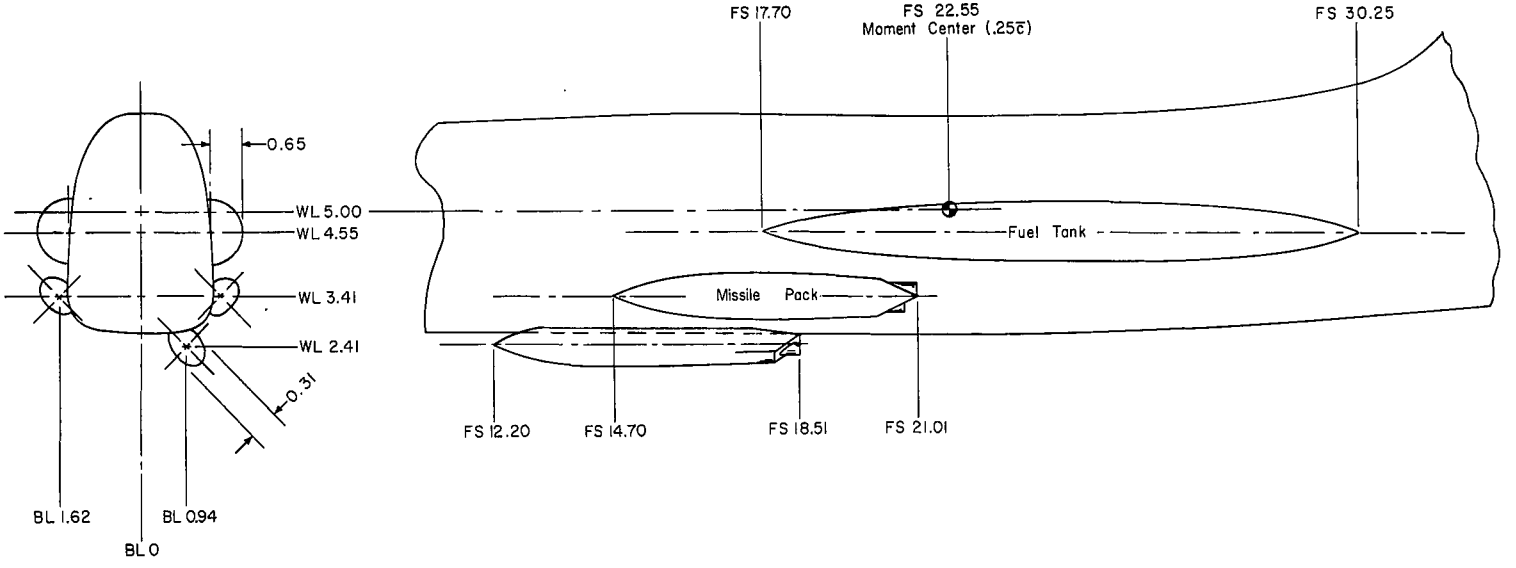

(c) External missile packs and fuel tanks.

Figure 2.- Concluded.

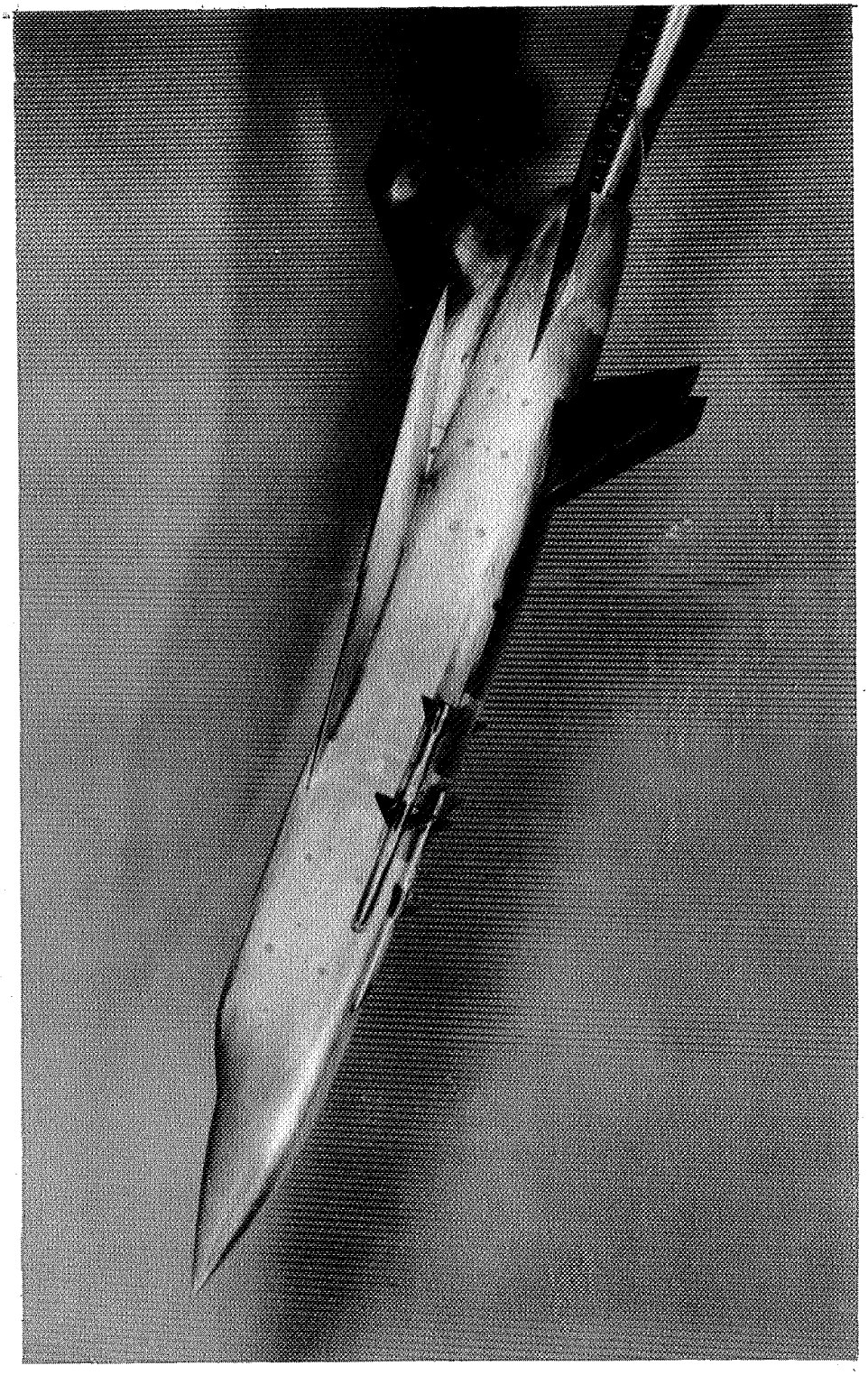

L-97106

(a) Basic model.

Figure 3.- Photographs of the model.

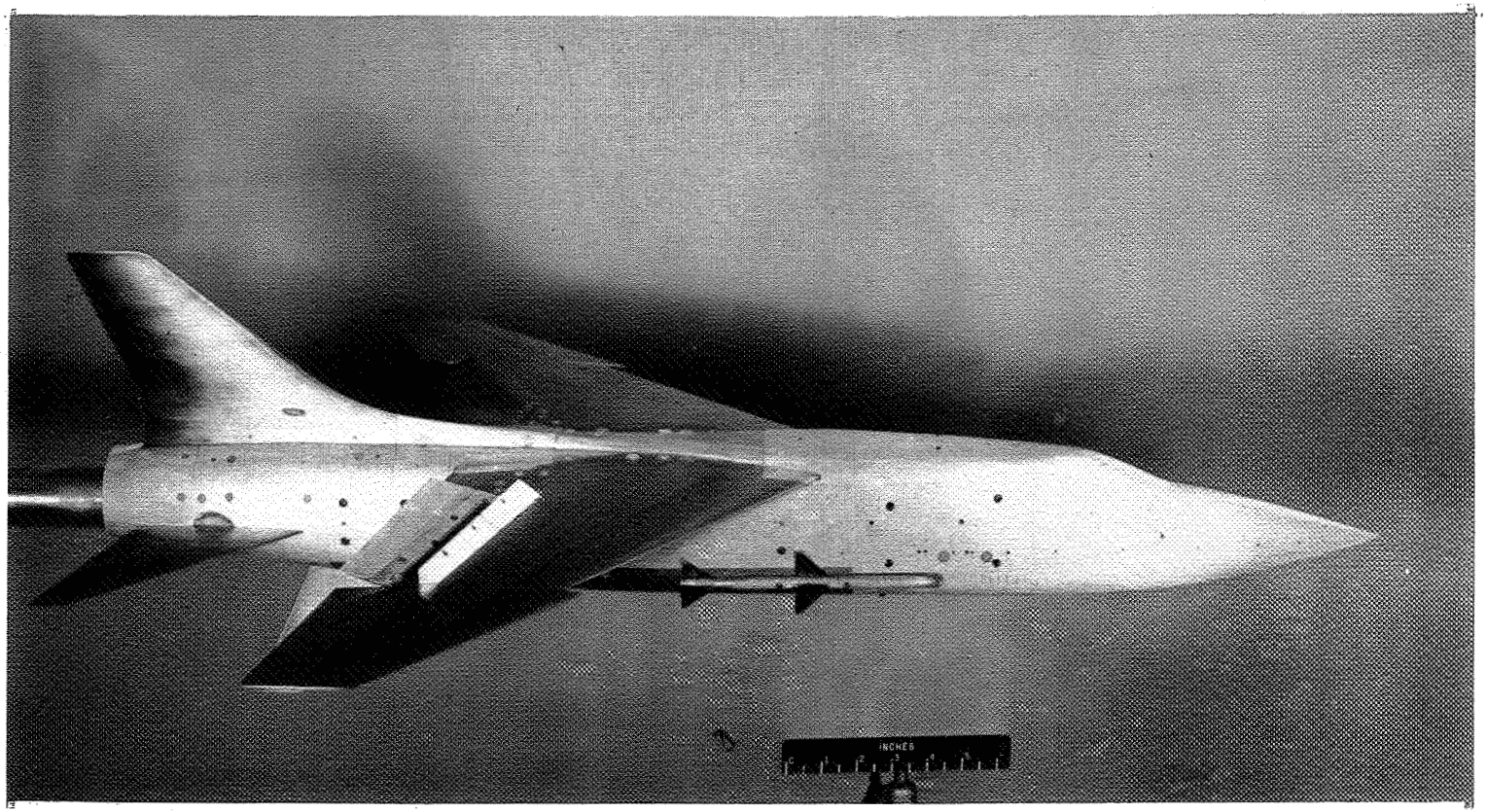

(b) Basic model with spoiler and ailerons deflected. L-57-861

Figure 3.- Continued.

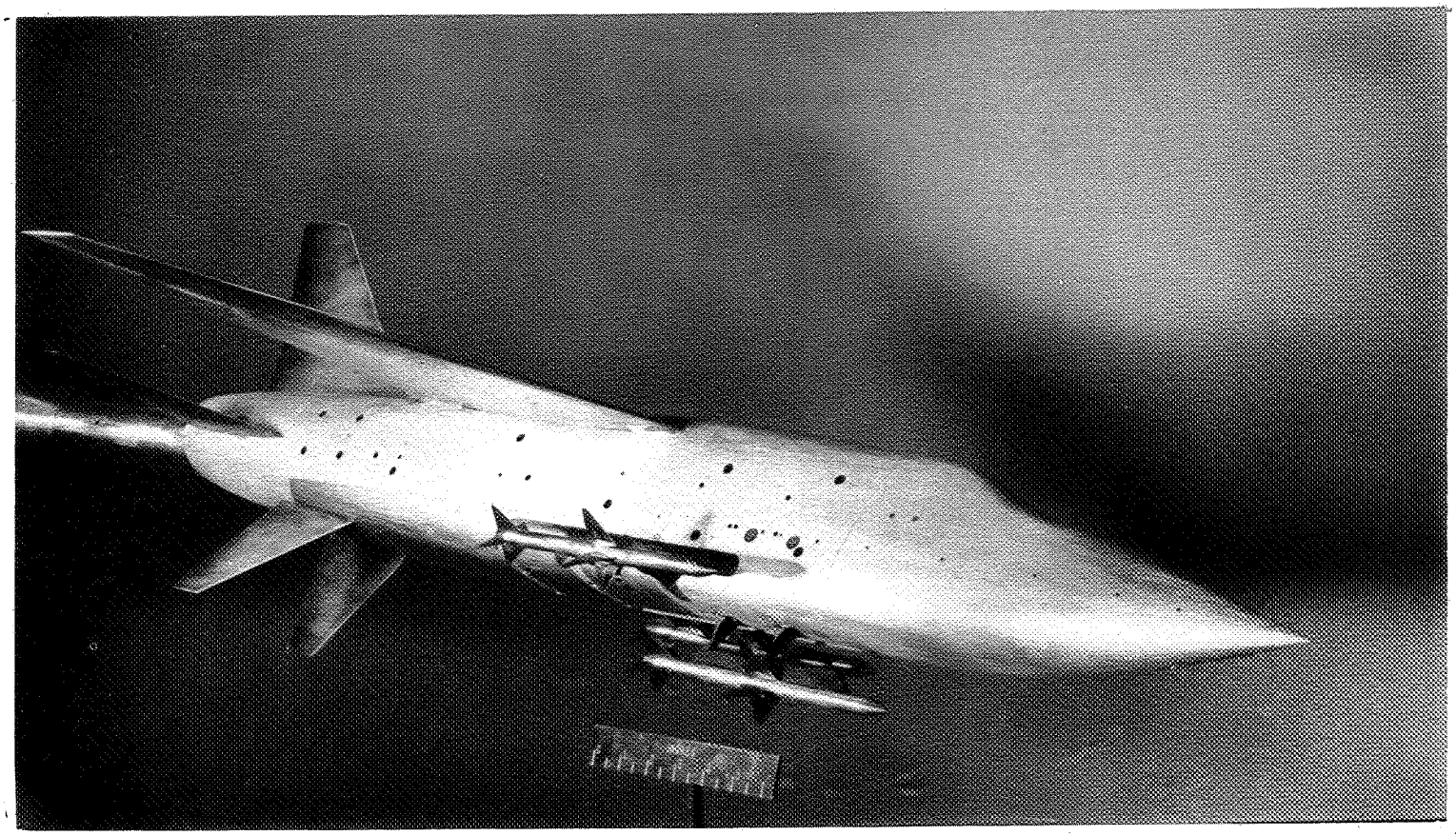

(c) Basic model with three missiles extended. L-57-857

Figure 3.- Continued.

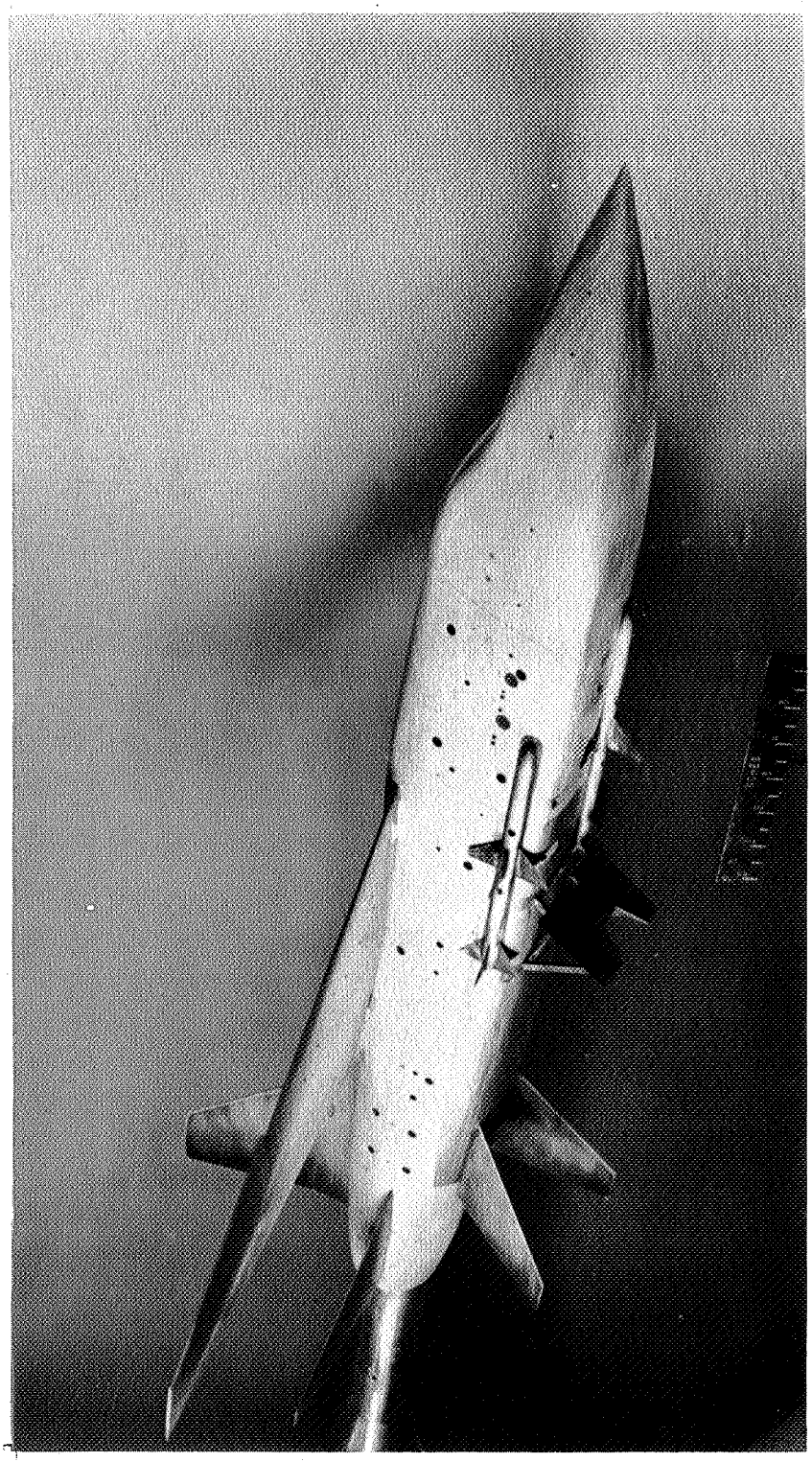

(d) Basic model with speed brake extended. L-57-859

Figure 3.- Continued.

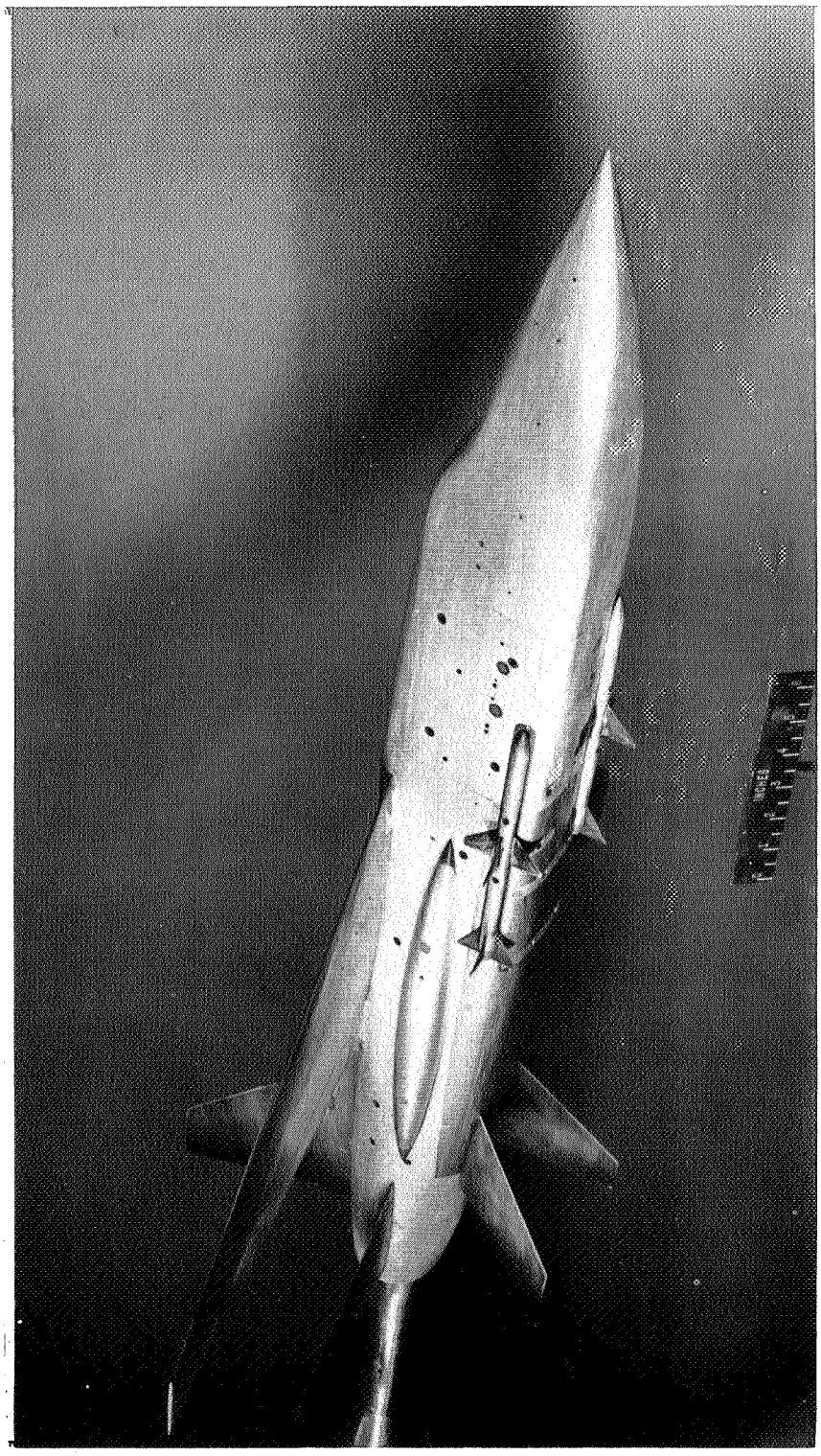

L-57-858

(e) Basic model with external fuel tanks.

Figure 3.- Continued.

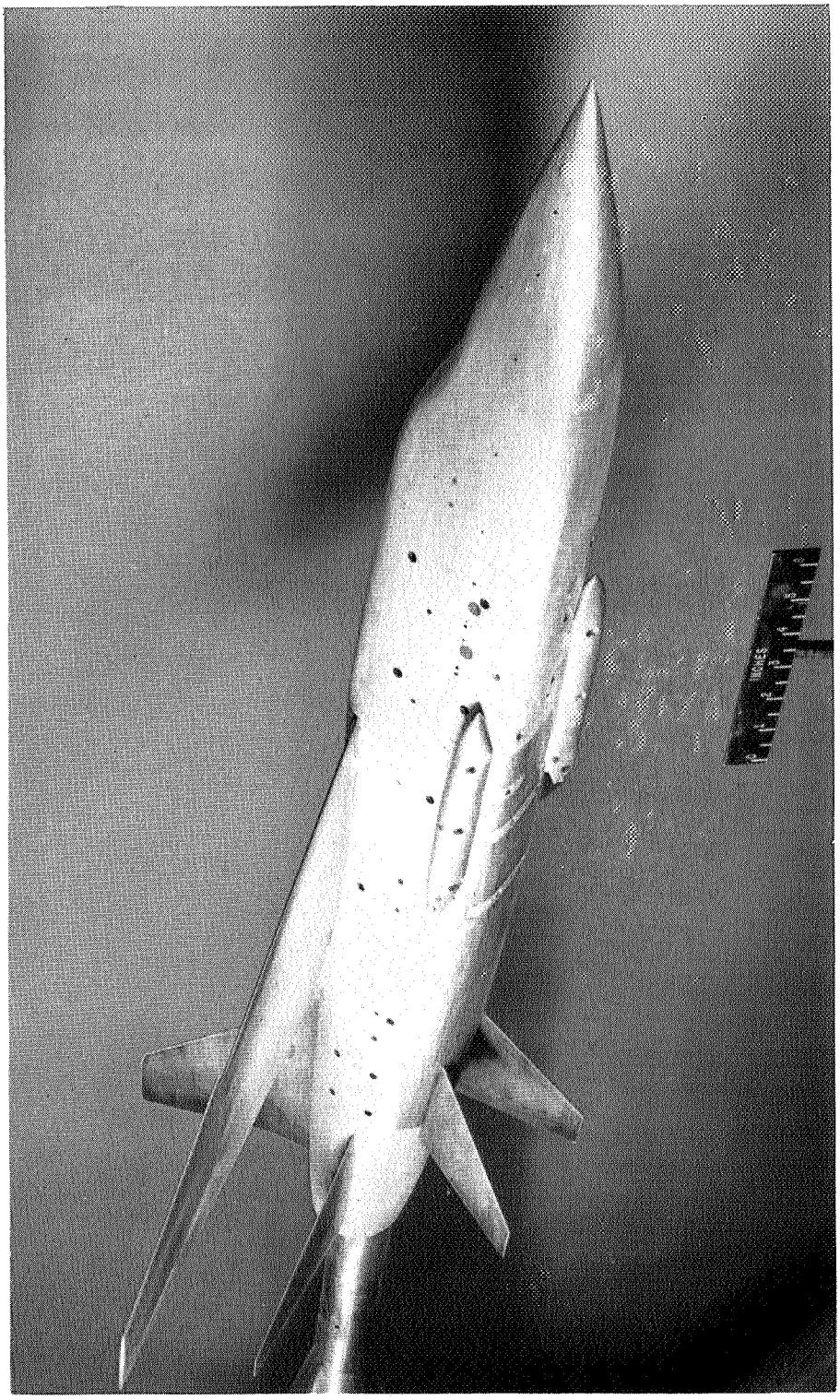

(f) Basic model with three external missile packs. L-57-860

Figure 3.- Continued.

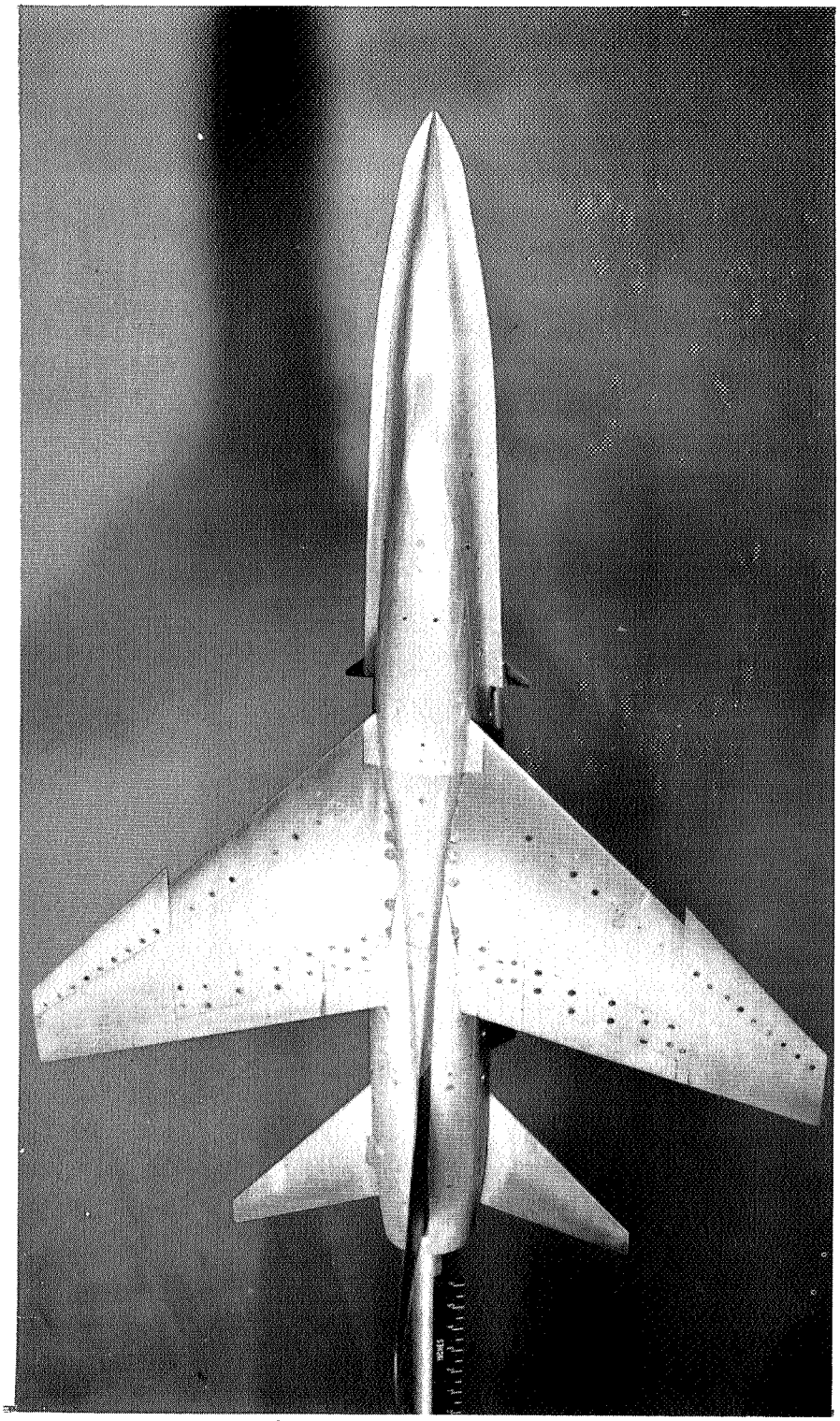

(g) Basic model with strakes installed. L-57-855

Figure 3.- Concluded.

α=-7.9°

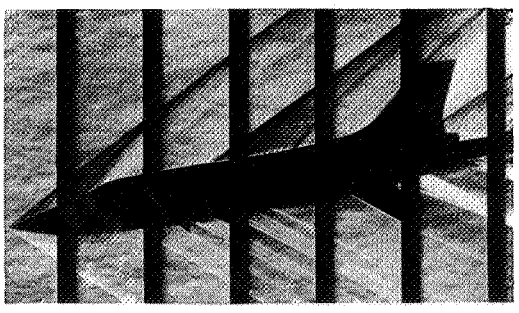

α=-7.6°

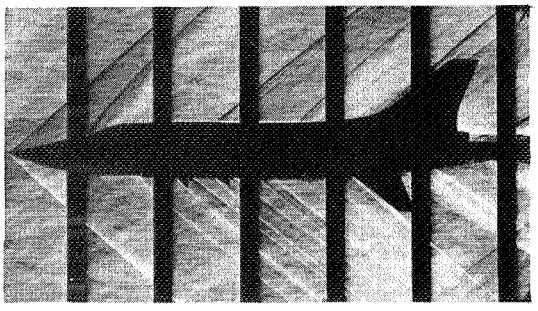

α= 1.6°

α= 1.8°

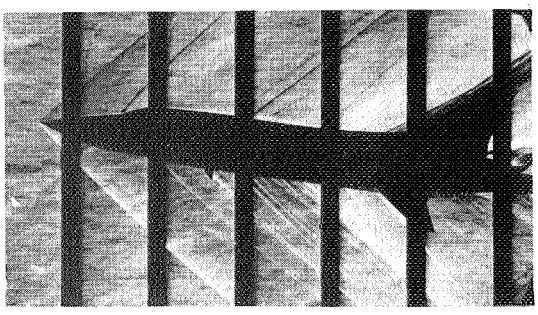

α= 8.8°

α= 9.0°

α=21.2°

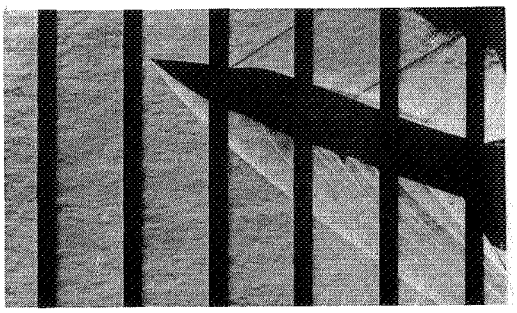

α=21.4°

(a) M = 1.60. (b) M = 1.90.

Figure 4.- Typical schlieren photographs.

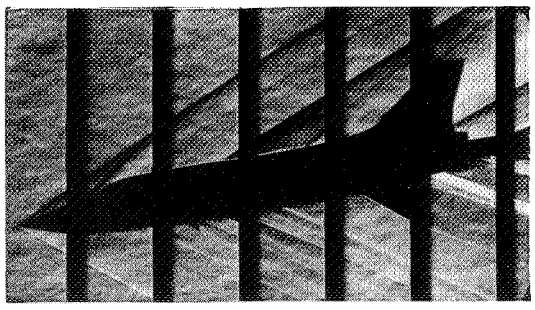

α=-7.1°

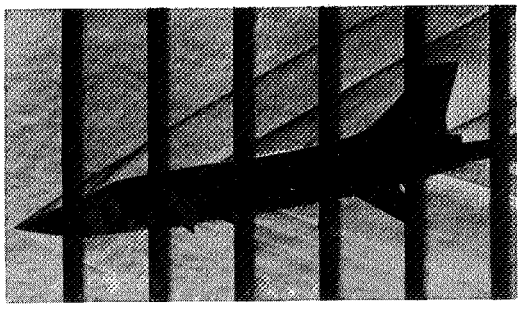

α=-7.8°

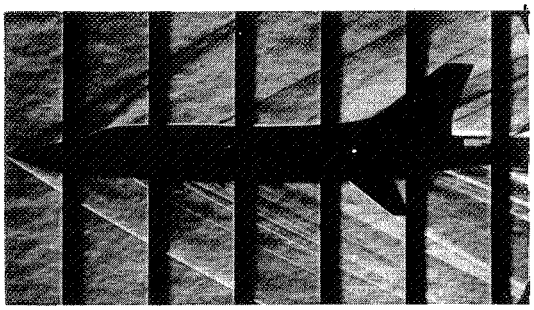

α = 2.3°

α = 1.5°

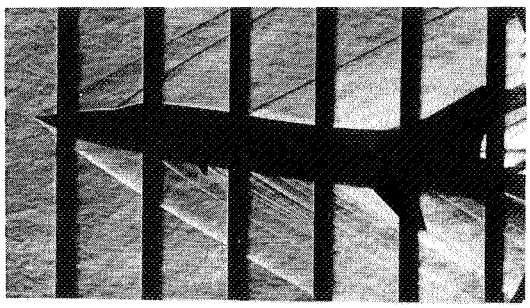

α = 9.5°

α = 8.7°

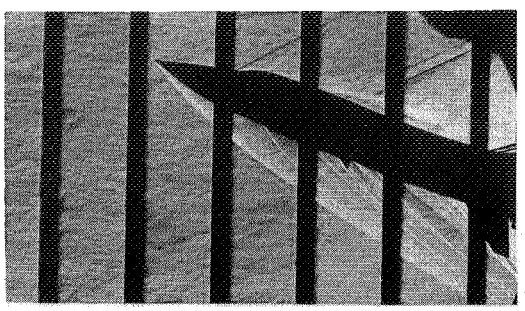

α =21.8°

α =21.0°

(c) M = 2.20. (d) M = 2.50. L-57-2793

Figure 4.- Concluded.

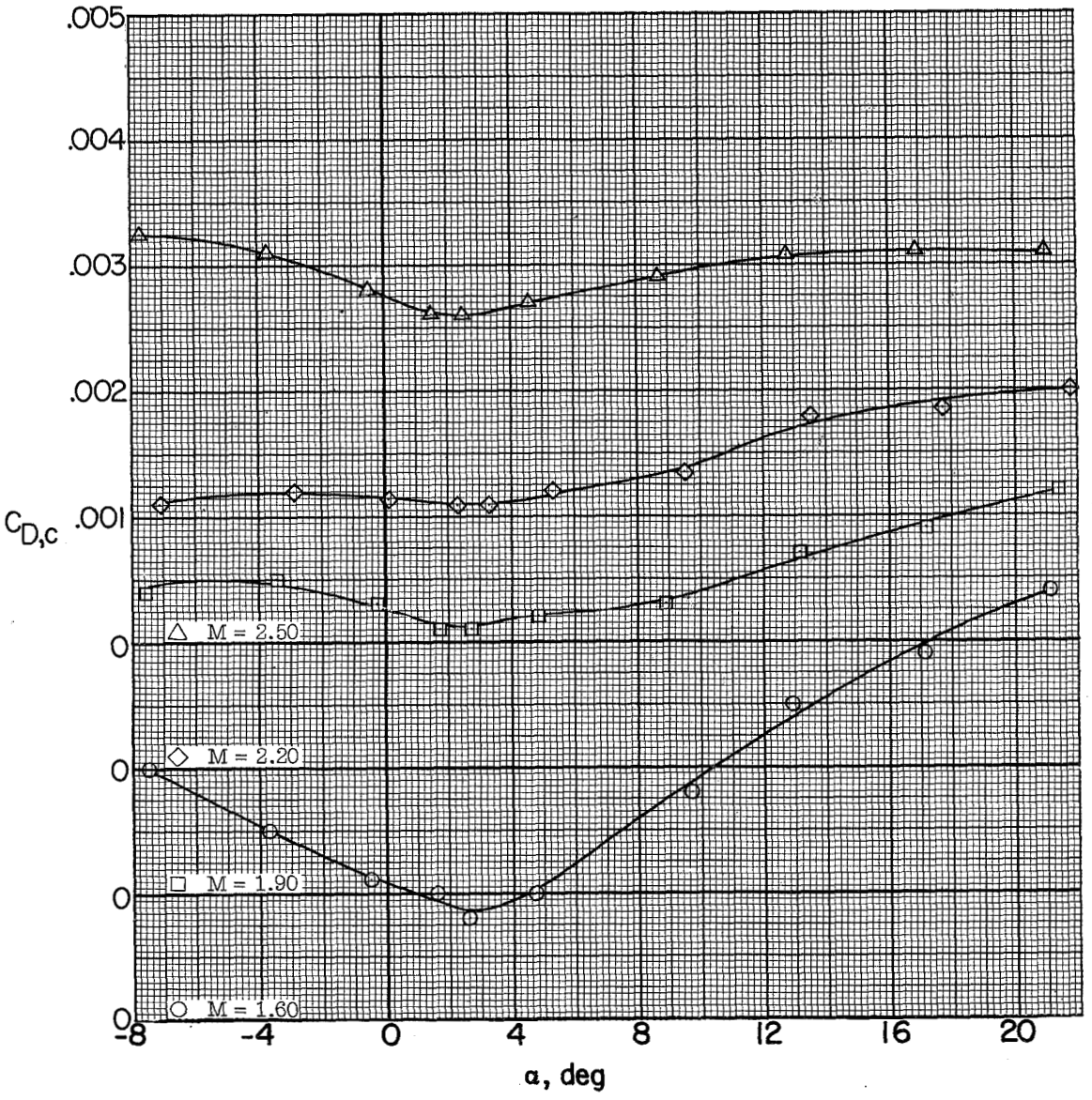

Figure 5.- Typical variation of balance-chamber drag coefficient with angle of attack. $\beta = 0^{\circ}$.

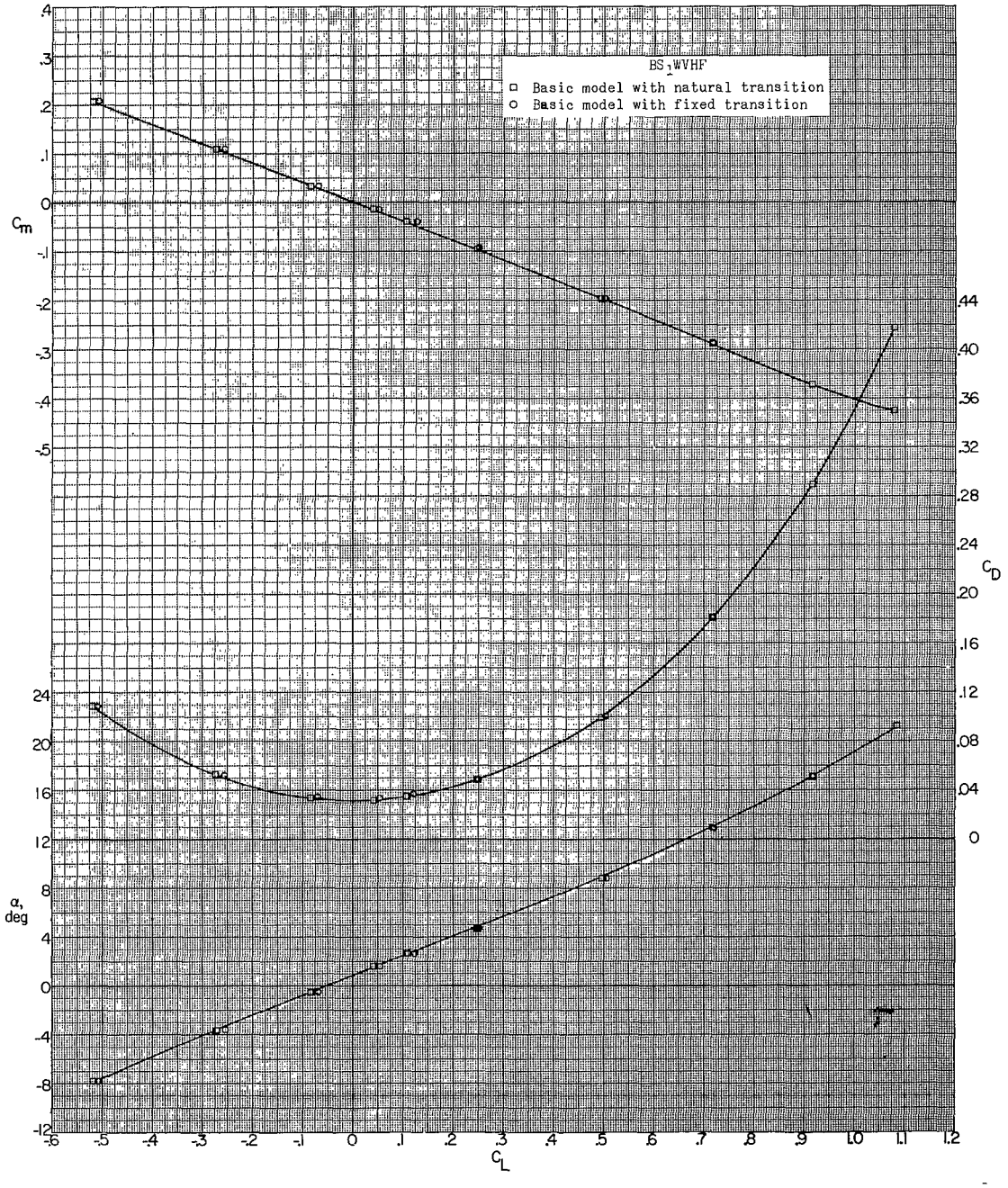

(a) M = 1.60.

Figure 6.- Effect of transition on aerodynamic characteristics in pitch. $\beta = 0^{\circ}$.

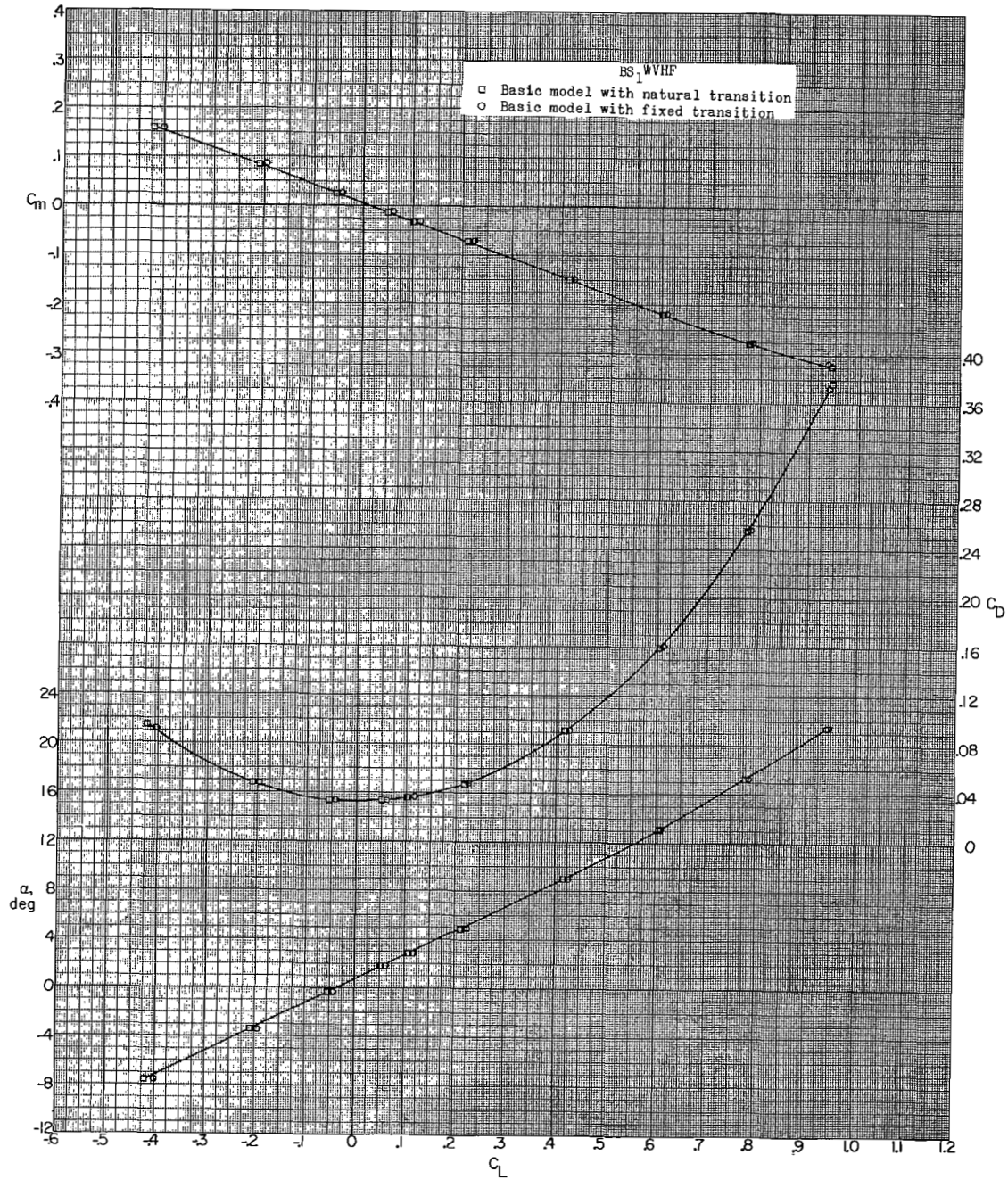

(b) M = 1.90.

Figure 6.- Continued.

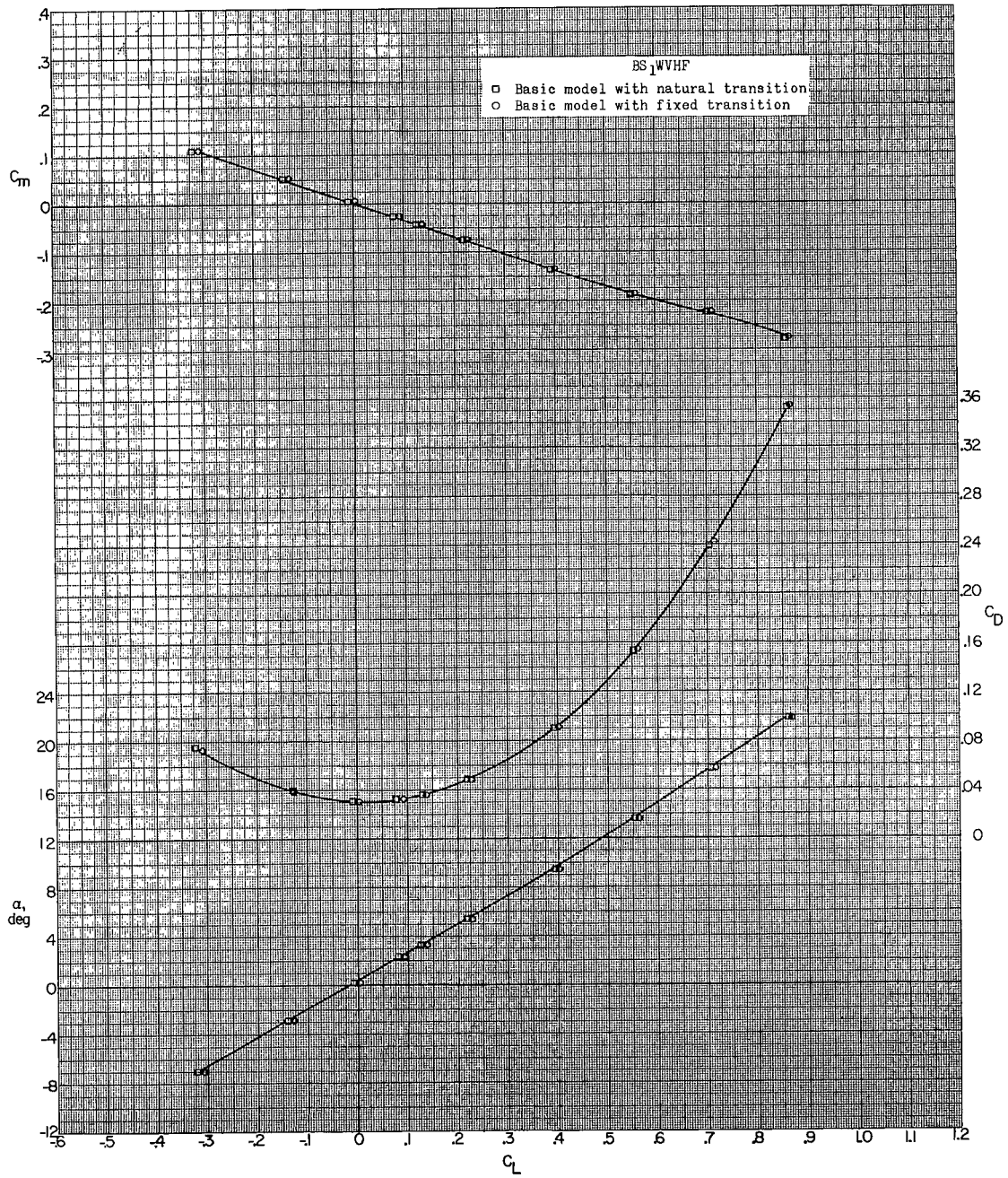

(c) M = 2.20.

Figure 6.- Concluded.

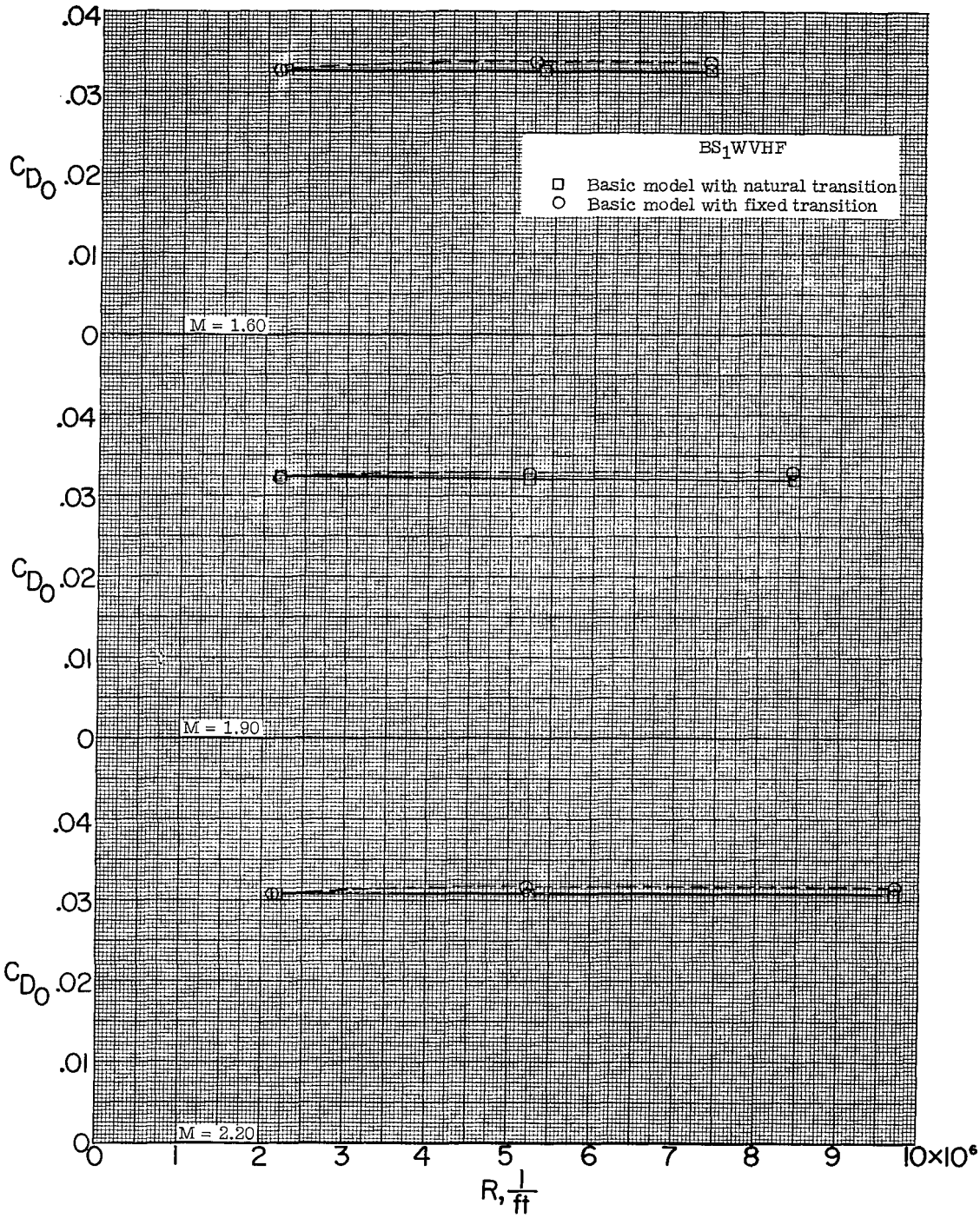

Figure 7.- Effect of Reynolds number on zero-lift drag for natural and fixed transition.

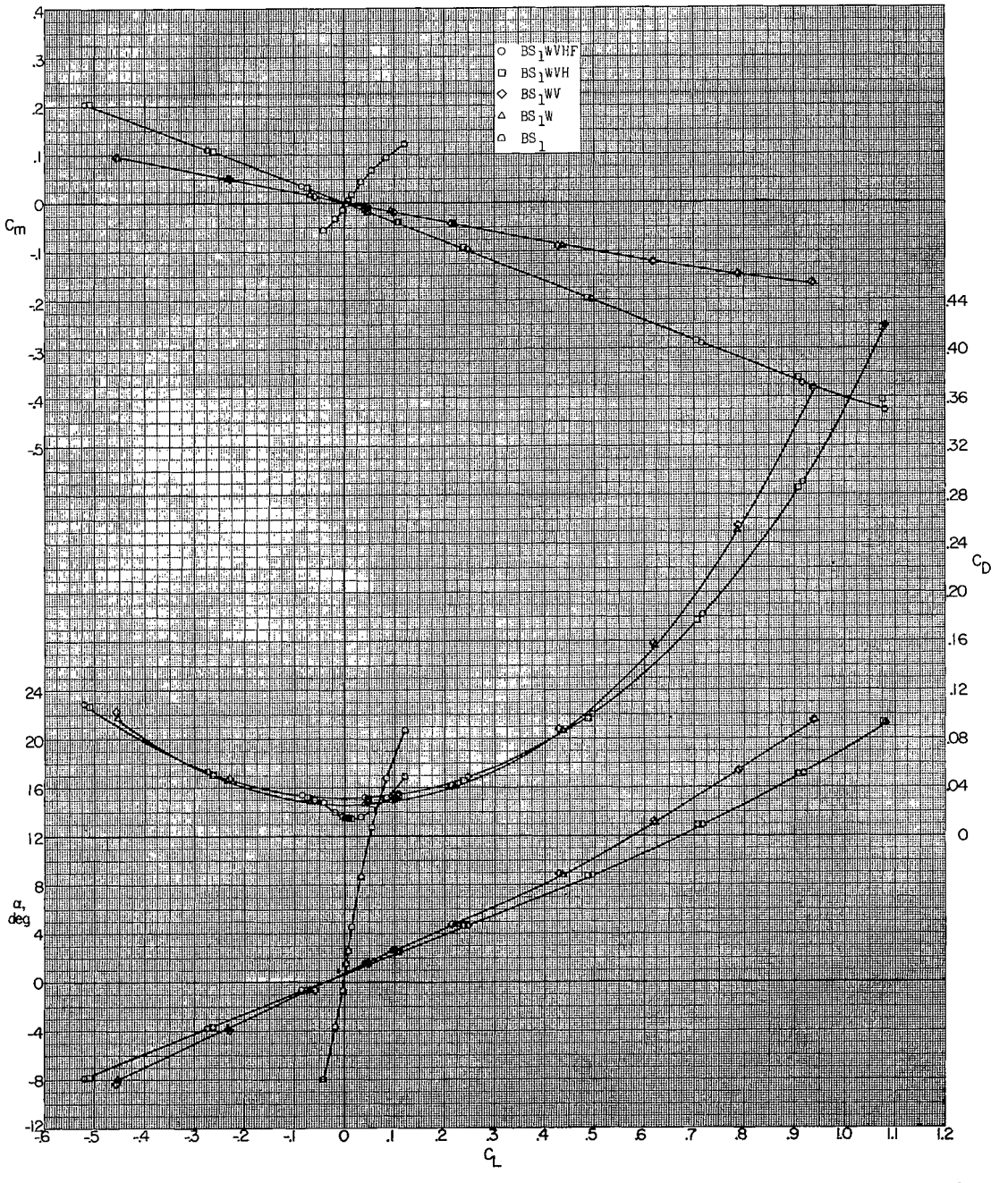

(a) M = 1.60; $\beta = 0^{\circ}$.

Figure 8.- Effect of model-component breakdown on aerodynamic characteristics in pitch.

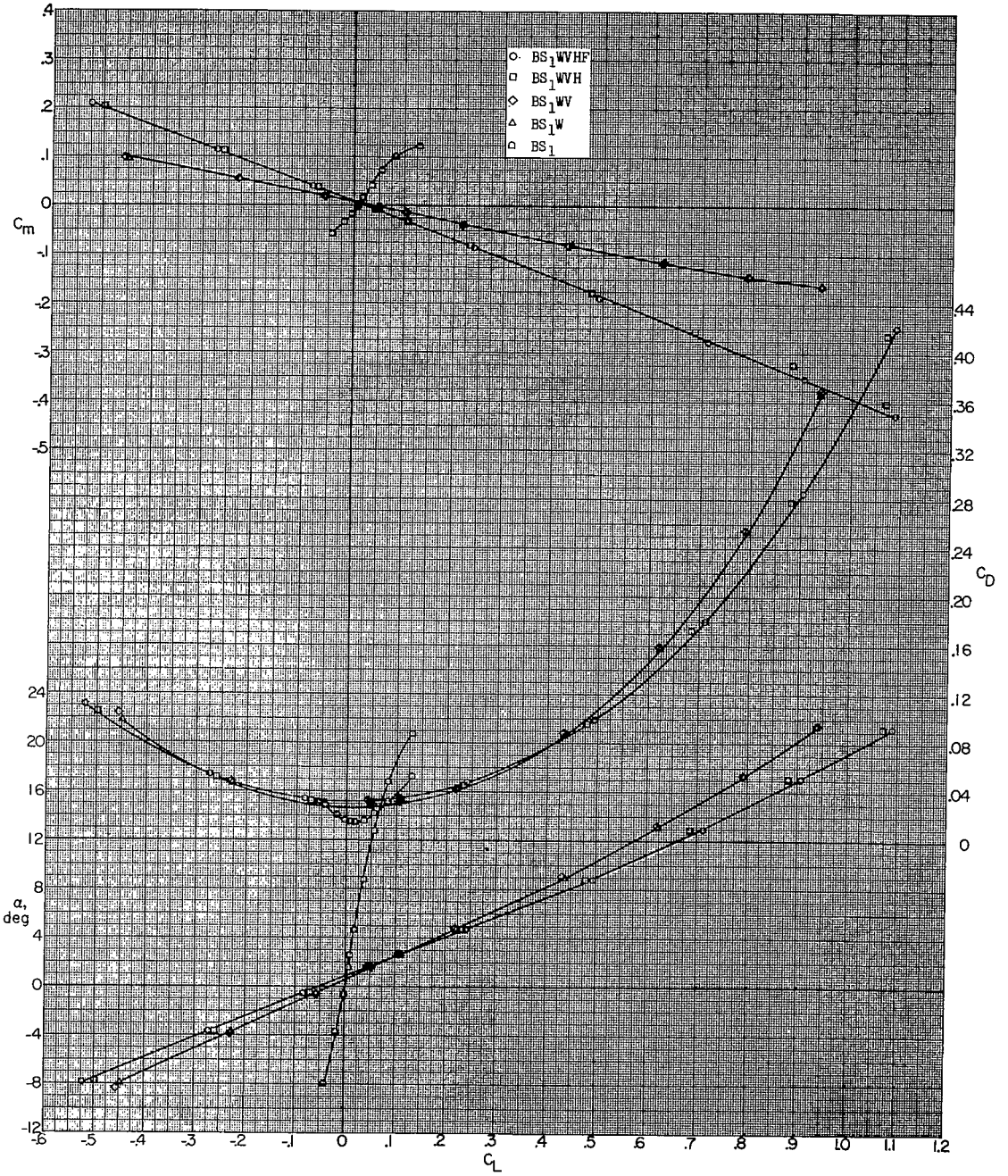

(b) M = 1.60; $\beta = 5.0^{\circ}$.

Figure 8.- Continued.

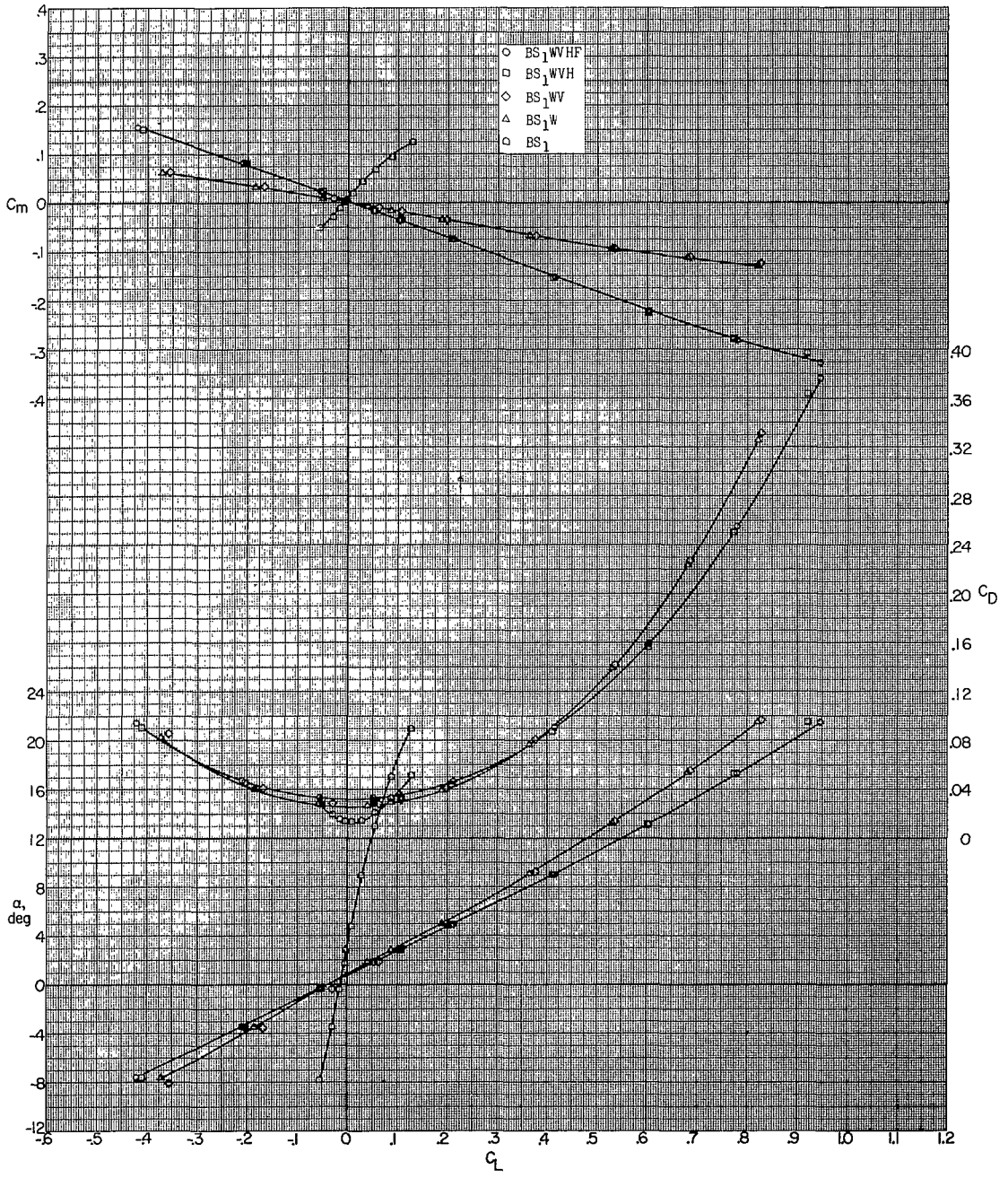

(c) M = 1.90; $\beta = 0^{\circ}$.

Figure 8.- Continued.

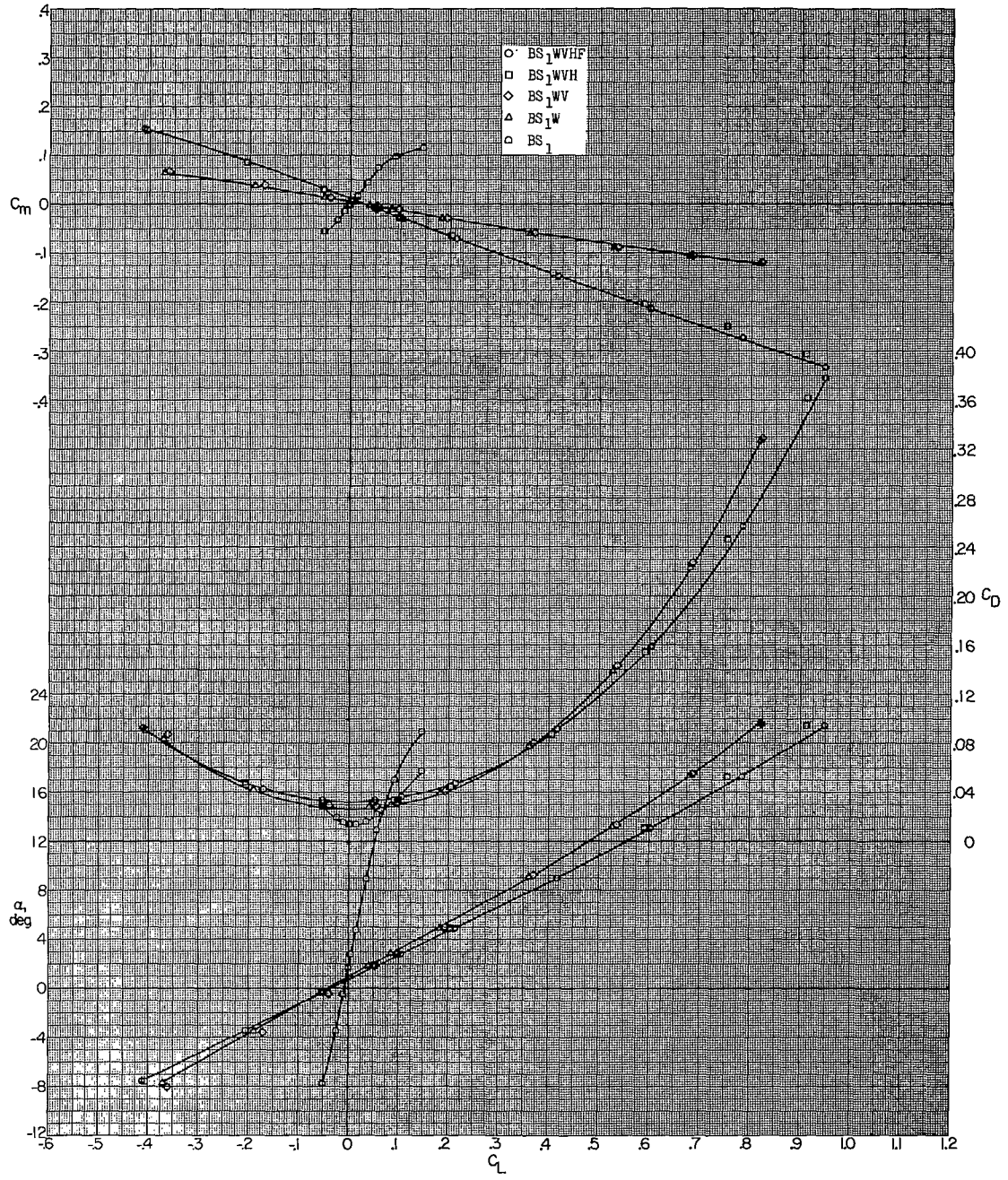

(d) M = 1.90; β = 5.0°.

Figure 8.- Continued.

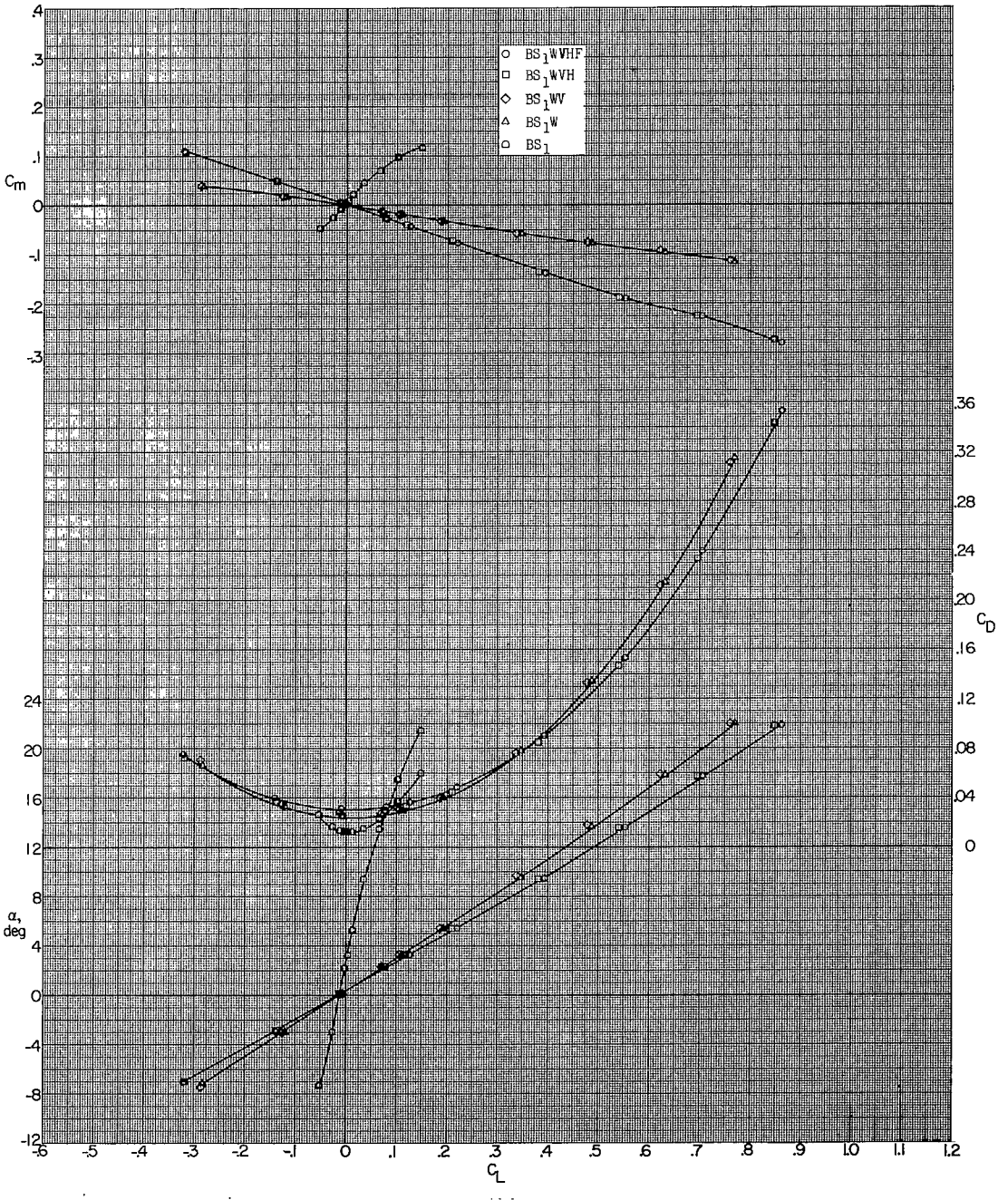

(e) M = 2.20; β = 0°.

Figure 8.- Continued.

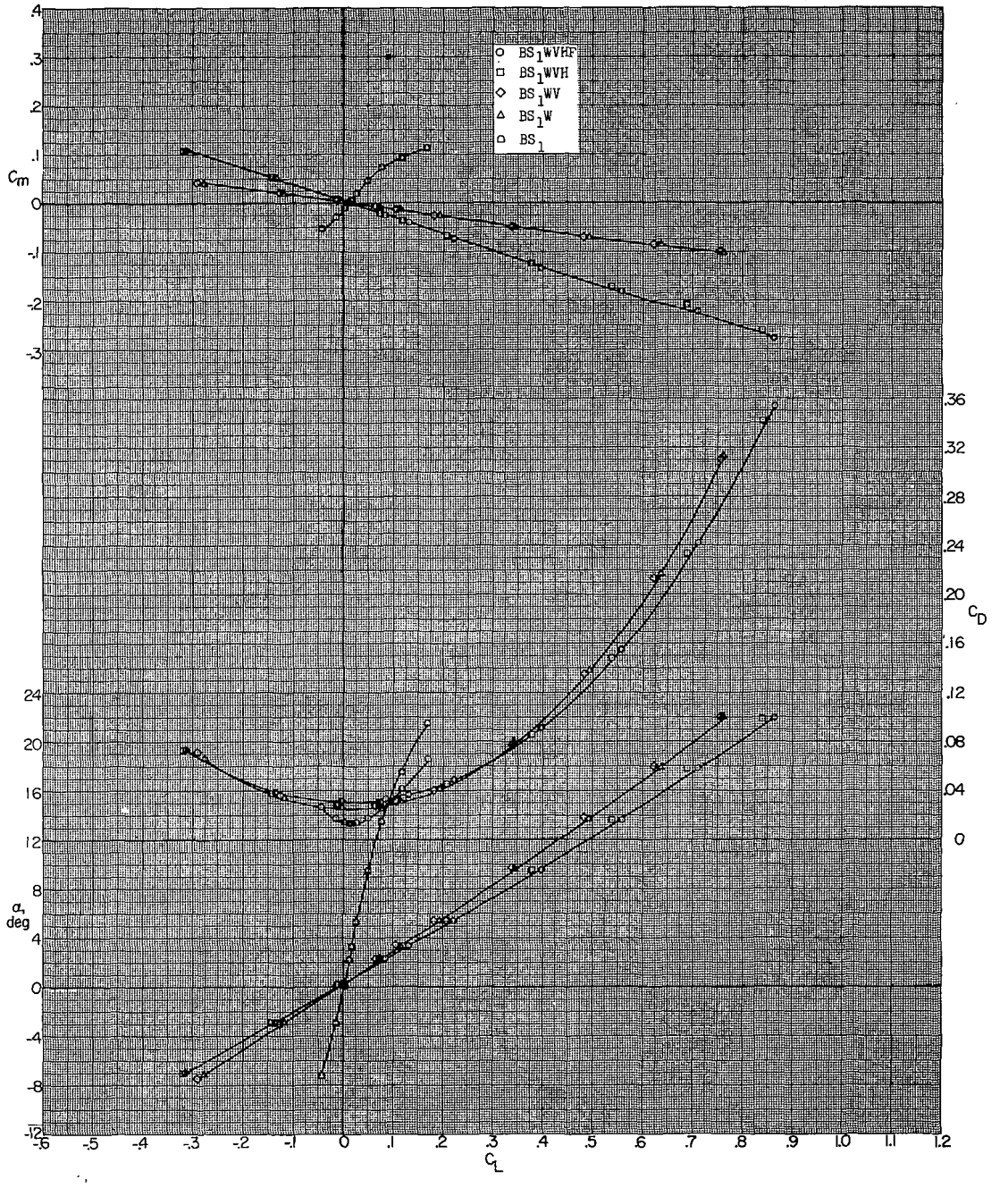

(f) M = 2.20; $\beta = 5.0^{\circ}$.

Figure 8.- Continued.

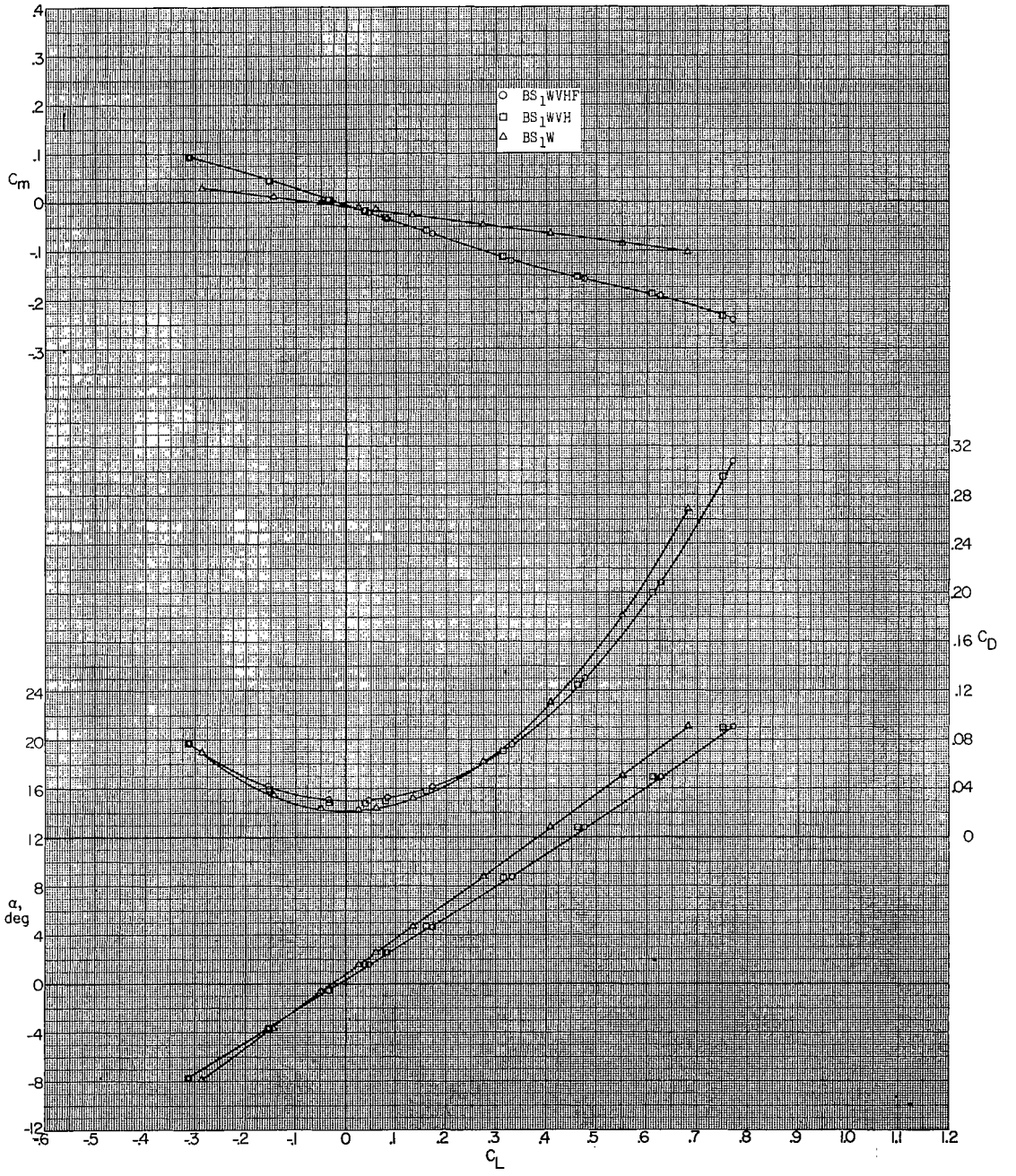

(g) M = 2.50; $\beta = 0^{\circ}$.

Figure 8.- Continued.

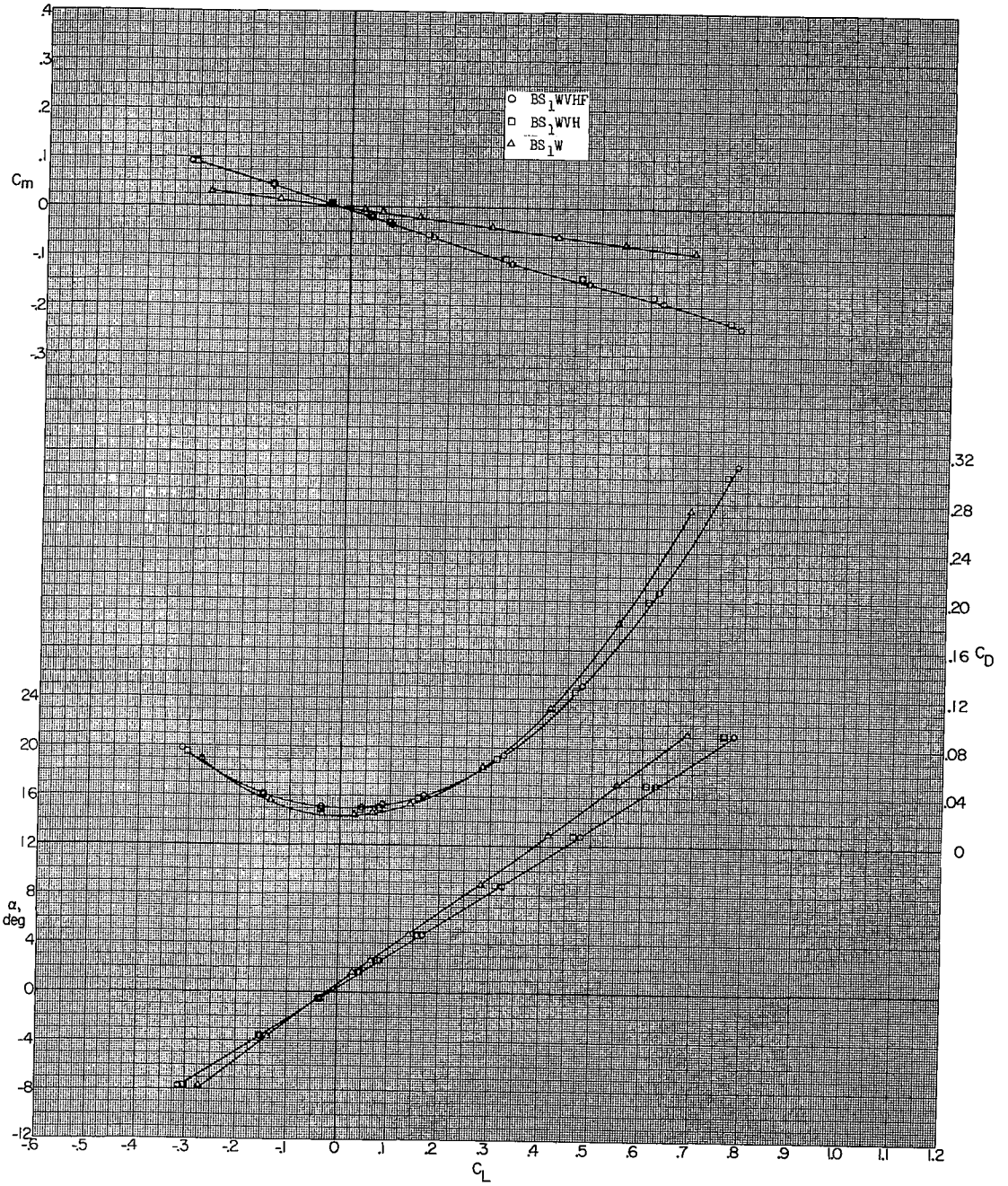

(h) M = 2.50; $\beta = 5.0^{\circ}$.

Figure 8.- Concluded.

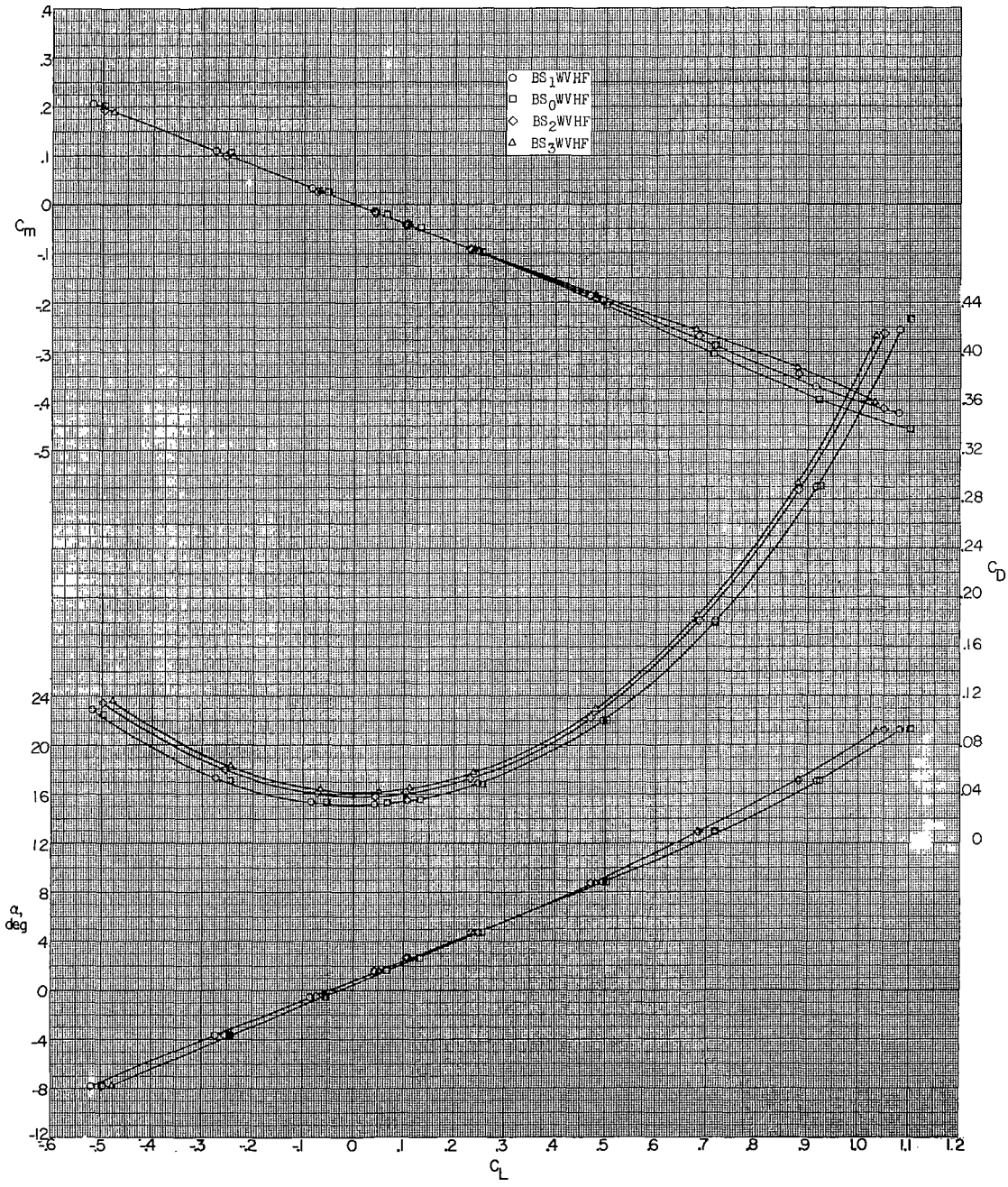

(a) M = 1.60; β = 0°.

Figure 9.- Effect of missiles on aerodynamic characteristics in pitch.

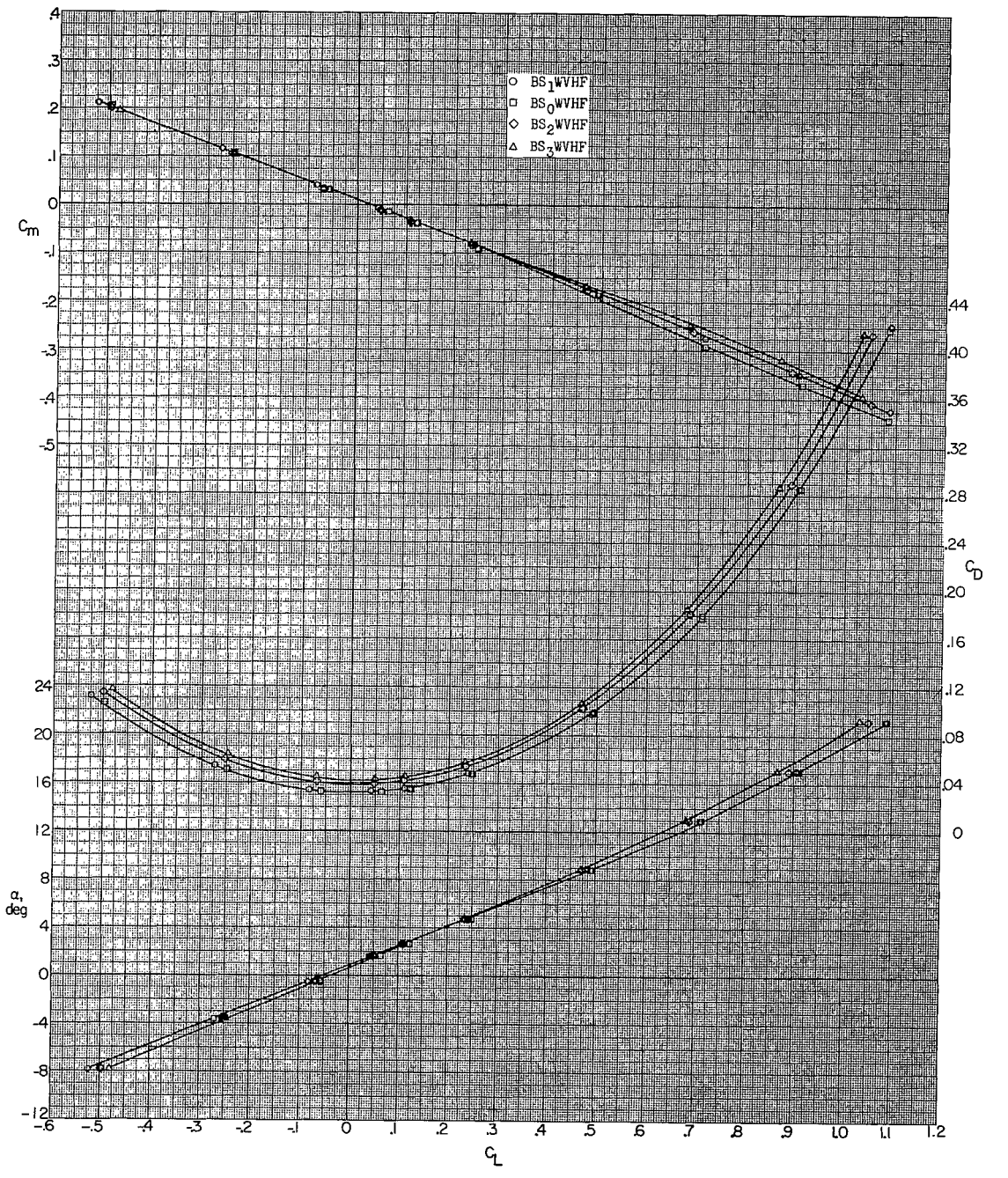

(b) M = 1.60; β = 5.0°.

Figure 9.- Continued.

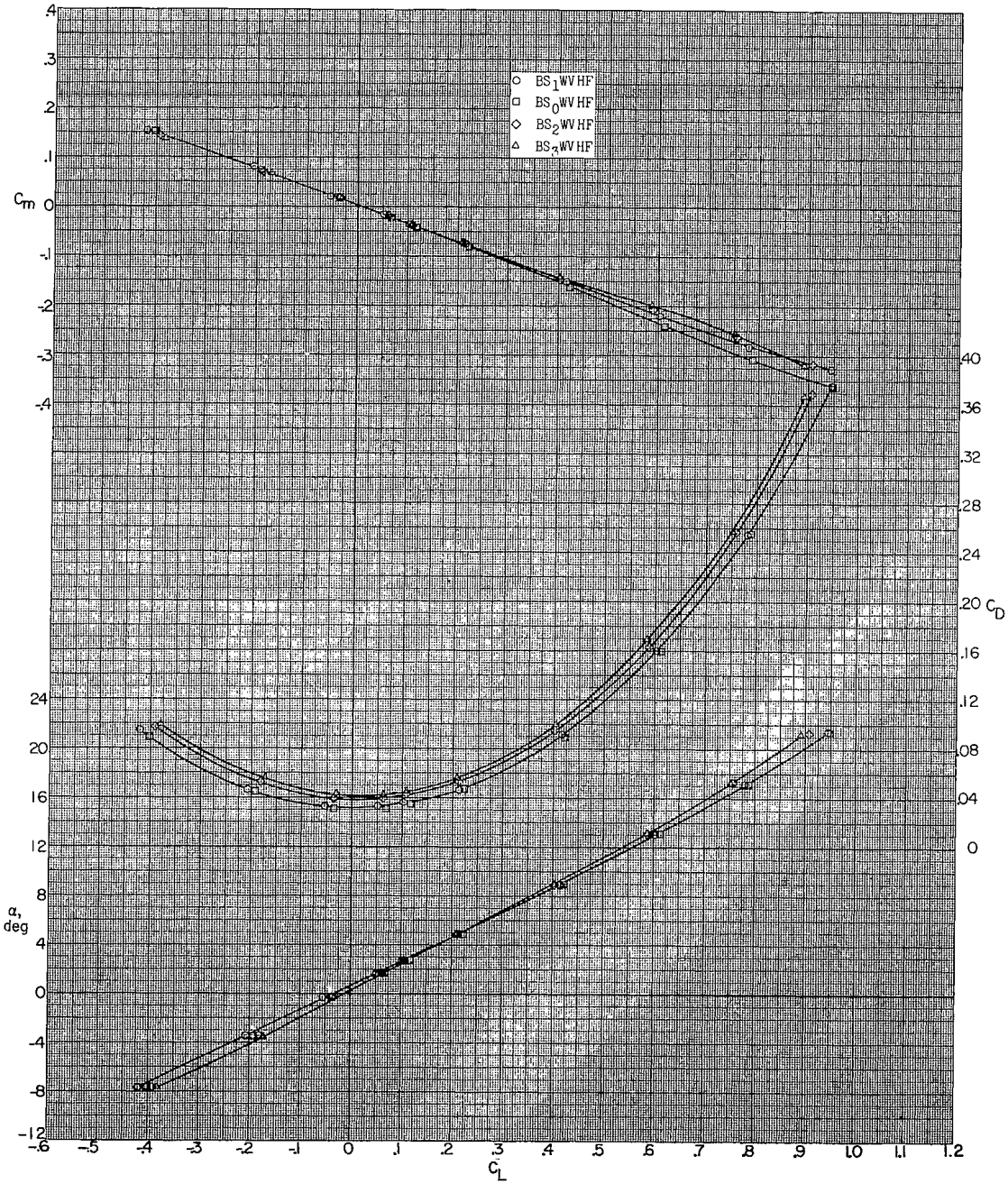

(c) M = 1.90; $\beta = 0^{\circ}$.

Figure 9.- Continued.

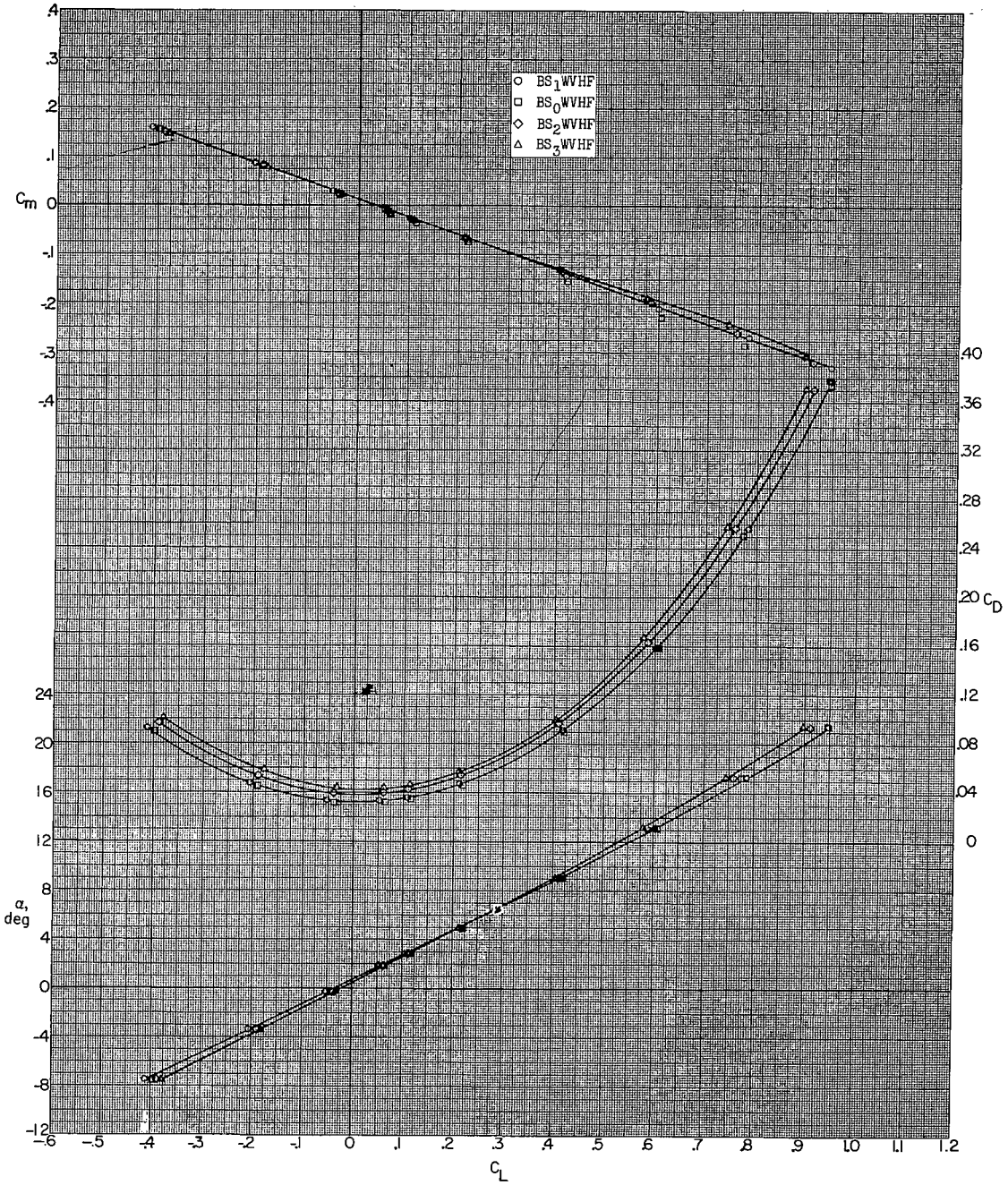

(d) M = 1.90; $\beta = 5.0^{\circ}$.

Figure 9.- Continued.

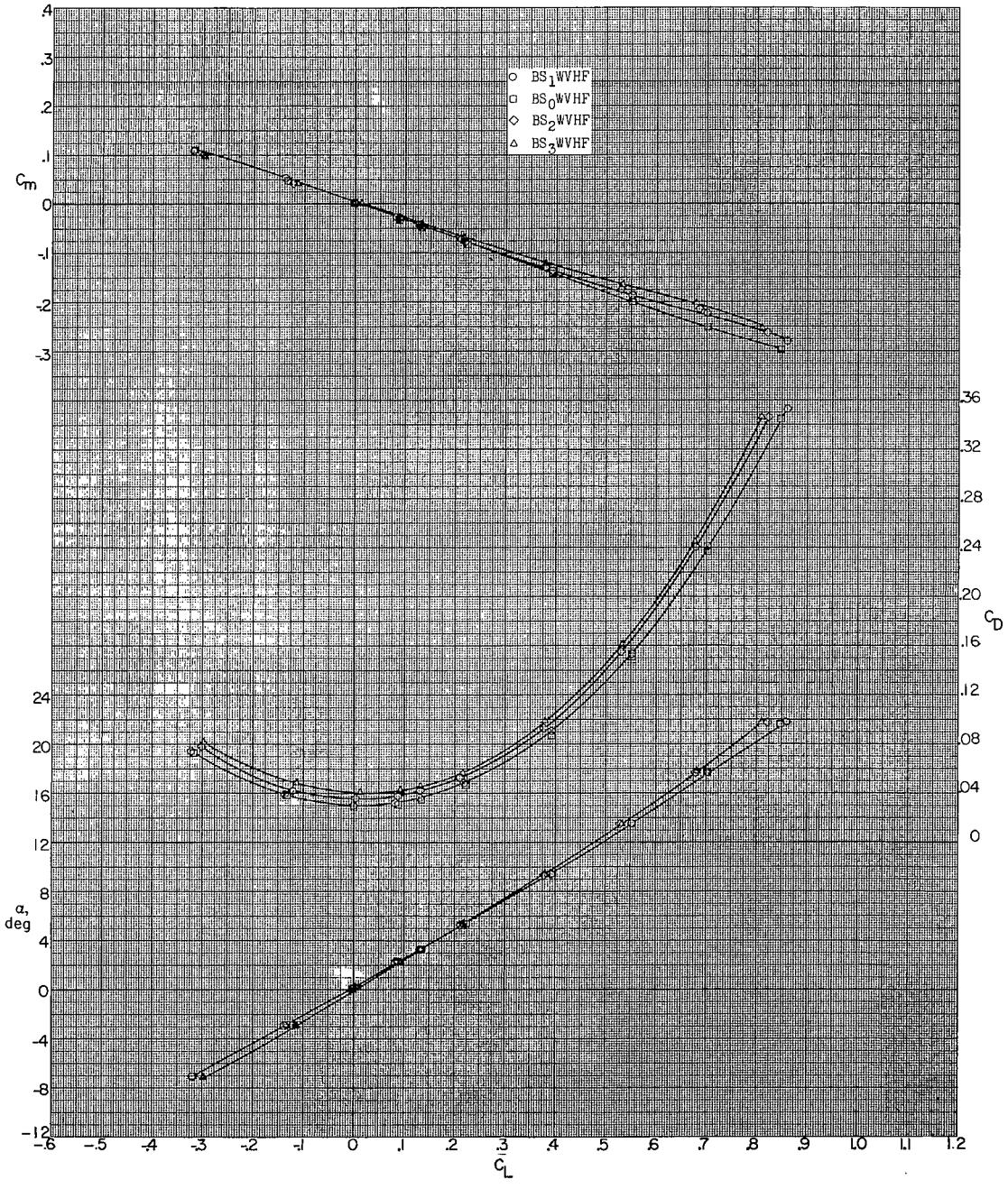

(e) M = 2.20; β = 0°.

Figure 9.- Continued.

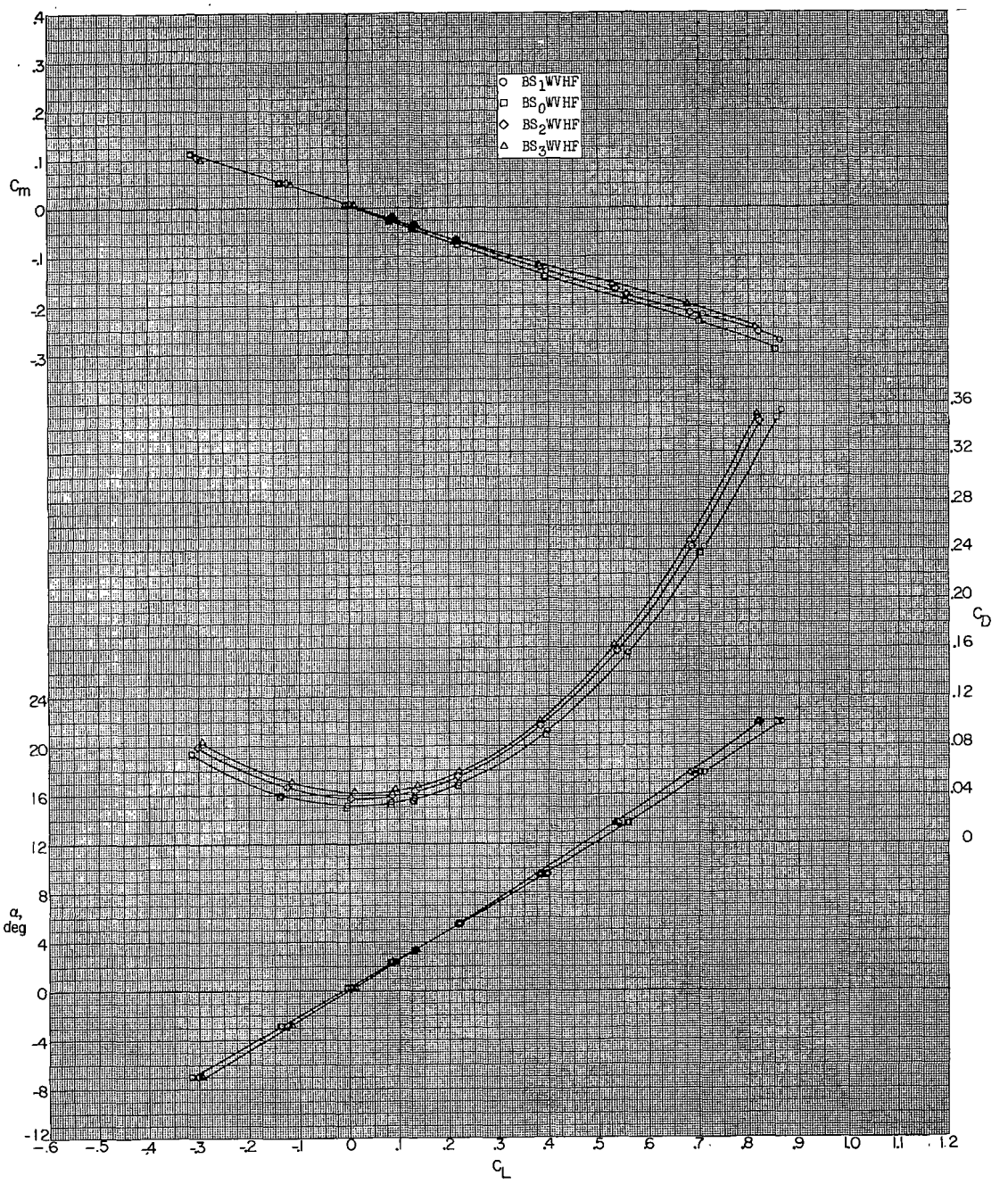

(f) M = 2.20; $\beta = 5.0^{\circ}$.

Figure 9.- Concluded.

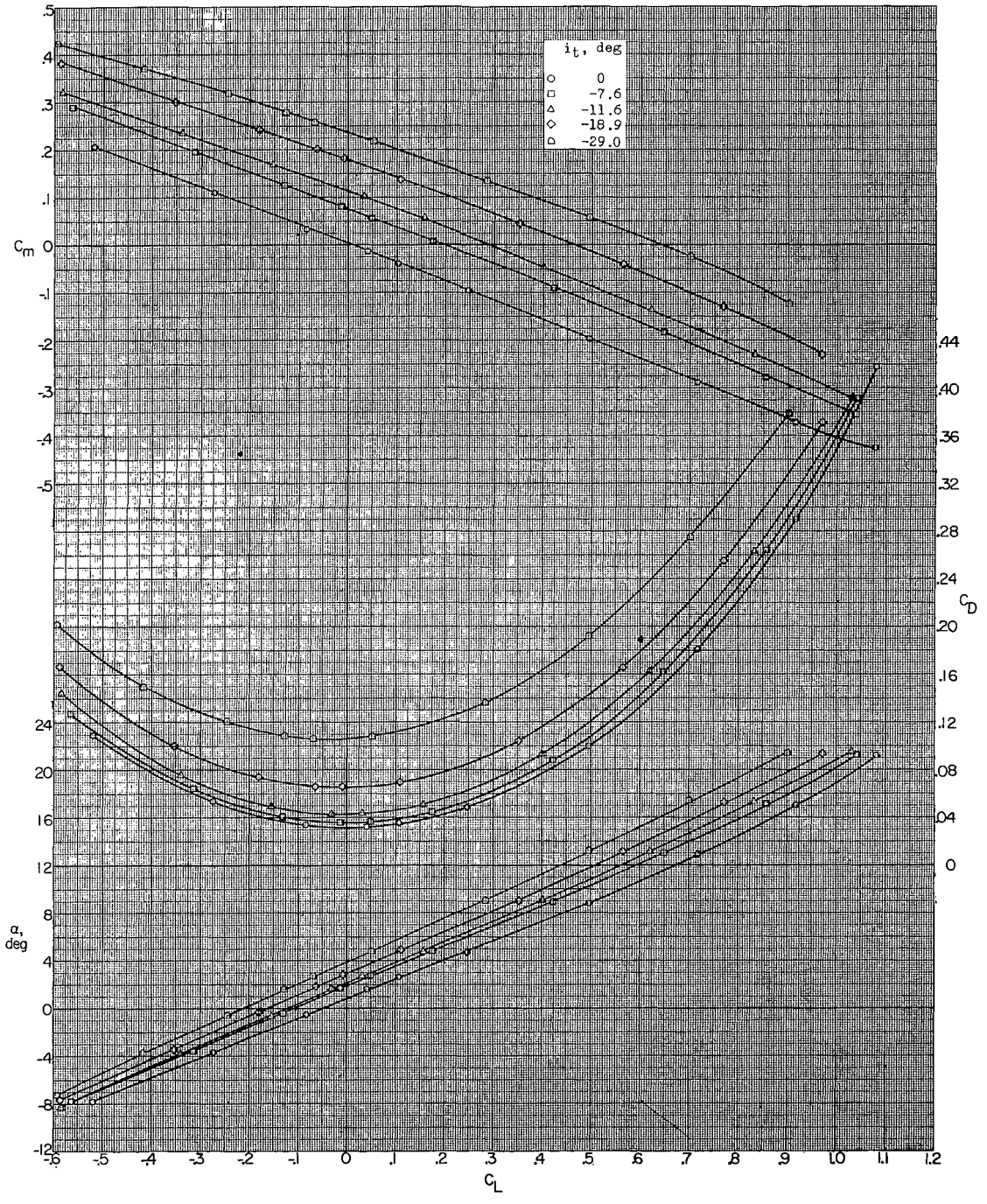

(a) M = 1.60.

Figure 10.- Effect of horizontal stabilizer incidence on aerodynamic characteristics in pitch. BS_1WVHF; $\beta = 0^o$.

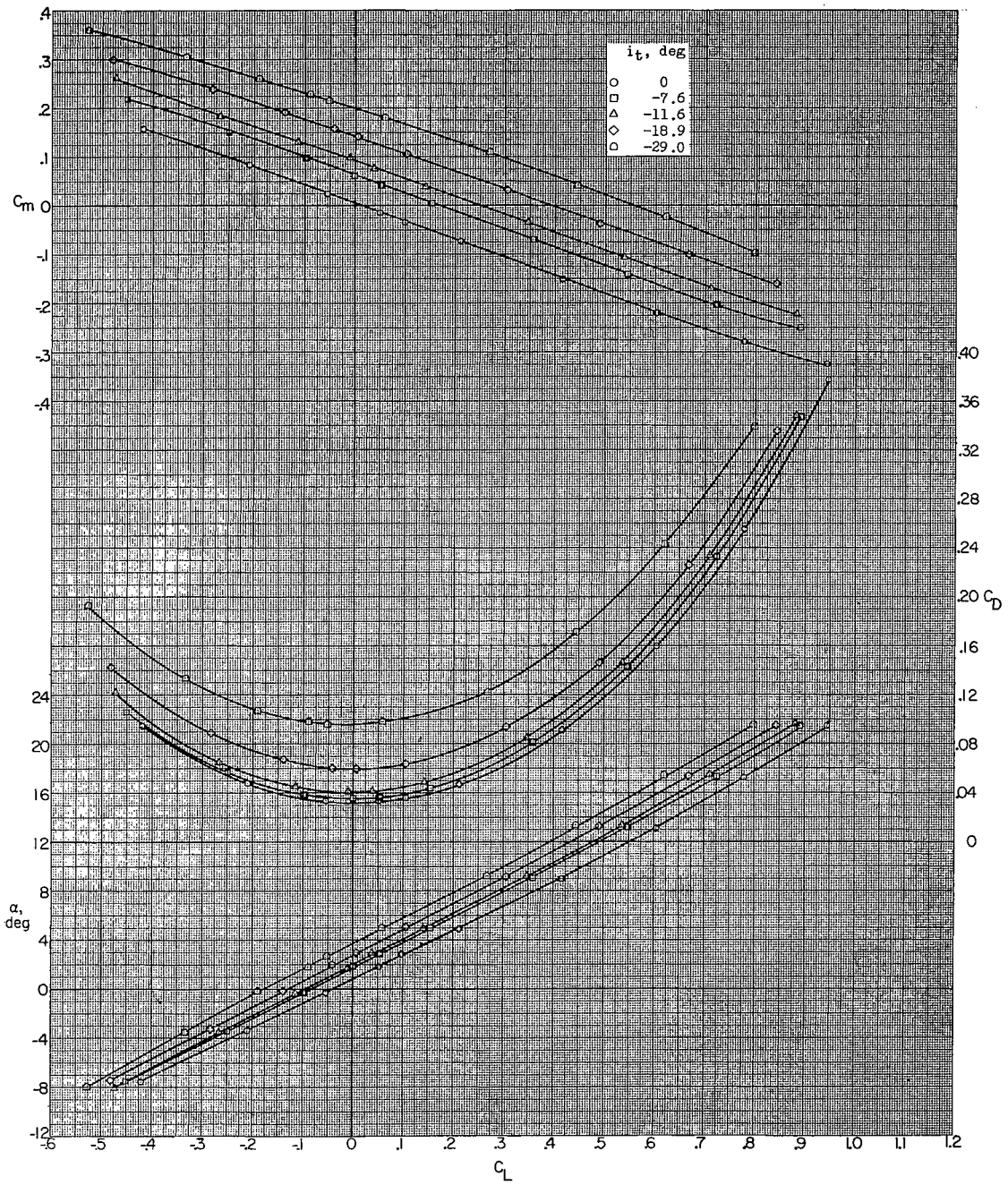

(b) M = 1.90.

Figure 10.- Continued.

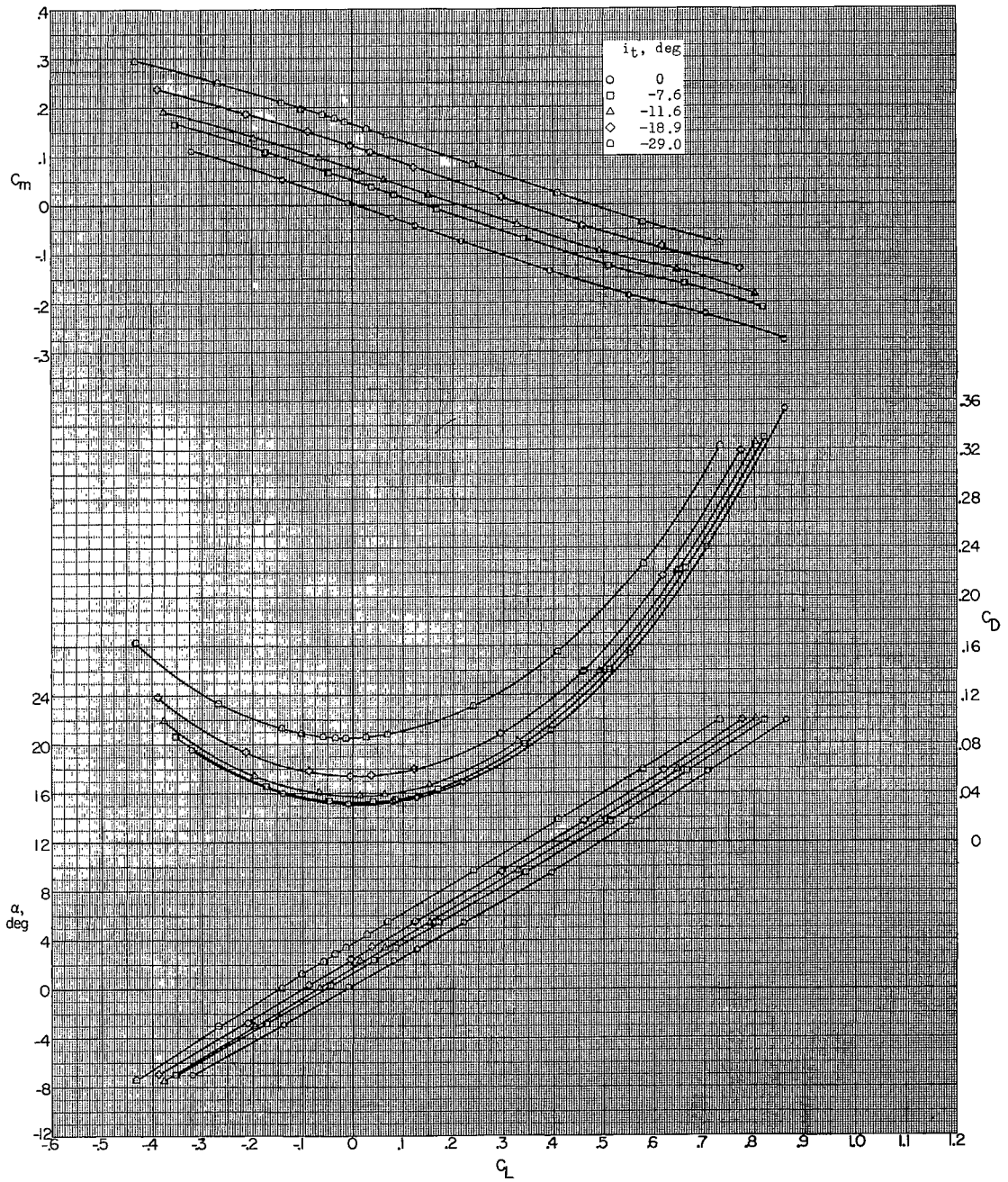

(c) M = 2.20.

Figure 10.- Continued.

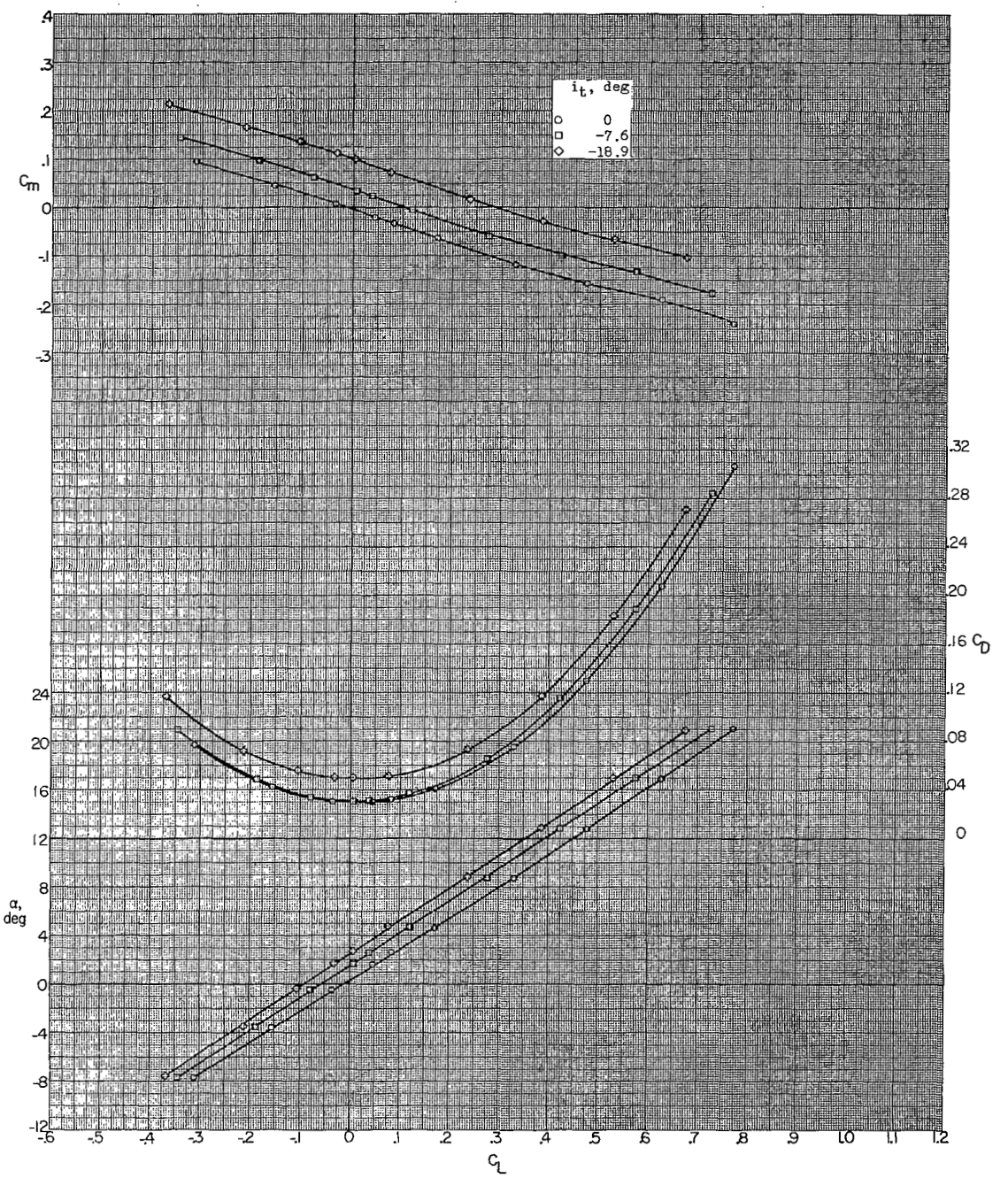

(d) M = 2.50.

Figure 10.- Concluded.

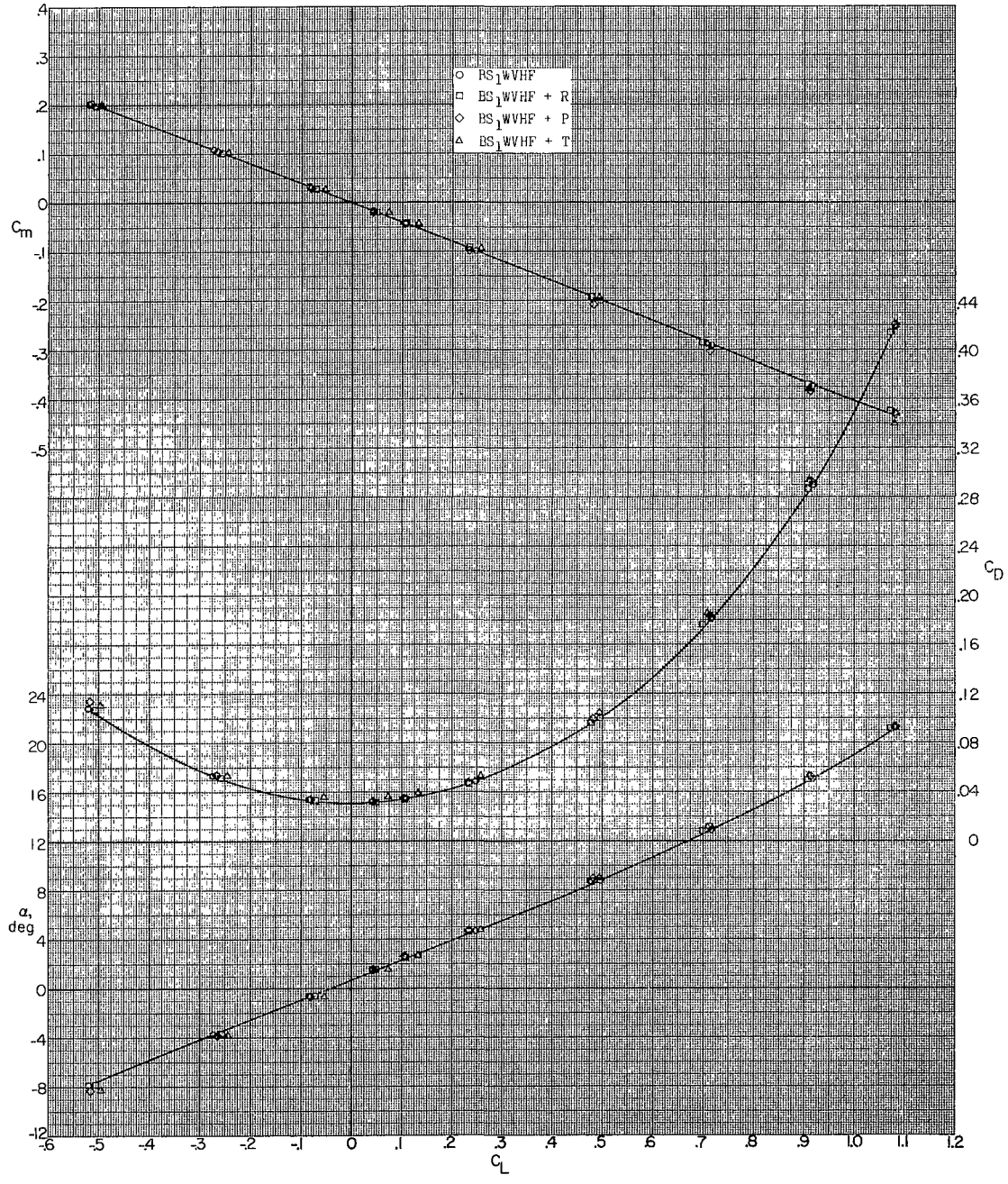

(a) M = 1.60; $\beta = 0^{\circ}$.

Figure 11.- Effect of some of the model modifications on aerodynamic characteristics in pitch.

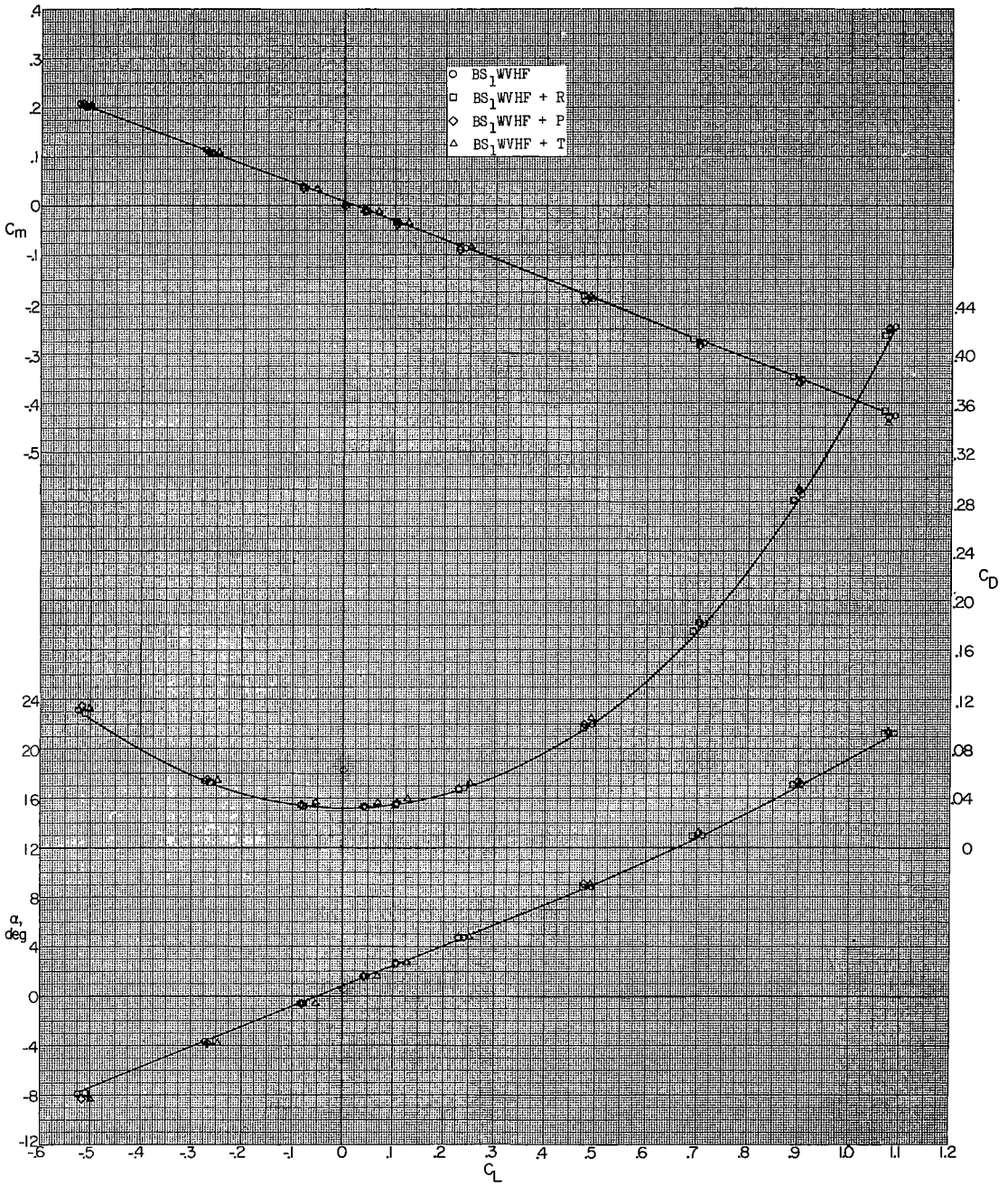

(b) M = 1.60; β = 5.0°.

Figure 11.- Continued.

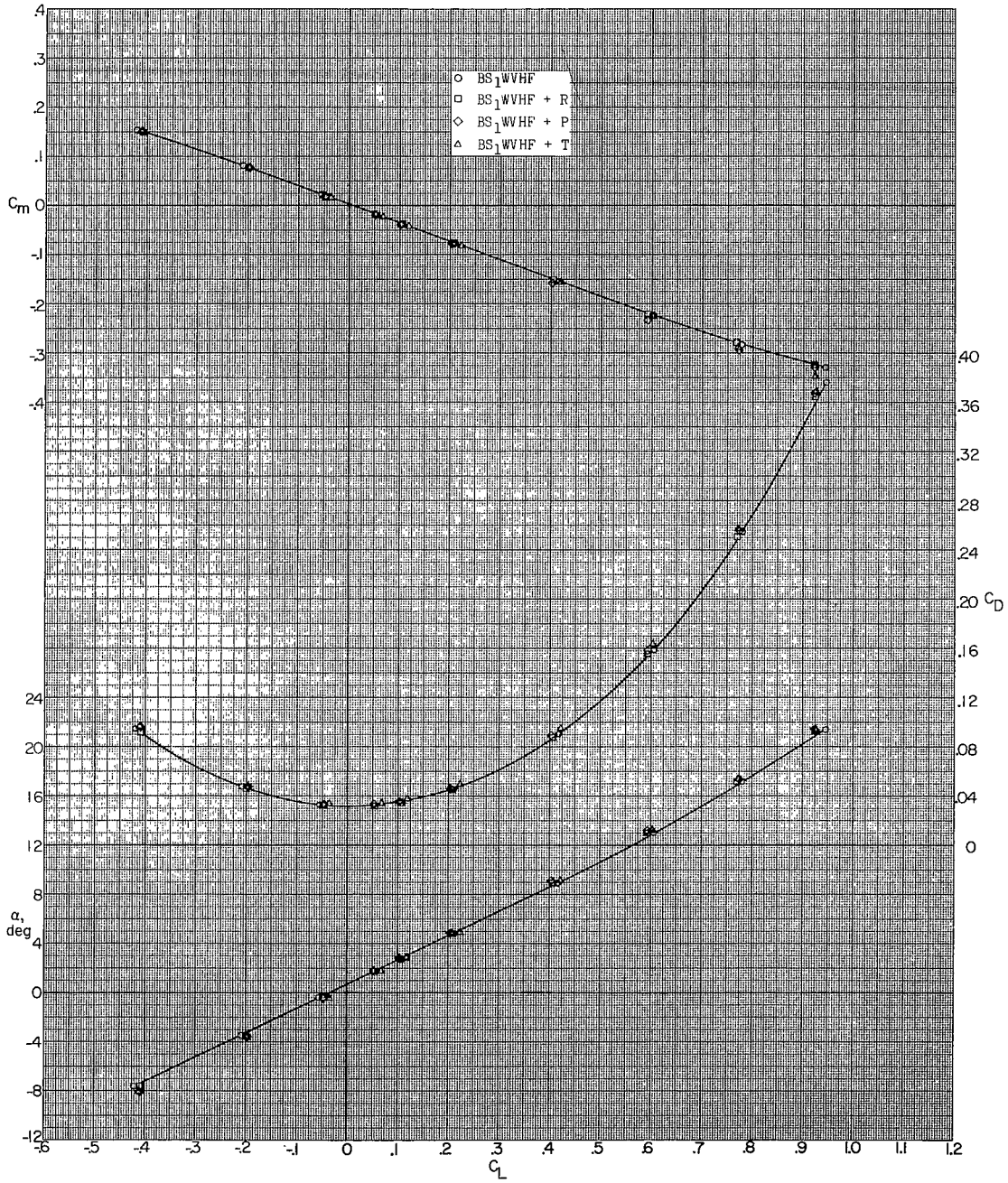

(c) M = 1.90; $\beta = 0^{\circ}$.

Figure 11.- Continued.

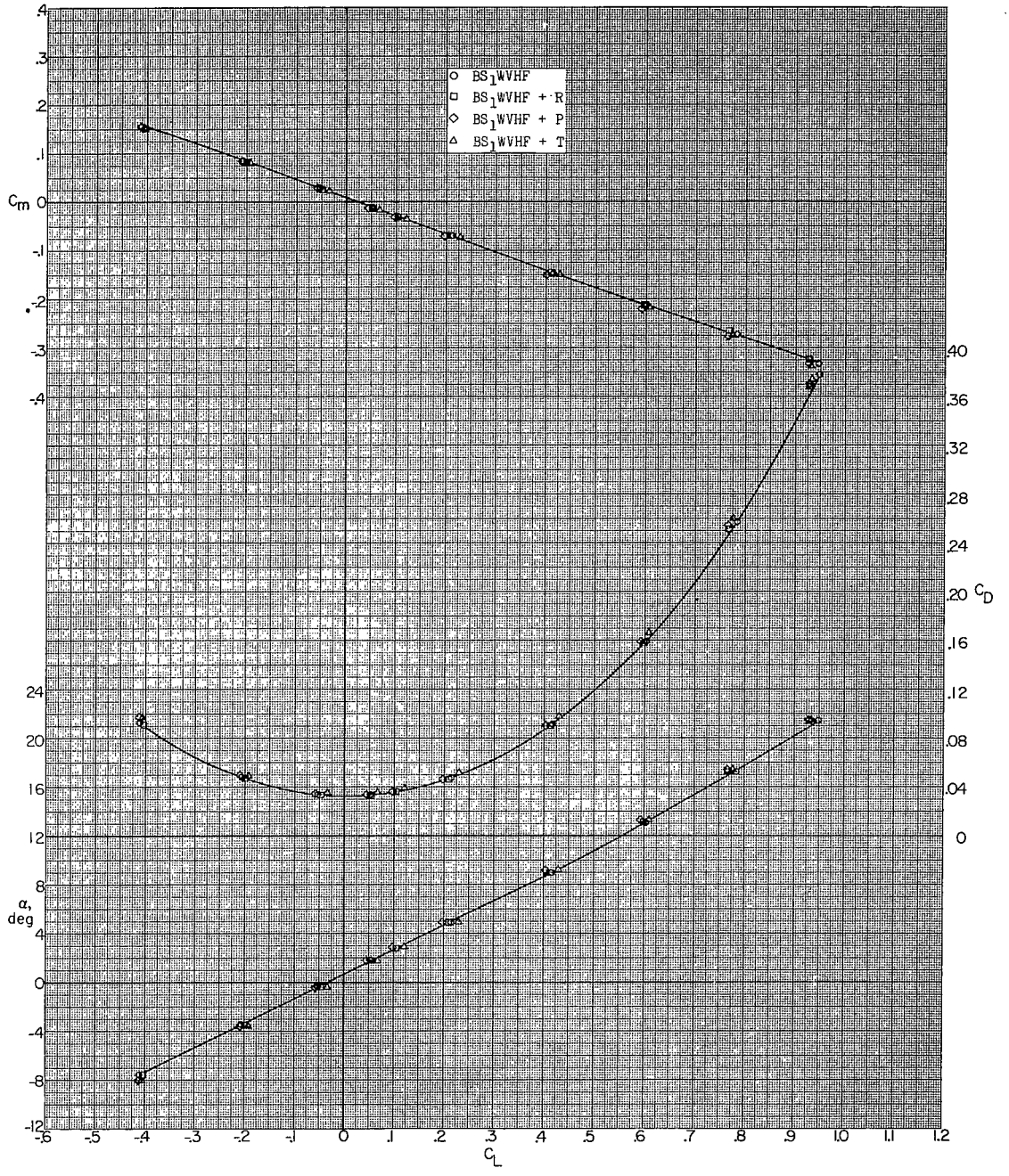

(d) M = 1.90; β = 5.0°.

Figure 11.- Continued.

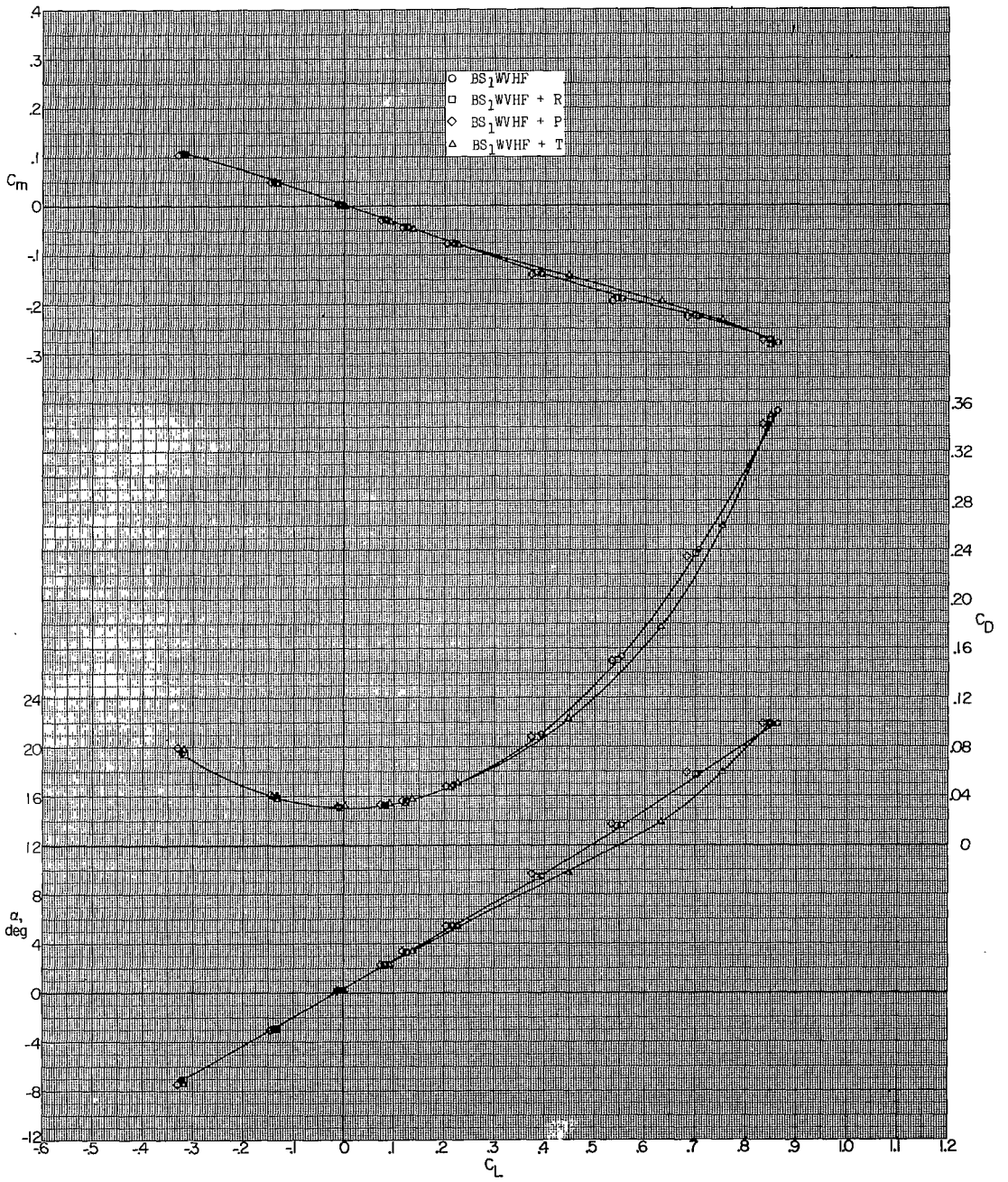

(e) M = 2.20; $\beta = 0^{\circ}$.

Figure 11.- Continued.

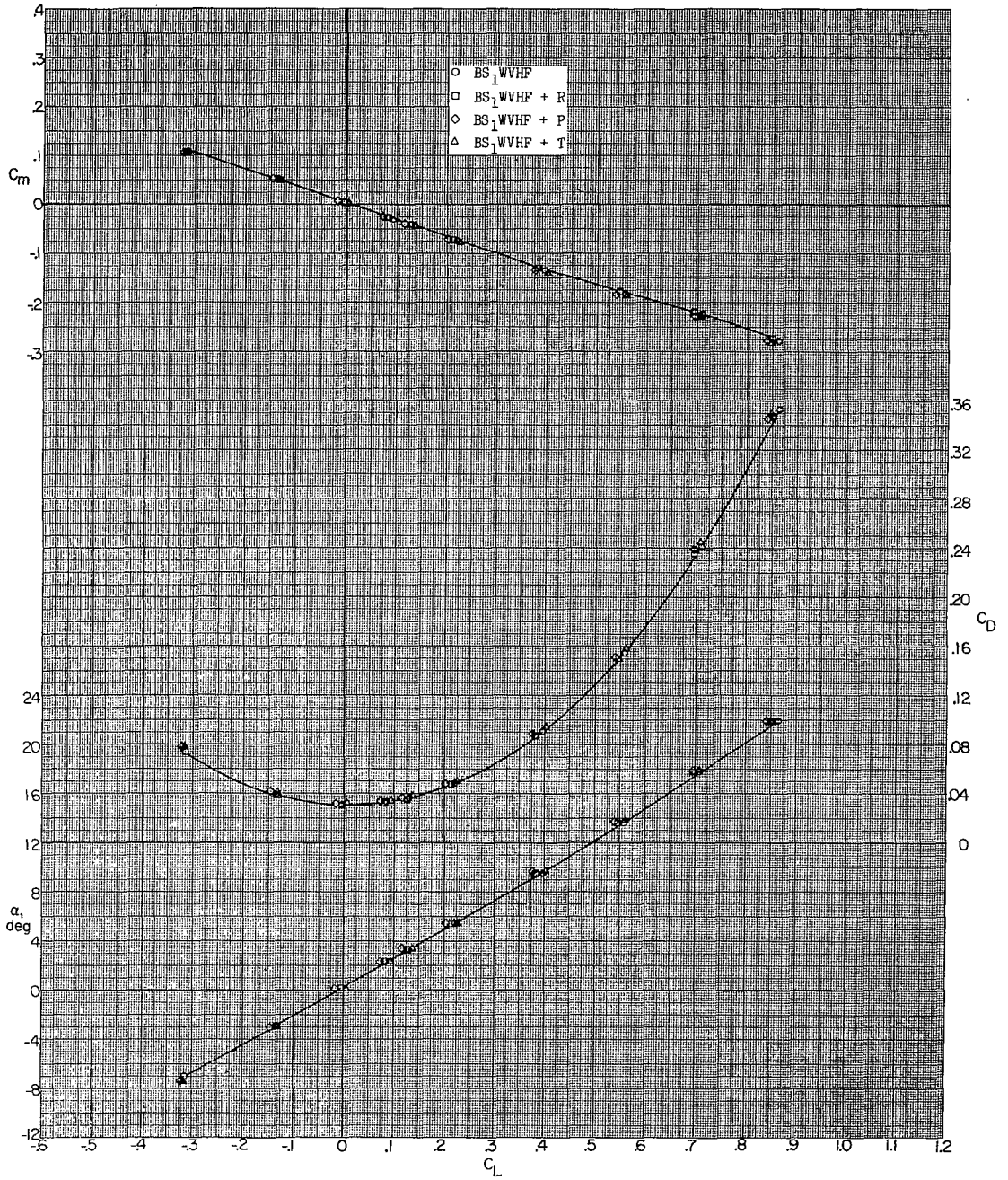

(f) M = 2.20; β = 5.0°.

Figure 11.- Continued.

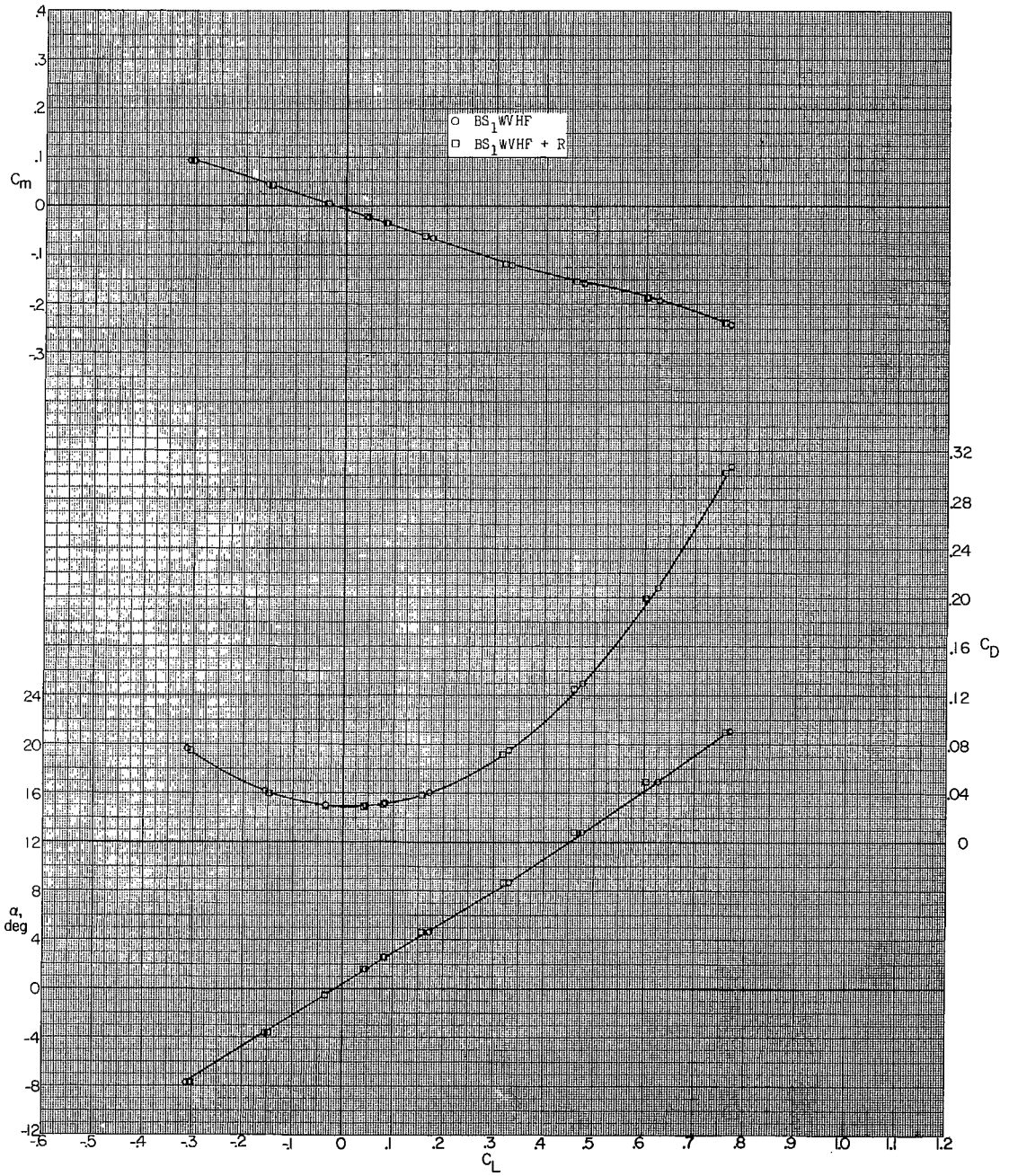

(g) M = 2.50; $\beta = 0^{\circ}$.

Figure 11.- Continued.

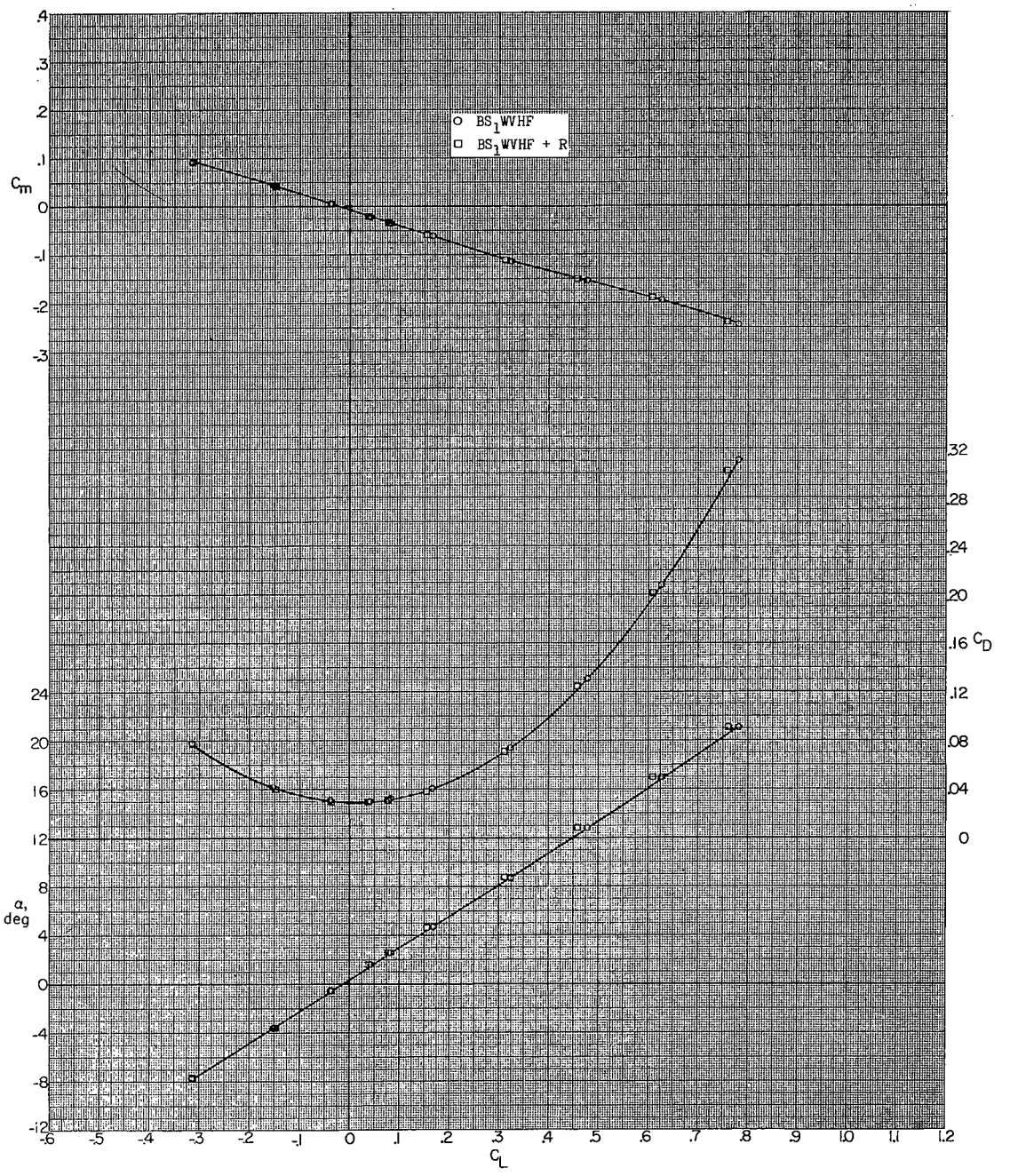

(h) M = 2.50; $\beta = 5.0^{\circ}$.

Figure 11.- Concluded.

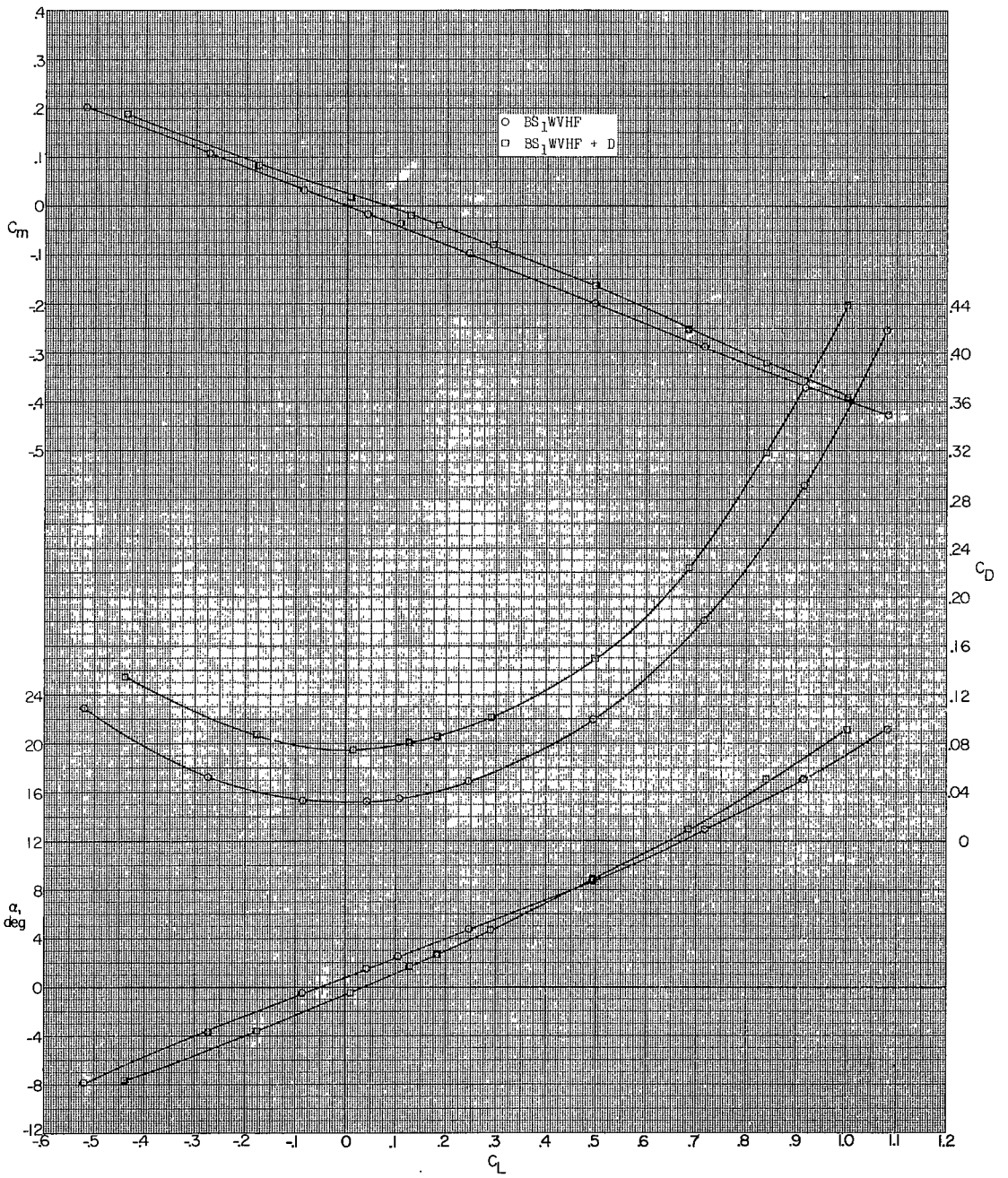

(a) M = 1.60; $\beta = 0^{\circ}$.

Figure 12.- Effect of speed brake on aerodynamic characteristics in pitch.

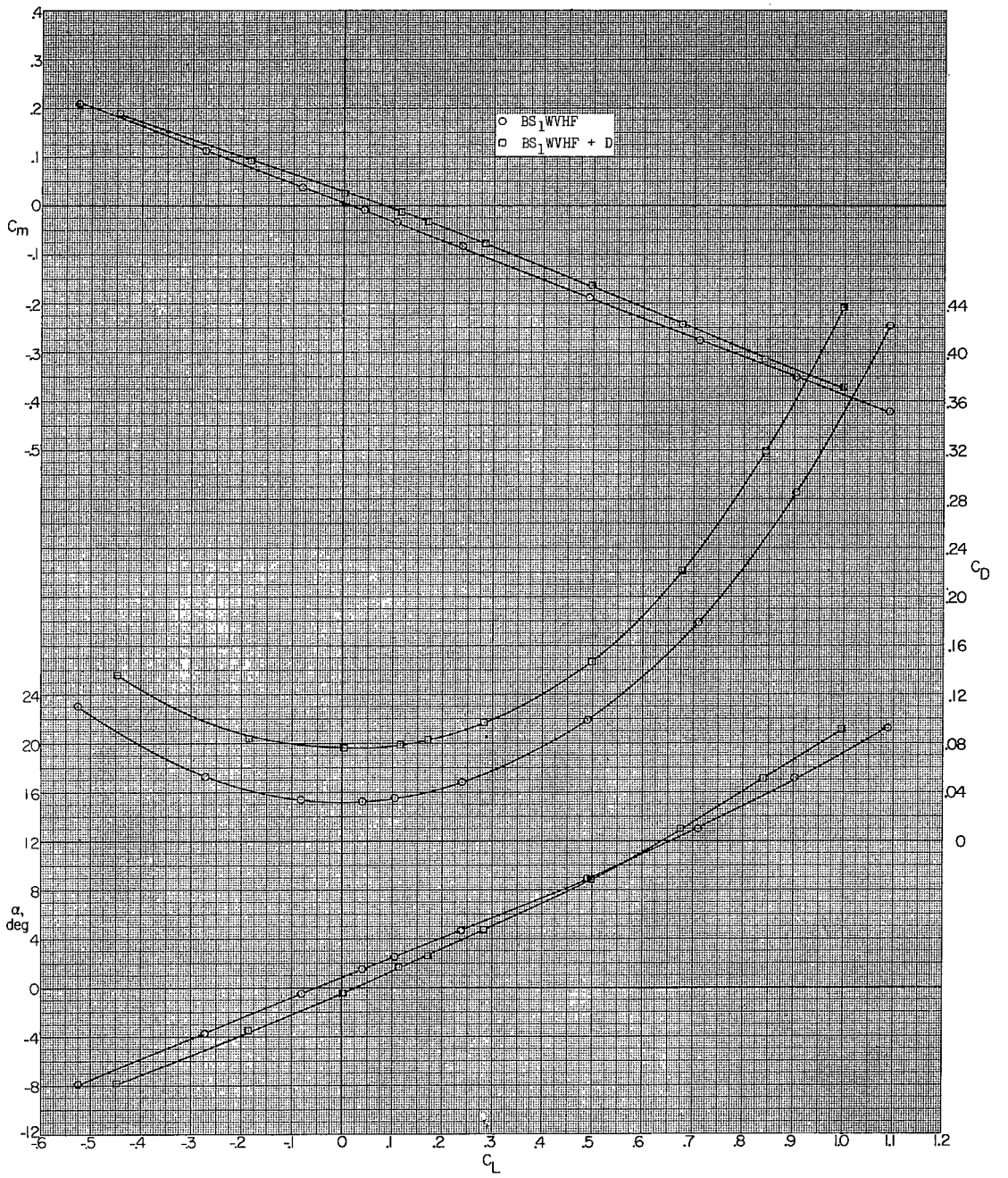

(b) M = 1.60; β = 5.0°.

Figure 12.- Continued.

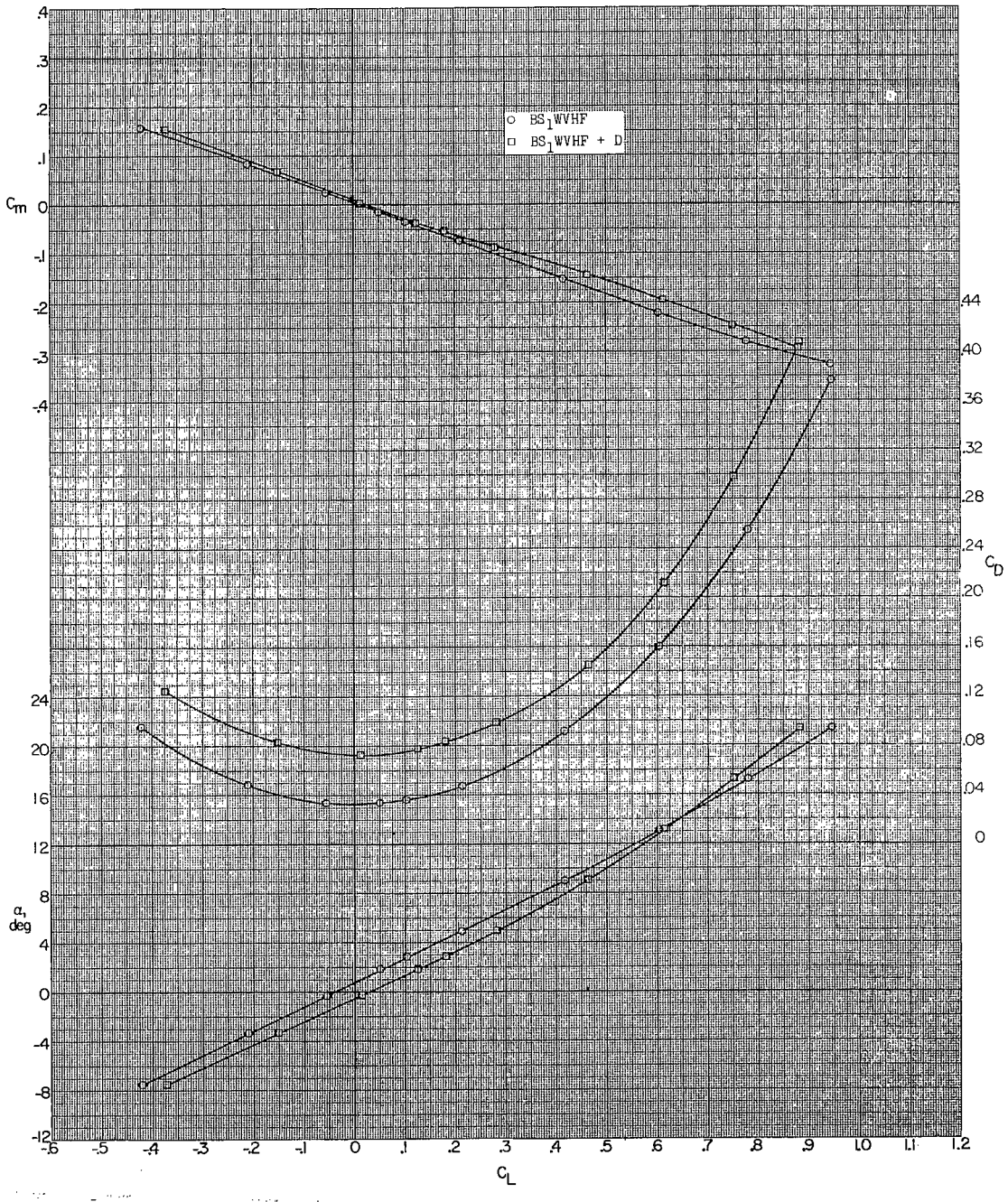

(c) M = 1.90; β = 0°.

Figure 12.- Continued.

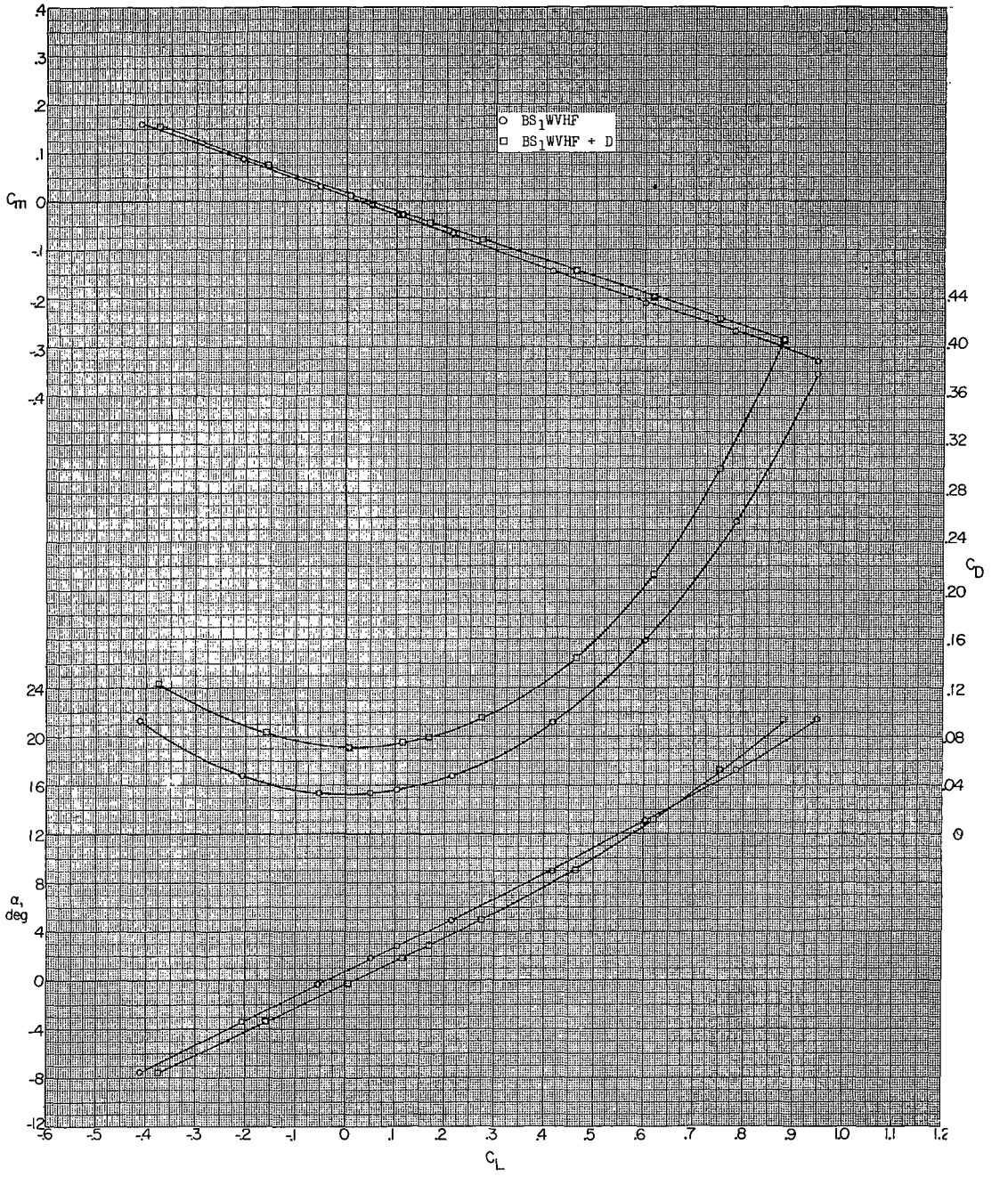

(d) M = 1.90; $\beta = 5.0^{\circ}$.

Figure 12.- Continued.

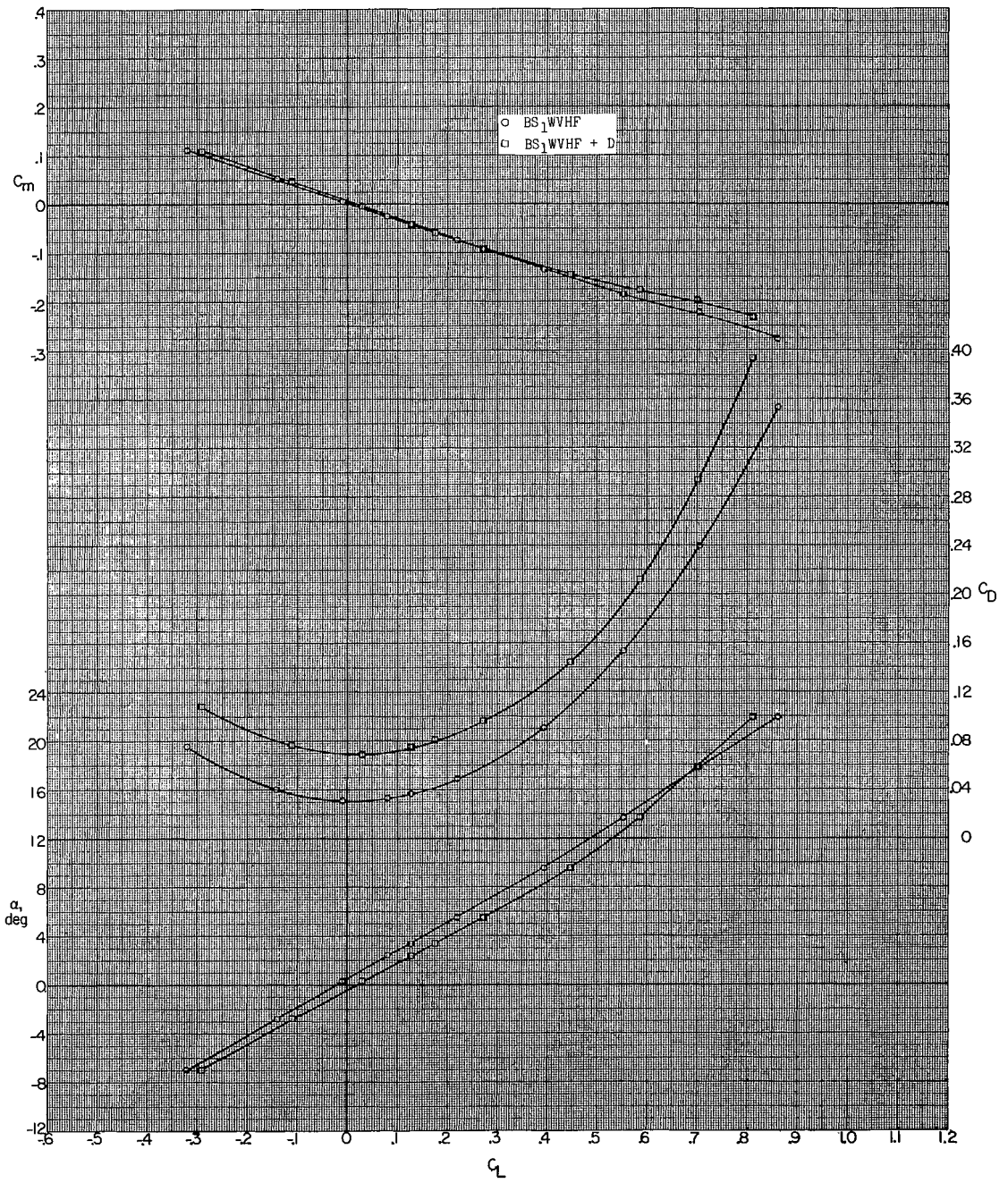

(e) M = 2.20; β = 0°.

Figure 12.- Continued.

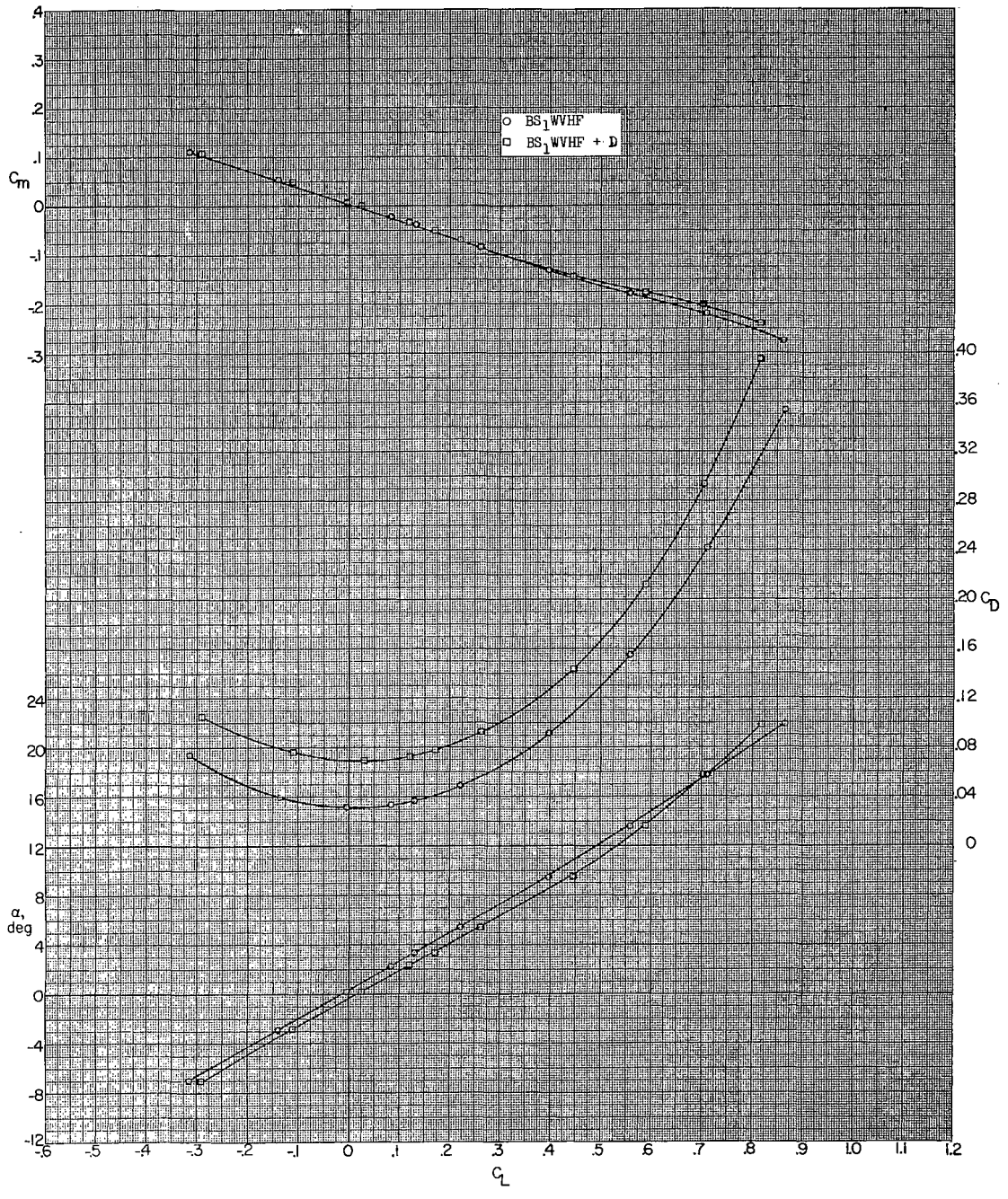

(f) M = 2.20; $\beta = 5.0^{\circ}$.

Figure 12.- Concluded.

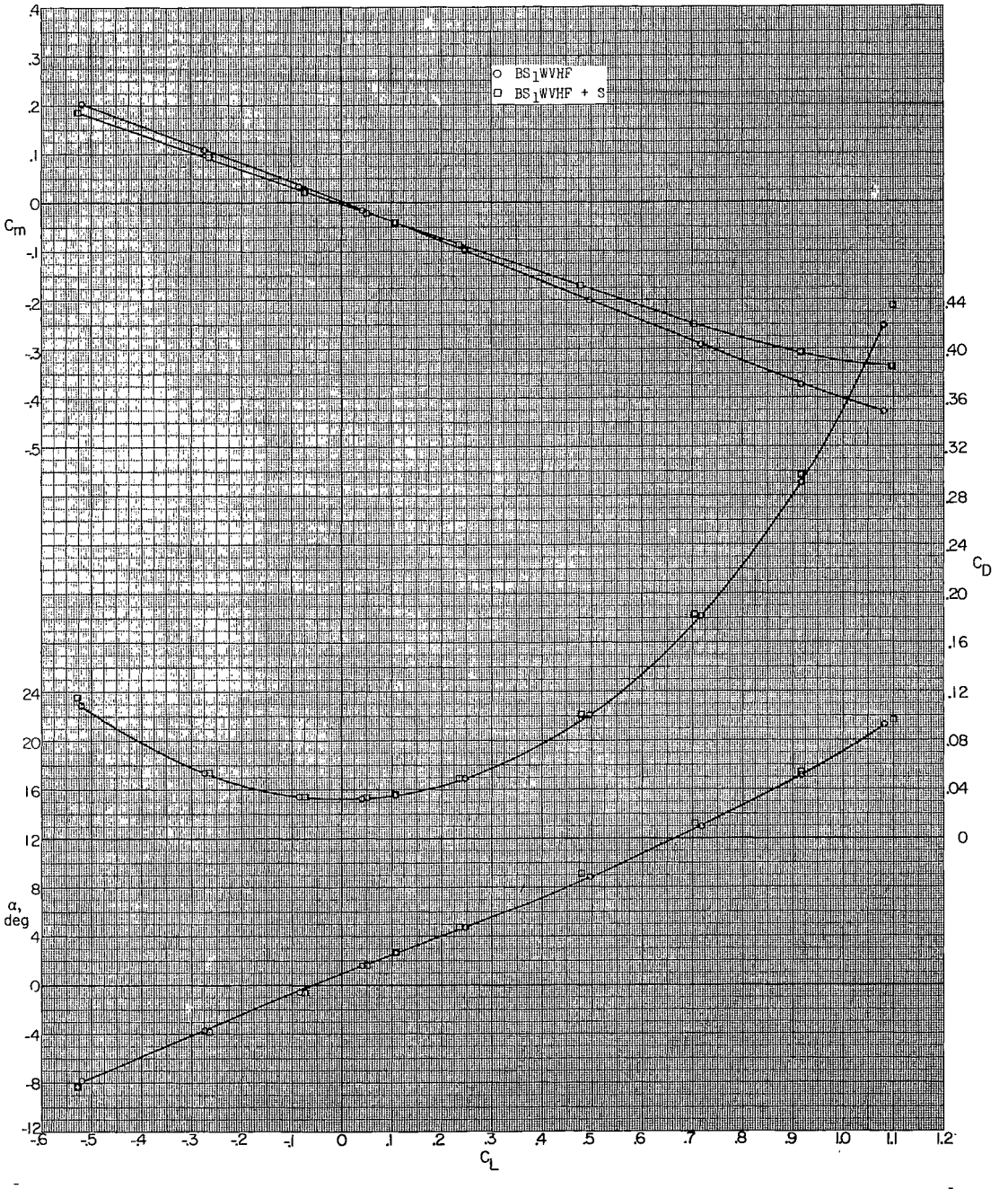

(a) M = 1.60.

Figure 13.- Effect of strakes on aerodynamic characteristics in pitch. $\beta = 0^{\circ}$.

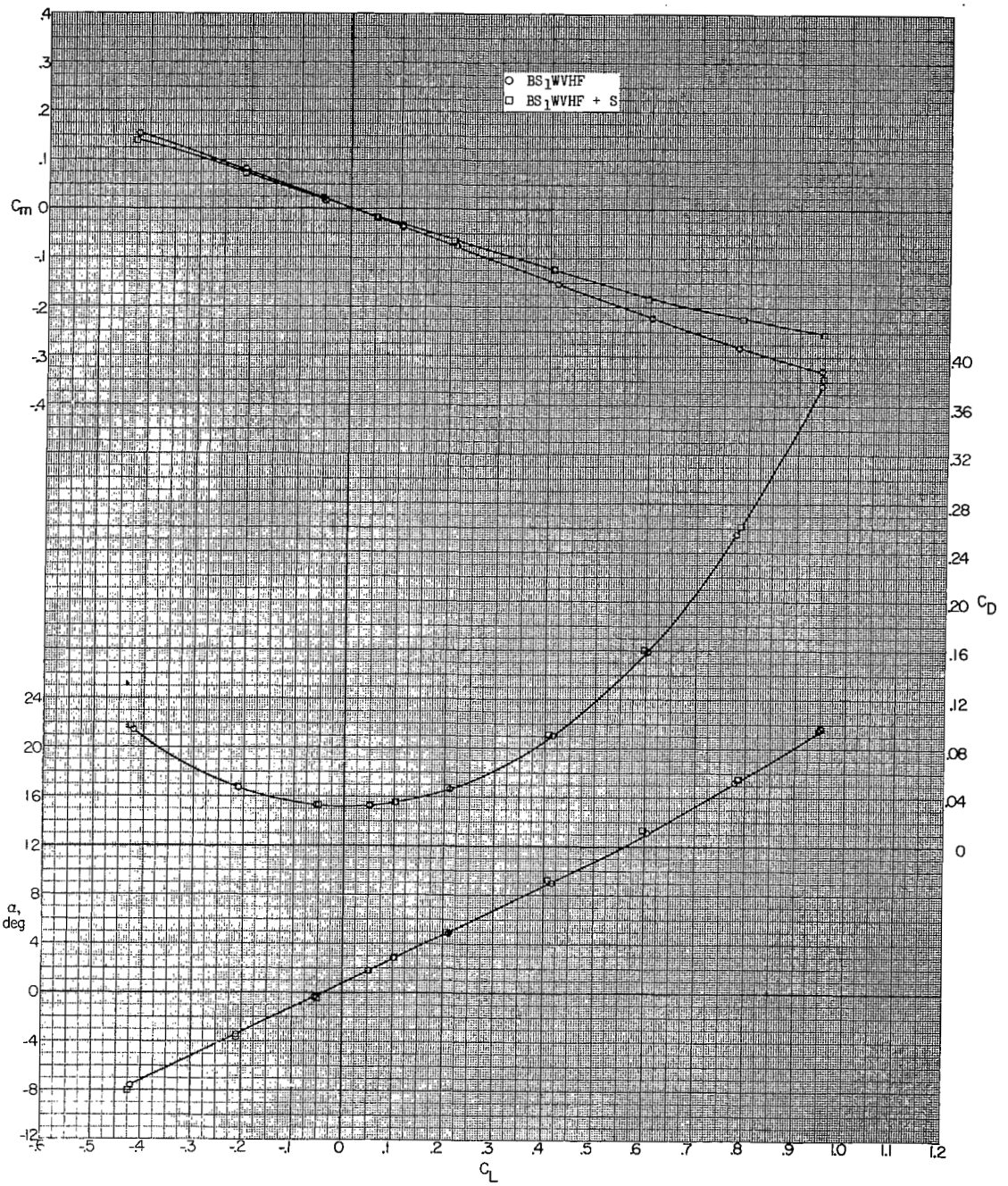

(b) M = 1.90.

Figure 13.- Continued.

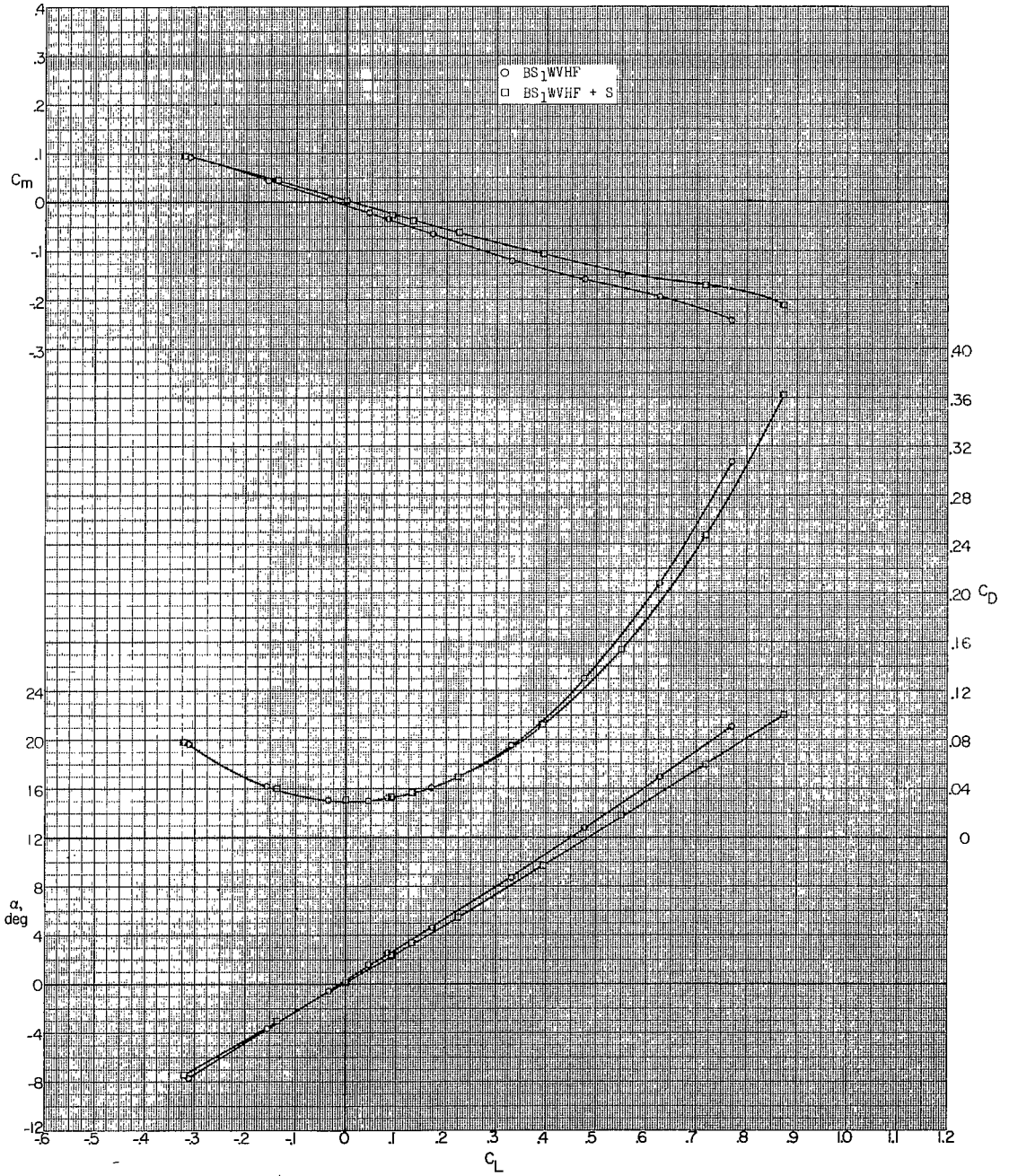

(c) M = 2.20.

Figure 13.- Concluded.

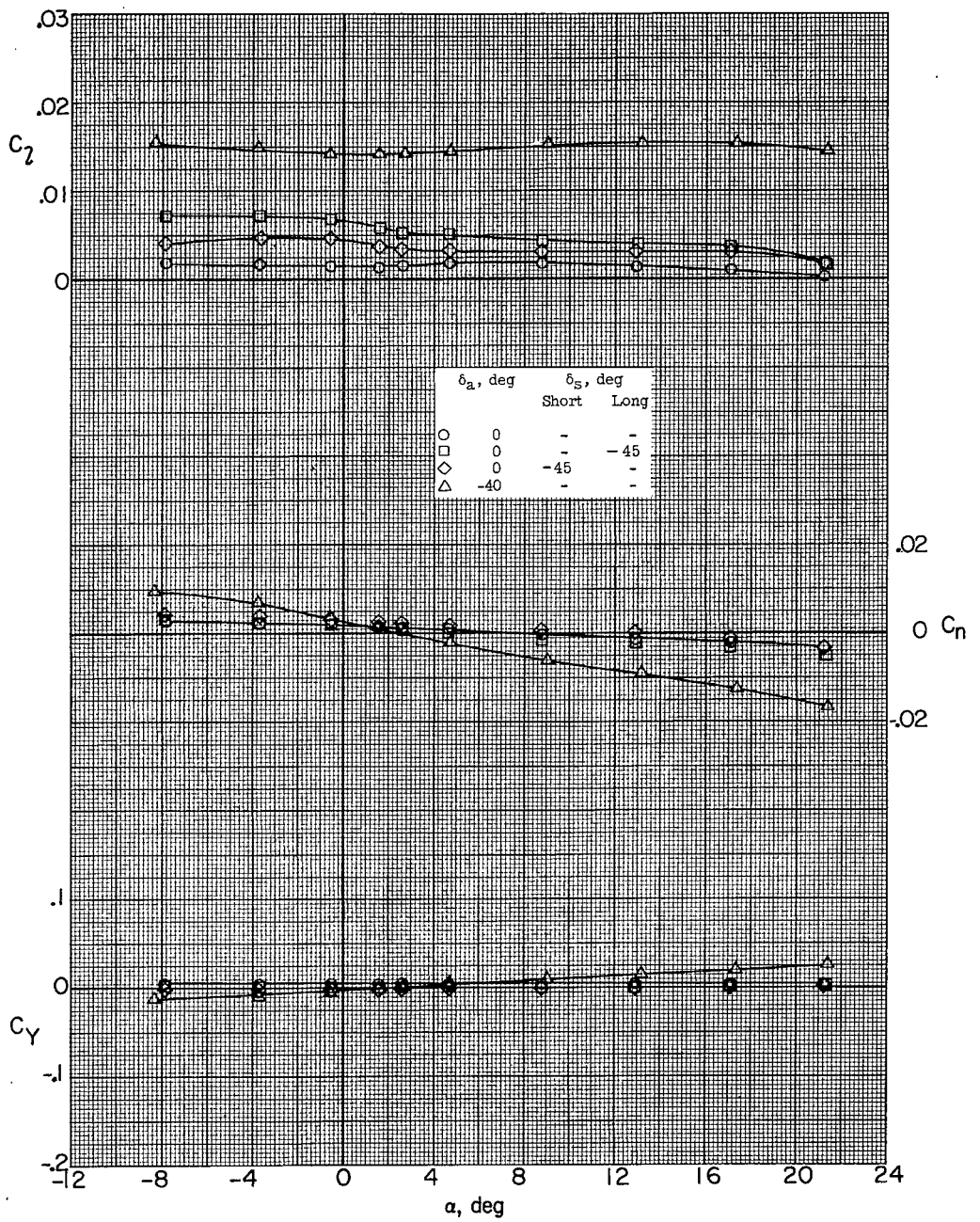

(a) M = 1.60.

Figure 14.- Effect of separate deflections of aileron and long and short spoilers on aerodynamic characteristics in pitch. BS_1WVHF; $\beta = 0^\circ$.

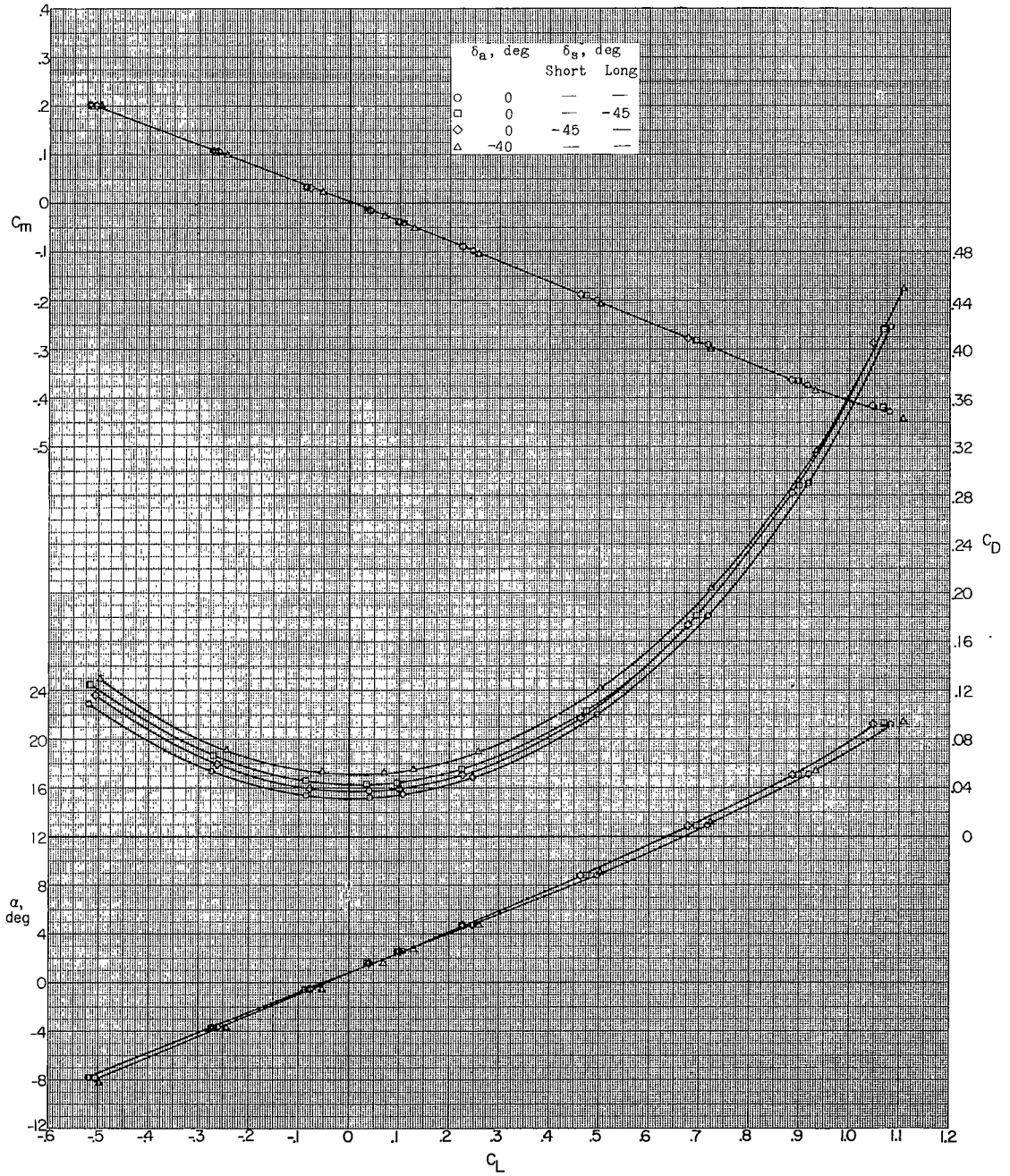

(a) Concluded.

Figure 14.- Continued.

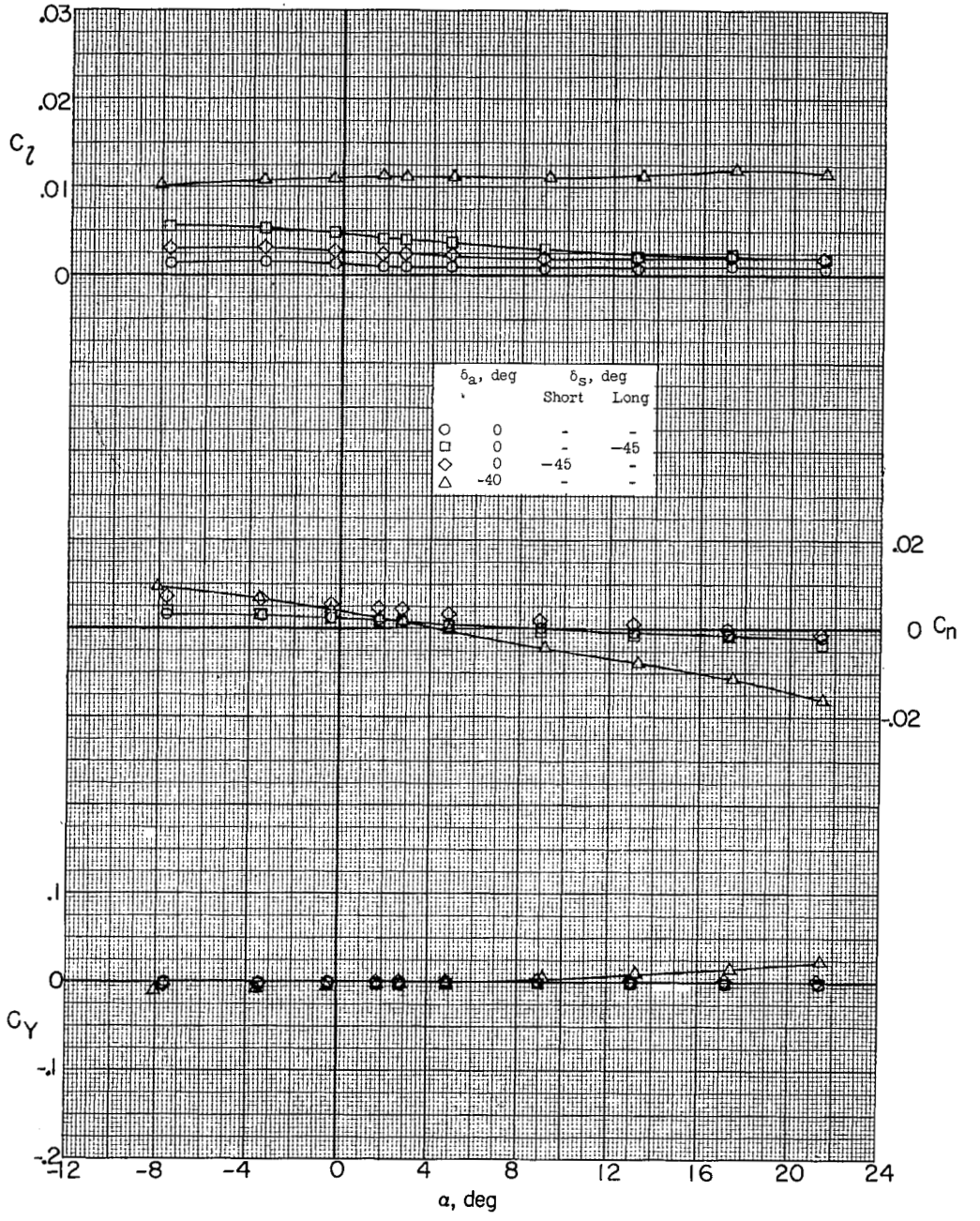

(b) M = 1.90.

Figure 14.- Continued.

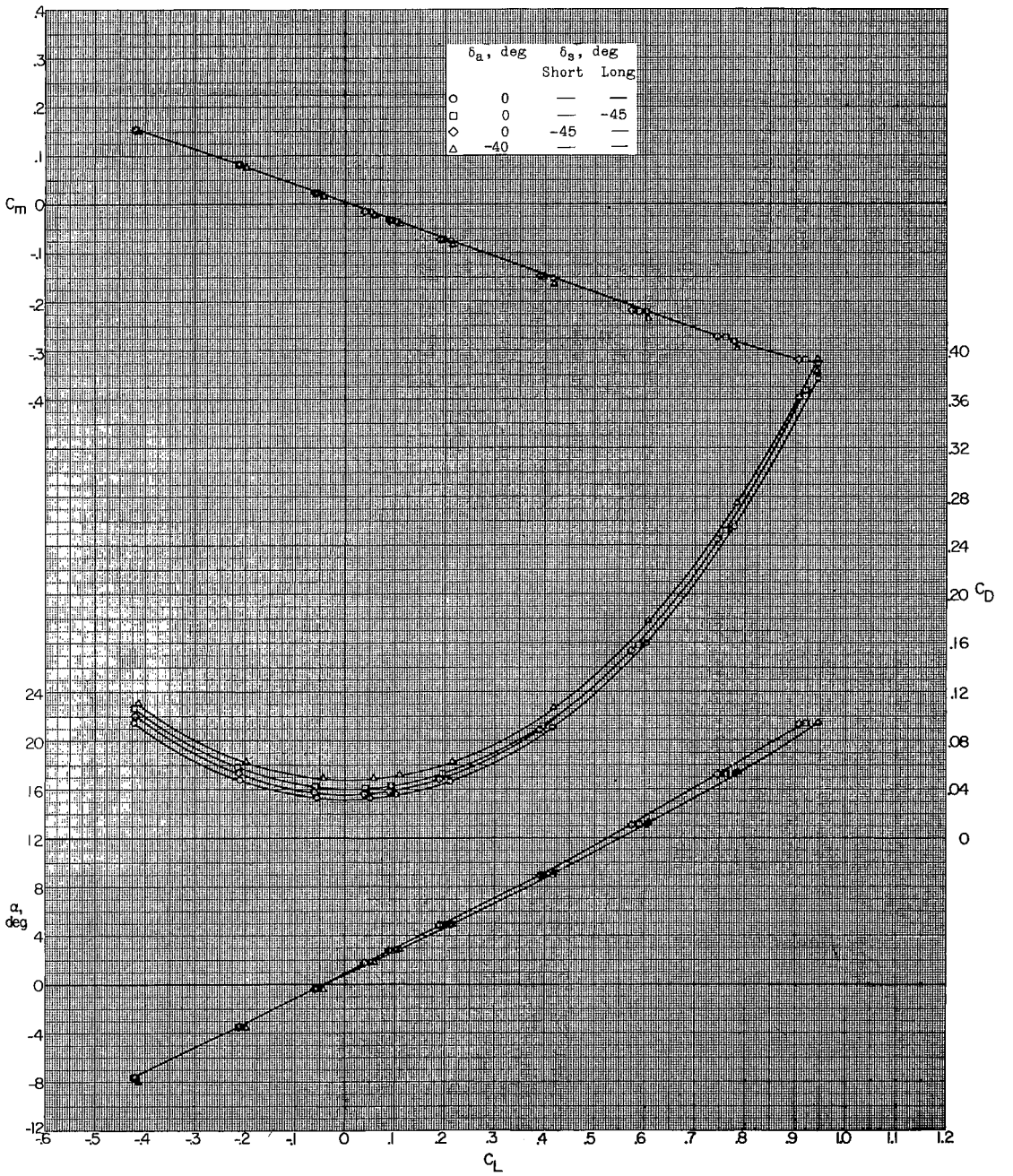

(b) Concluded.

Figure 14.- Continued.

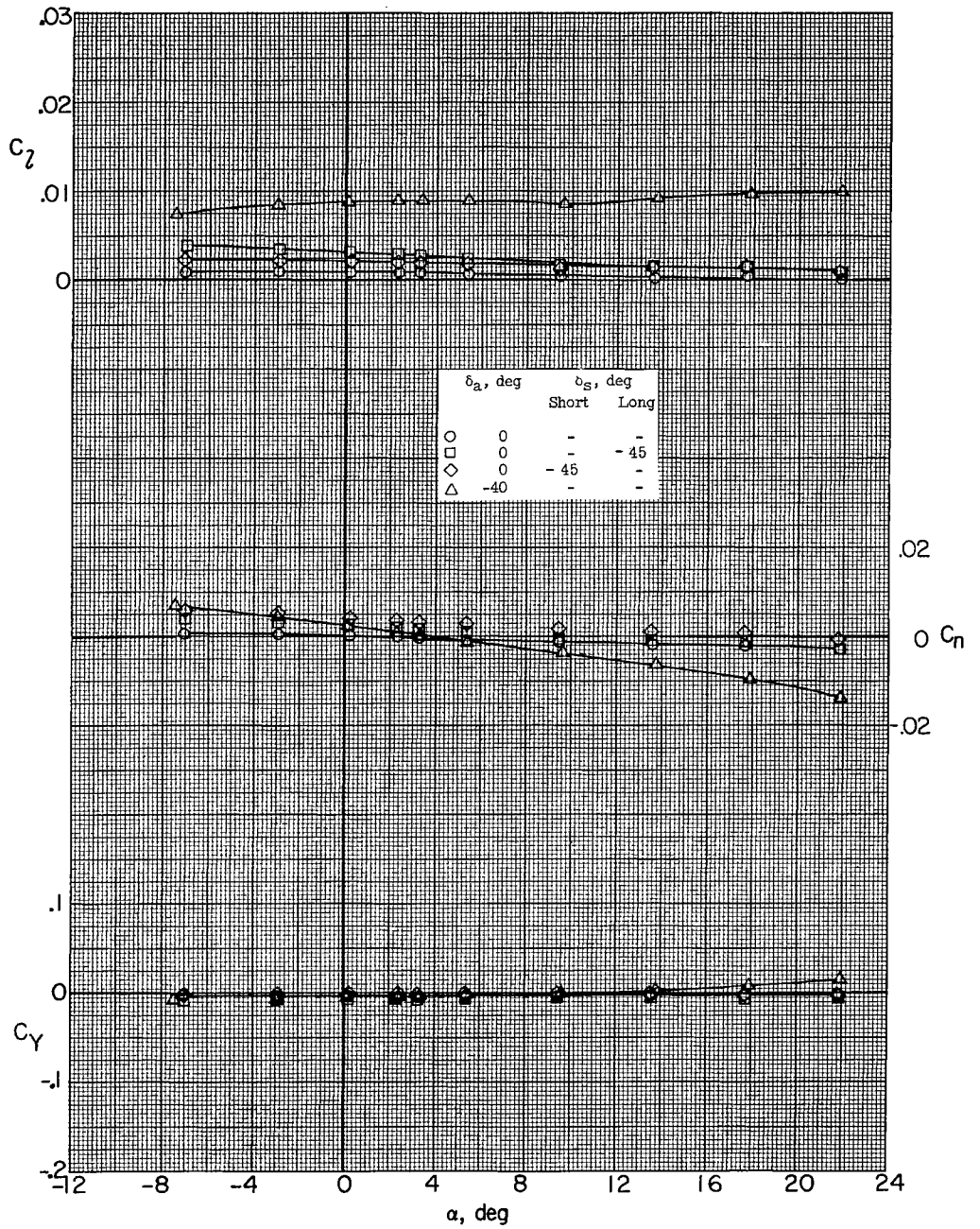

(c) M = 2.20.

Figure 14.- Continued.

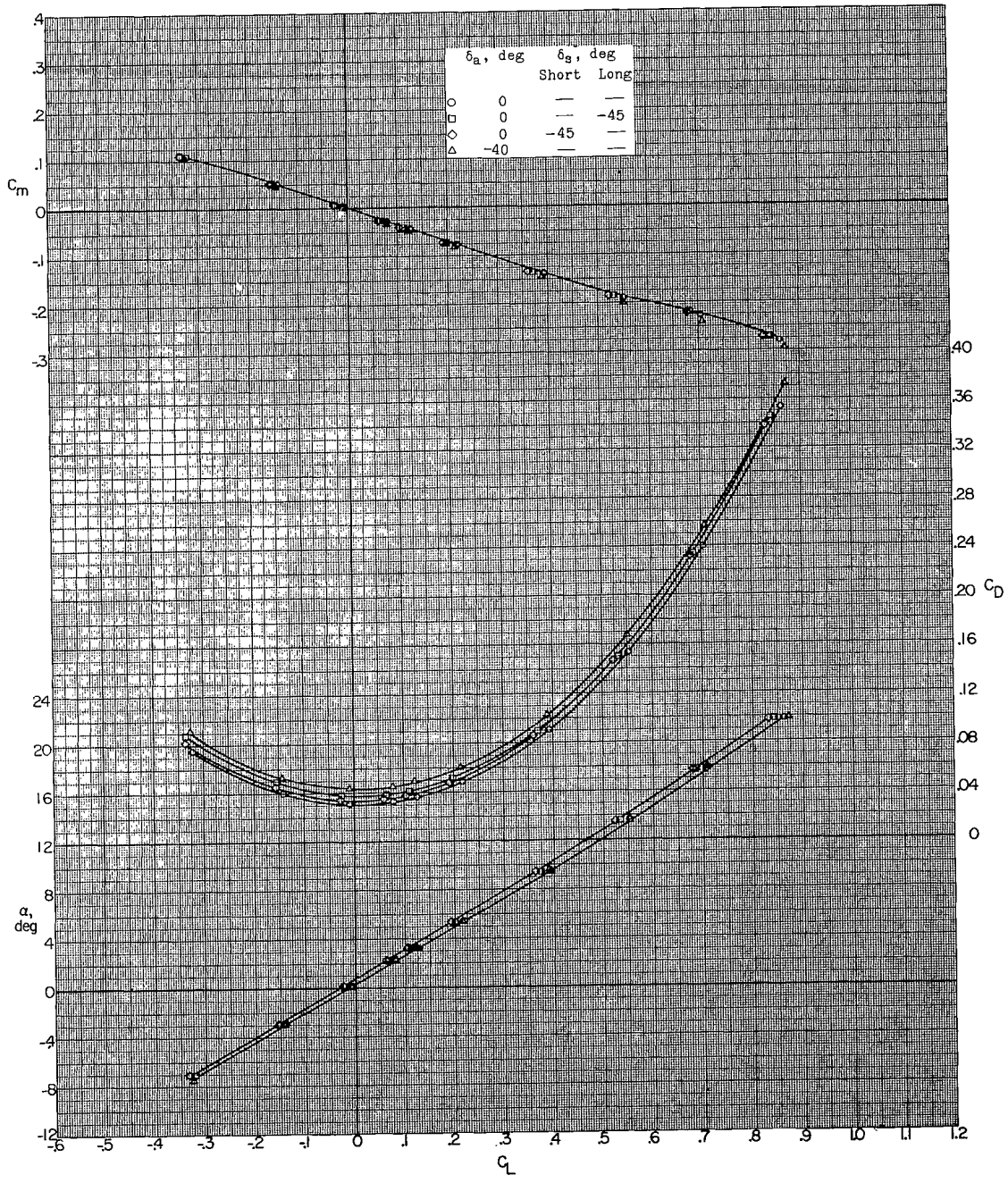

(c) Concluded.

Figure 14.- Concluded.

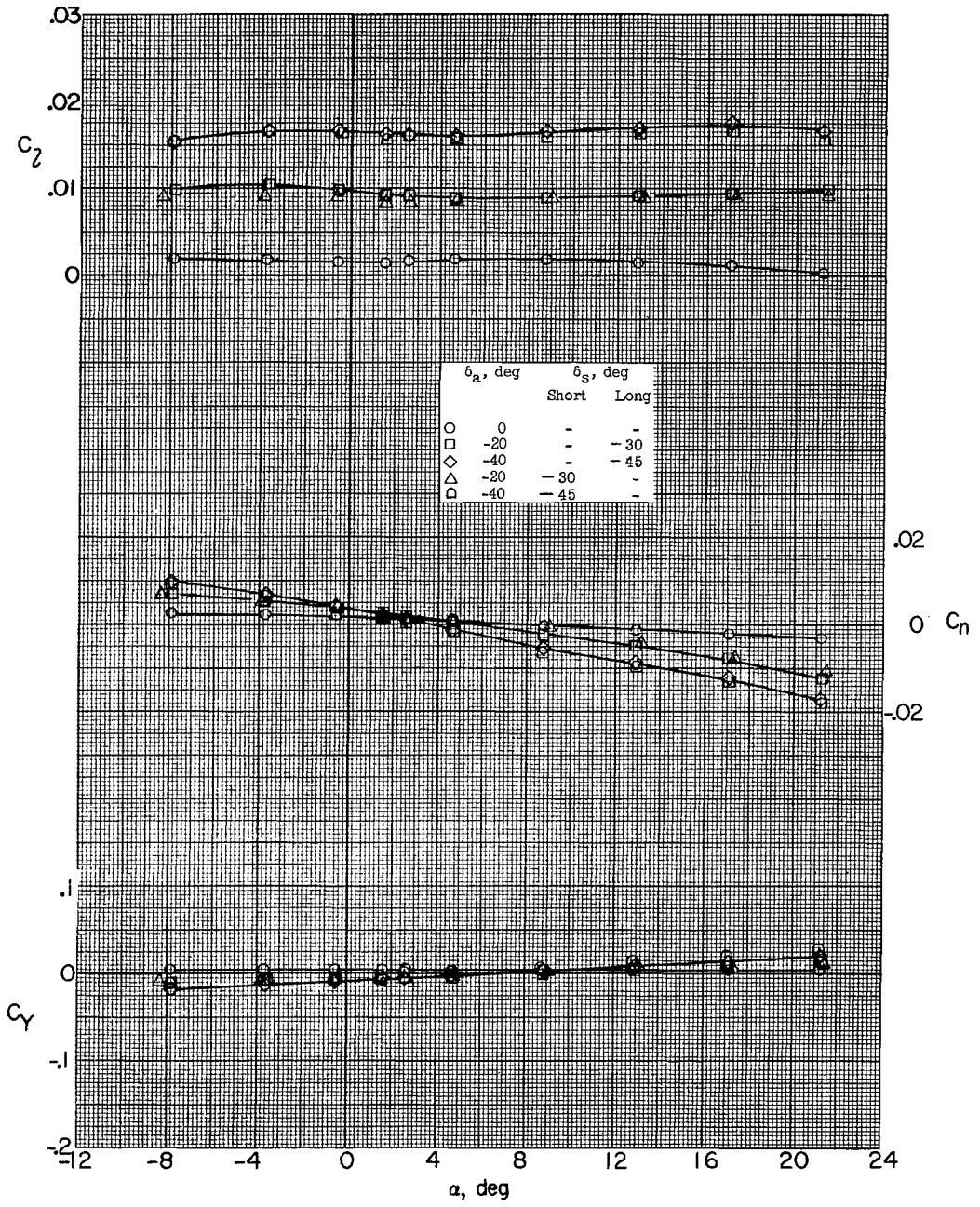

(a) M = 1.60.

Figure 15.- Effect of combined deflections of aileron and long and short spoilers on aerodynamic characteristics in pitch. BS_1WVHF; $\beta = 0^\circ$.

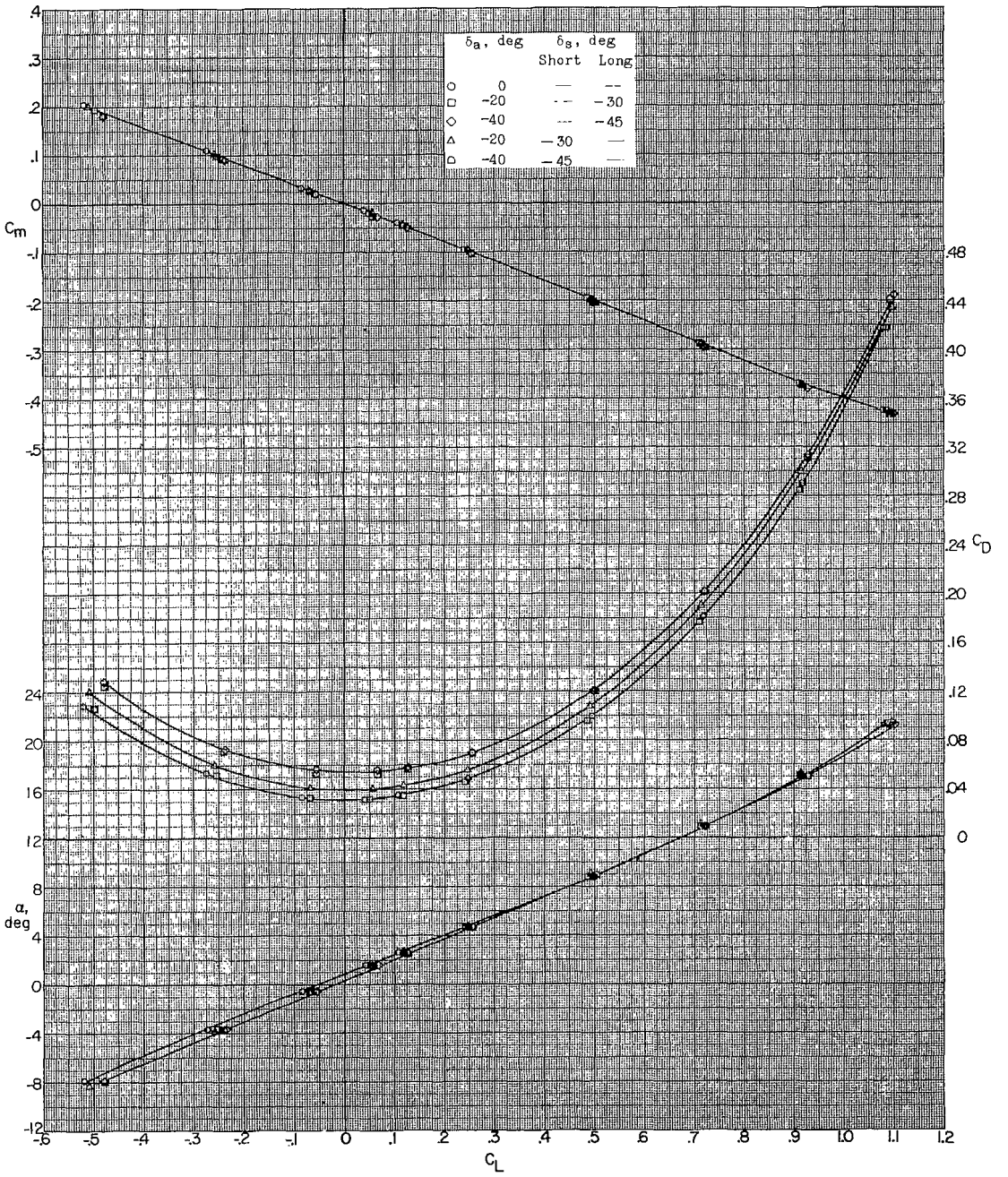

(a) Concluded.

Figure 15.- Continued.

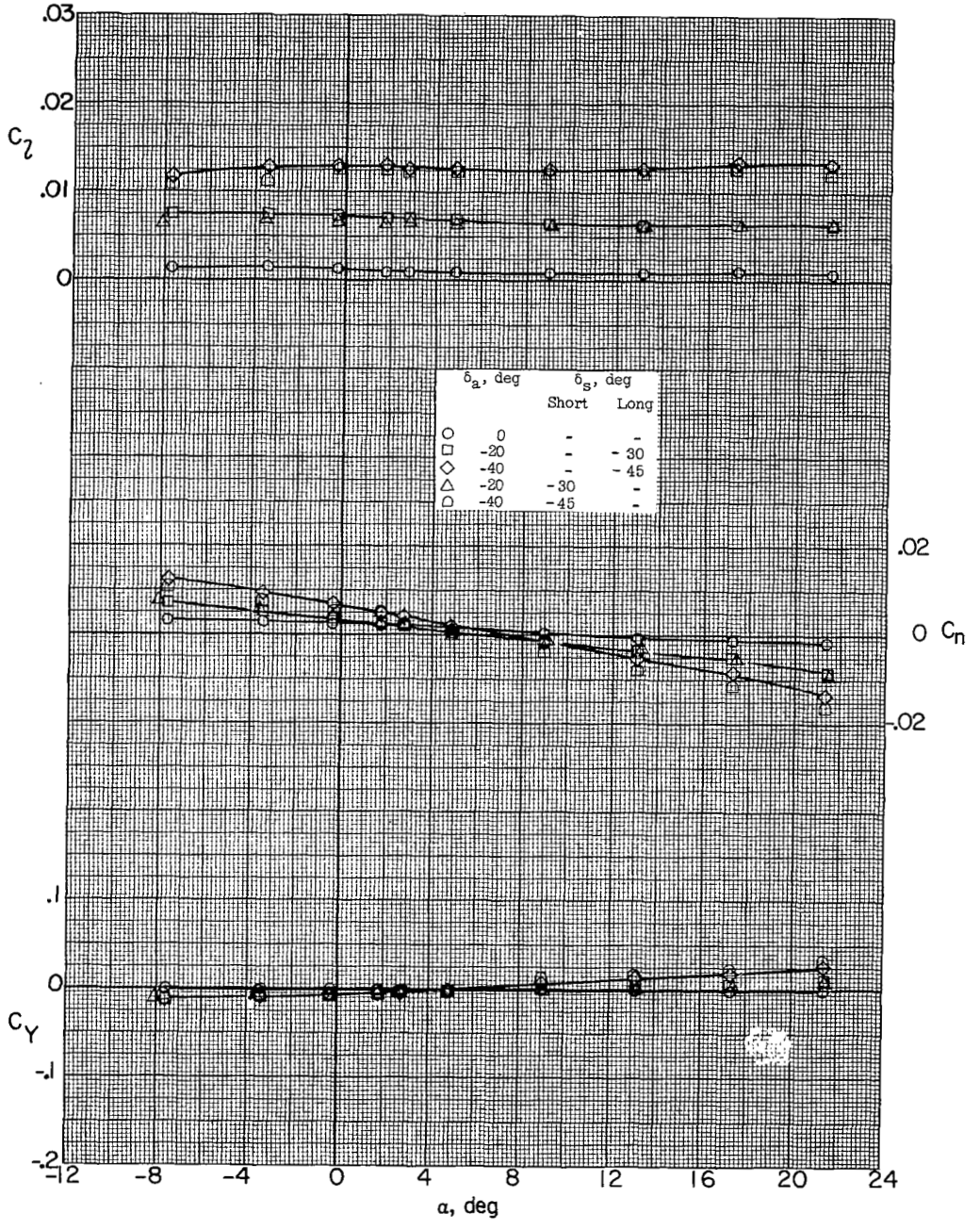

(b) M = 1.90.

Figure 15.- Continued.

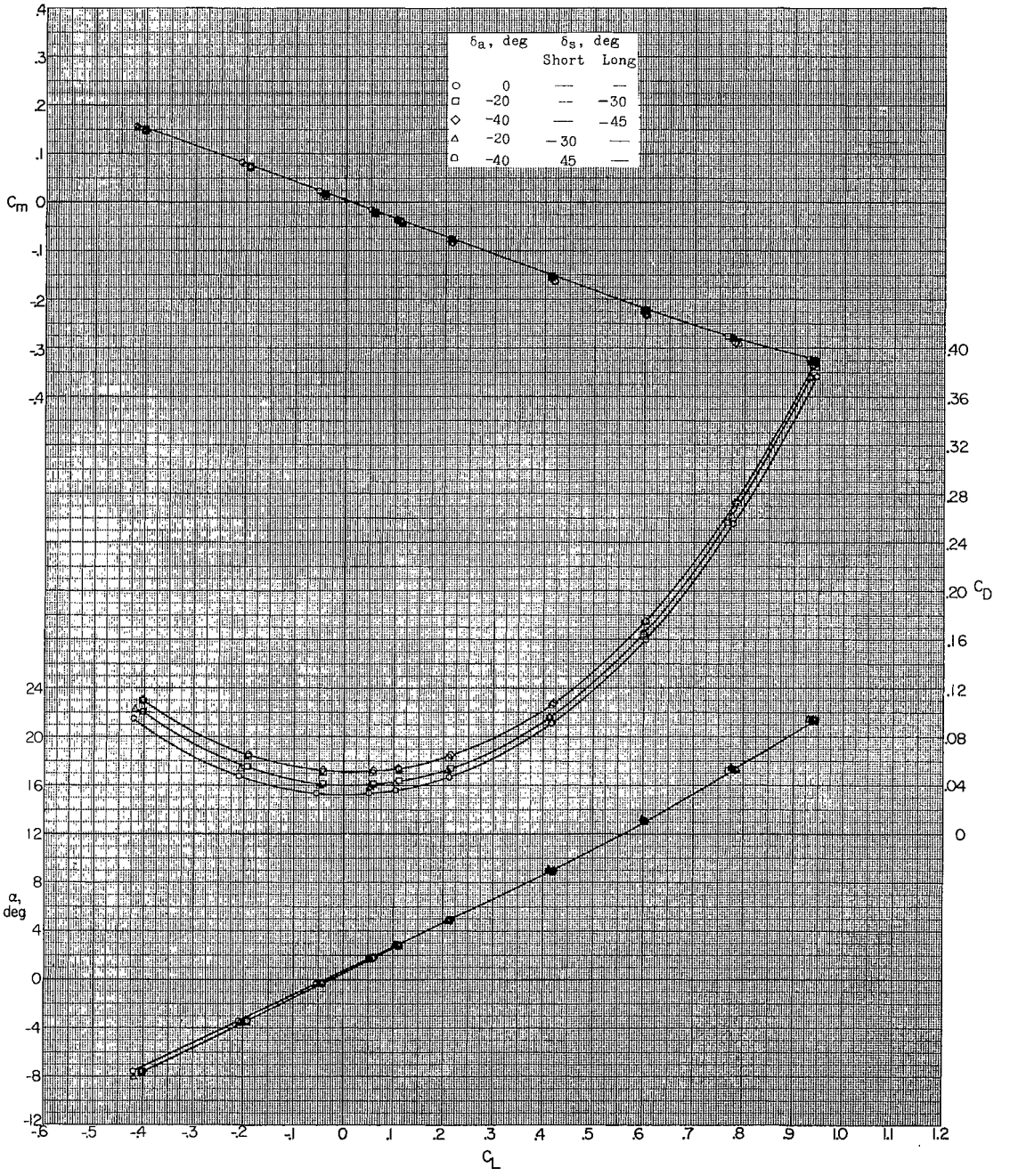

(b) Concluded.

Figure 15.- Continued.

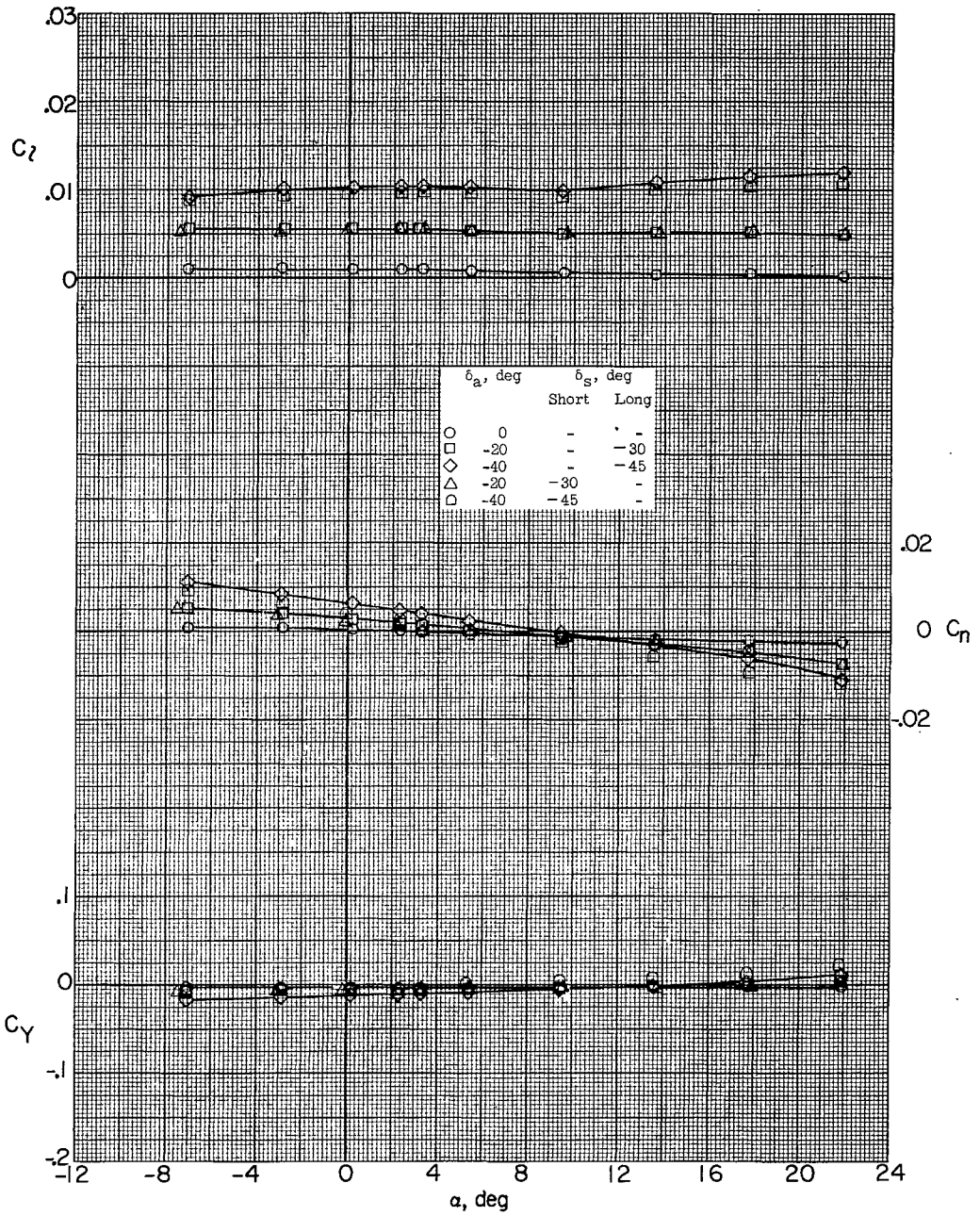

(c) M = 2.20.

Figure 15.- Continued.

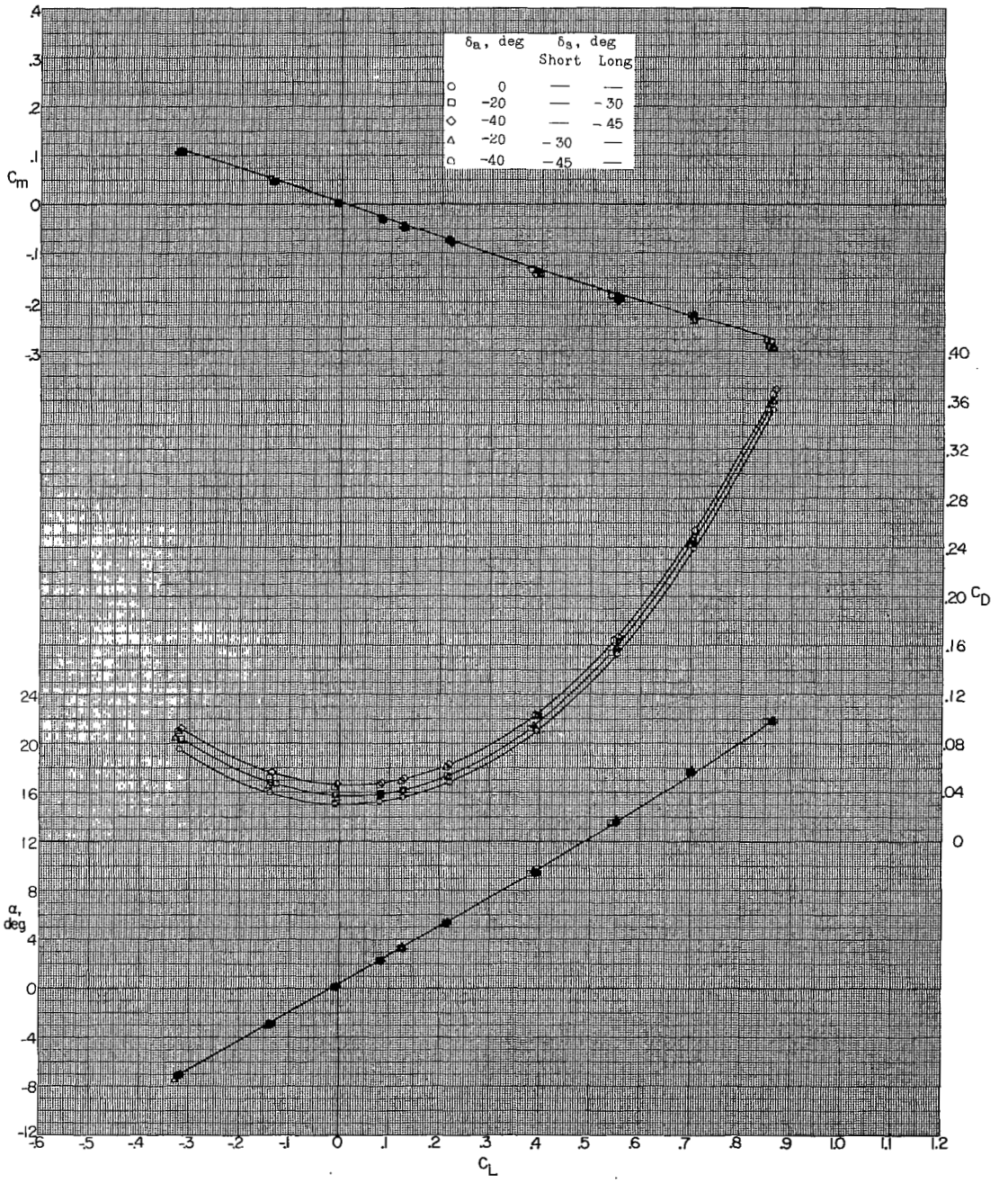

(c) Concluded.

Figure 15.- Continued.

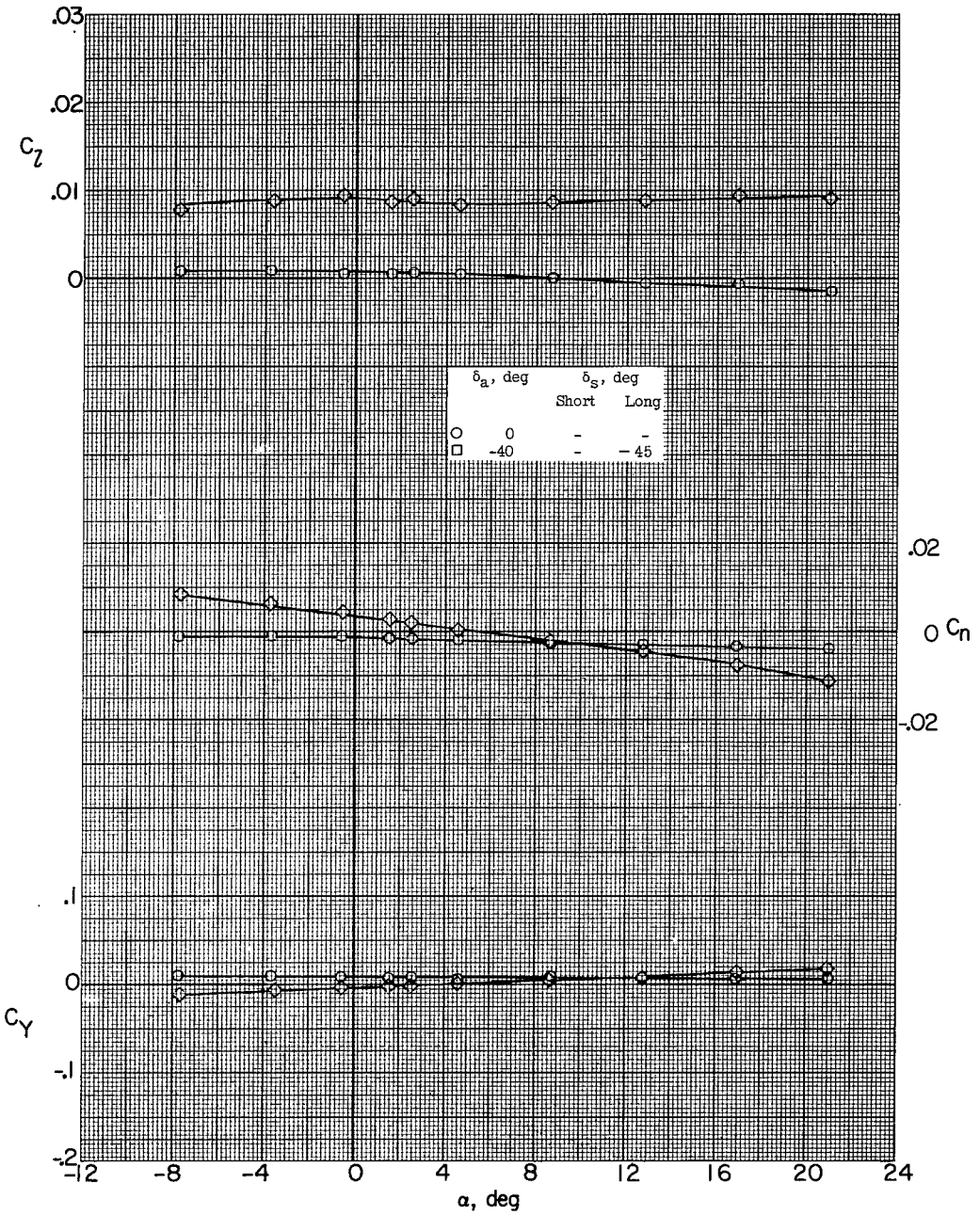

(d) M = 2.50.

Figure 15.- Continued.

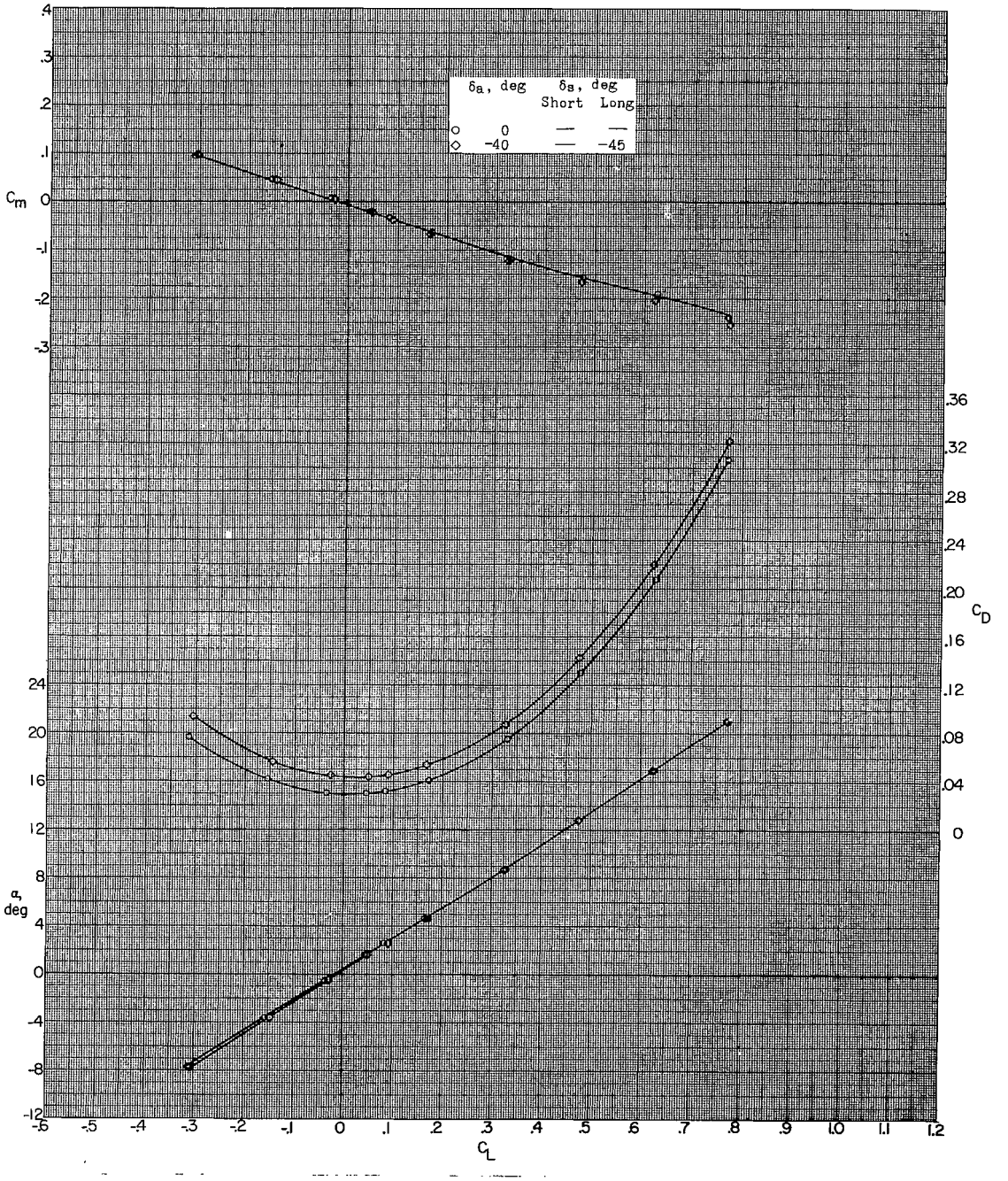

(d) Concluded.

Figure 15.- Concluded.

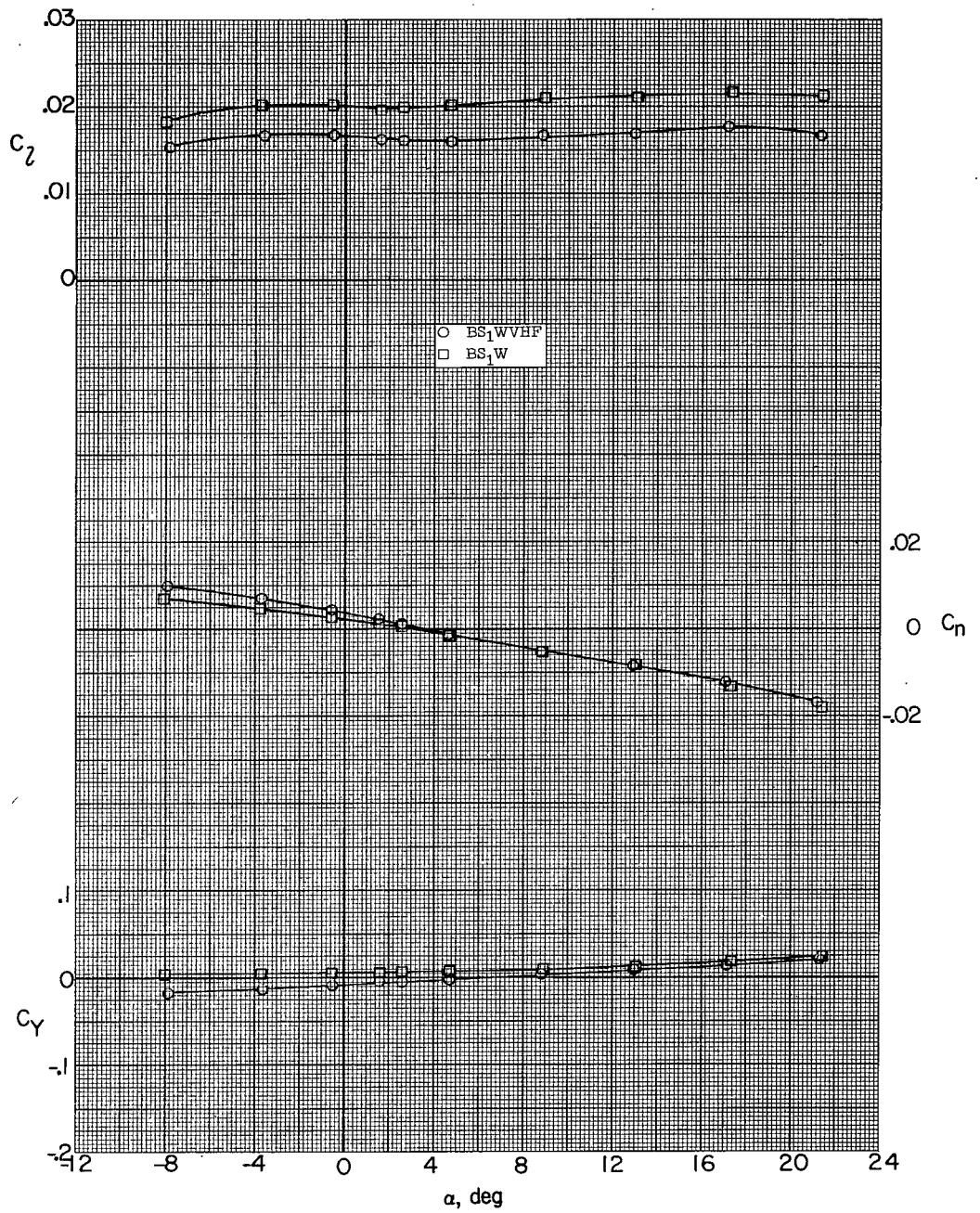

(a) M = 1.60.

Figure 16.- Effect of the tails on the aerodynamic characteristics in pitch of a combined spoiler and aileron deflection. $\delta_a = -40^\circ$; $\delta_s(\text{long}) = -45^\circ$; $\beta = 0^\circ$.

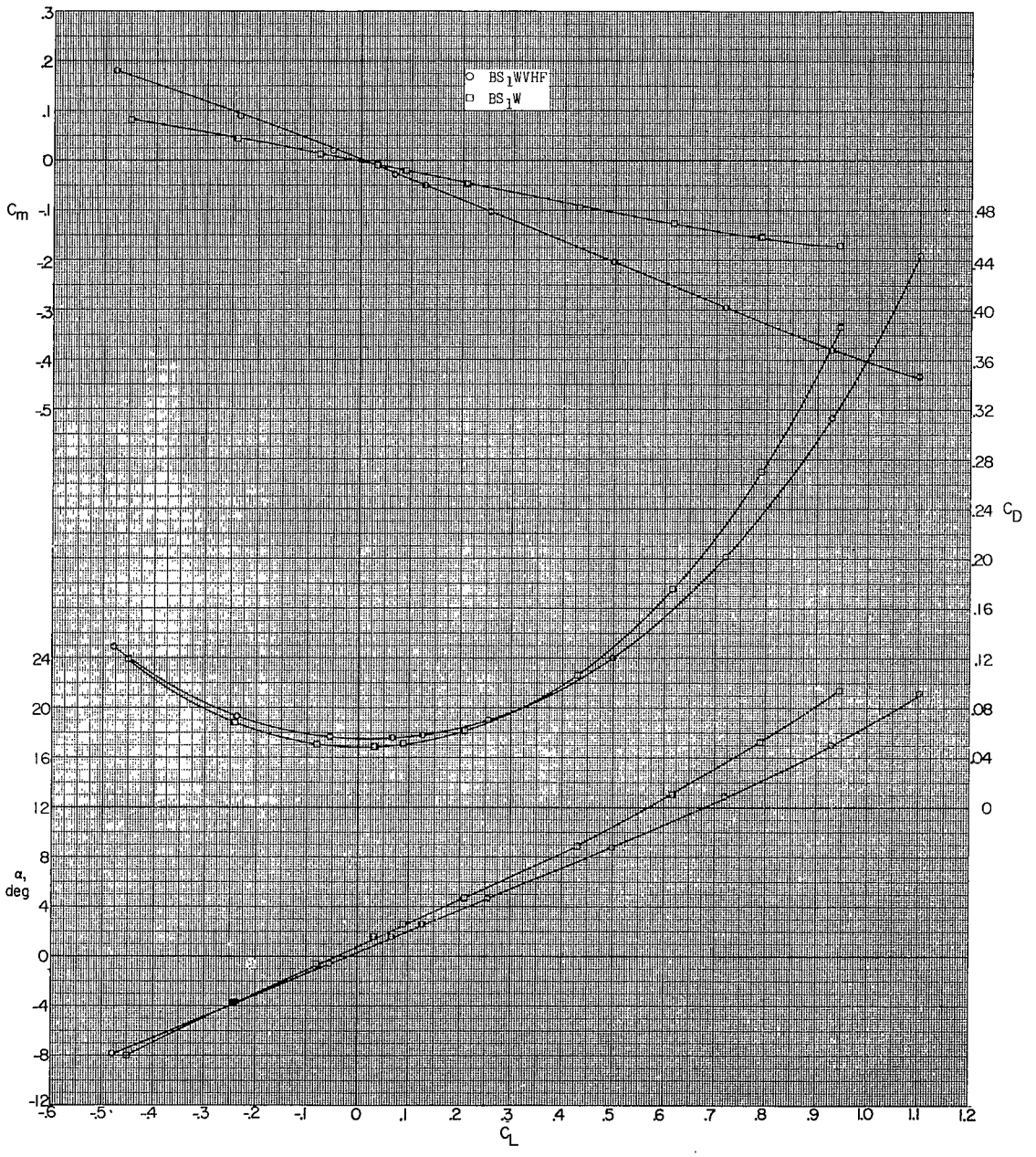

(a) Concluded.

Figure 16.- Continued.

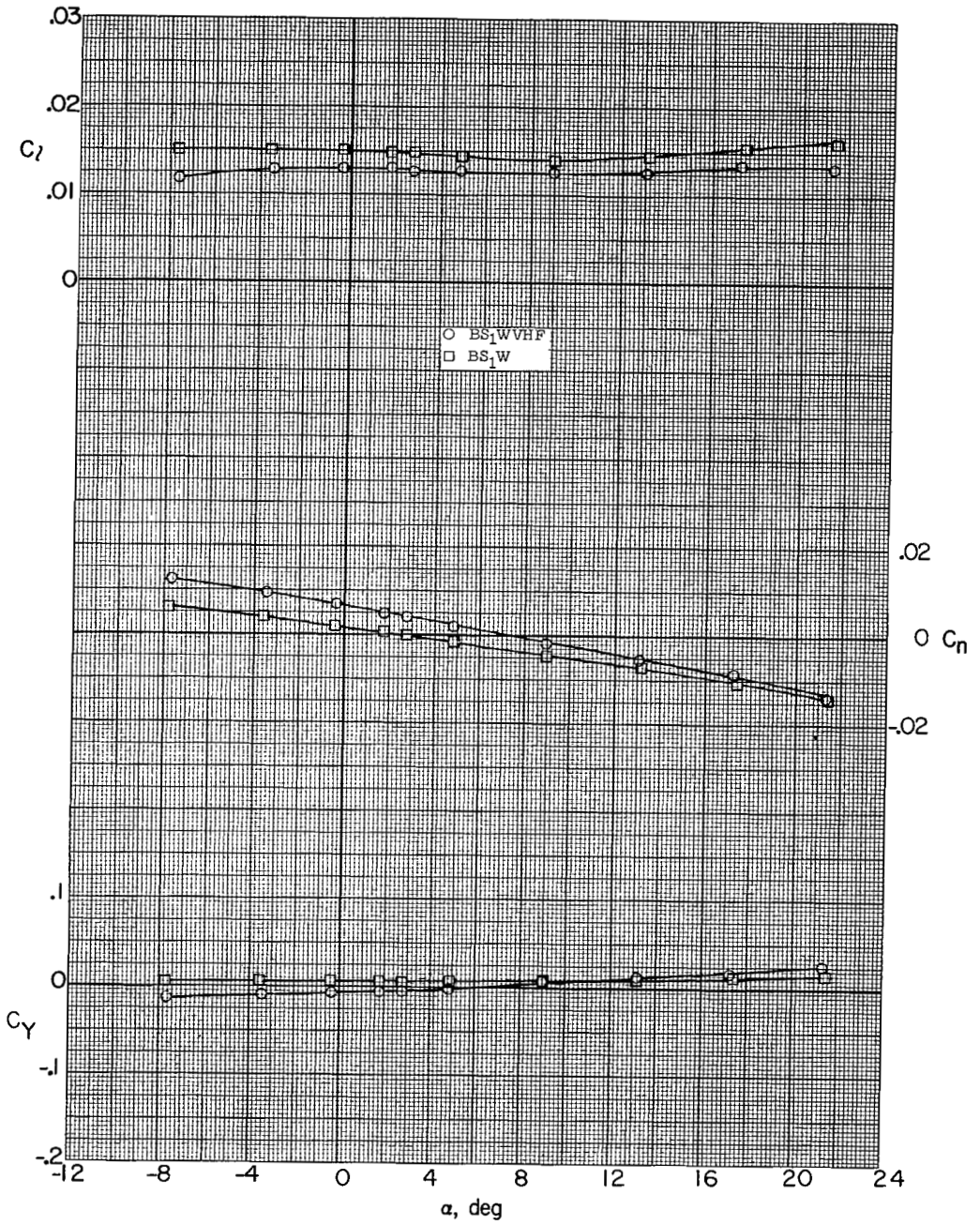

(b) M = 1.90.

Figure 16.- Continued.

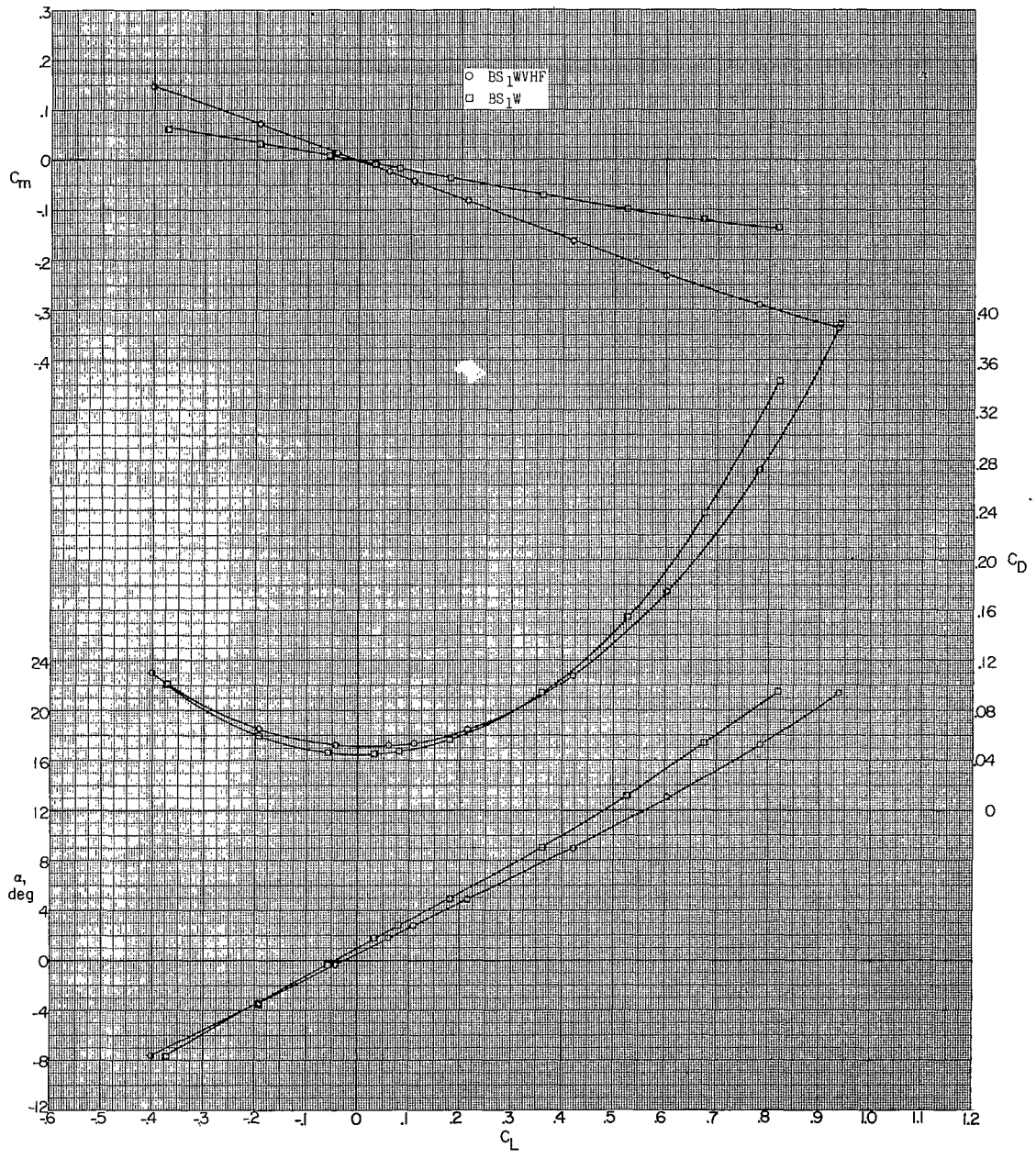

(b) Concluded.

Figure 16.- Continued.

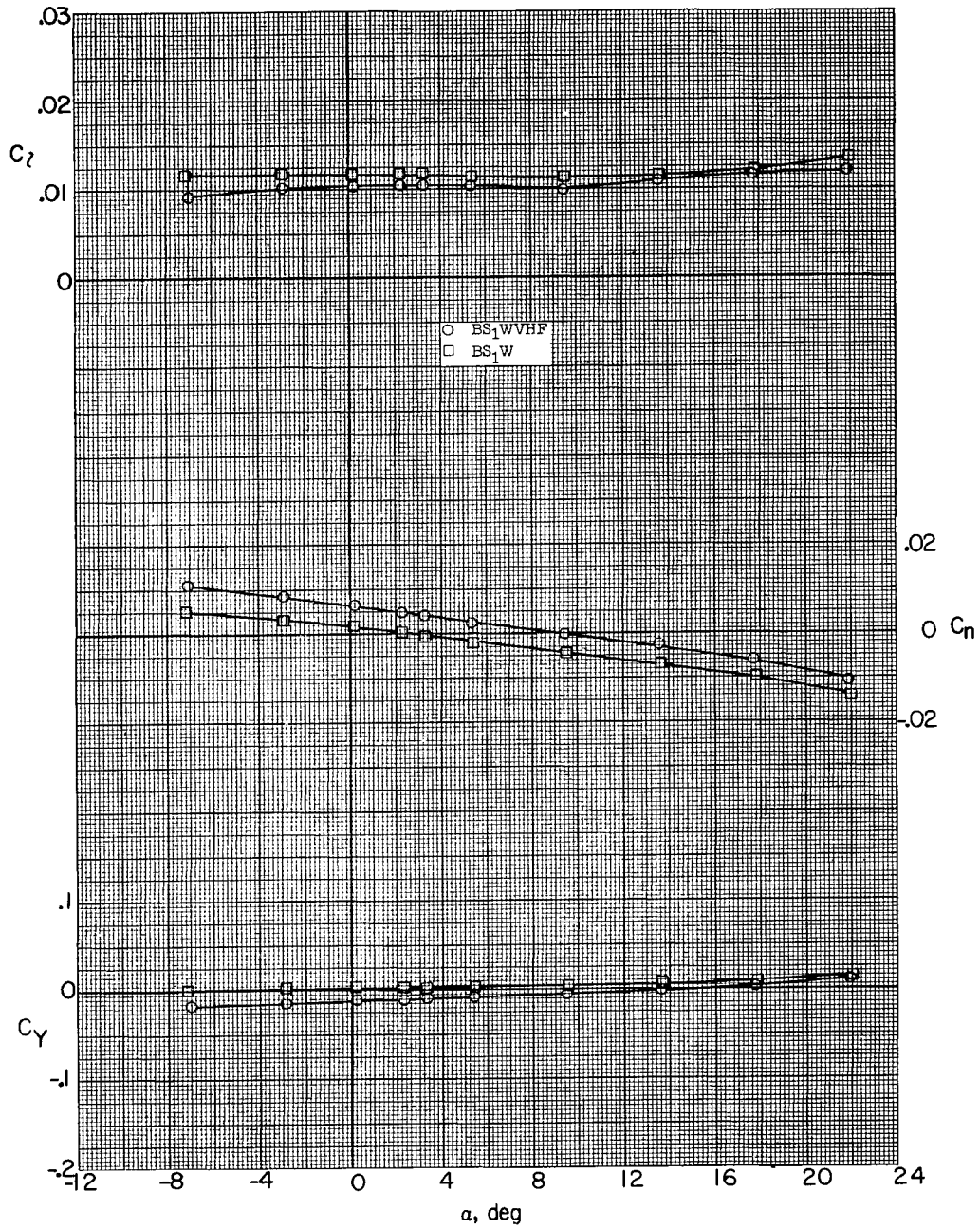

(c) M = 2.20.

Figure 16.- Continued.

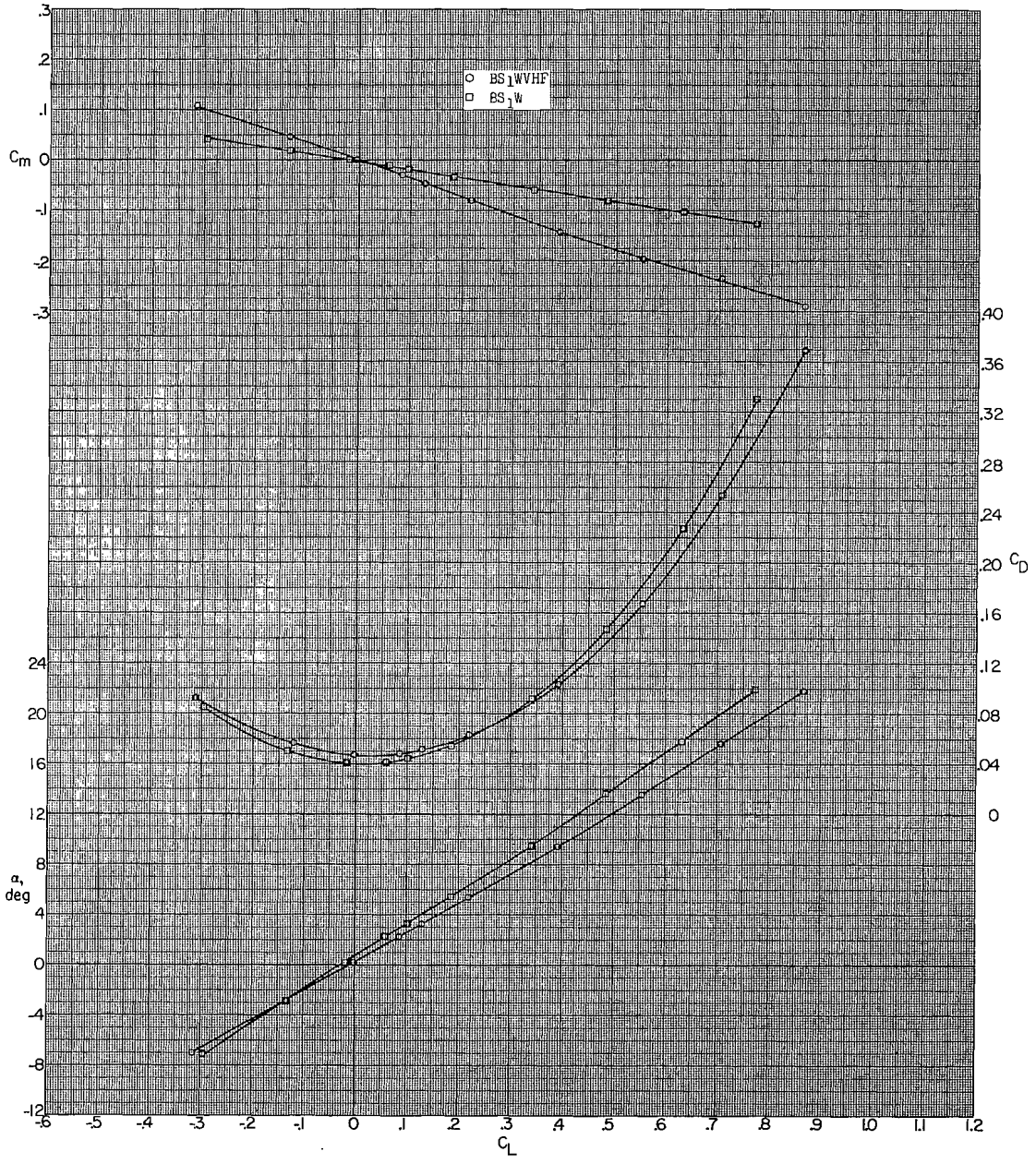

(c) Concluded.

Figure 16.- Concluded.

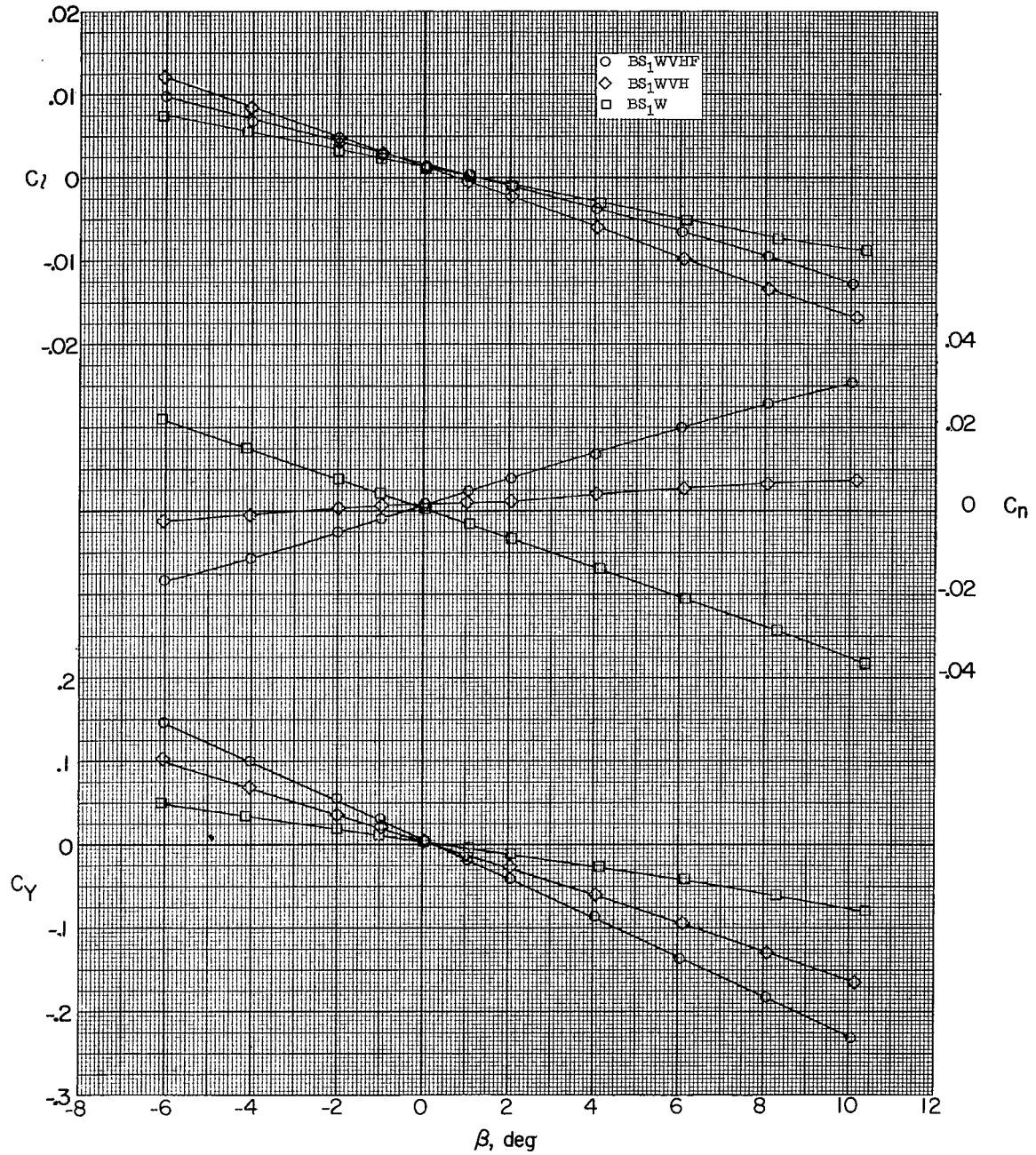

(a) M = 1.60; $\alpha = 0.5^{\circ}$.

Figure 17.- Effect of model-component breakdown on aerodynamic characteristic in sideslip.

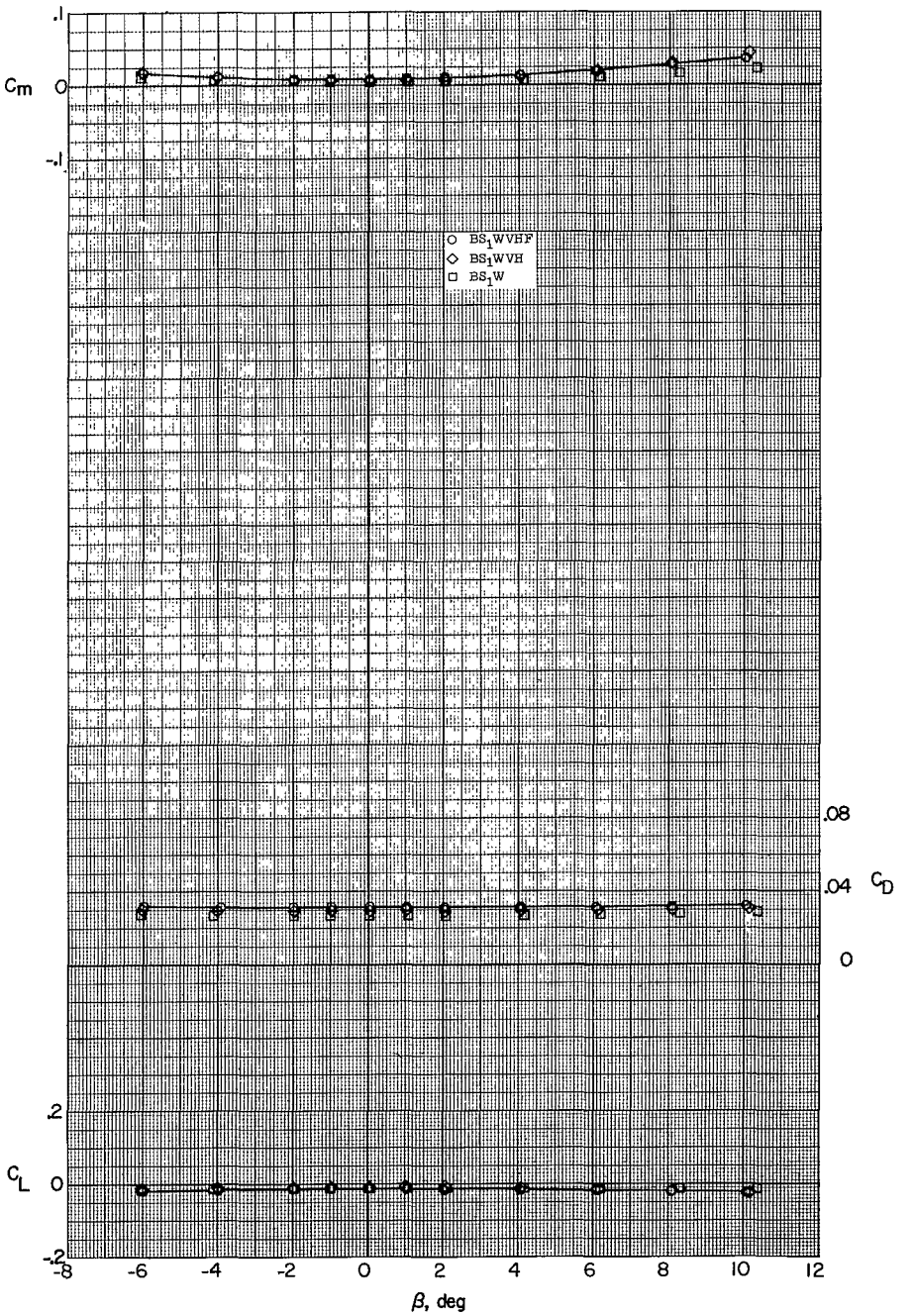

(a) Concluded.

Figure 17.- Continued.

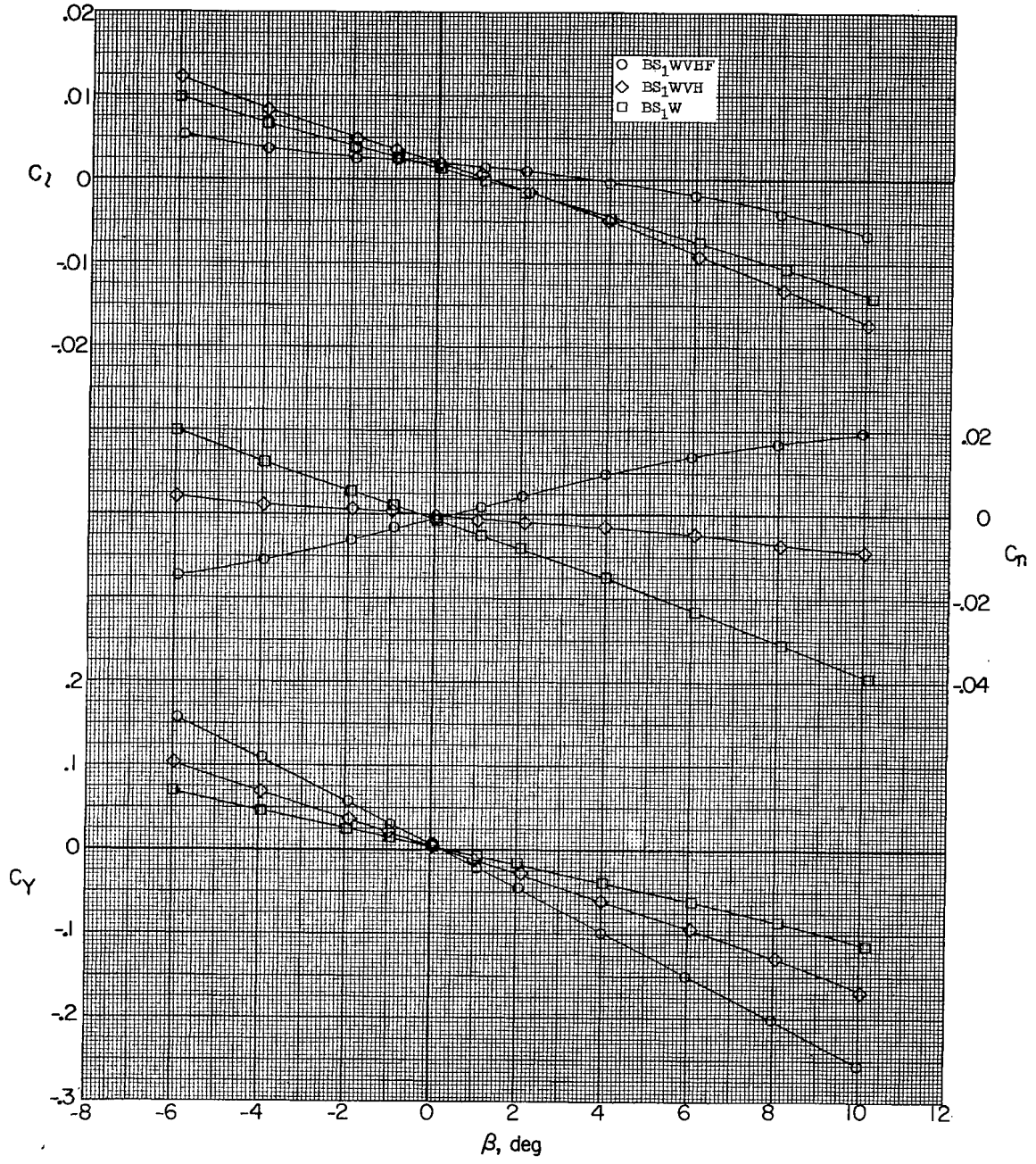

(b) M = 1.60; α = 10.9°.

Figure 17.- Continued.

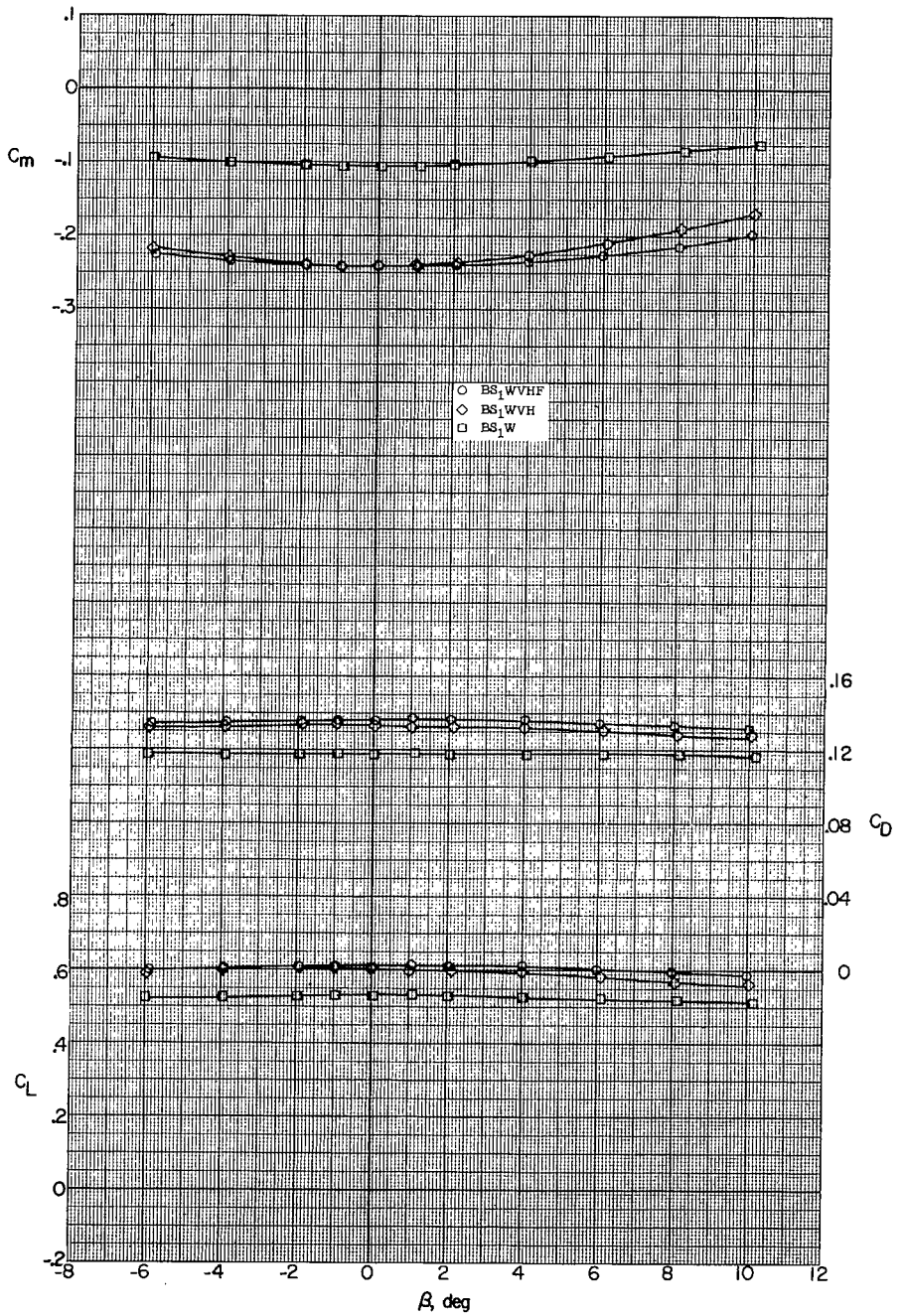

(b) Concluded.

Figure 17.- Continued.

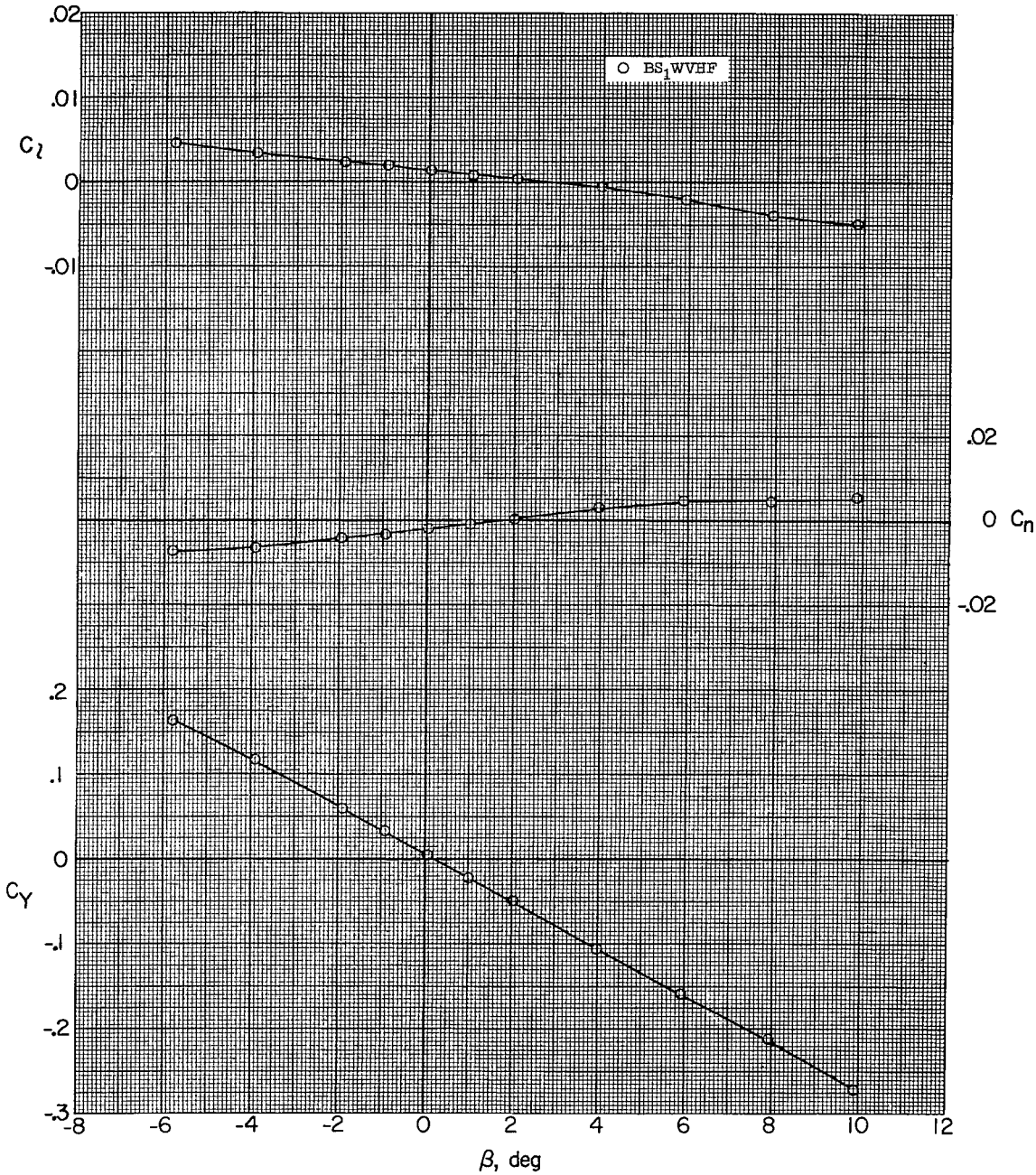

(c) M = 1.60; α = 16.1°.

Figure 17.- Continued.

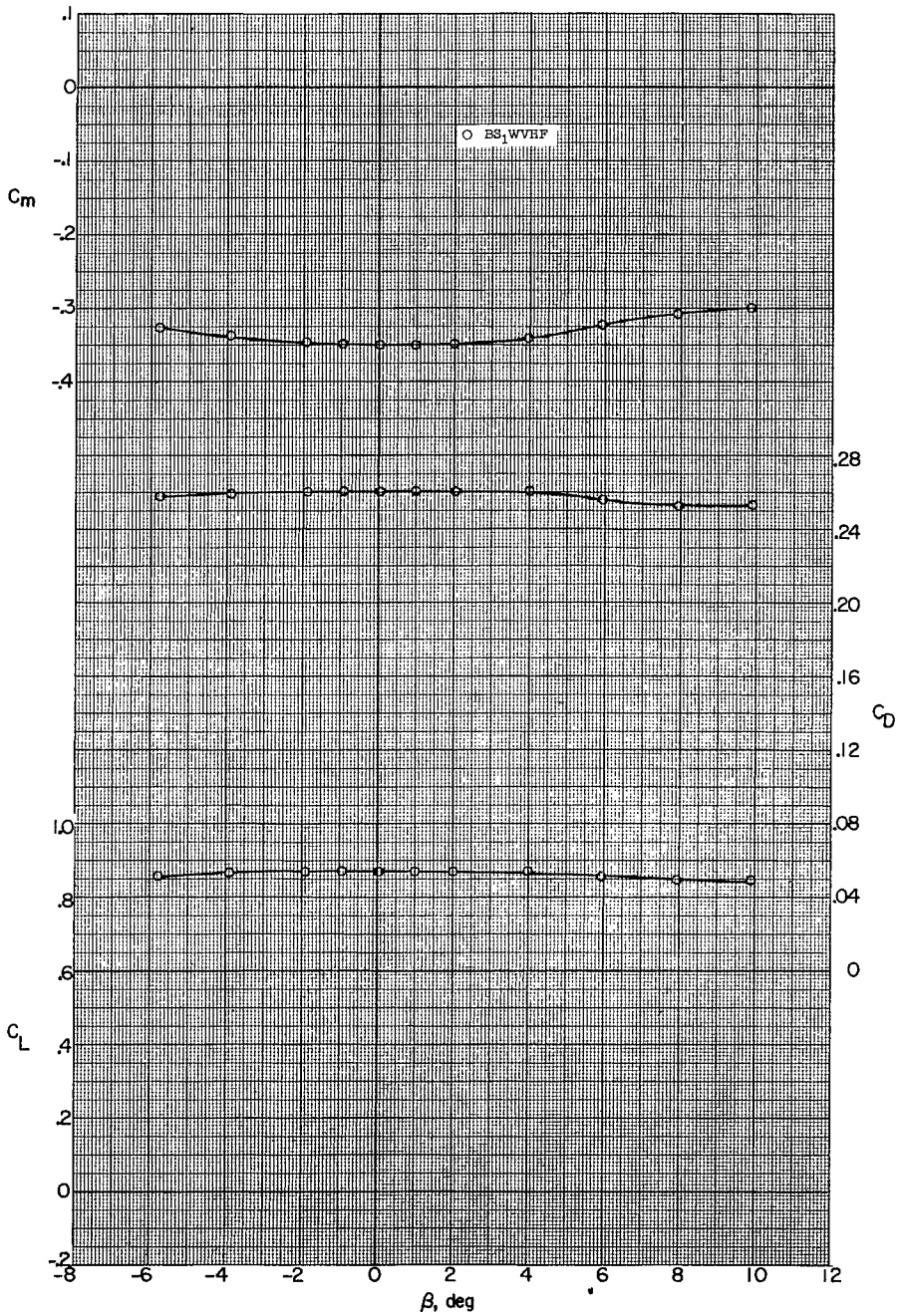

(c) Concluded.

Figure 17.- Continued.

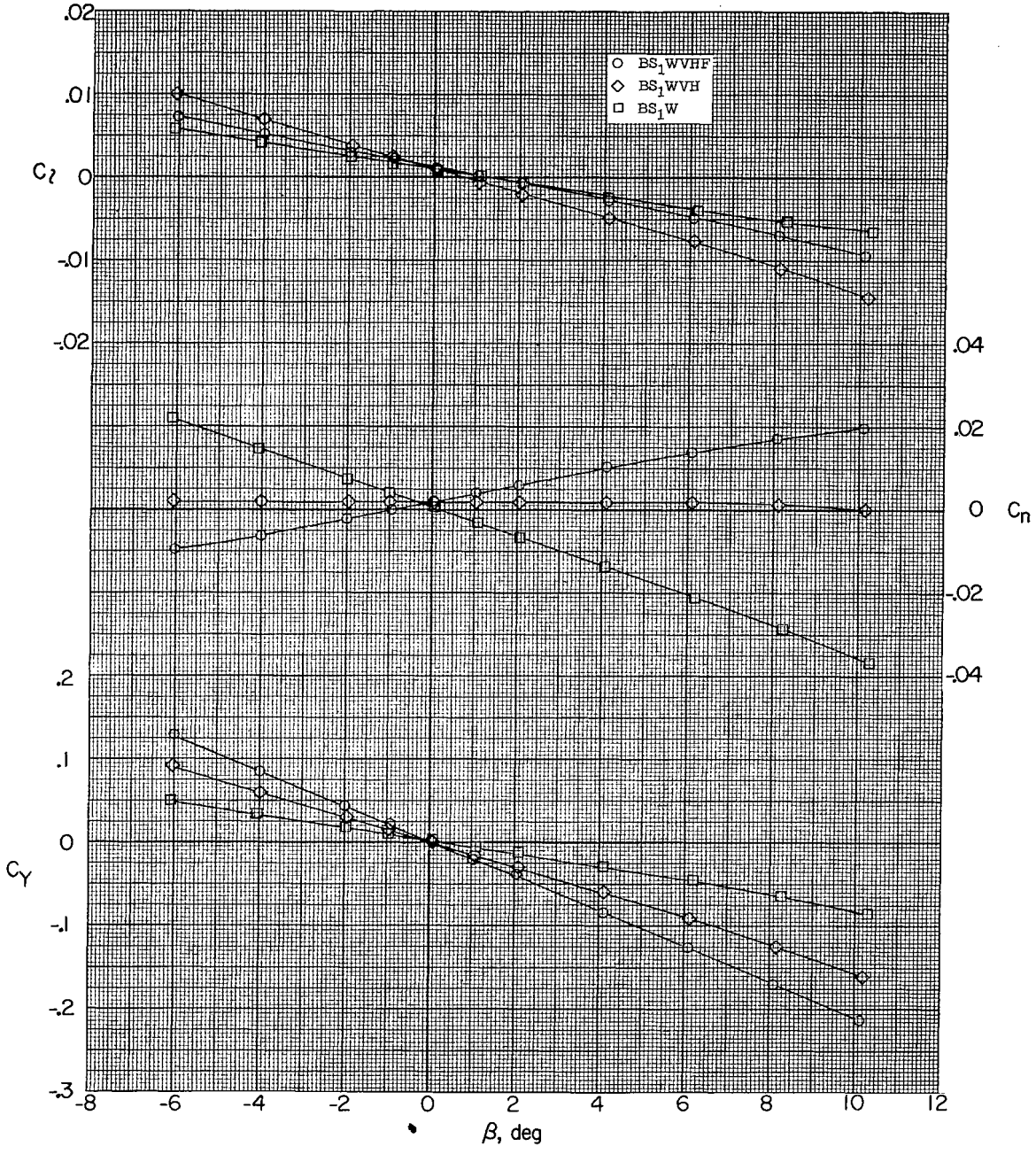

(d) M = 1.90; $\alpha = 0.7^{\circ}$.

Figure 17.- Continued.

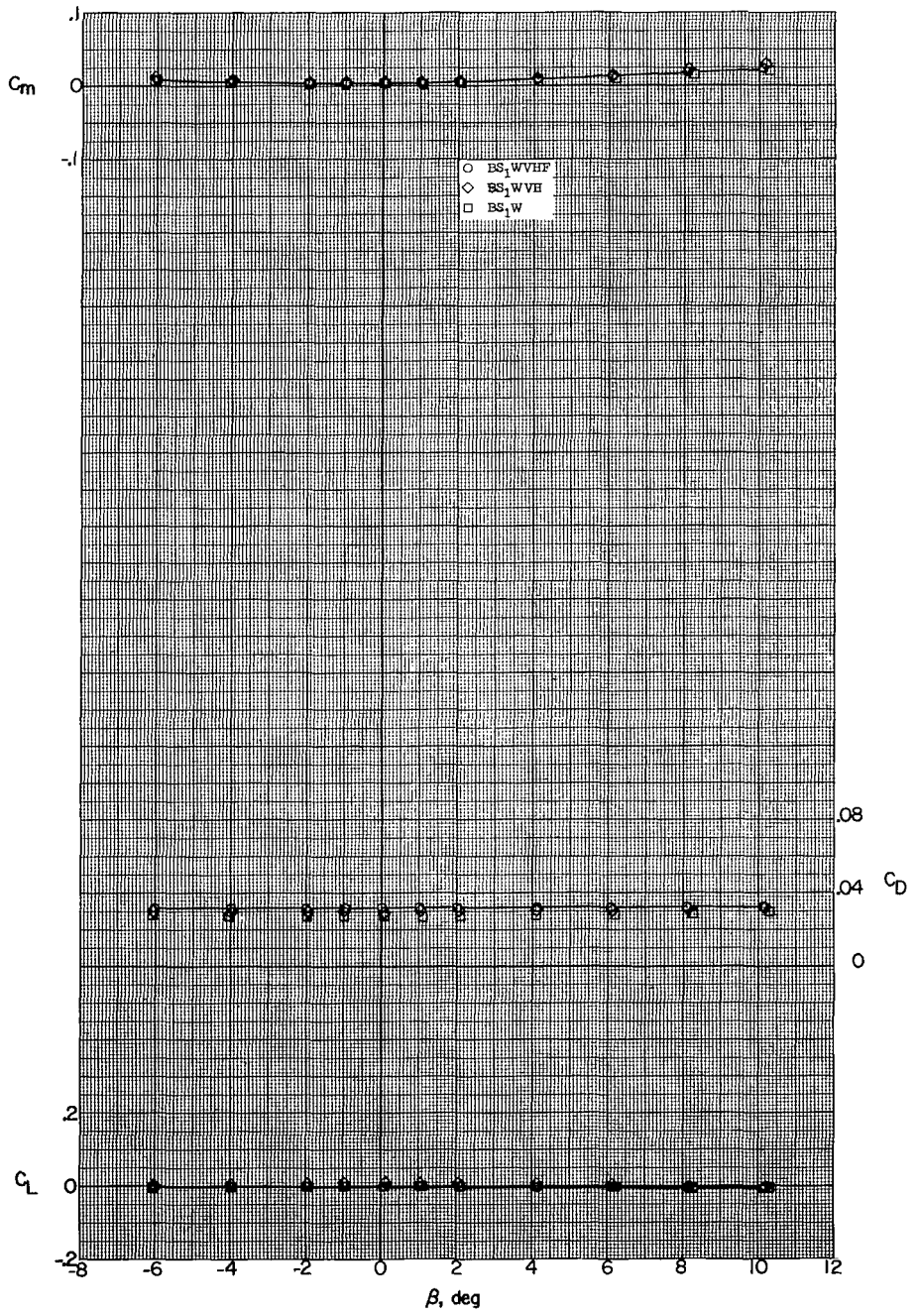

(d) Concluded.

Figure 17.- Continued.

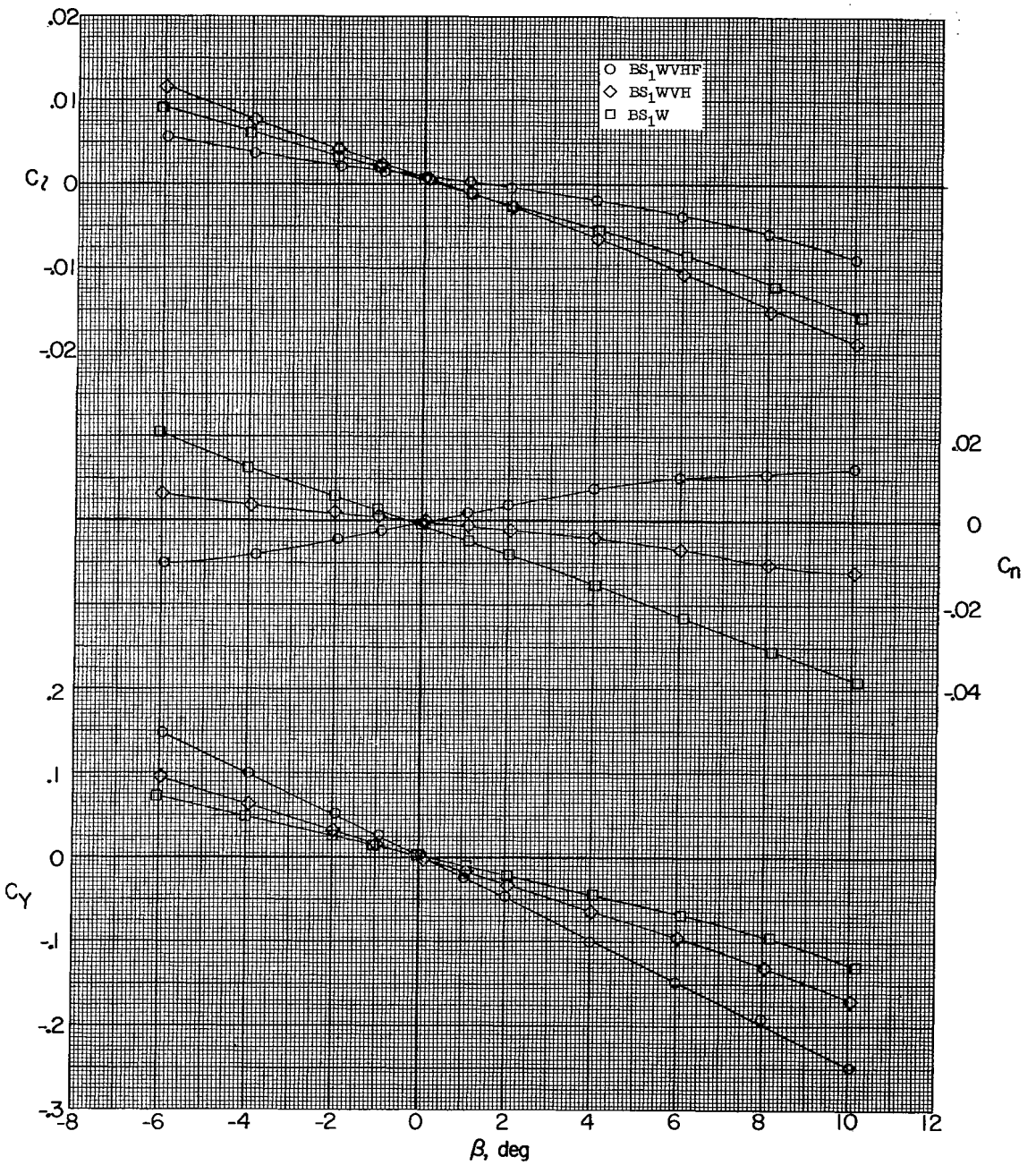

(e) M = 1.90; α = 11.1°.

Figure 17.- Continued.

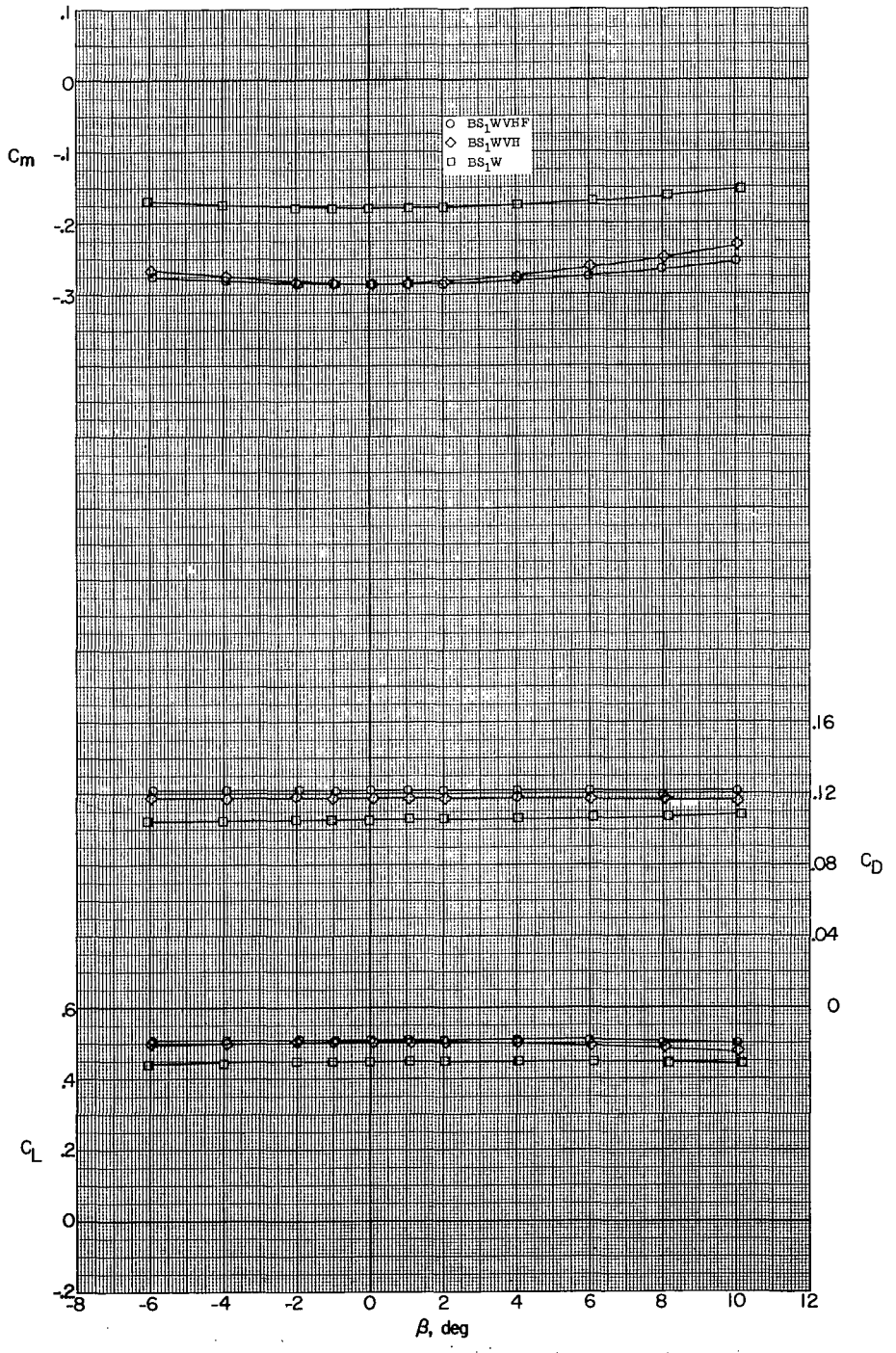

(e) Concluded.

Figure 17.- Continued.

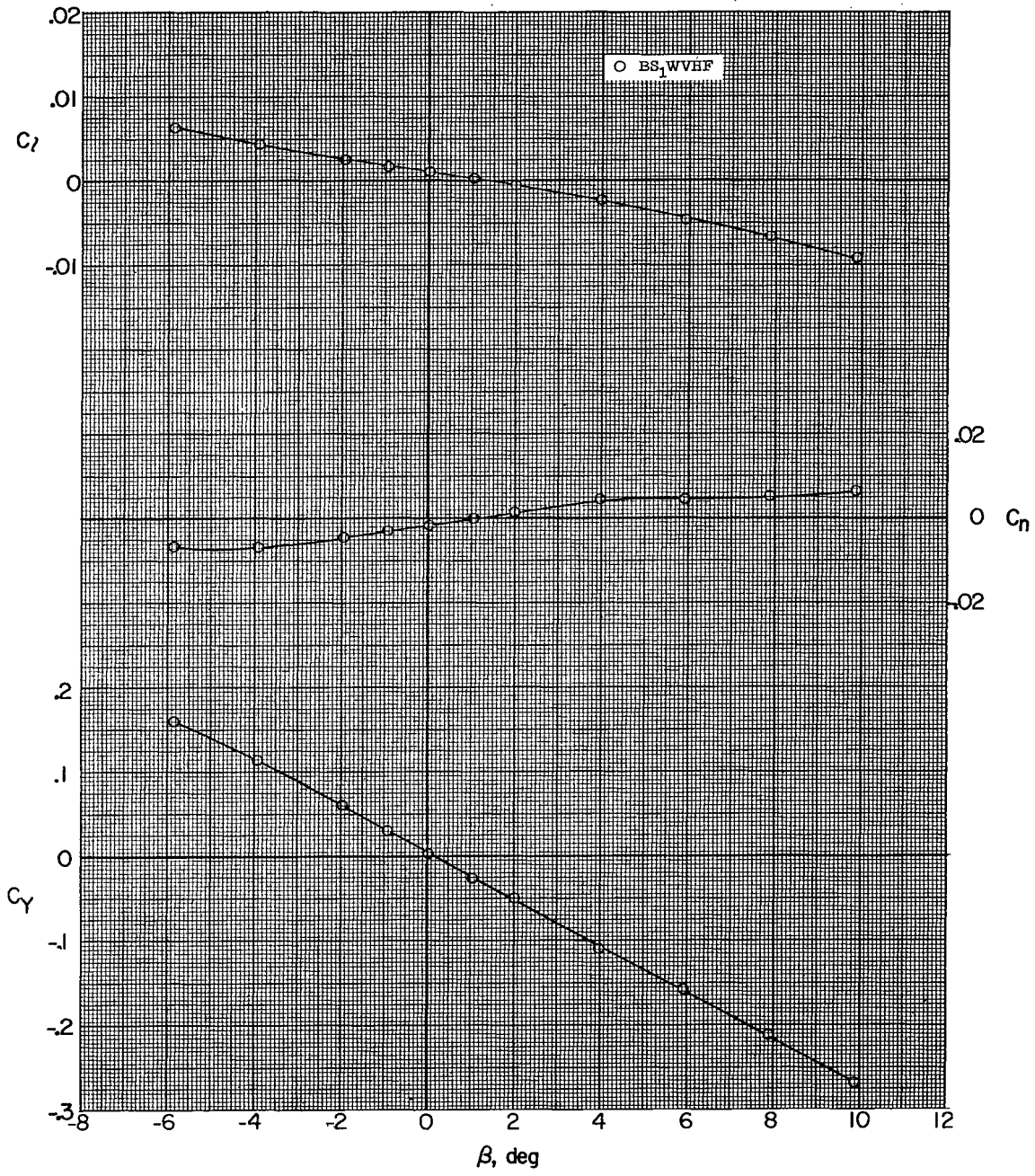

(f) M = 1.90; $\alpha = 16.2^{\circ}$.

Figure 17.- Continued.

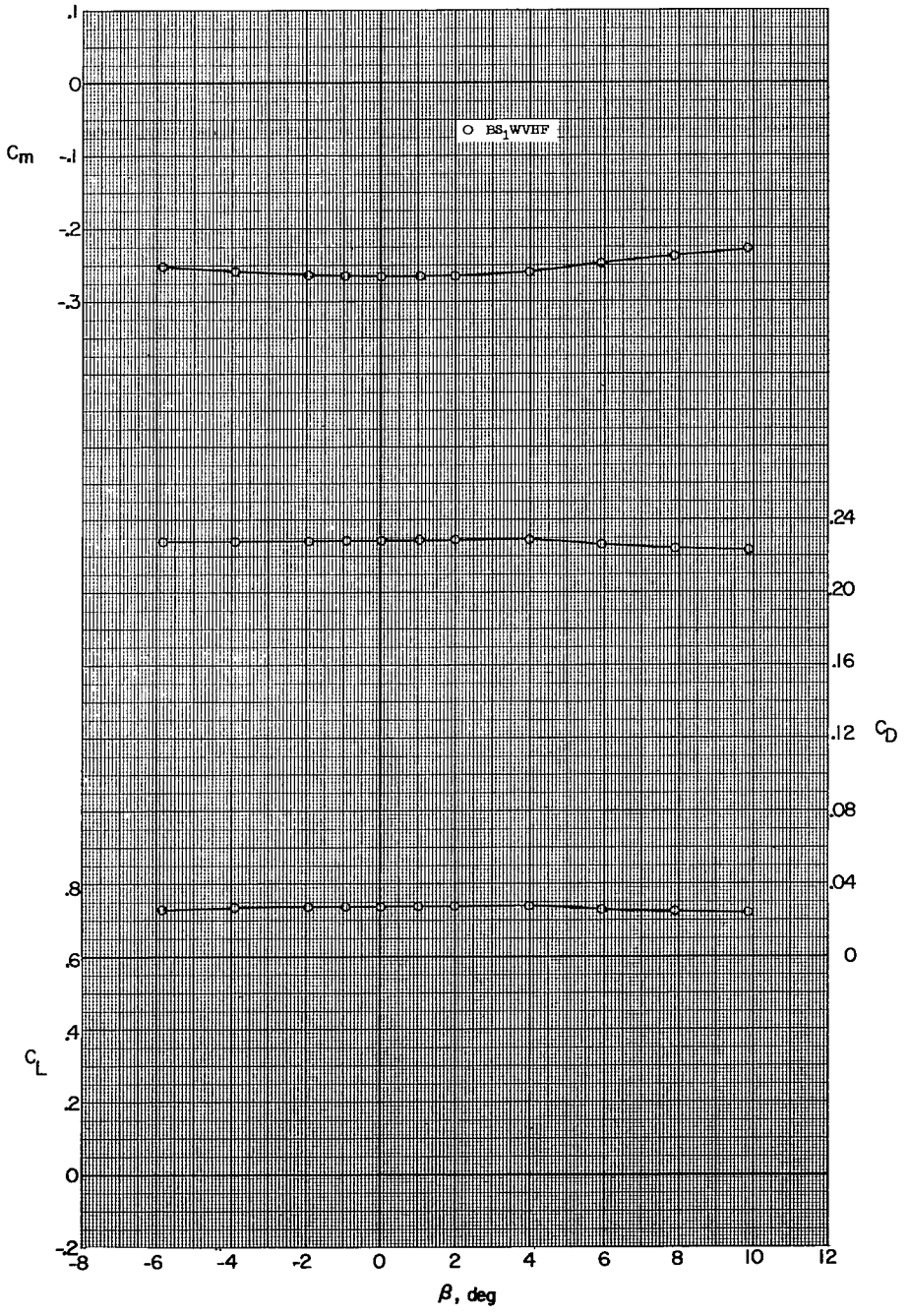

(f) Concluded.

Figure 17.- Continued.

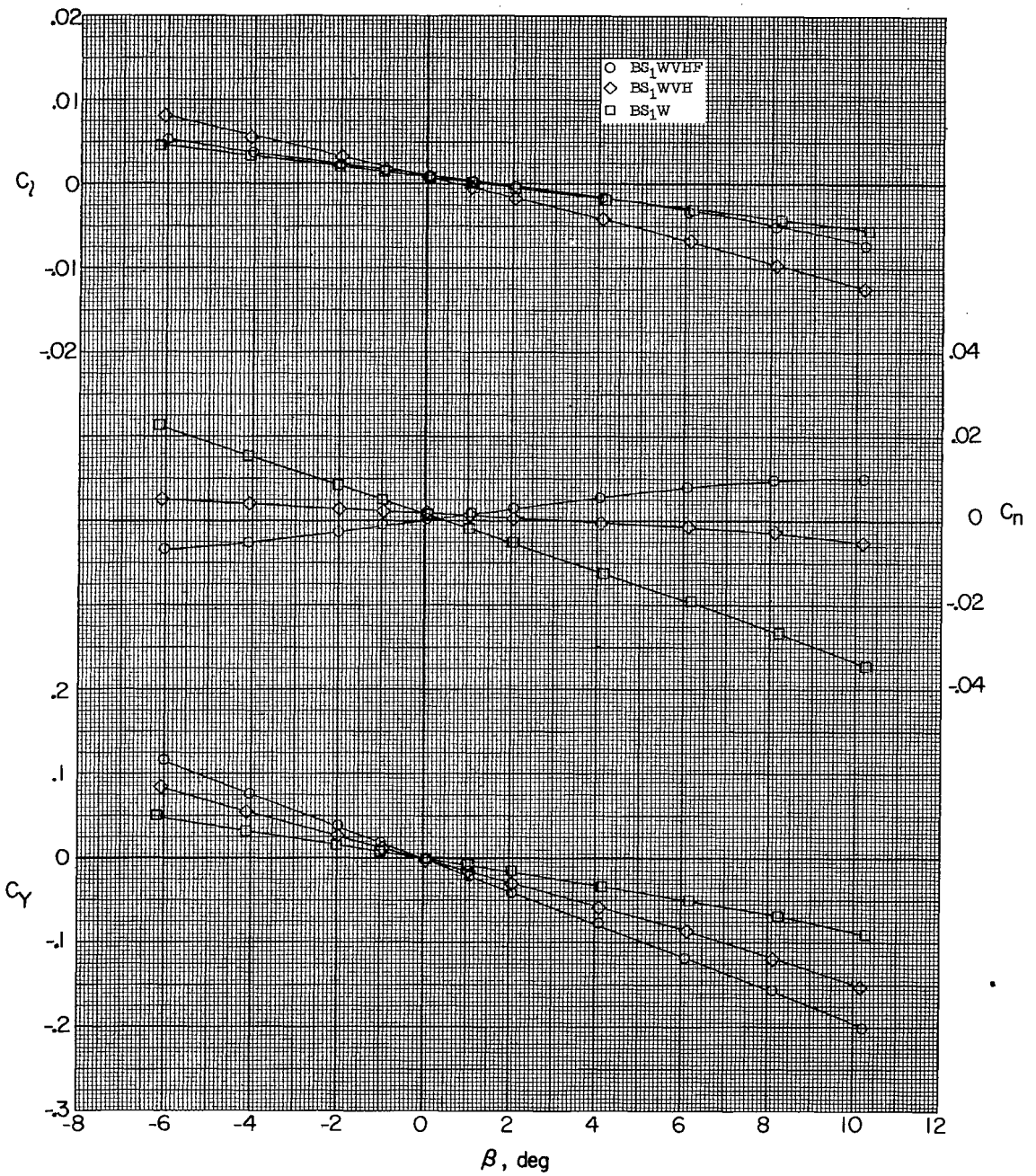

(g) M = 2.20; $\alpha = 1.2^{\circ}$.

Figure 17.- Continued.

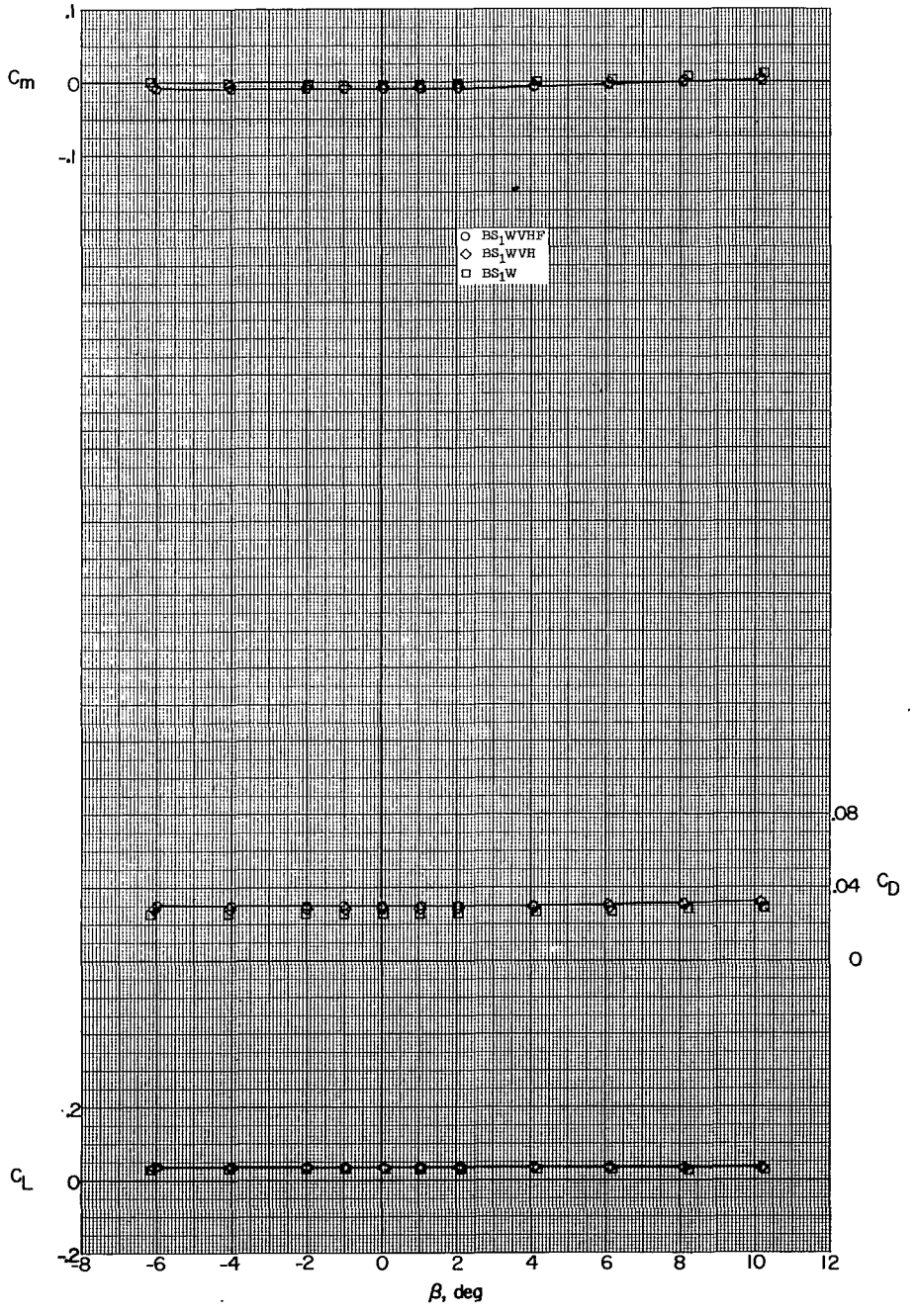

(g) Concluded.

Figure 17.- Continued.

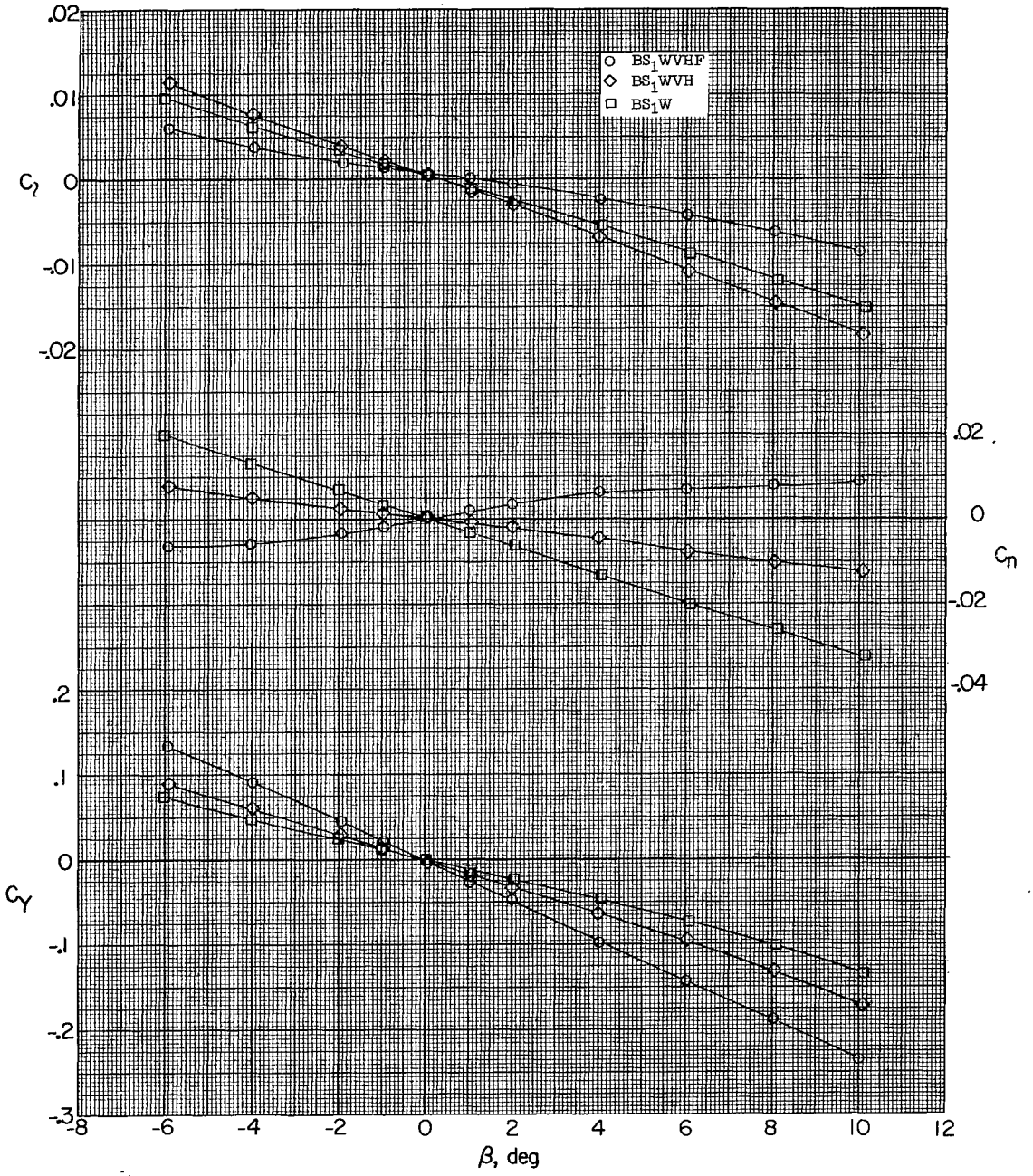

(h) M = 2.20; α = 11.6°.

Figure 17.- Continued.

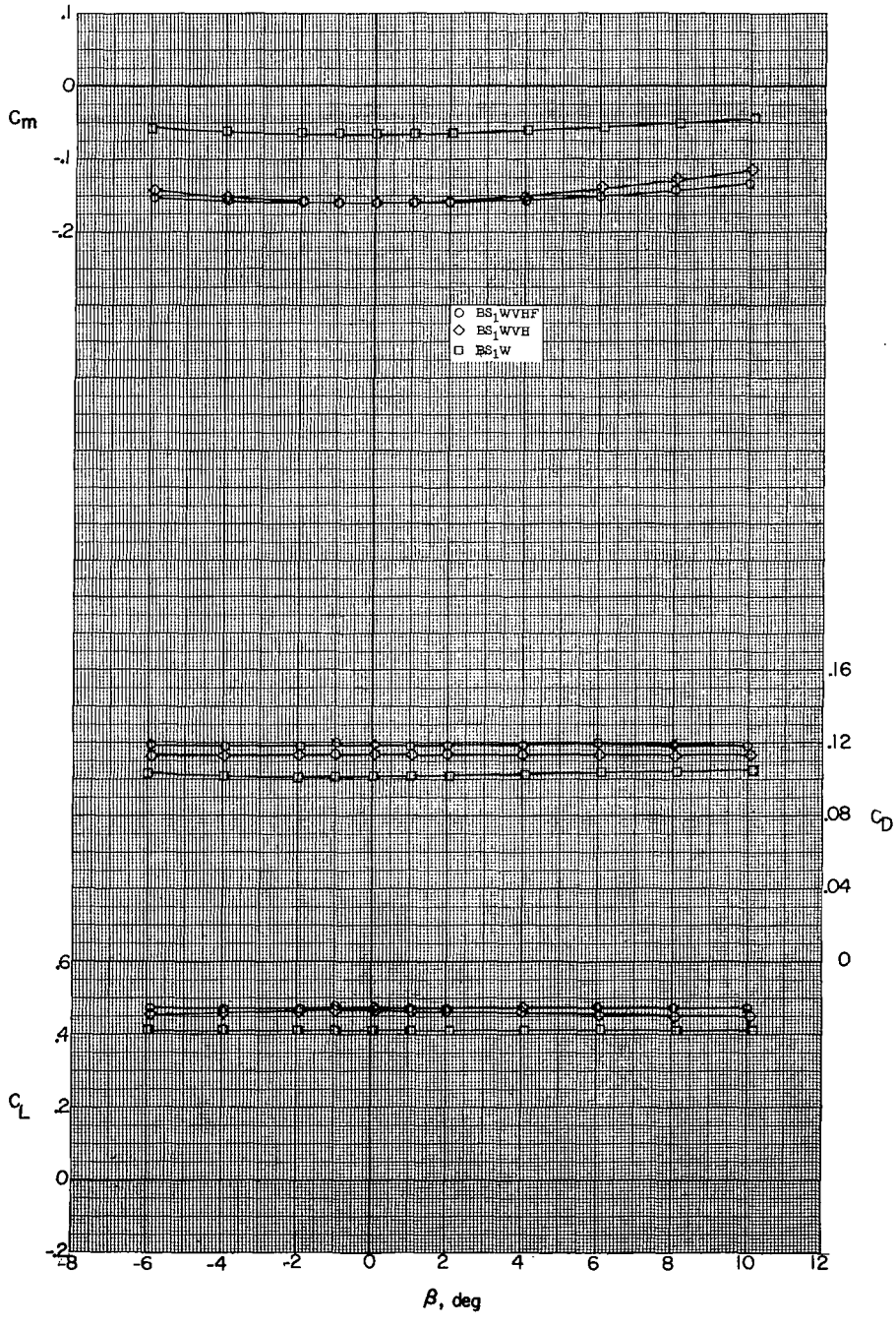

(h) Concluded.

Figure 17.- Continued.

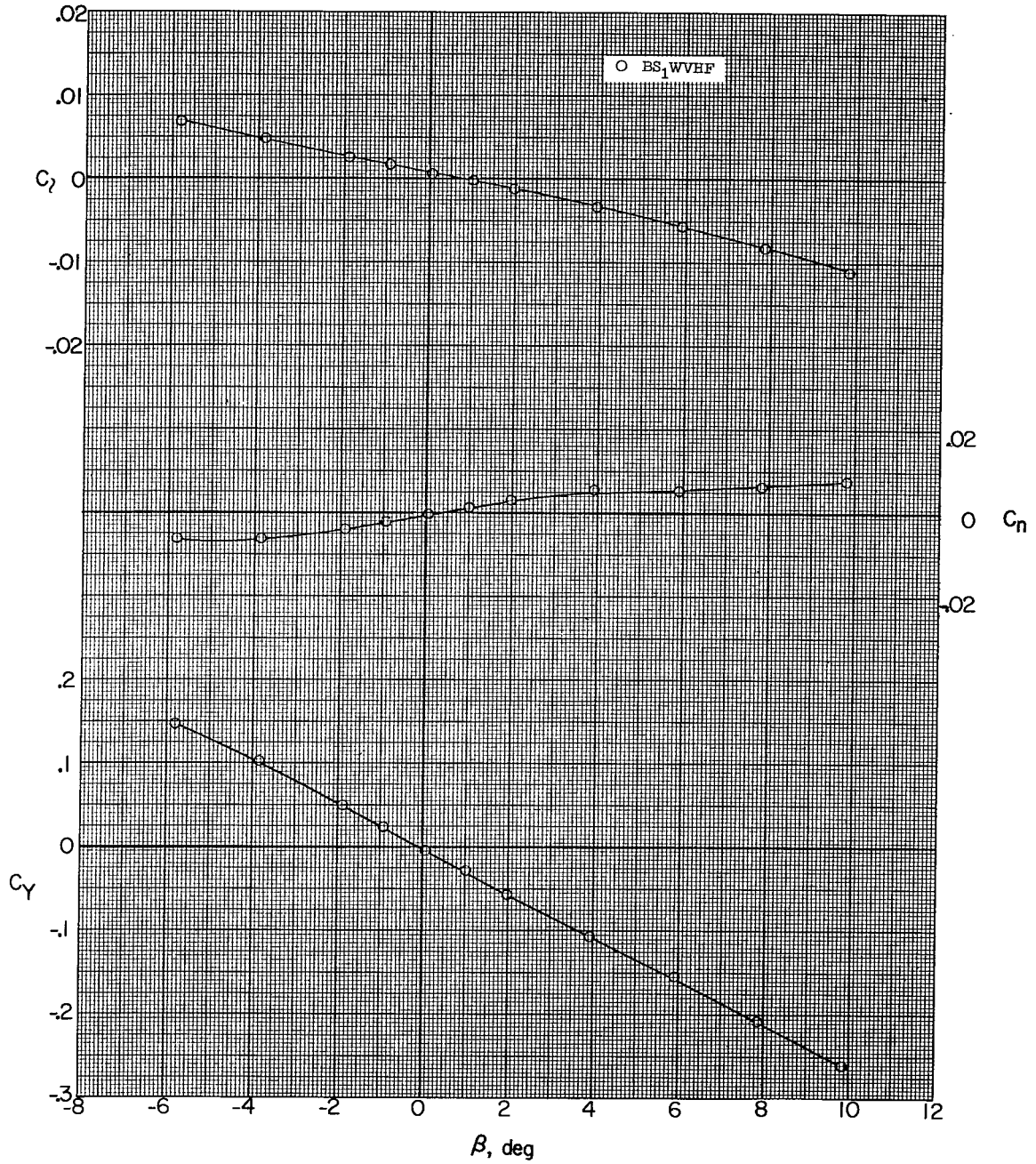

(i) M = 2.20; α = 16.7°.

Figure 17.- Continued.

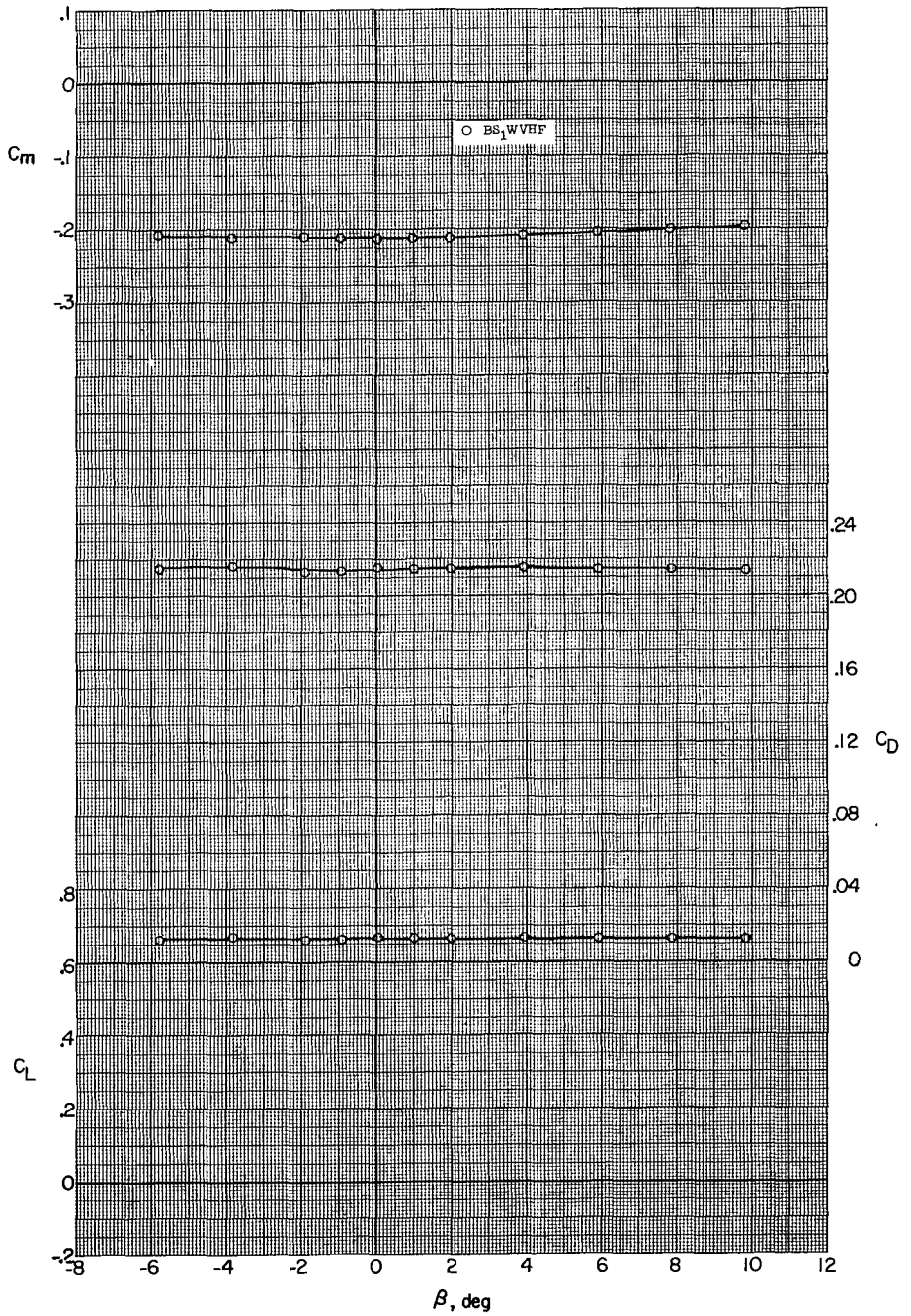

(i) Concluded.

Figure 17.- Continued.

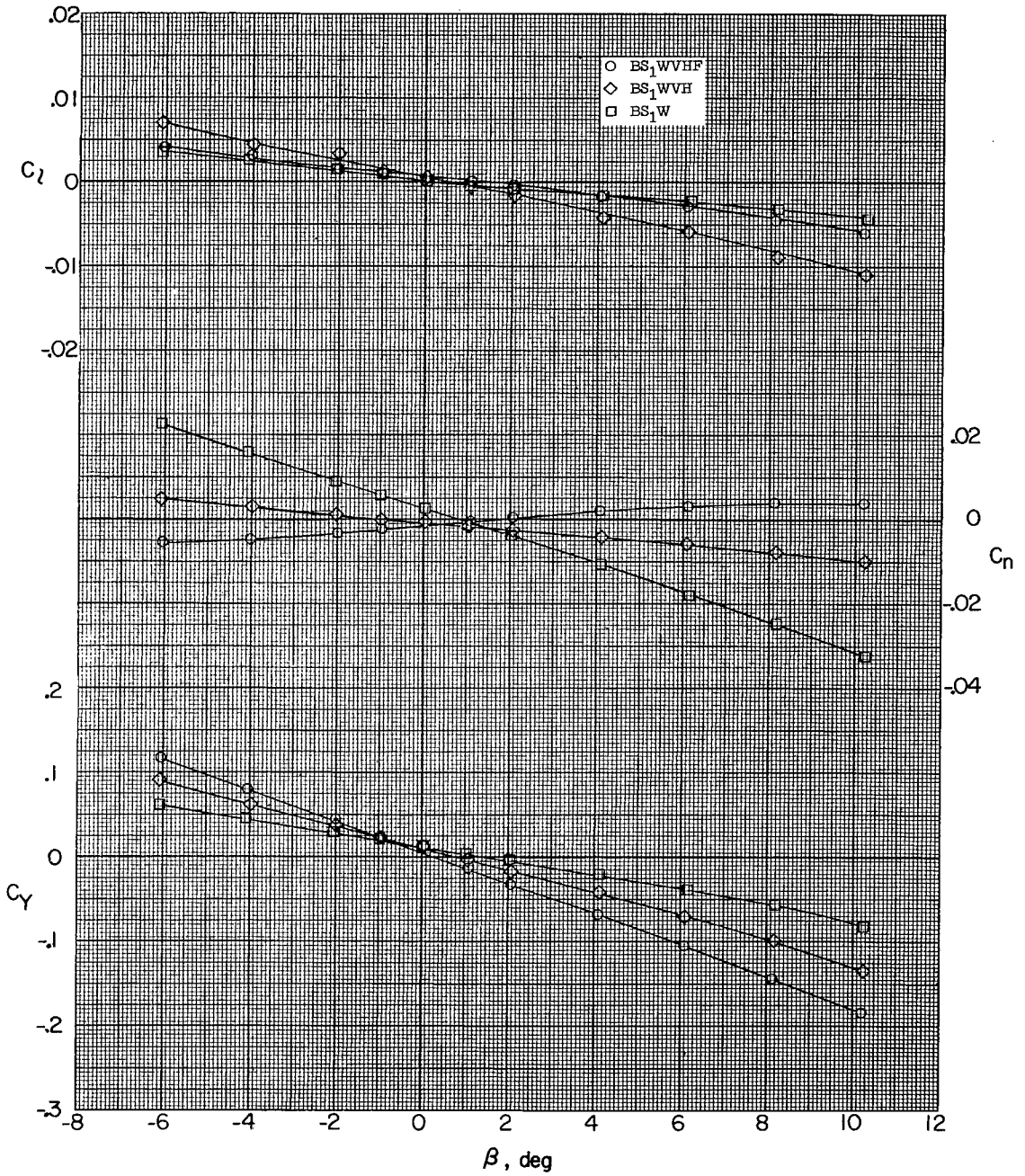

(j) M = 2.50; $\alpha = 0.5^{\circ}$.

Figure 17.- Continued.

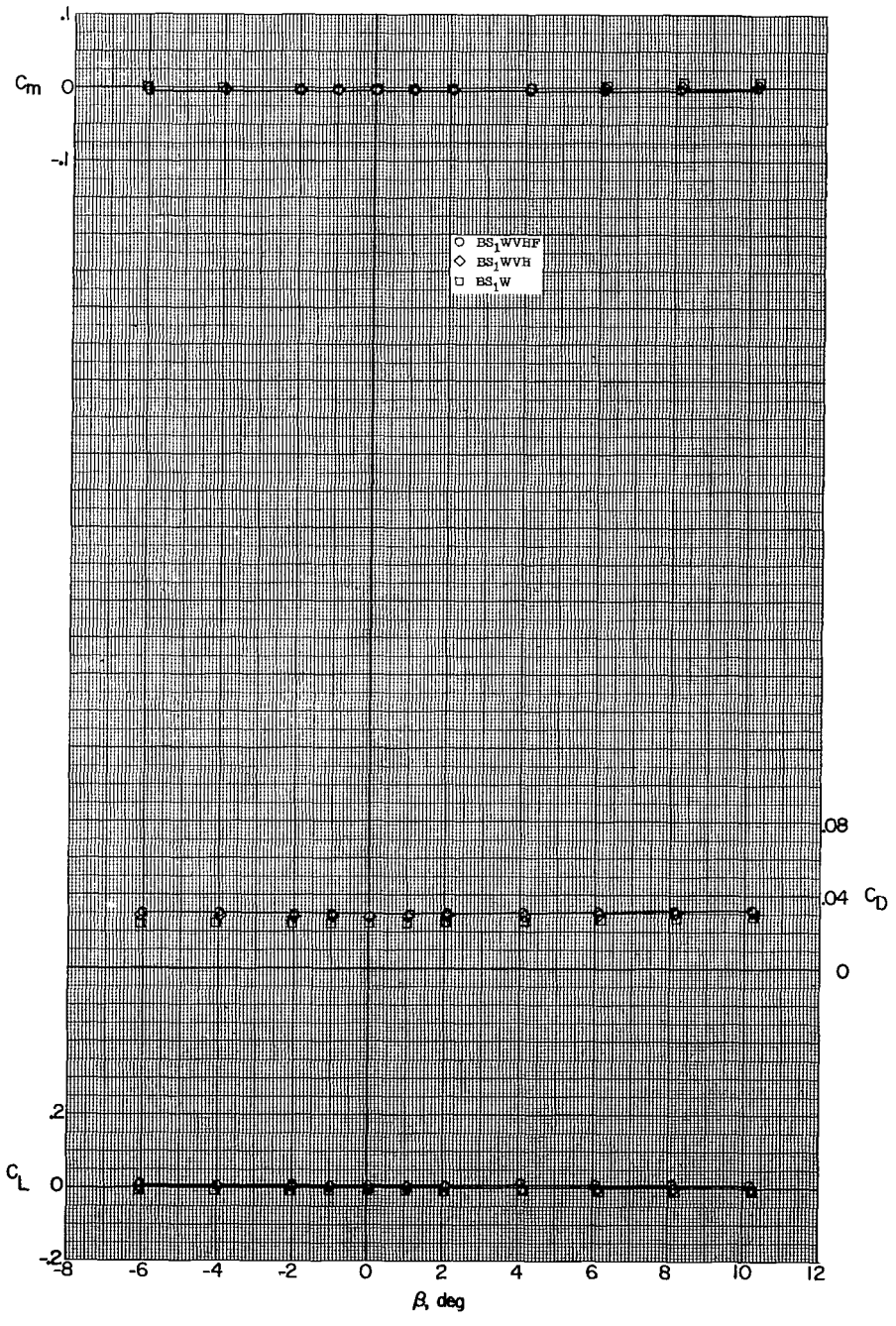

(j) Concluded.

Figure 17.- Continued.

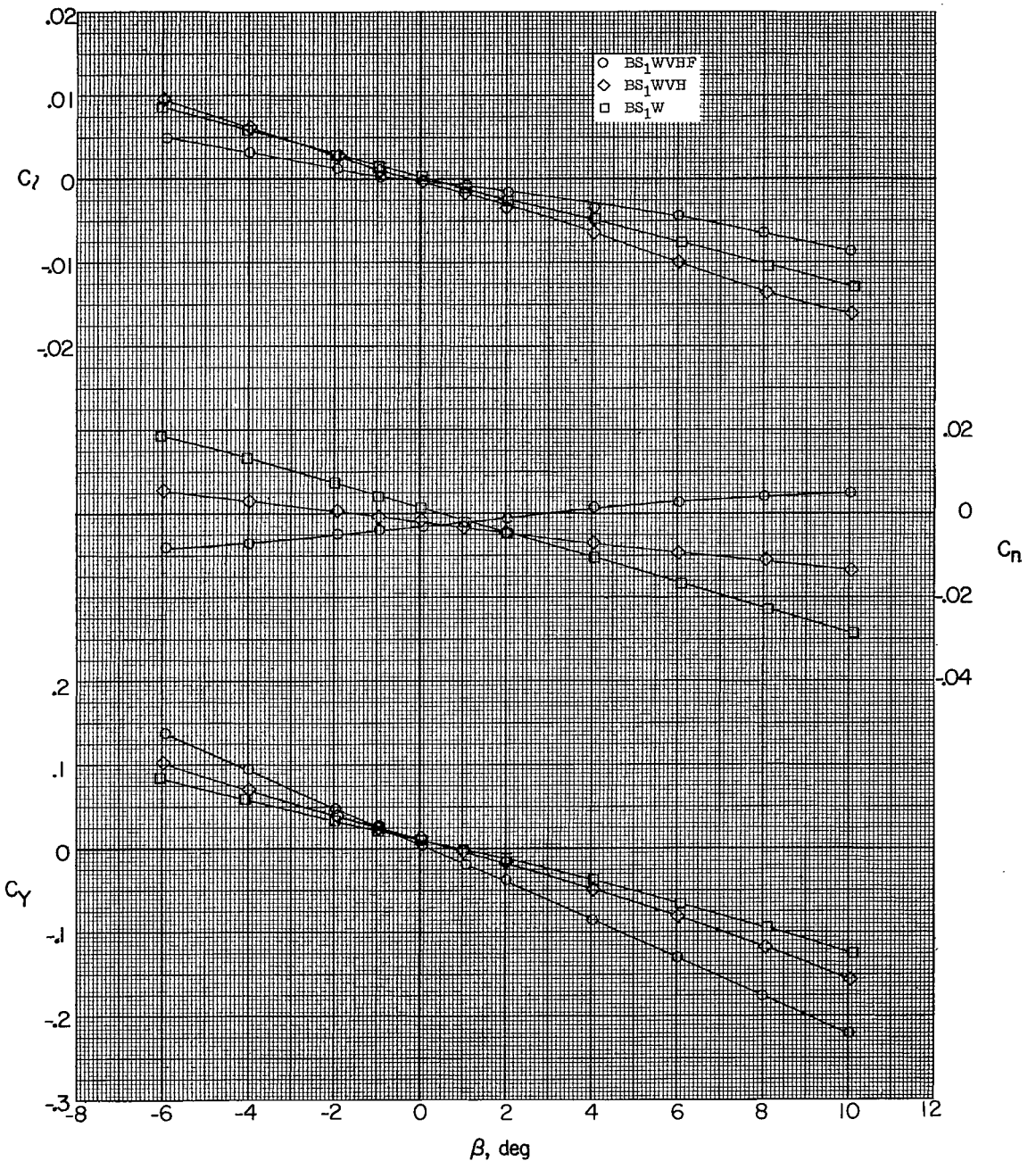

(k) M = 2.50; α = 10.8°.

Figure 17.- Continued.

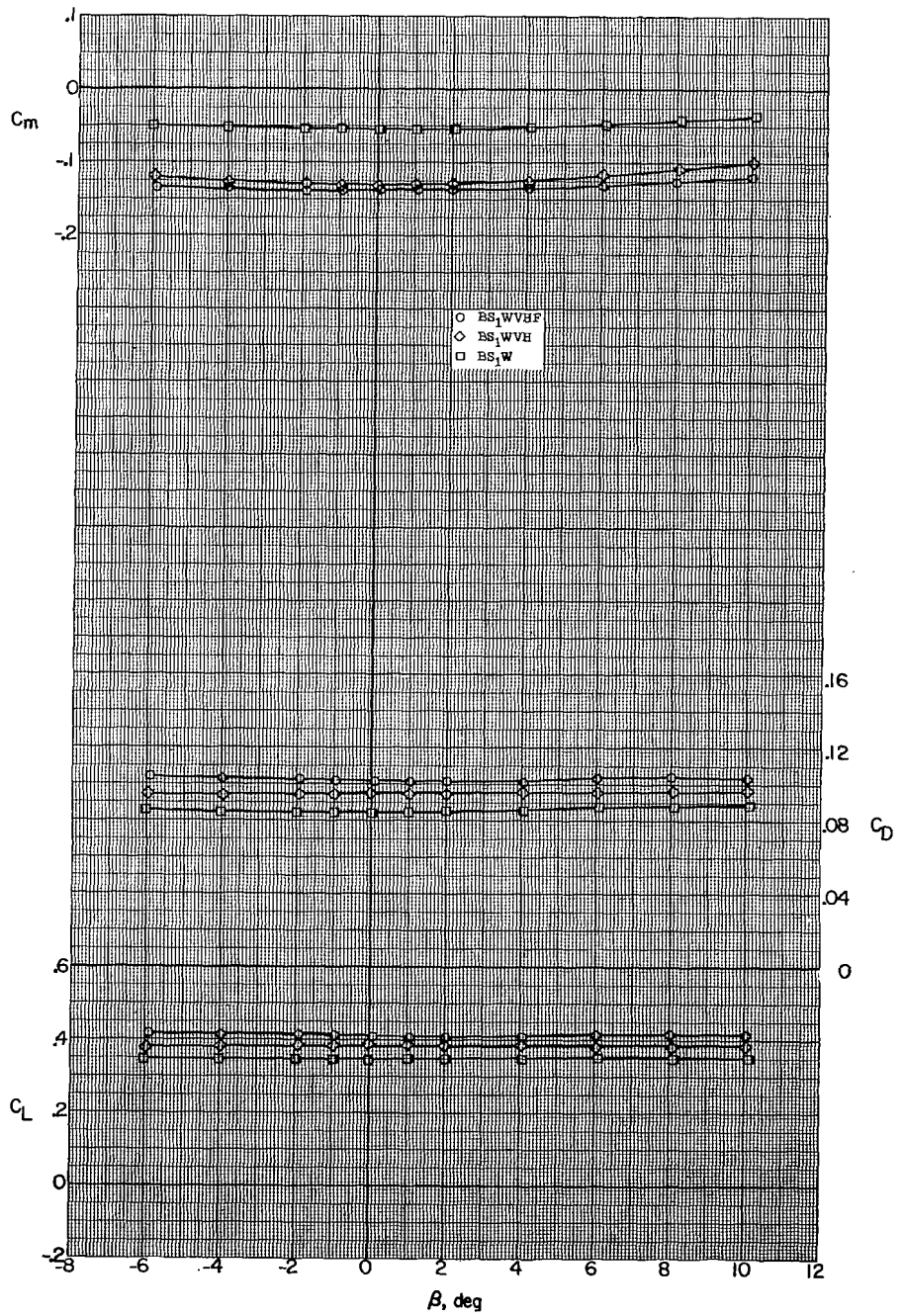

(k) Concluded.

Figure 17.- Continued.

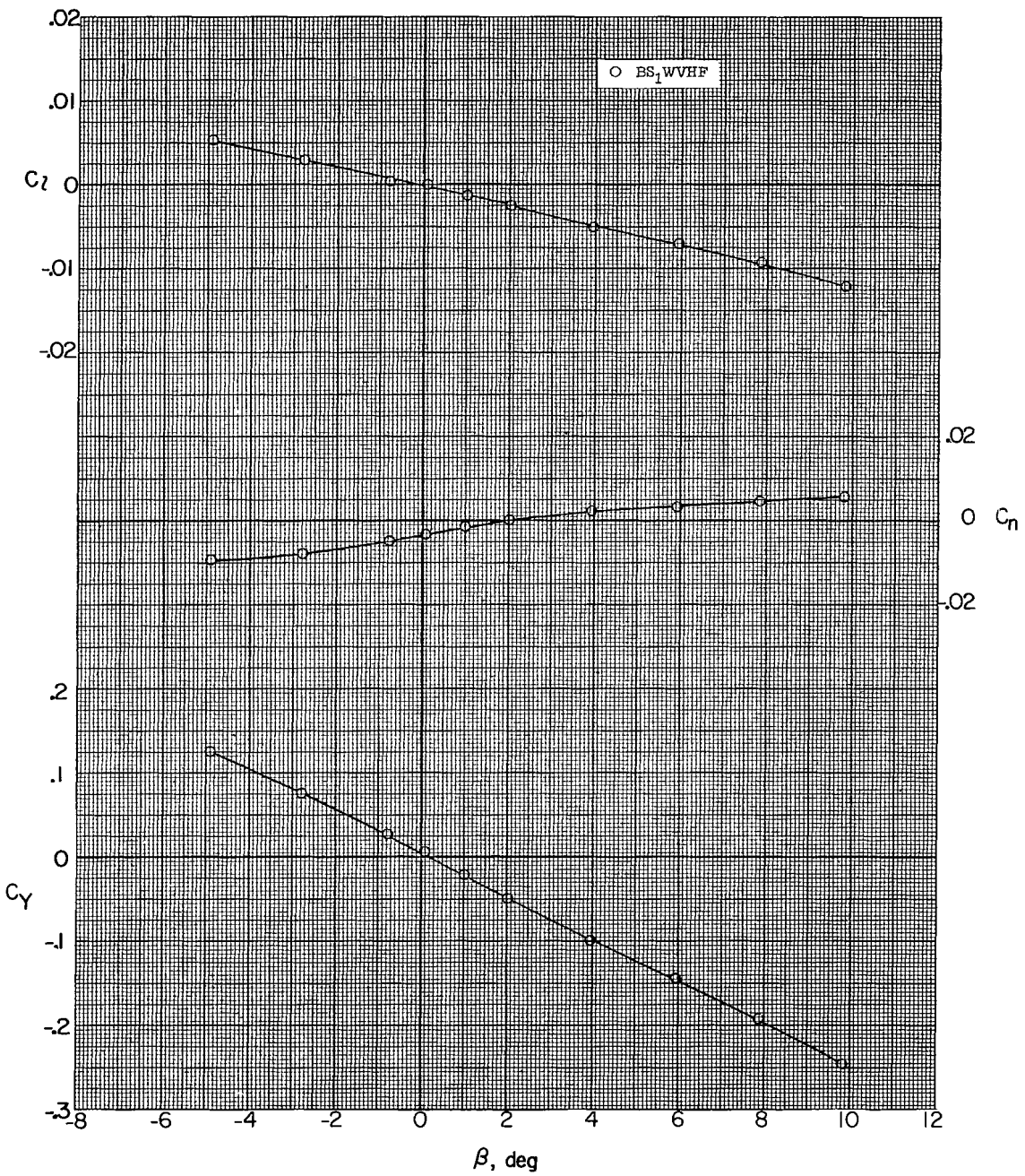

(*l*) M = 2.50; α = 15.9°.

Figure 17.- Continued.

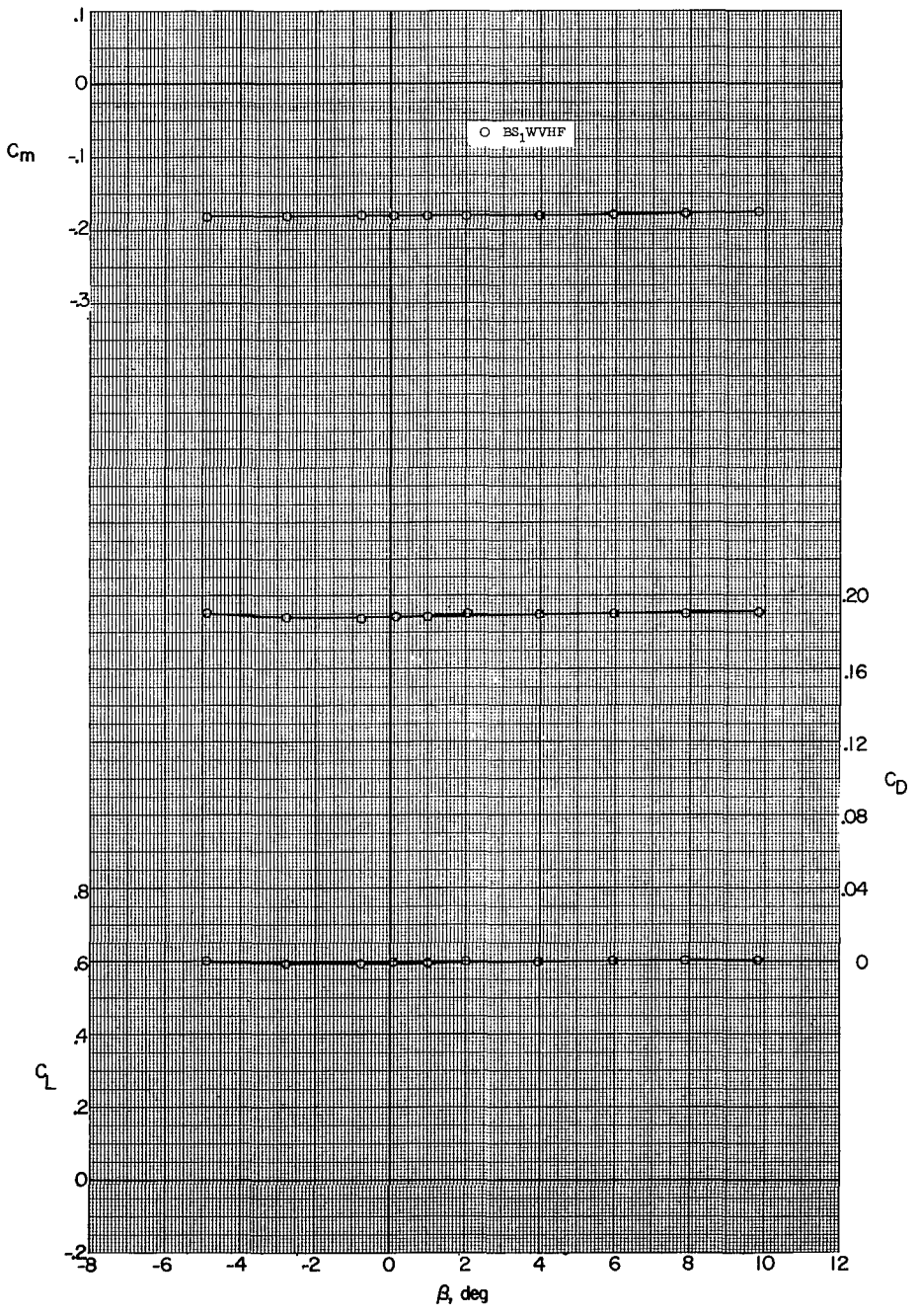

(l) Concluded.

Figure 17.- Concluded.

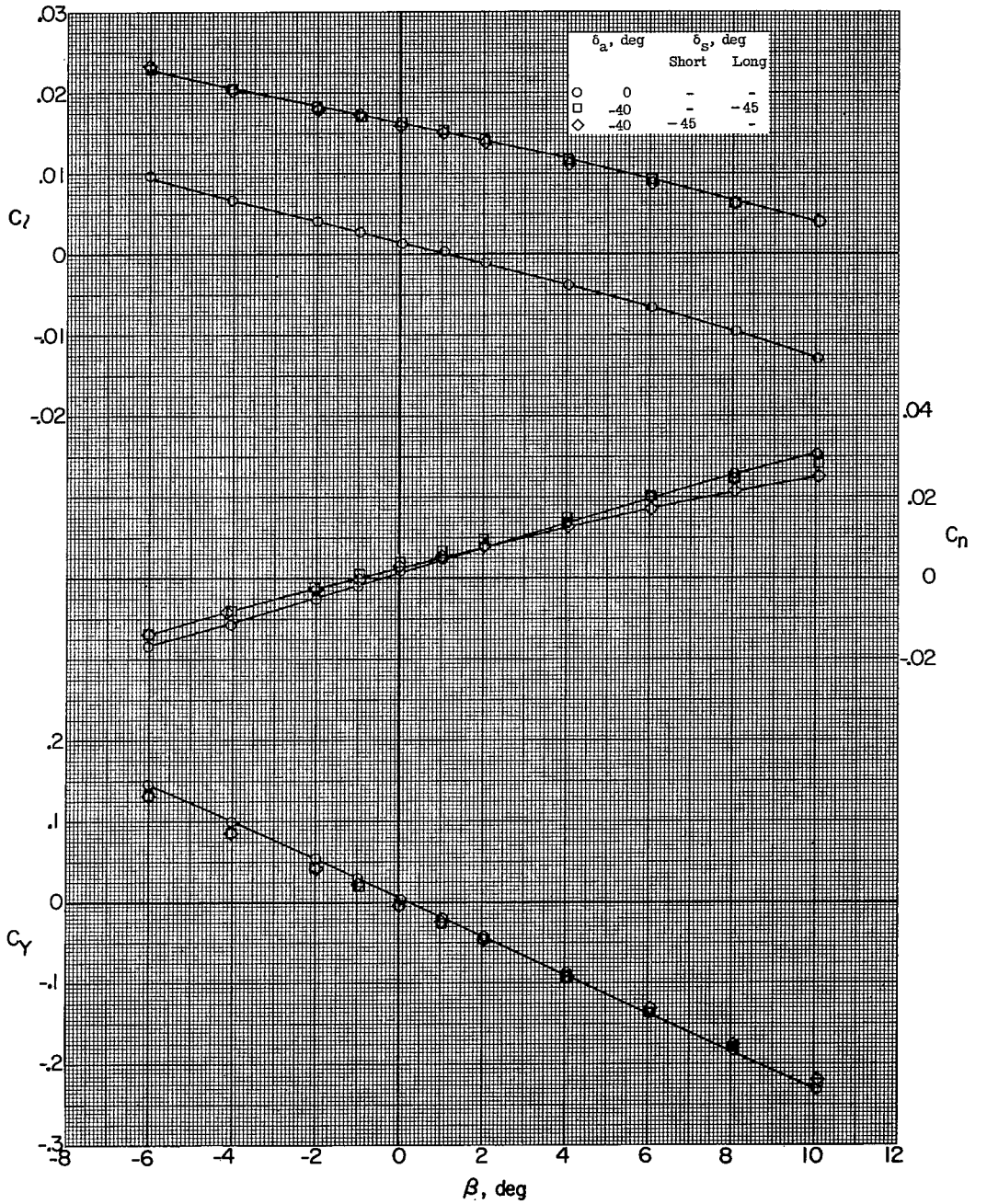

(a) M = 1.60; $\alpha = 0.5^\circ$.

Figure 18.- Effect of combined deflections of aileron and long and short spoilers on aerodynamic characteristics in sideslip. BS_1WVHF.

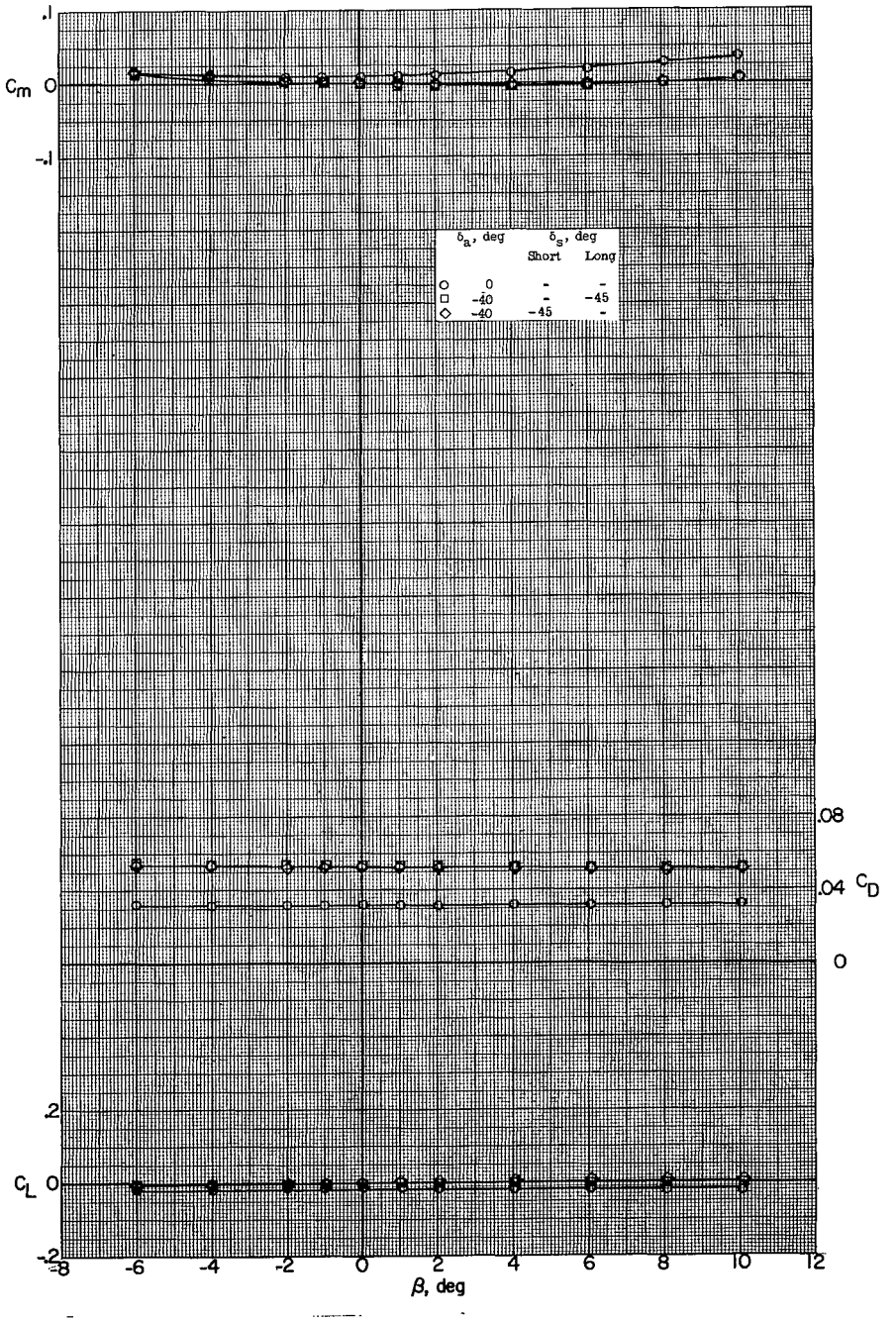

(a) Concluded.

Figure 18.- Continued.

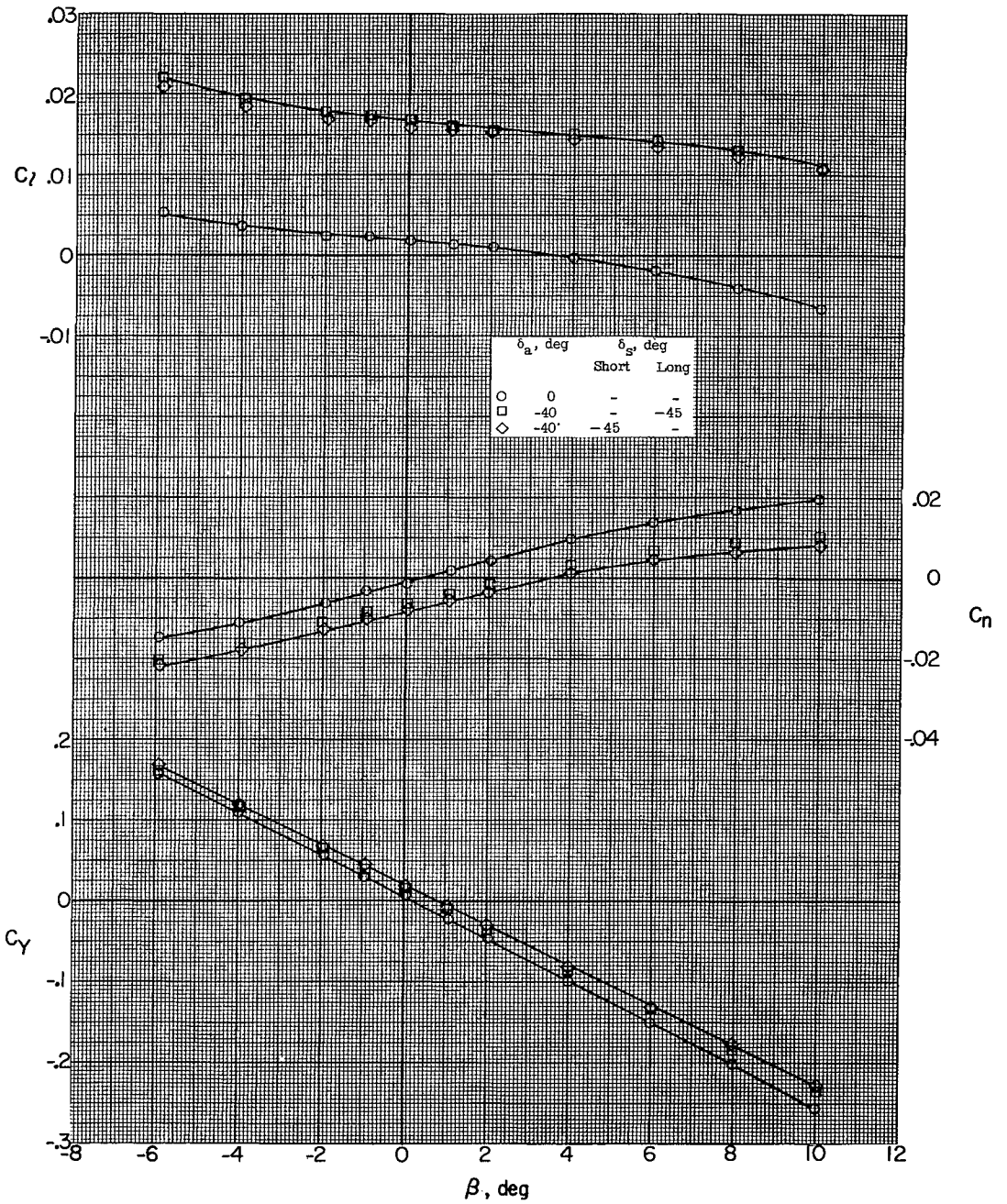

(b) M = 1.60; α = 10.9°.

Figure 18.- Continued.

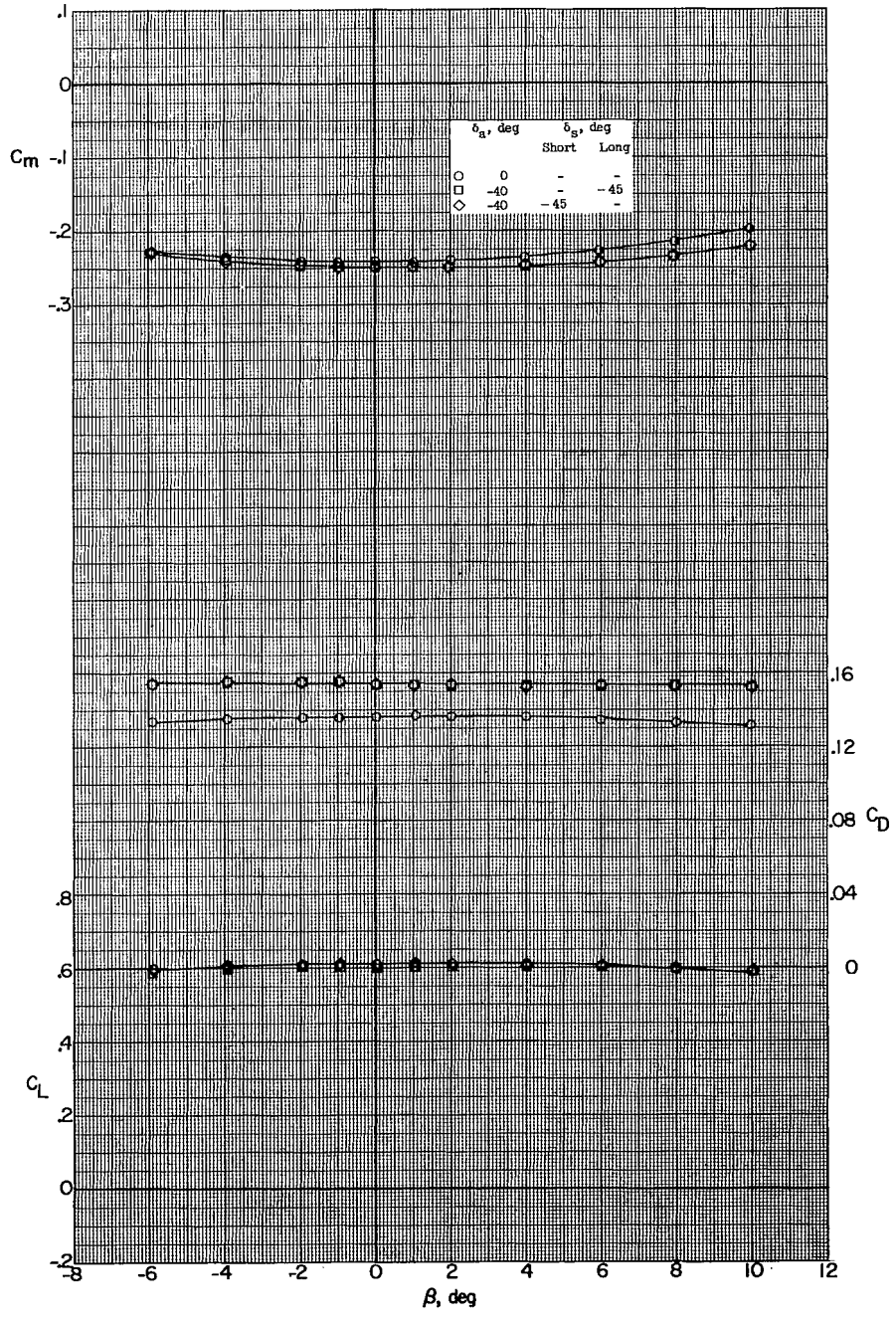

(b) Concluded.

Figure 18.- Continued.

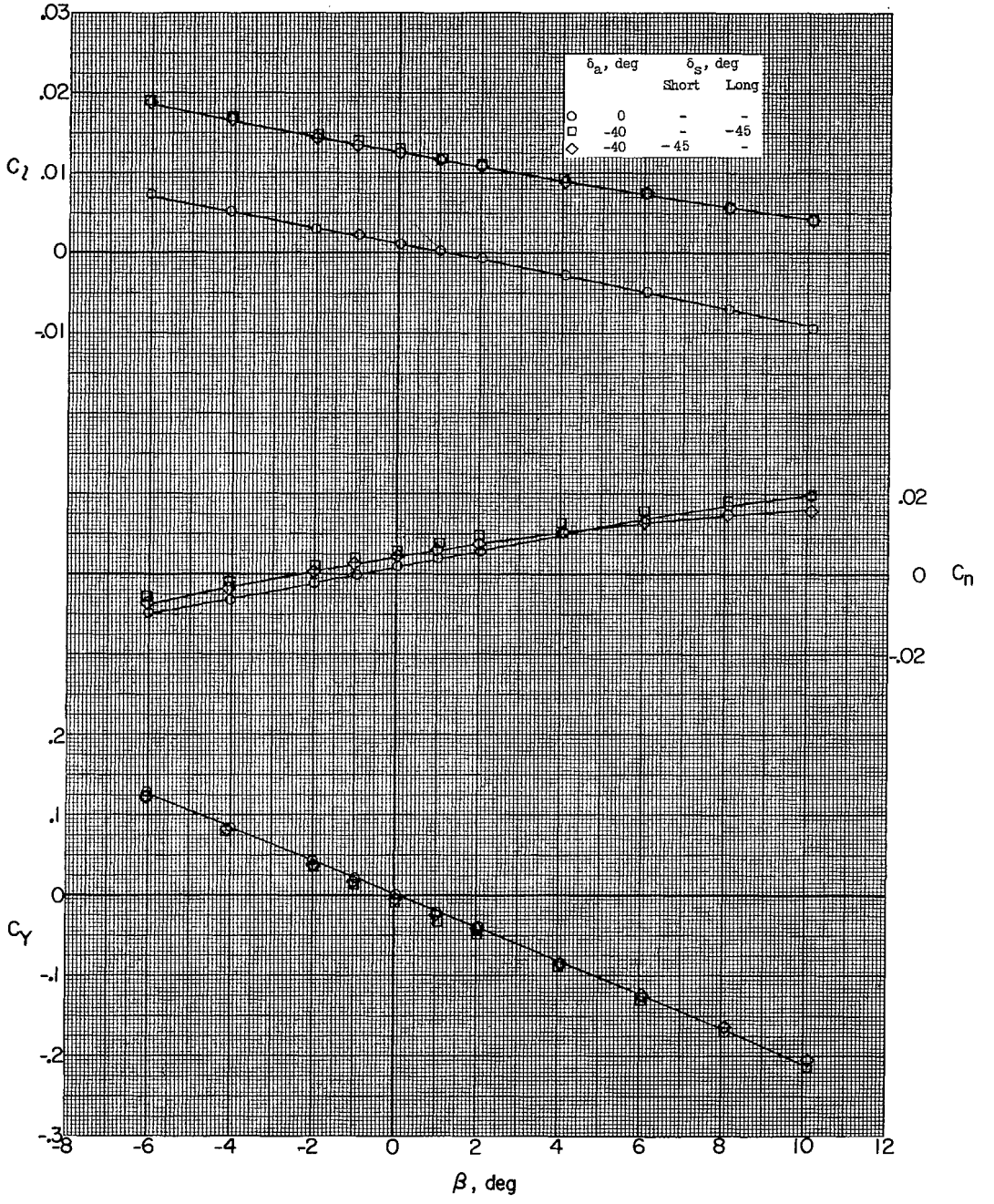

(c) M = 1.90; $\alpha = 0.7^{\circ}$.

Figure 18.- Continued.

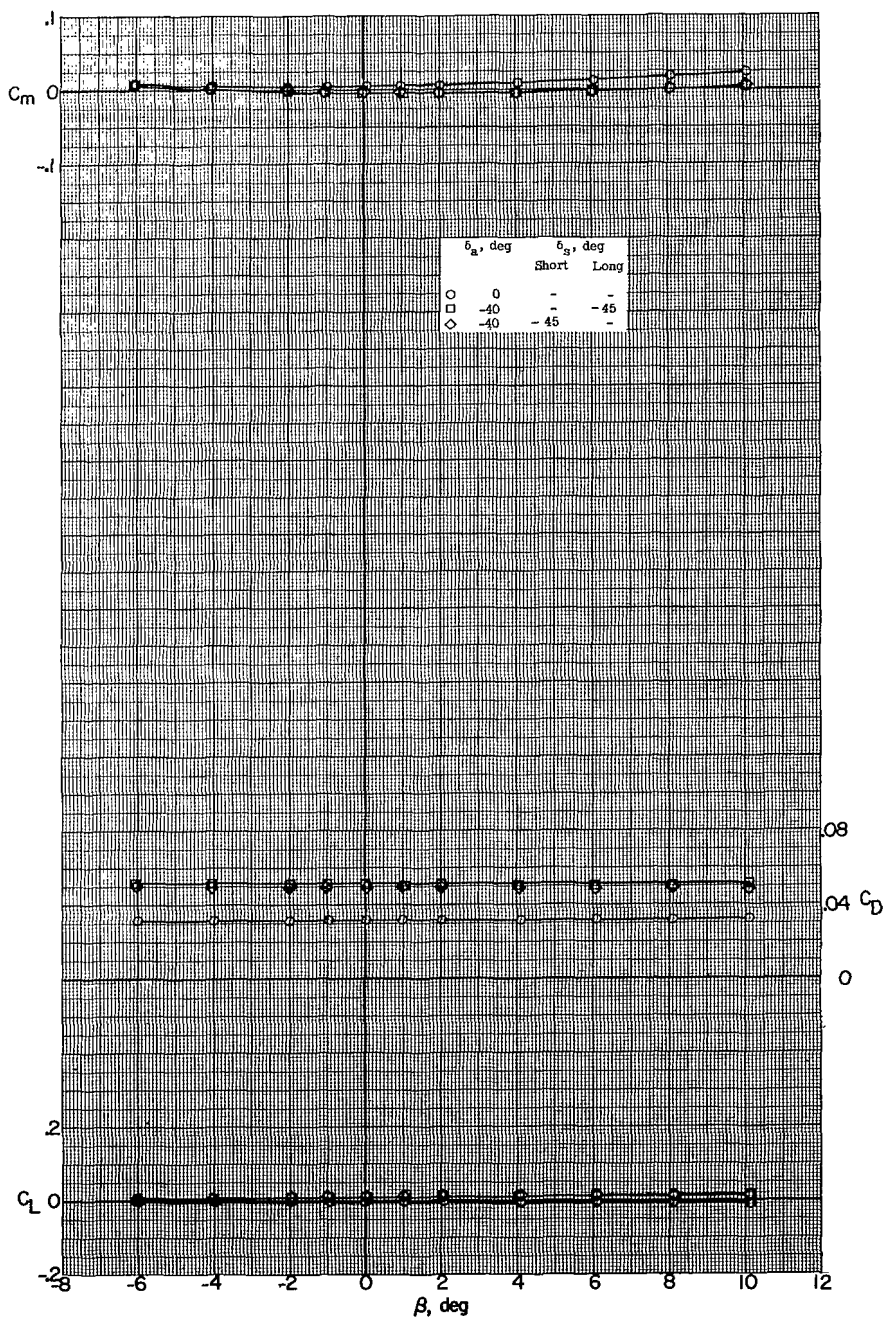

(c) Concluded.

Figure 18.- Continued.

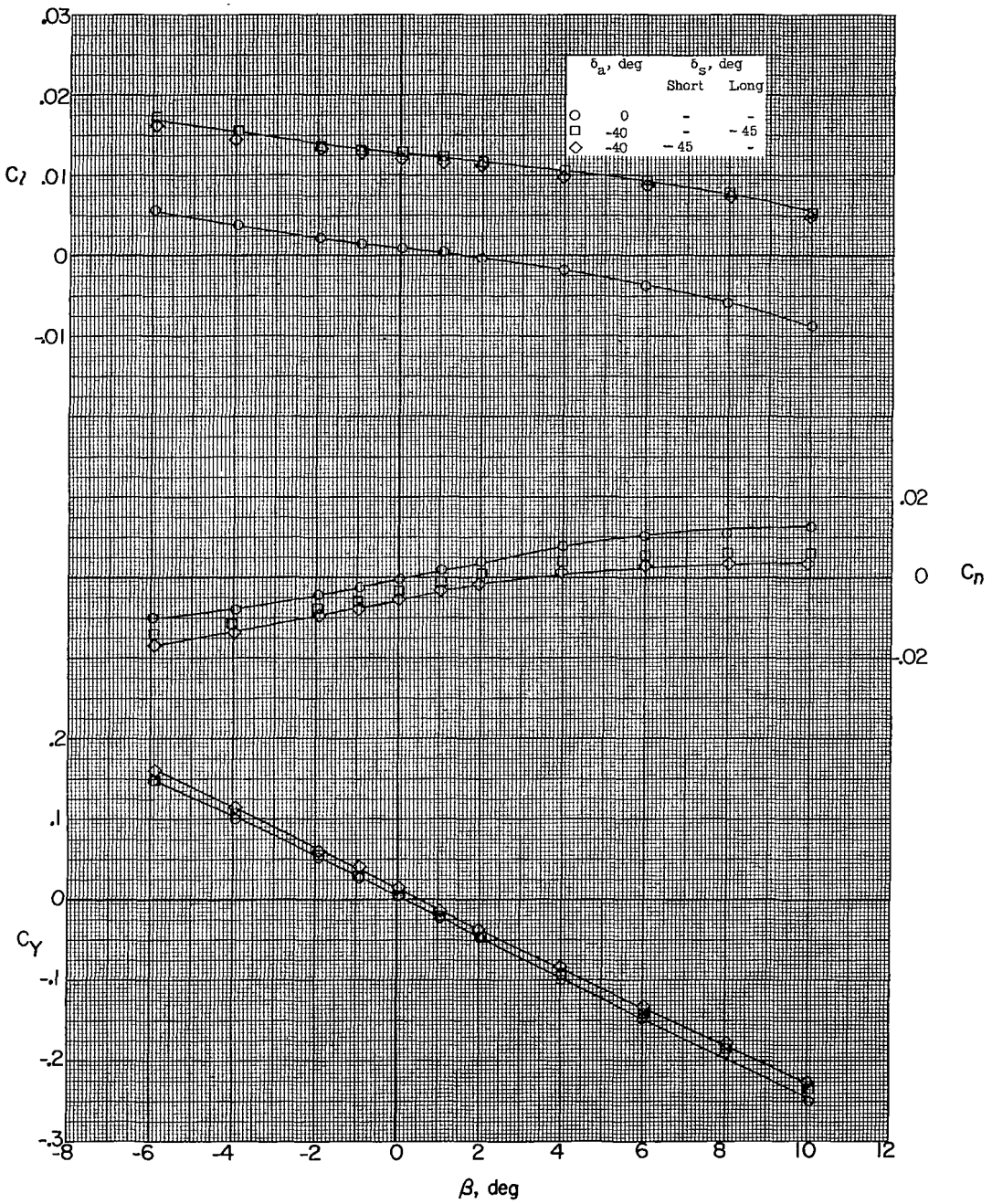

(d) M = 1.90; α = 11.0°.

Figure 18.- Continued.

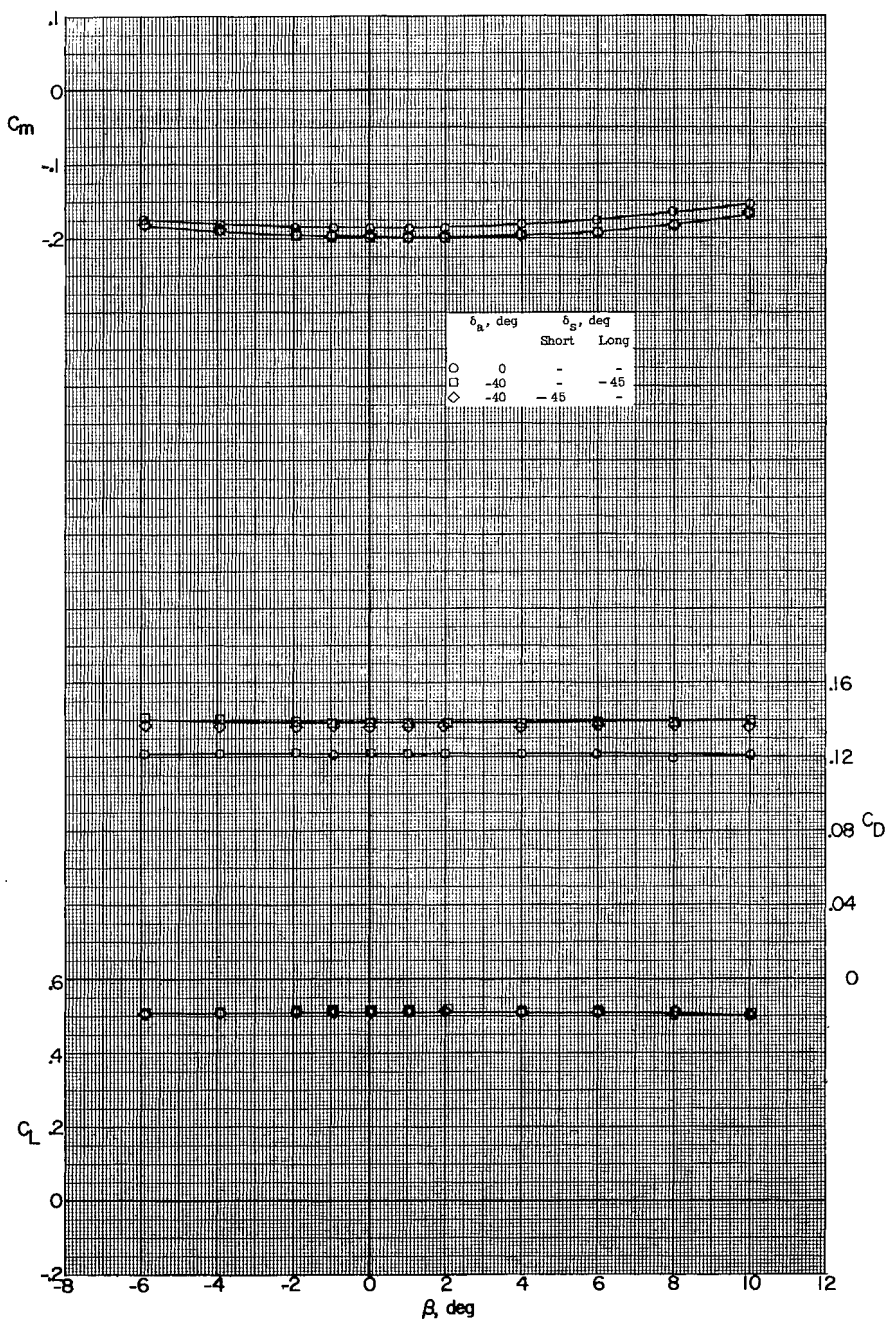

(d) Concluded.

Figure 18.- Continued.

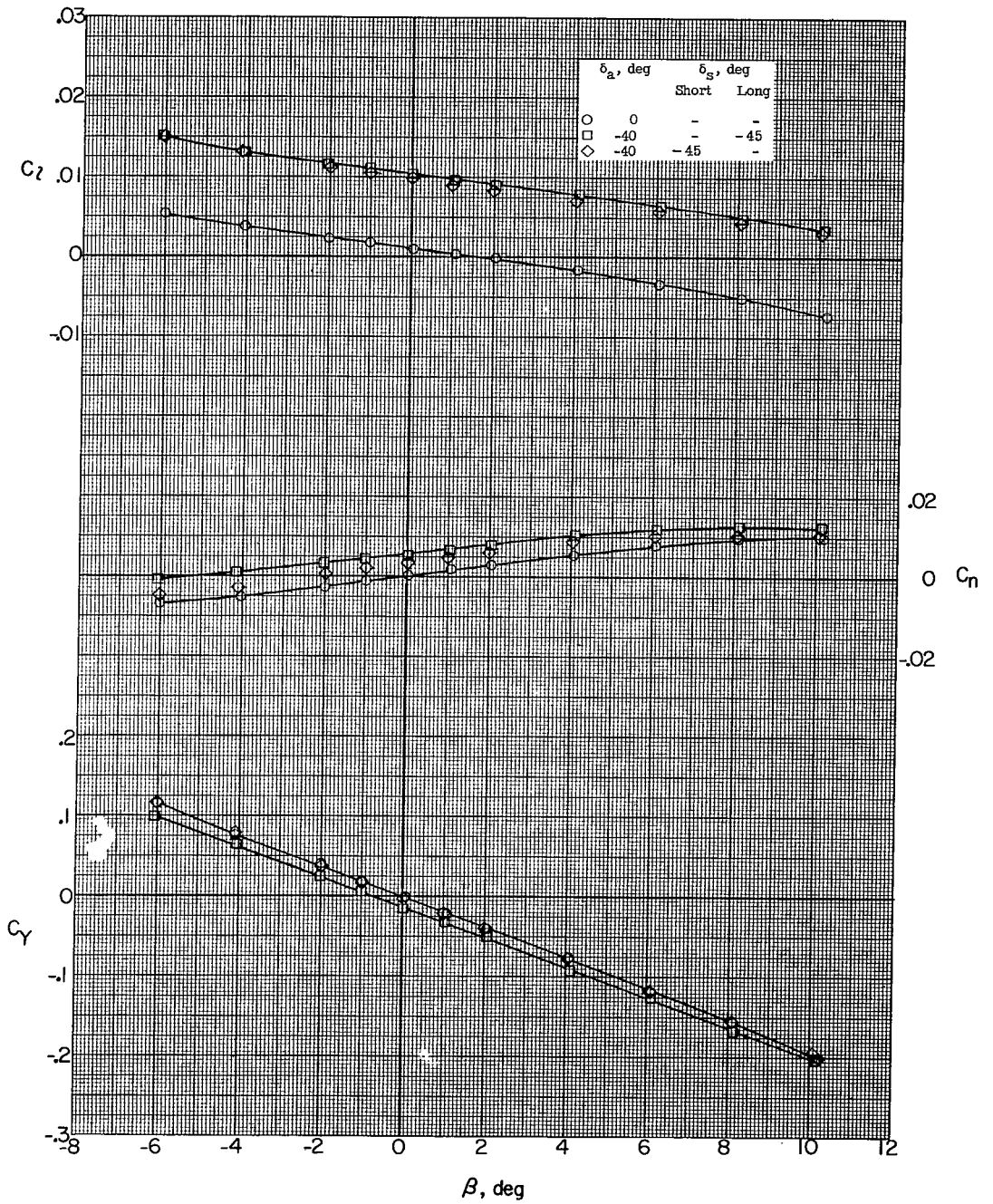

(e) M = 2.20; $\alpha = 1.2^\circ$.

Figure 18.- Continued.

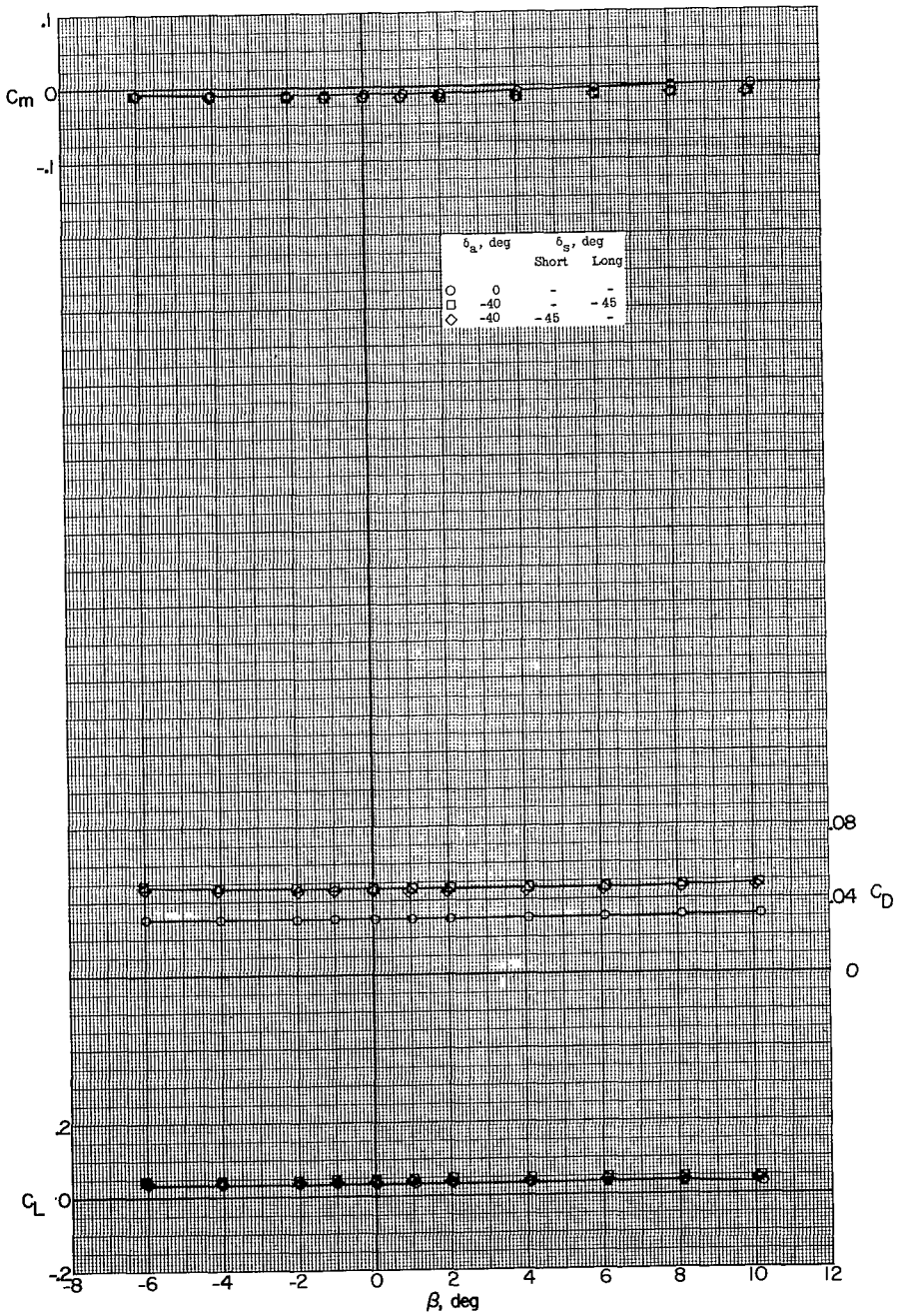

(e) Concluded.

Figure 18.- Continued.

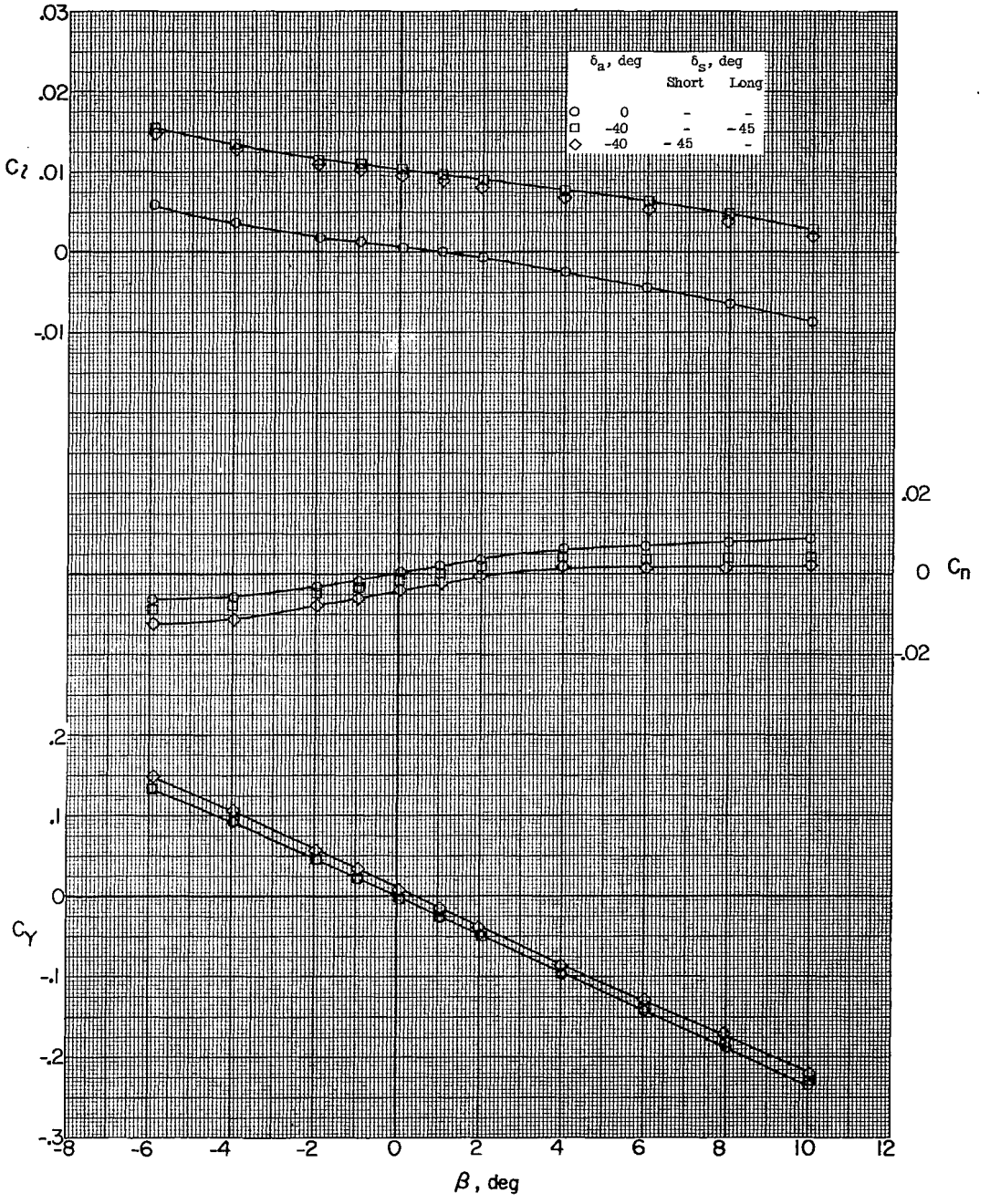

(f) M = 2.20; α = 11.5°.

Figure 18.- Continued.

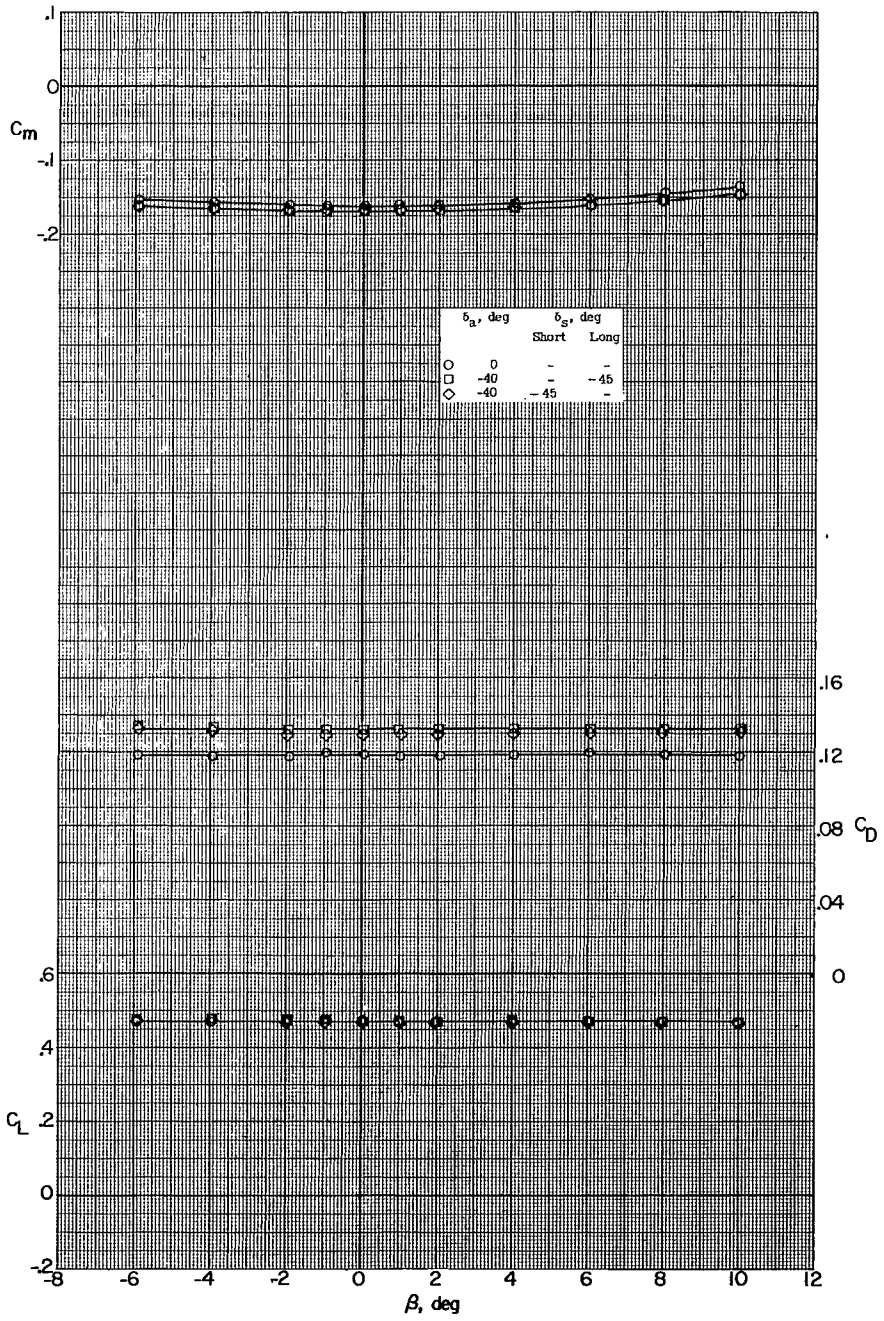

(f) Concluded.

Figure 18.- Continued.

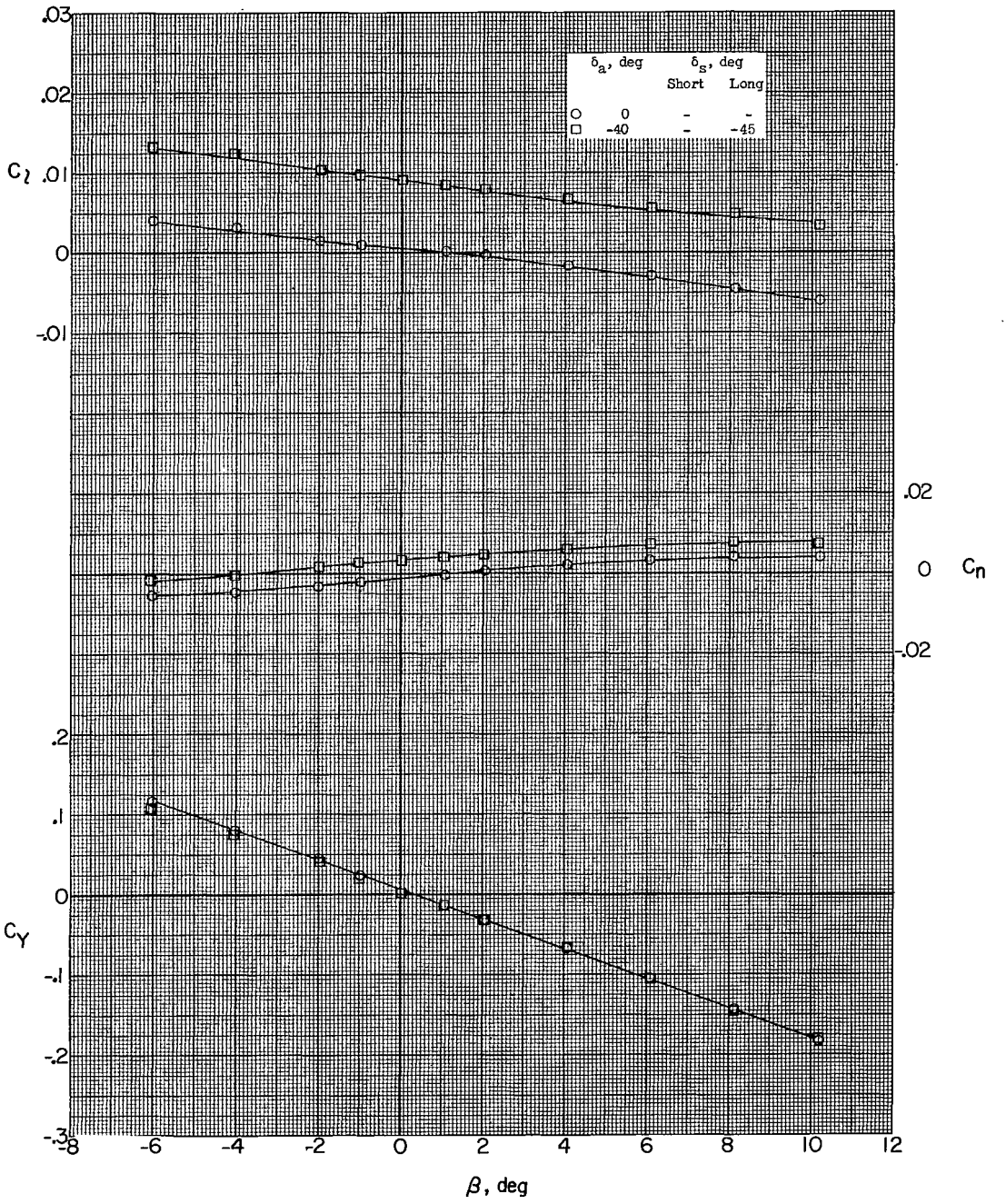

(g) M = 2.50; $\alpha = 0.5^\circ$.

Figure 18.- Continued.

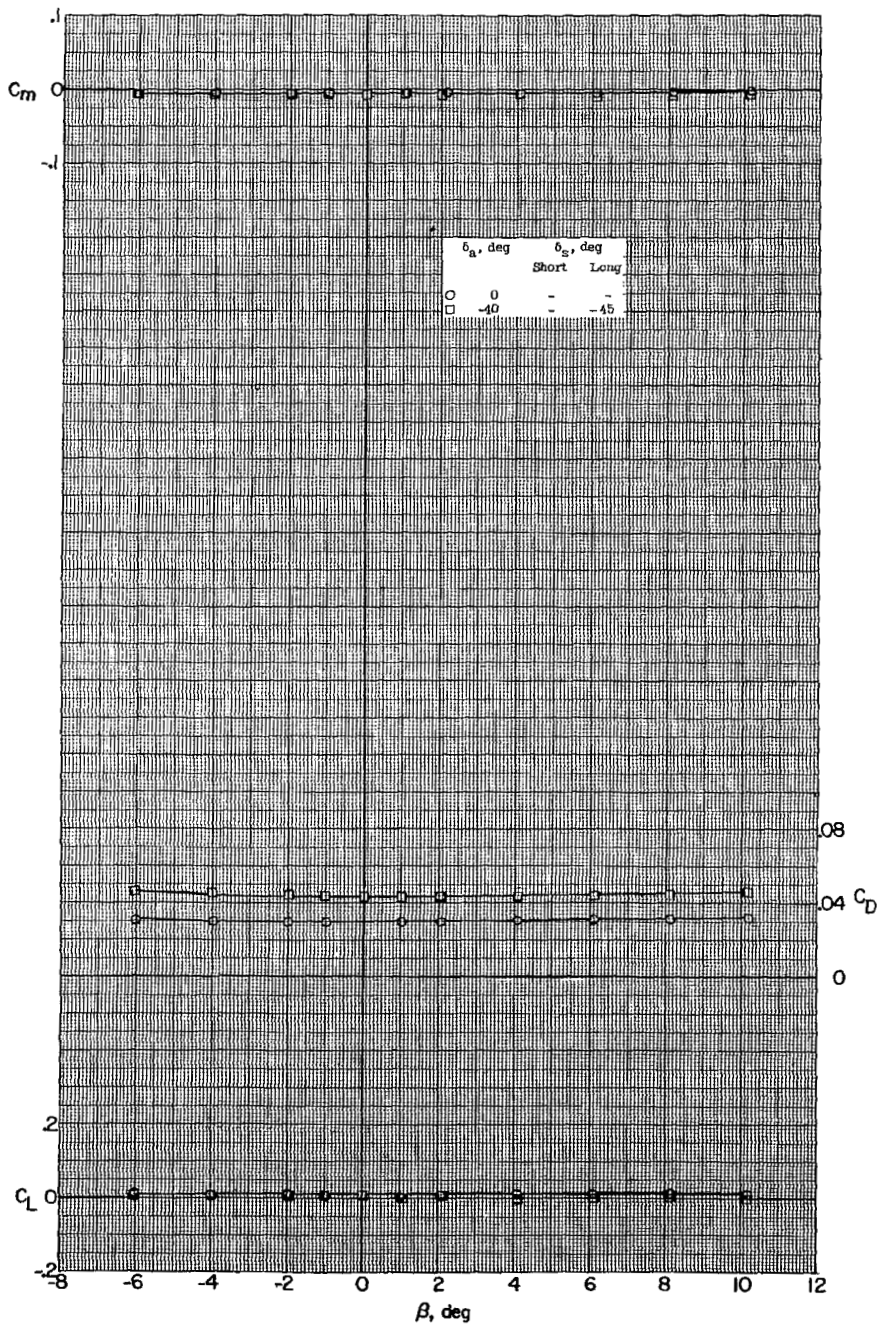

(g) Concluded.

Figure 18.- Continued.

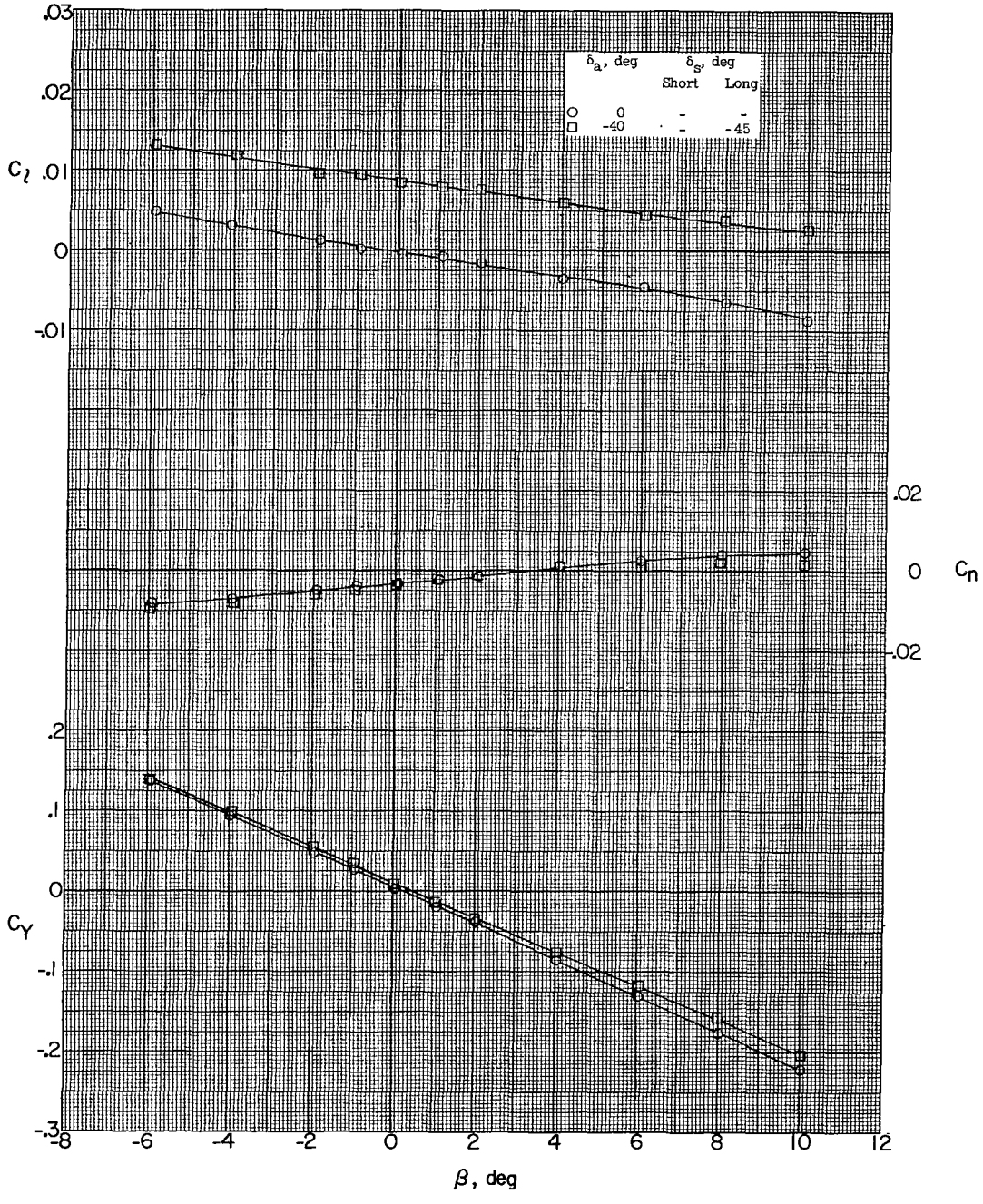

(h) M = 2.50; α = 10.8°.

Figure 18.- Continued.

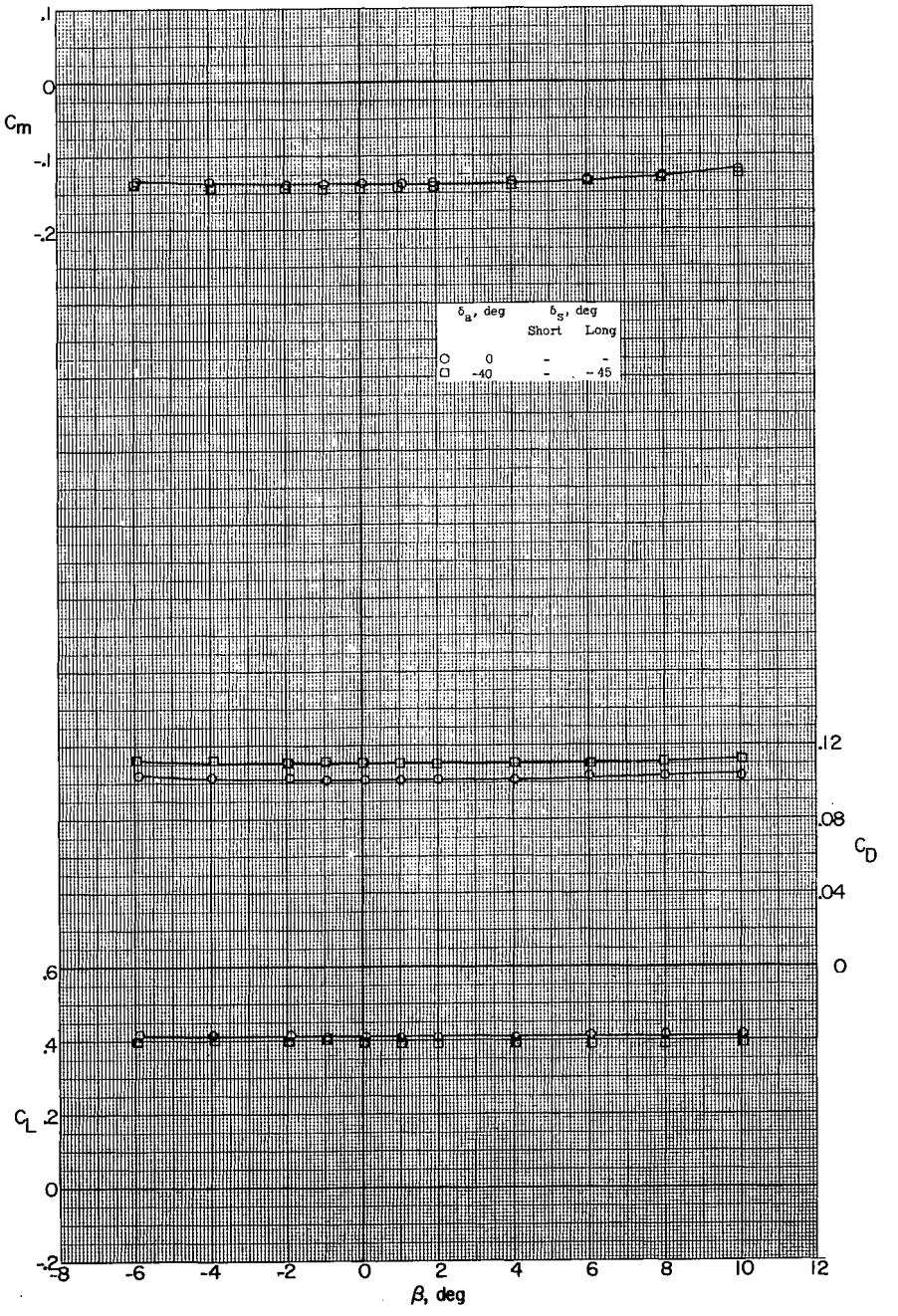

(h) Concluded.

Figure 18.- Concluded.

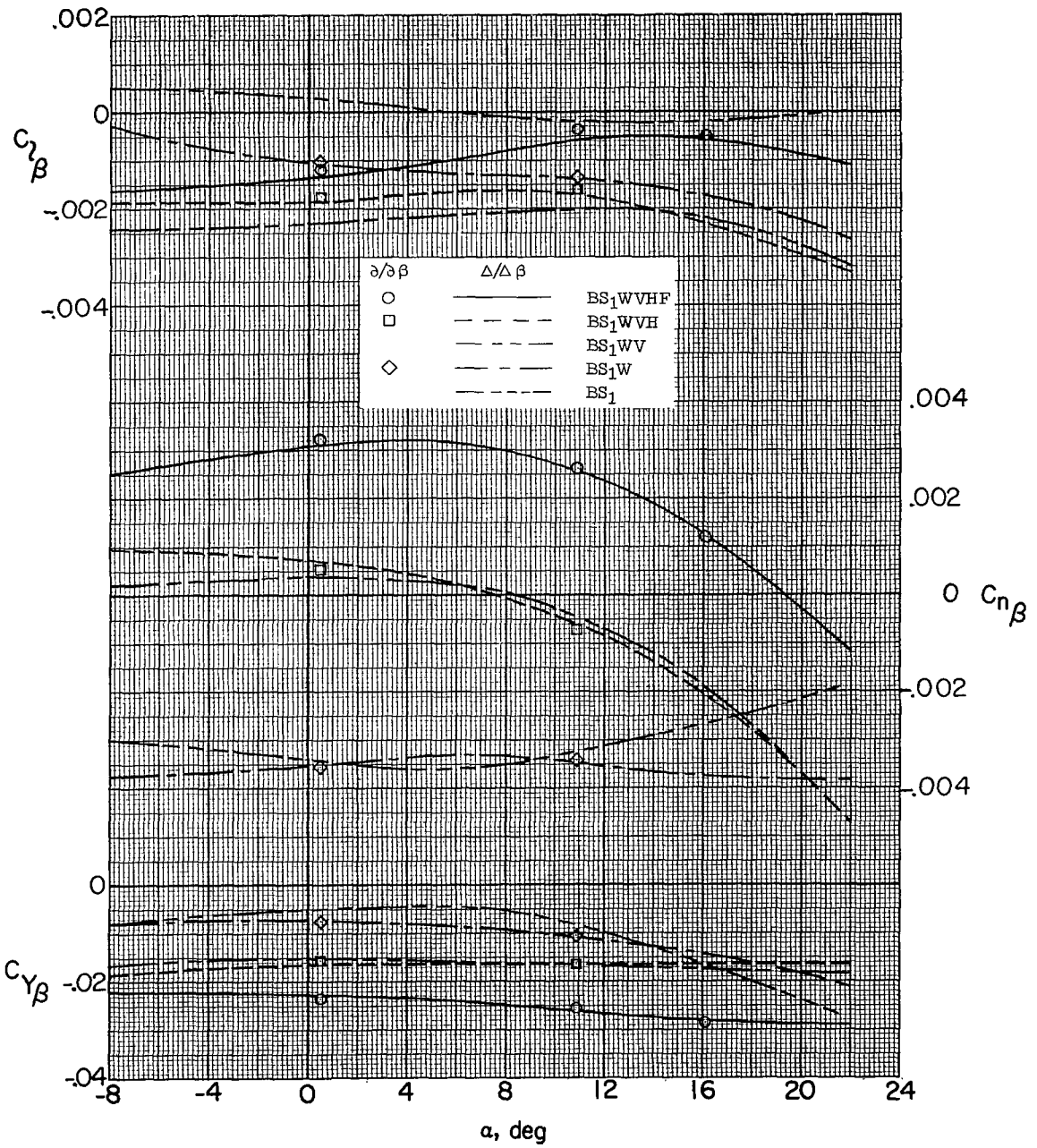

(a) M = 1.60.

Figure 19.- Effect of model-component breakdown on the variation of the static lateral stability parameters with angle of attack.

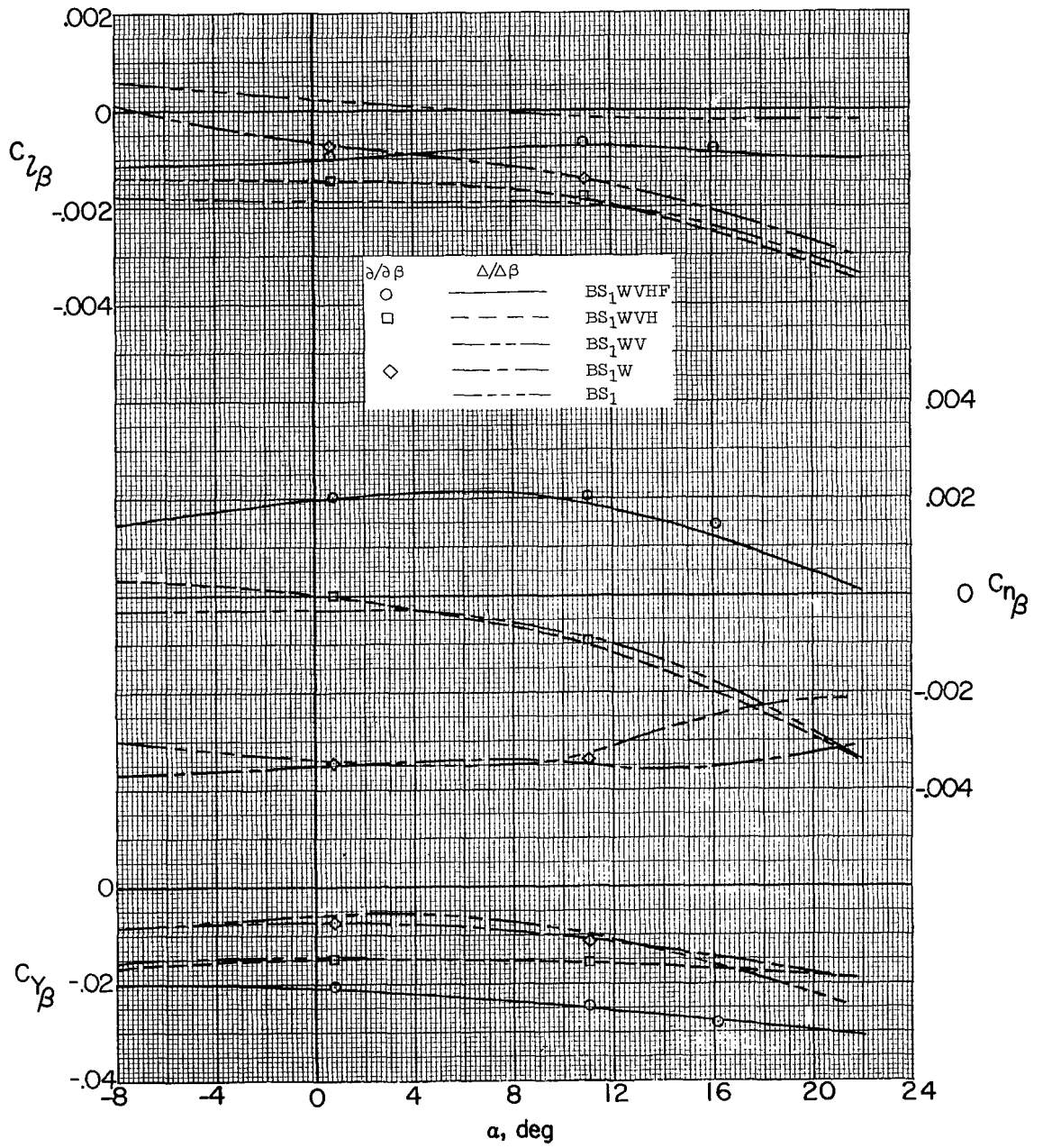

(b) M = 1.90.

Figure 19.- Continued.

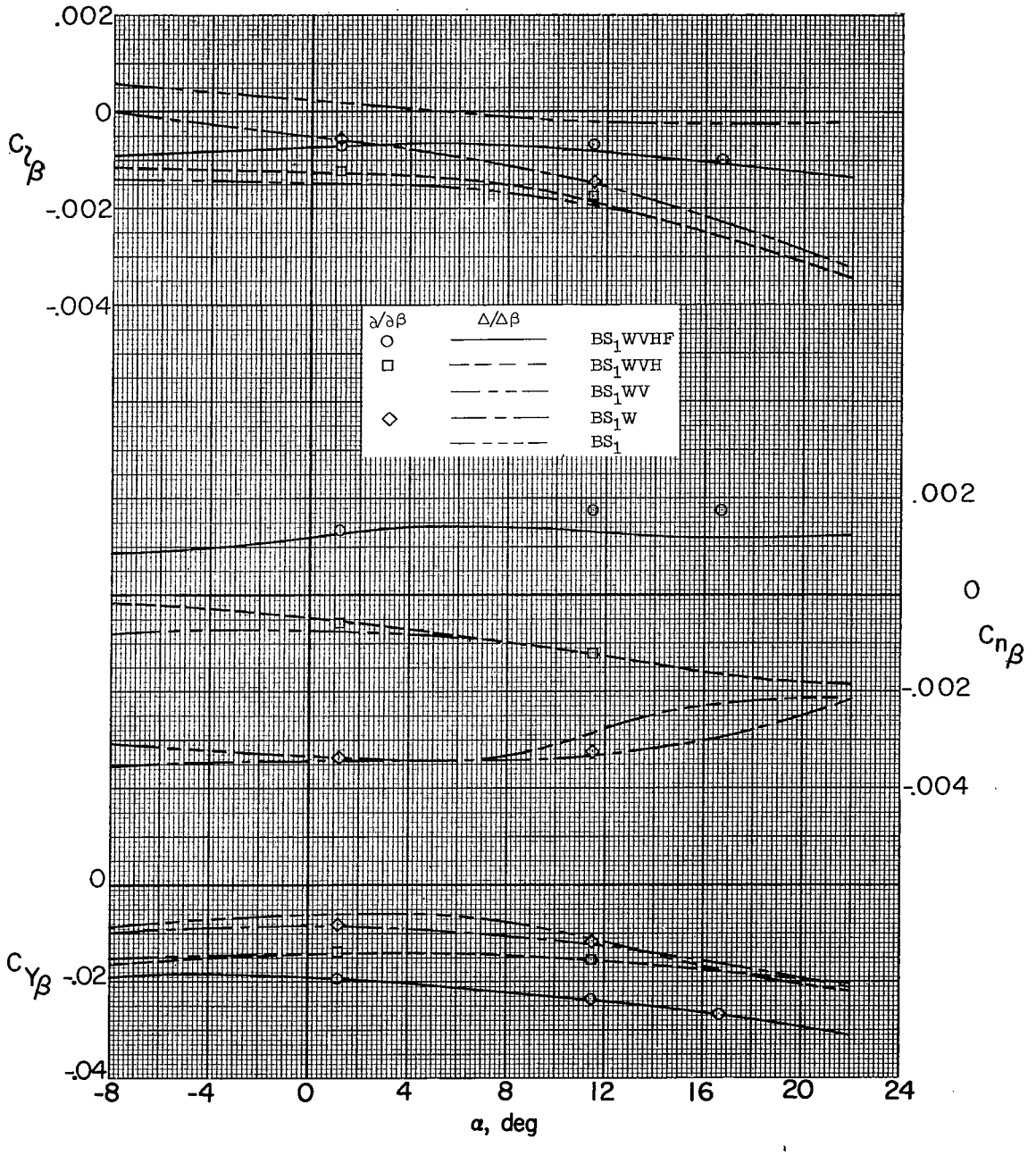

(c) M = 2.20.

Figure 19.- Continued.

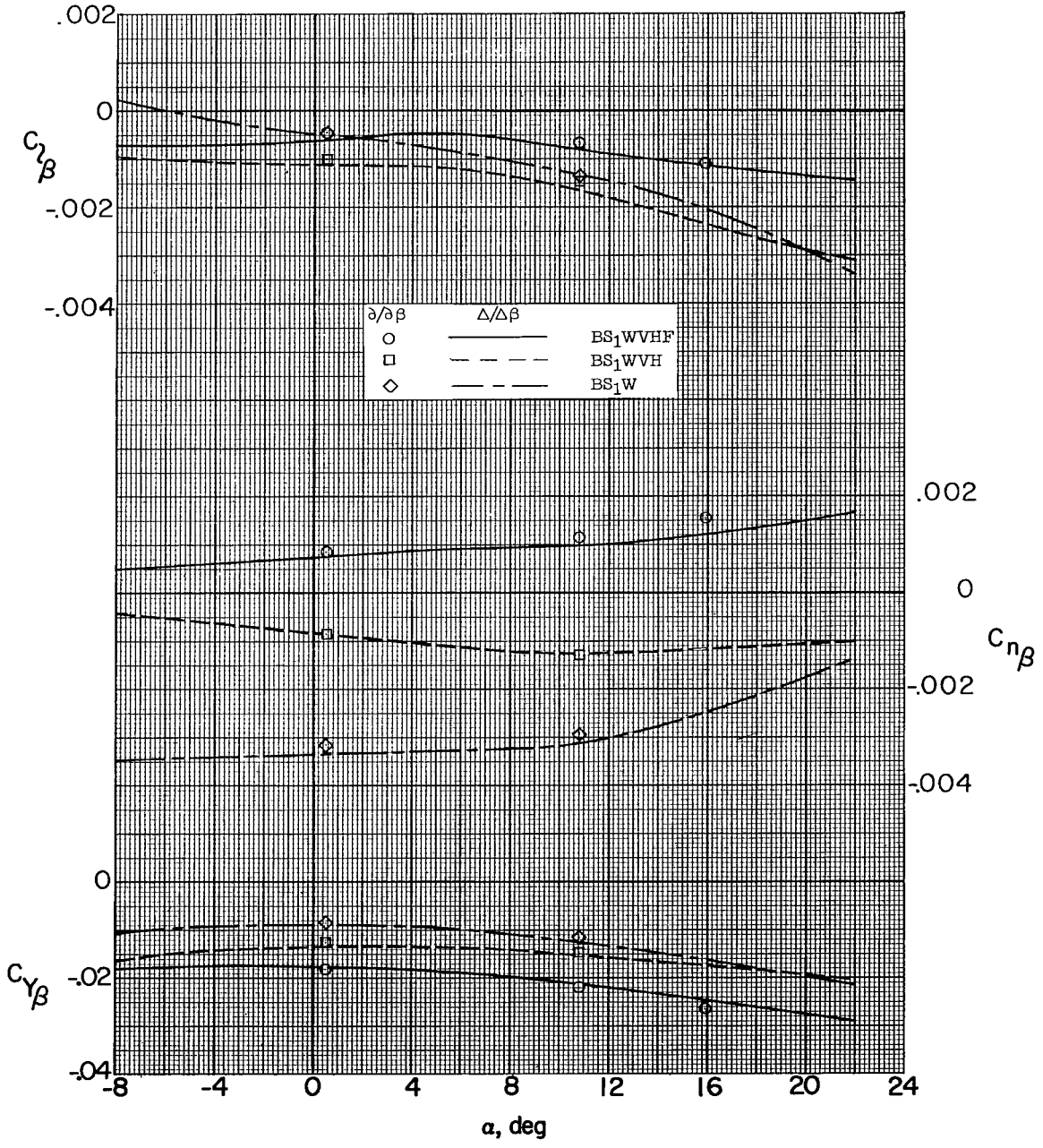

(d) M = 2.50.

Figure 19.- Concluded.

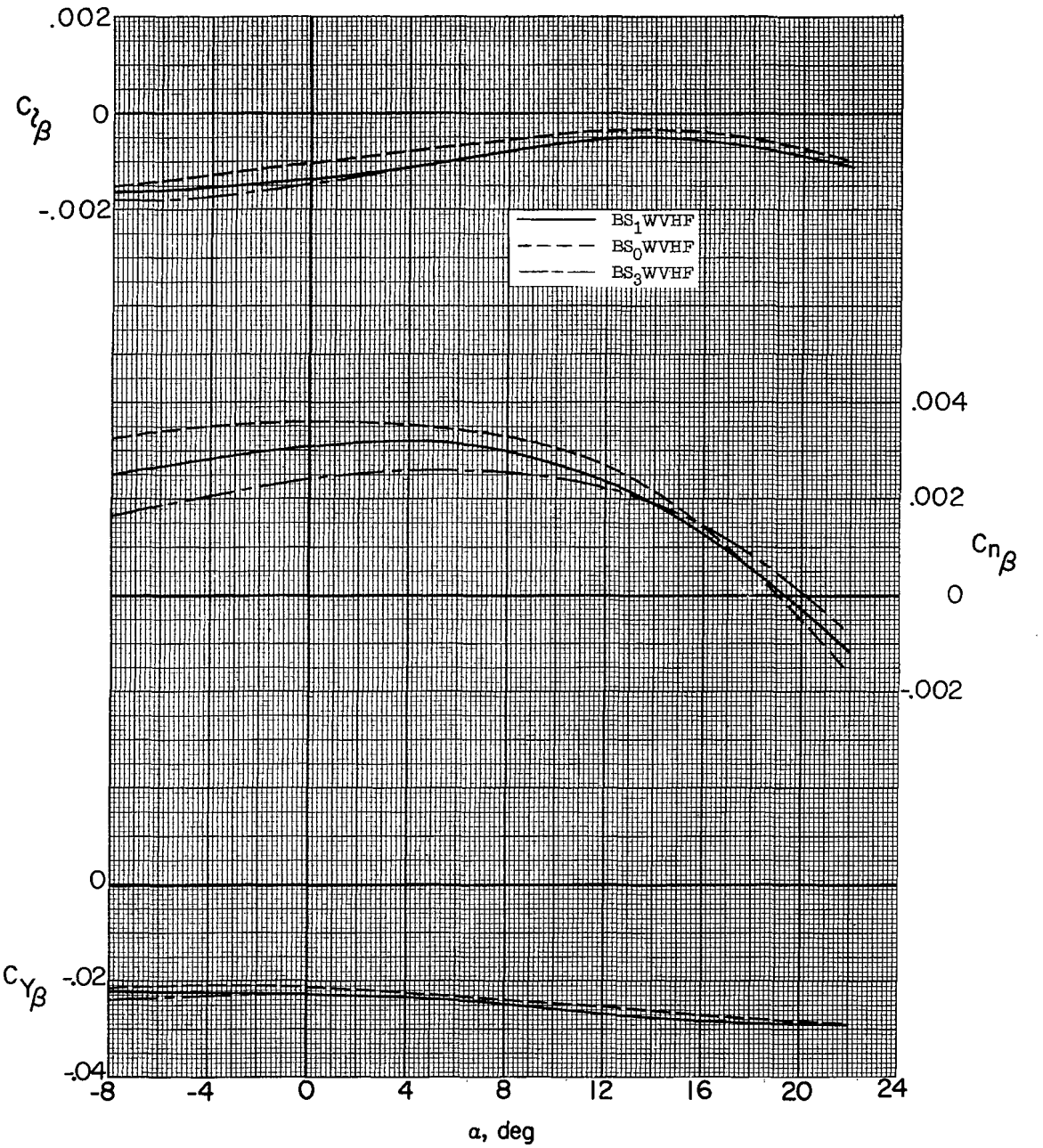

(a) M = 1.60.

Figure 20.- Effect of missiles on the variation of the static lateral stability parameters with angle of attack.

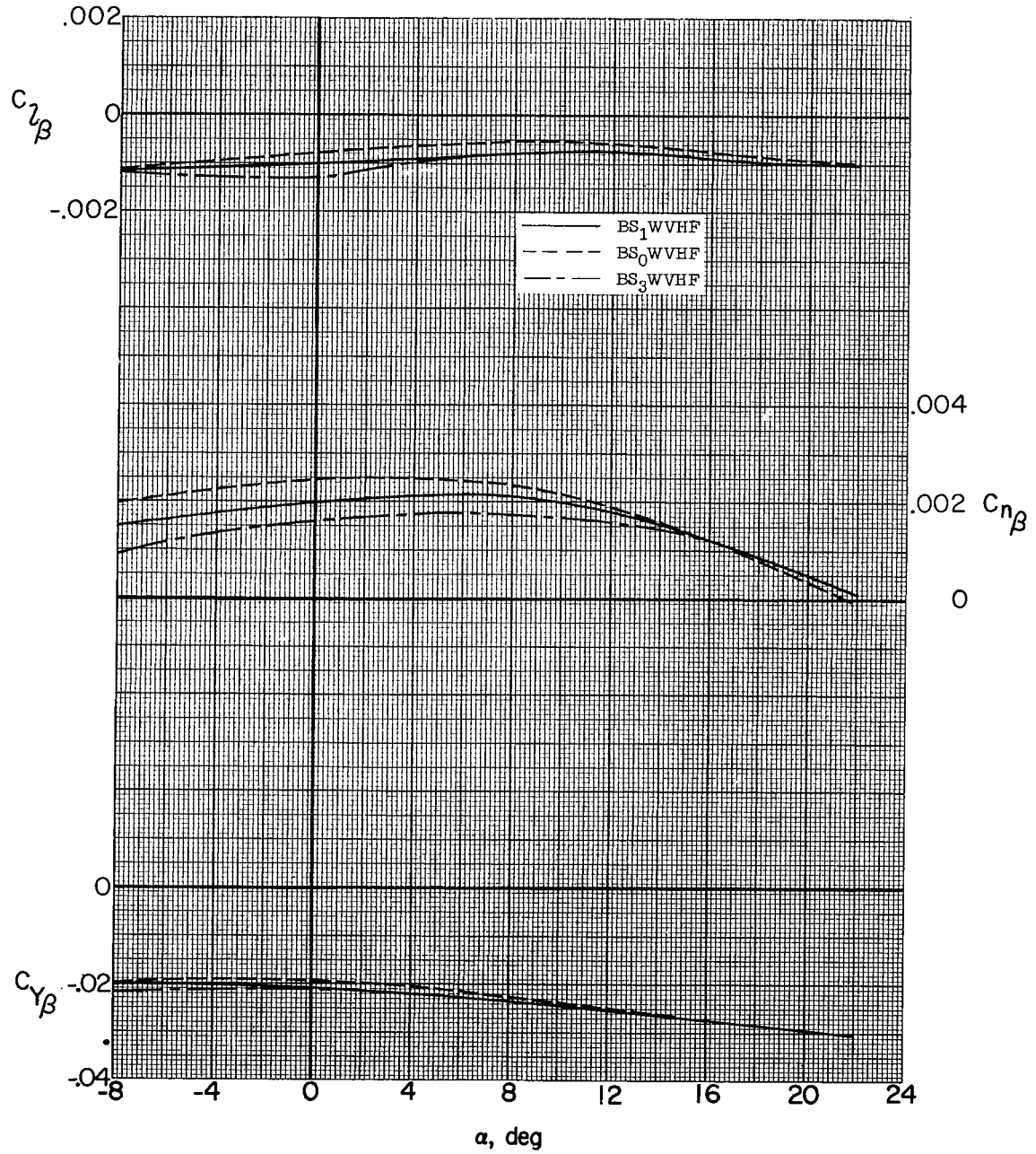

(b) M = 1.90.

Figure 20.- Continued.

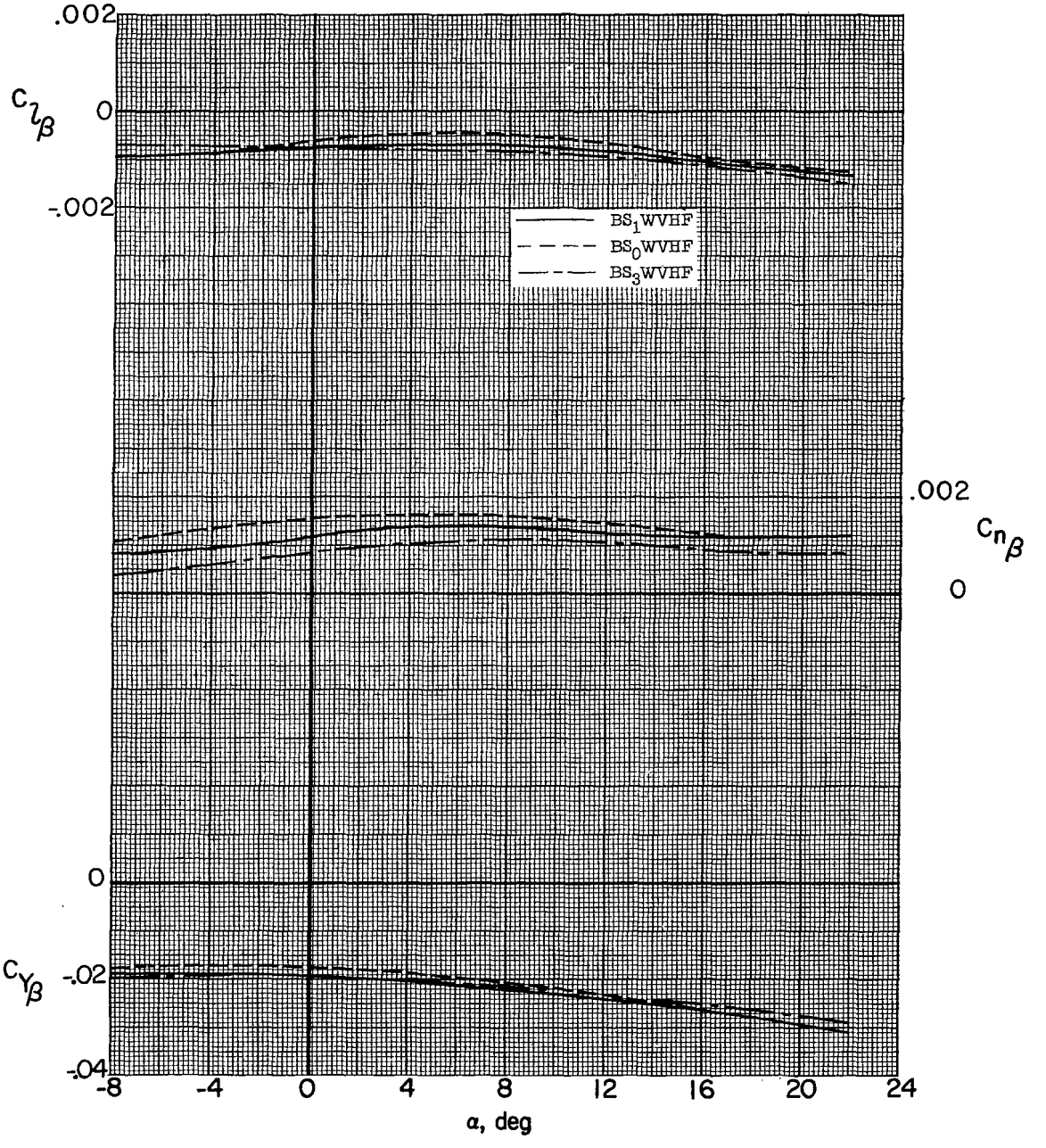

(c) M = 2.20.

Figure 20.- Concluded.

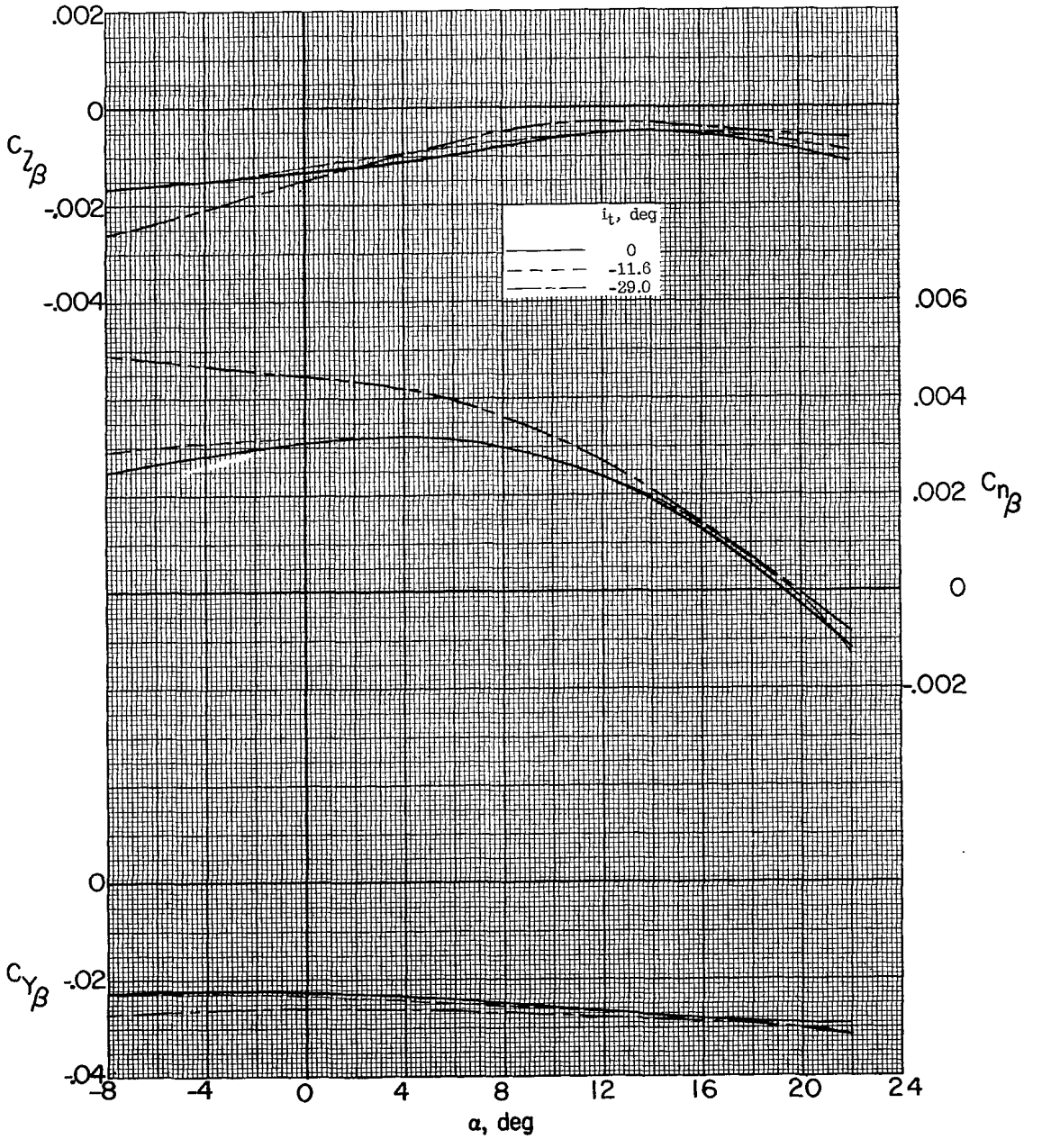

(a) M = 1.60.

Figure 21.- Effect of horizontal stabilizer incidence on the variation of the static lateral stability parameters with angle of attack. BS_1WVHF.

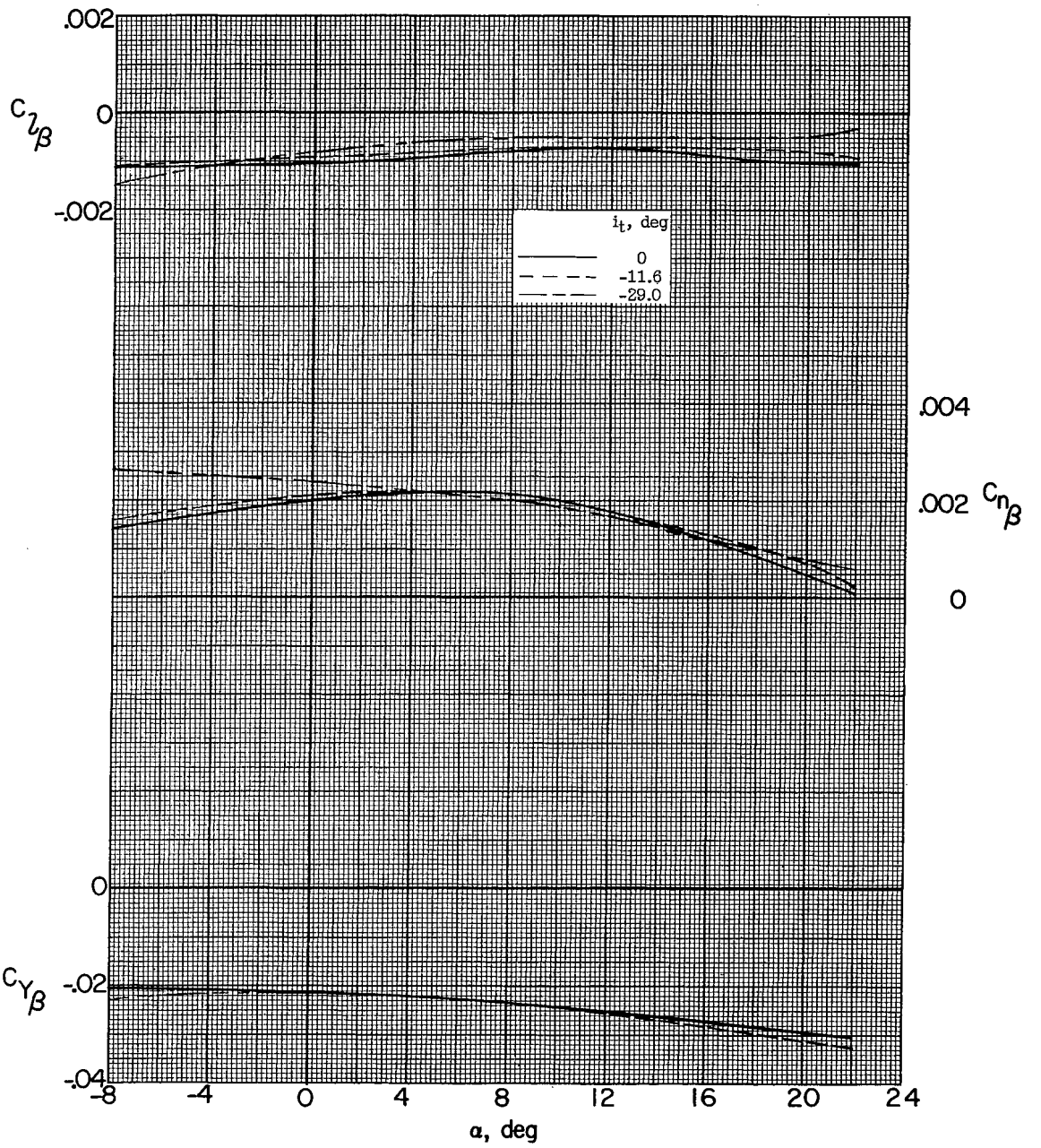

(b) M = 1.90.

Figure 21.- Continued.

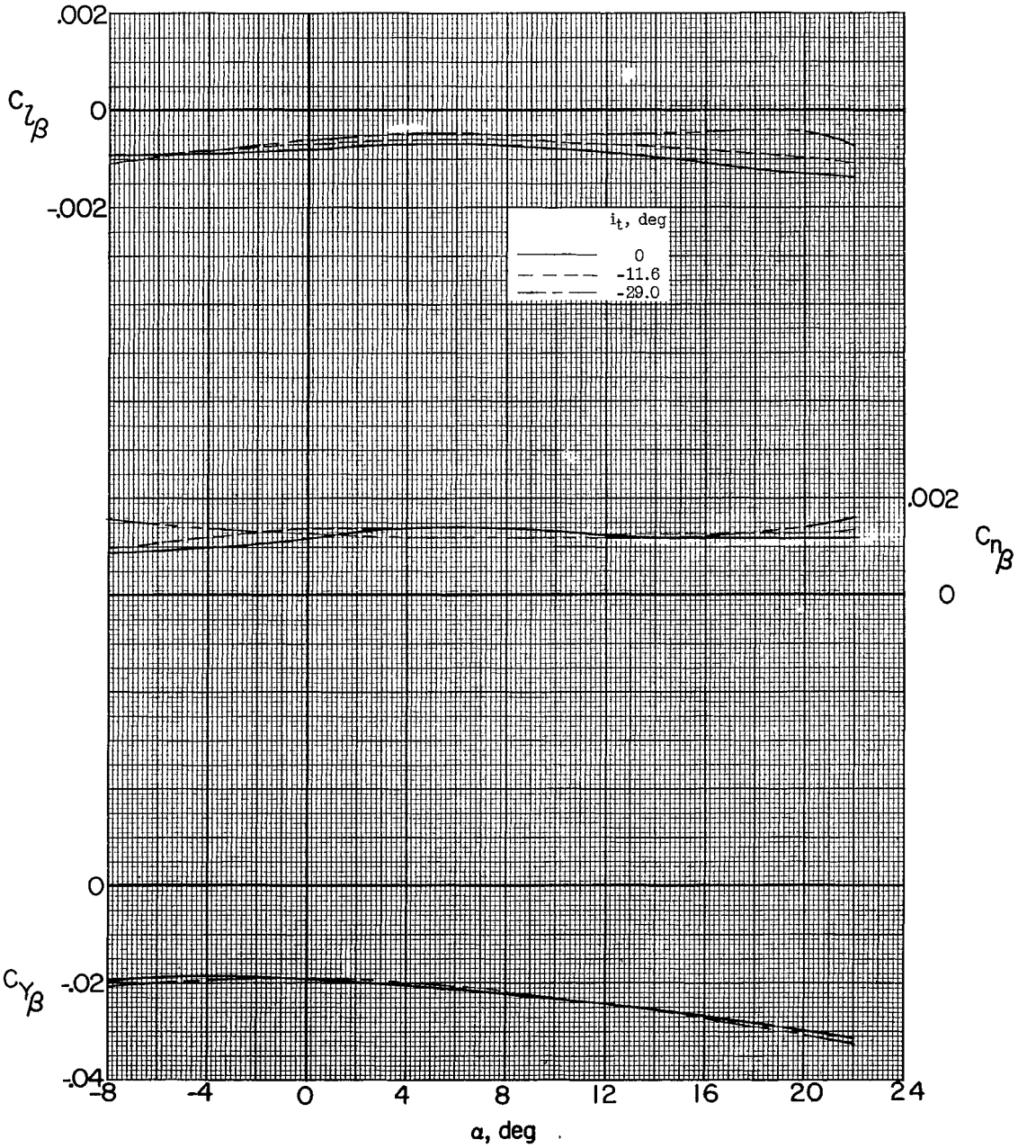

(c) M = 2.20.

Figure 21.- Concluded.

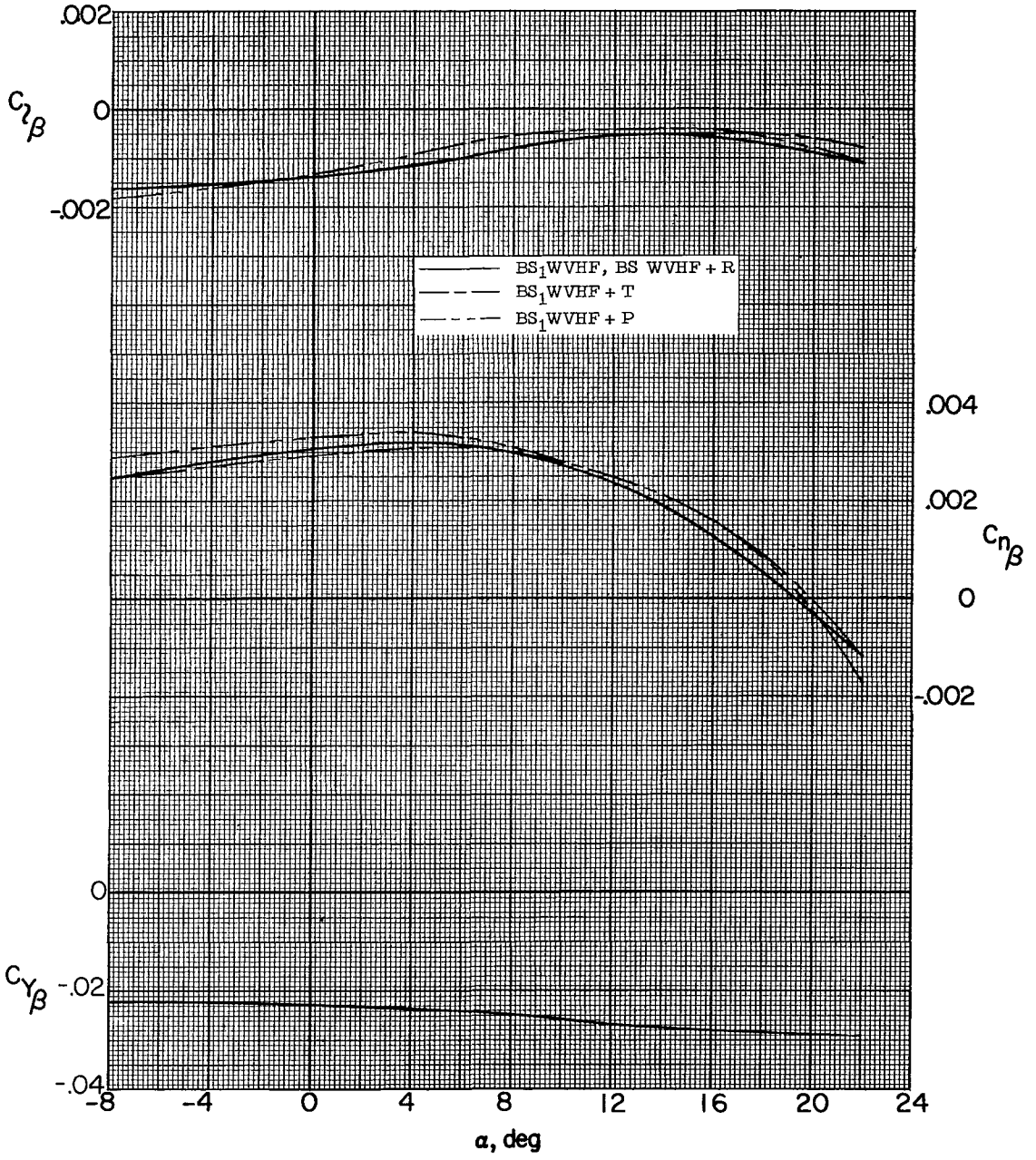

(a) M = 1.60.

Figure 22.- Effect of some of the model modifications on the variation of the static lateral stability parameters with angle of attack.

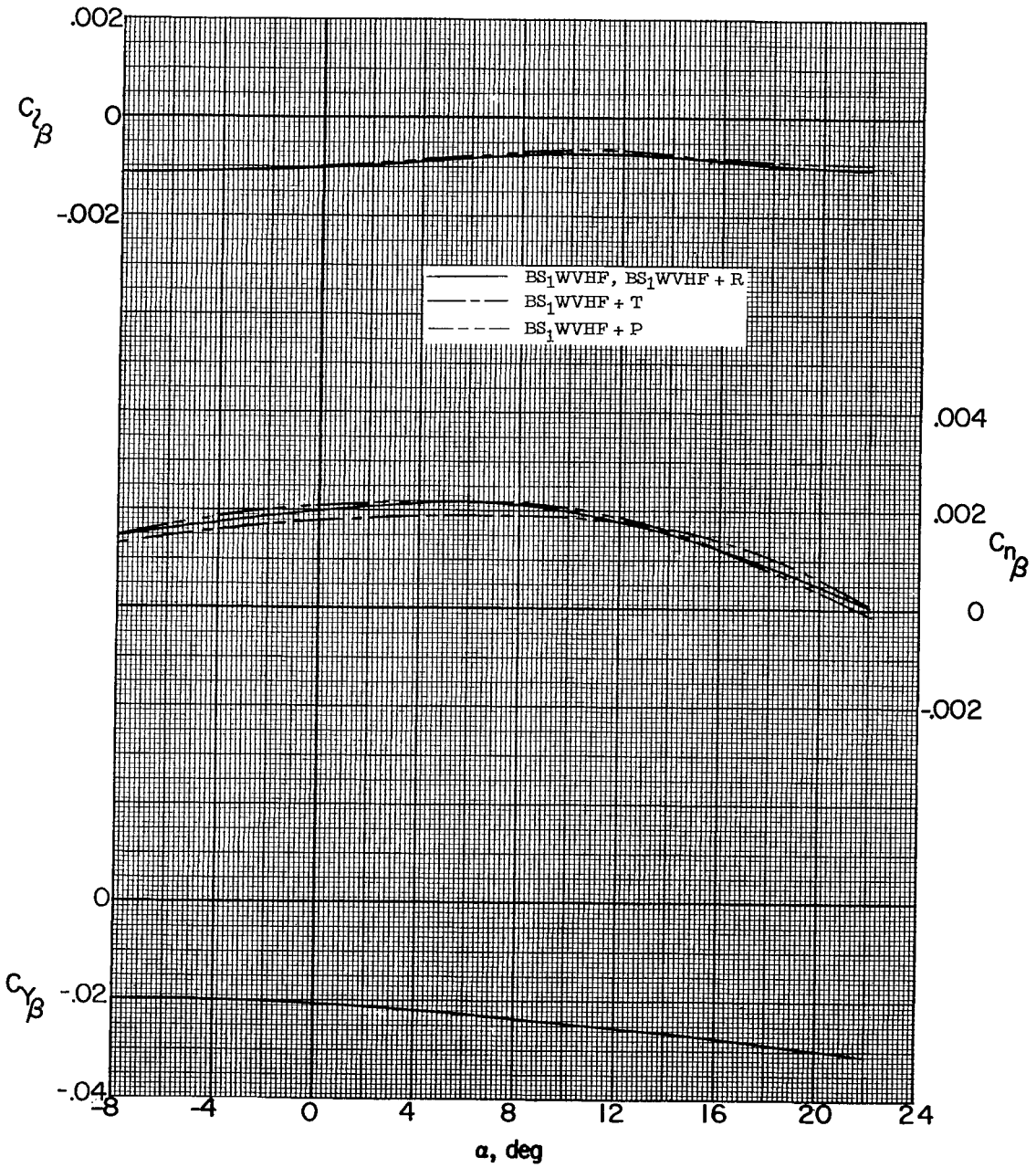

(b) M = 1.90.

Figure 22.- Continued.

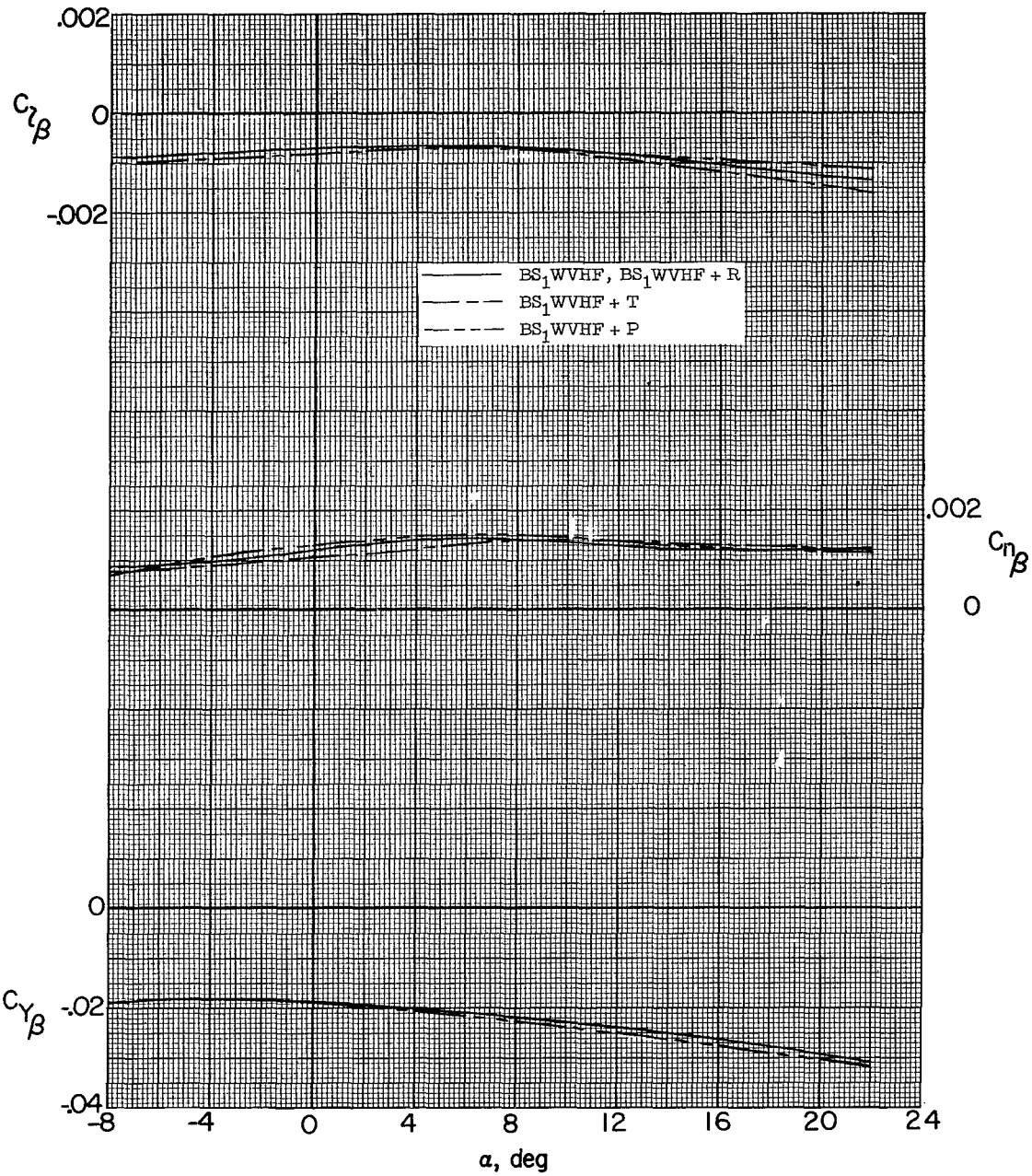

(c) M = 2.20.

Figure 22.- Concluded.

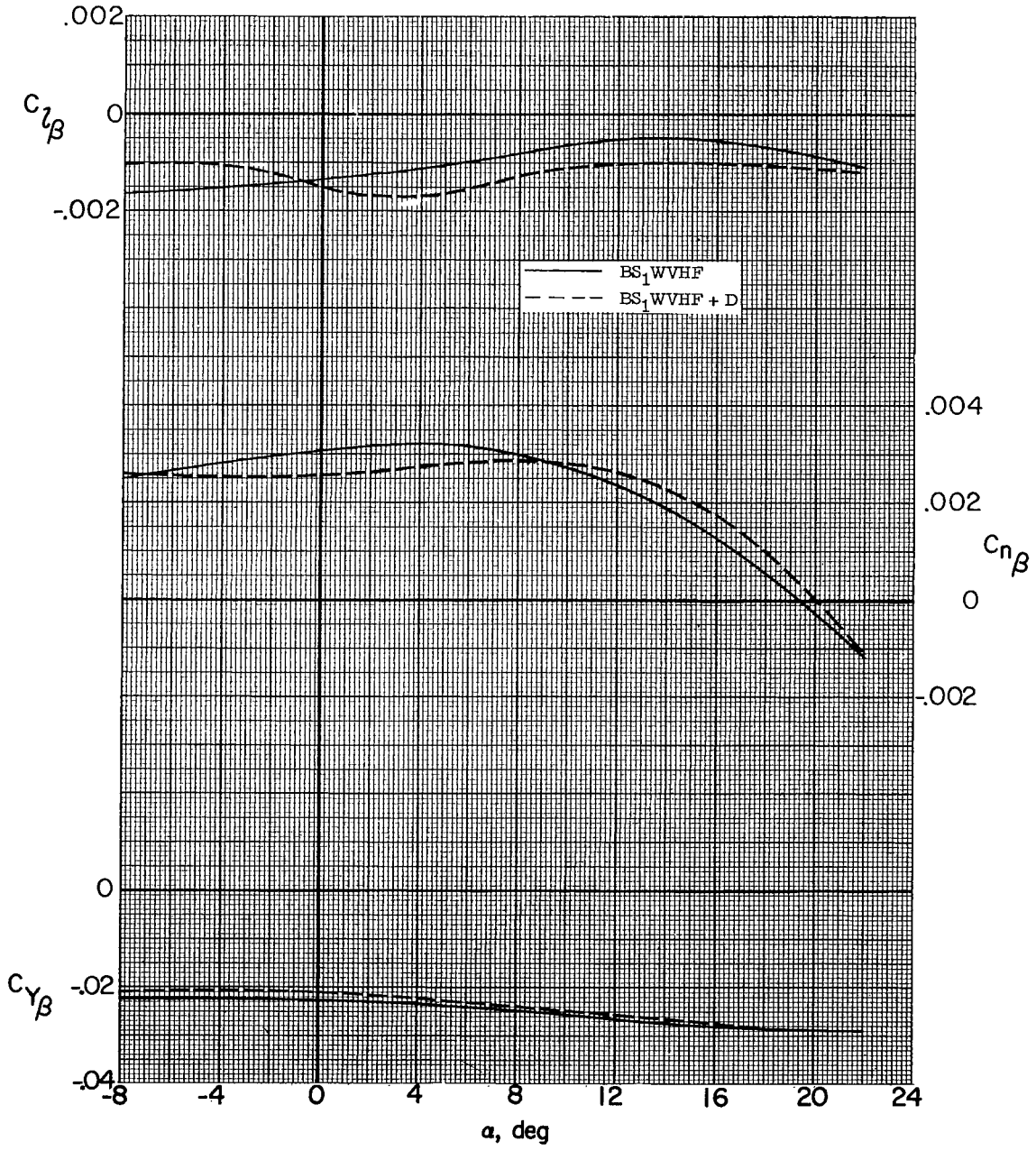

(a) M = 1.60.

Figure 23.- Effect of speed brake on the variation of the static lateral stability parameters with angle of attack.

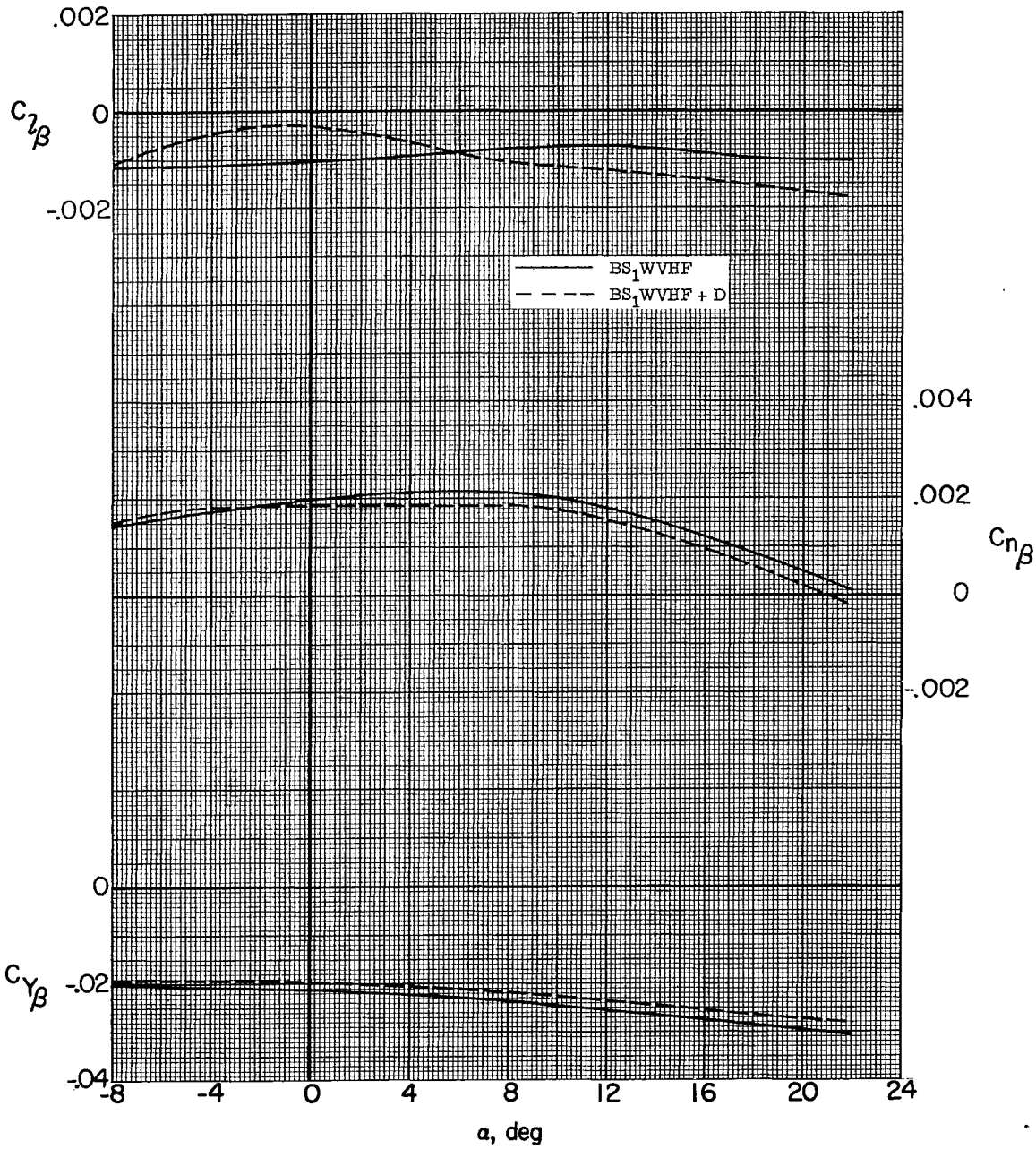

(b) M = 1.90.

Figure 23.- Continued.

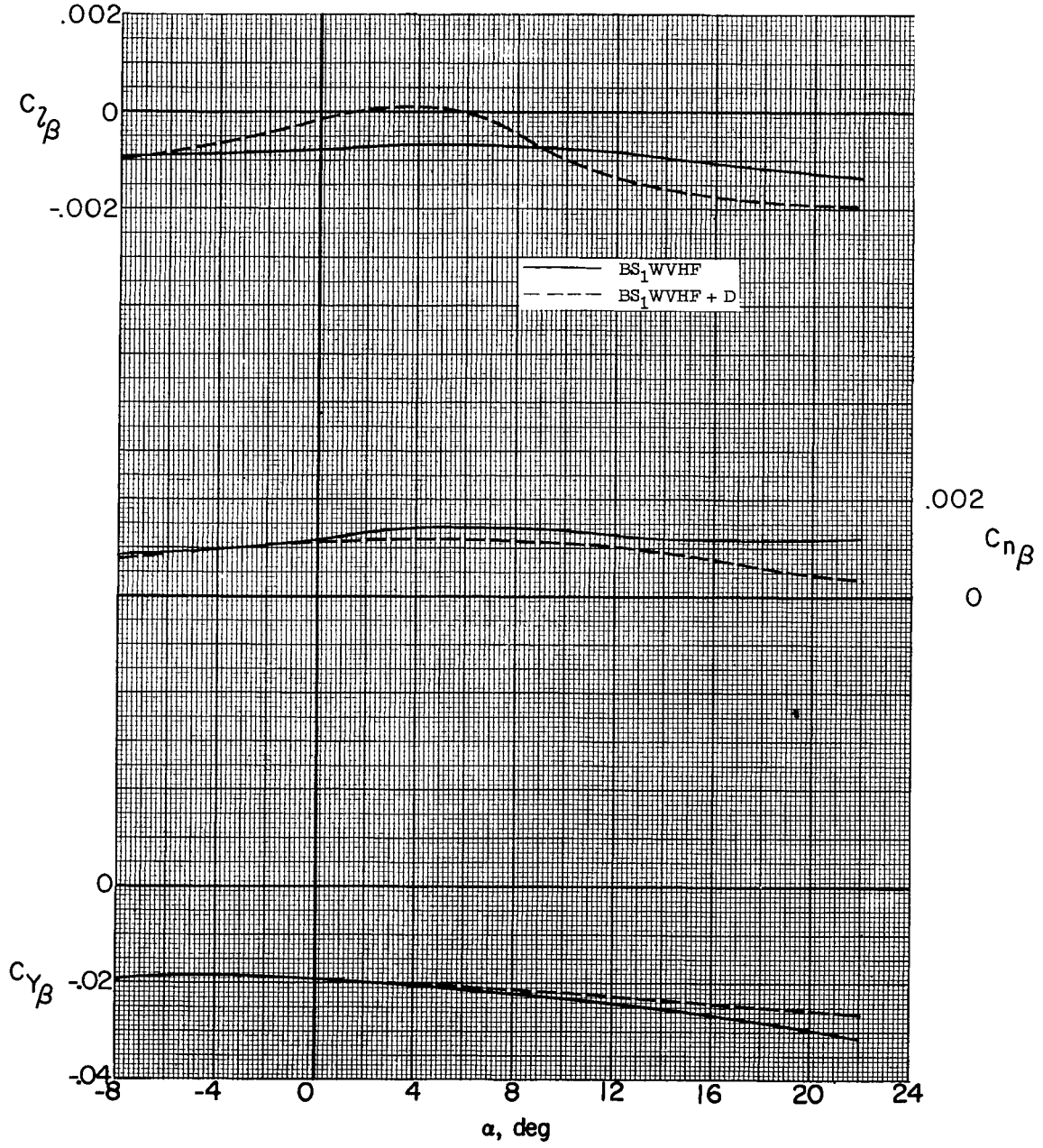

(c) M = 2.20.

Figure 23.- Concluded.

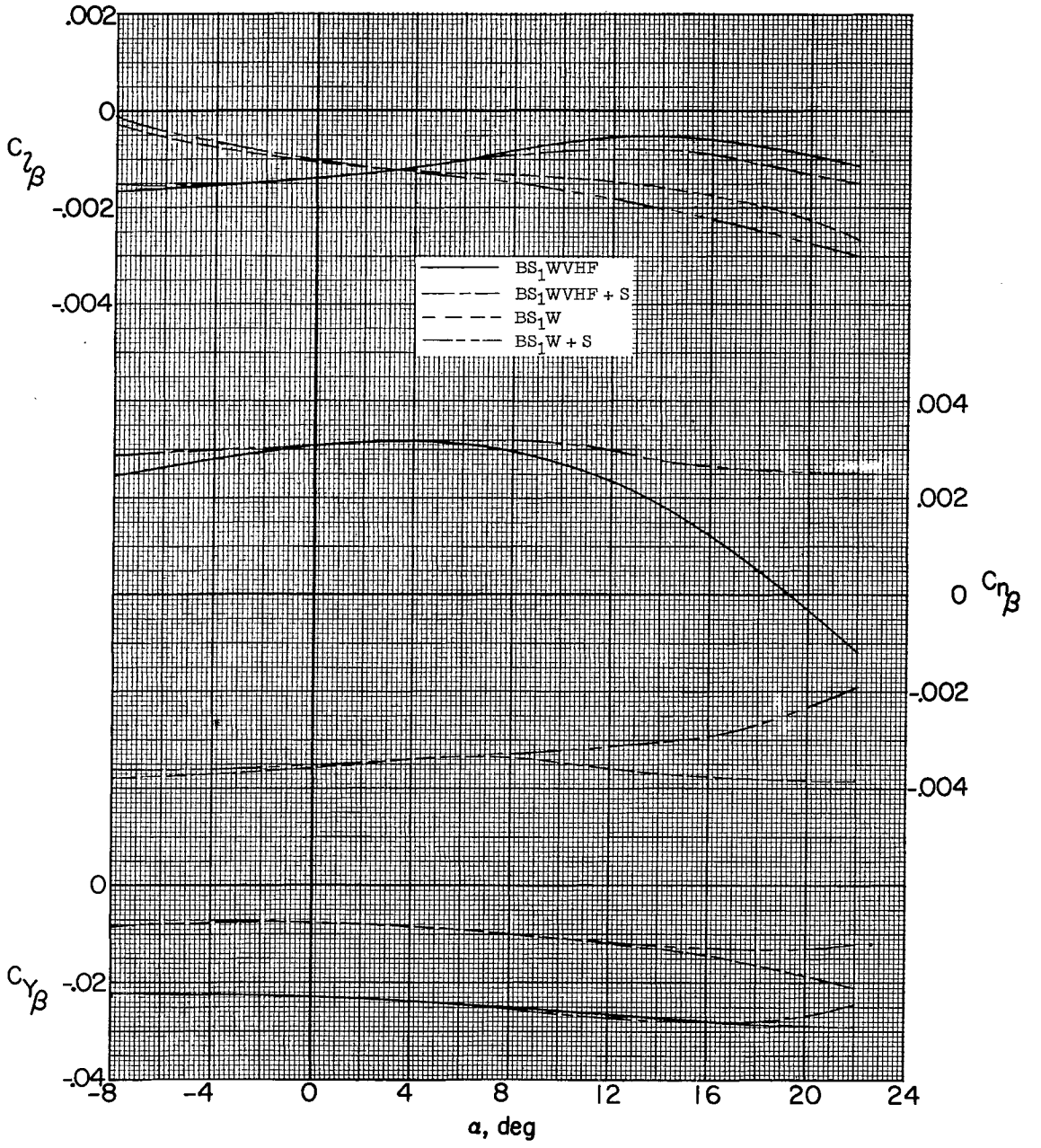

(a) M = 1.60.

Figure 24.- Effect of strakes on the variation of the static lateral stability parameters with angle of attack.

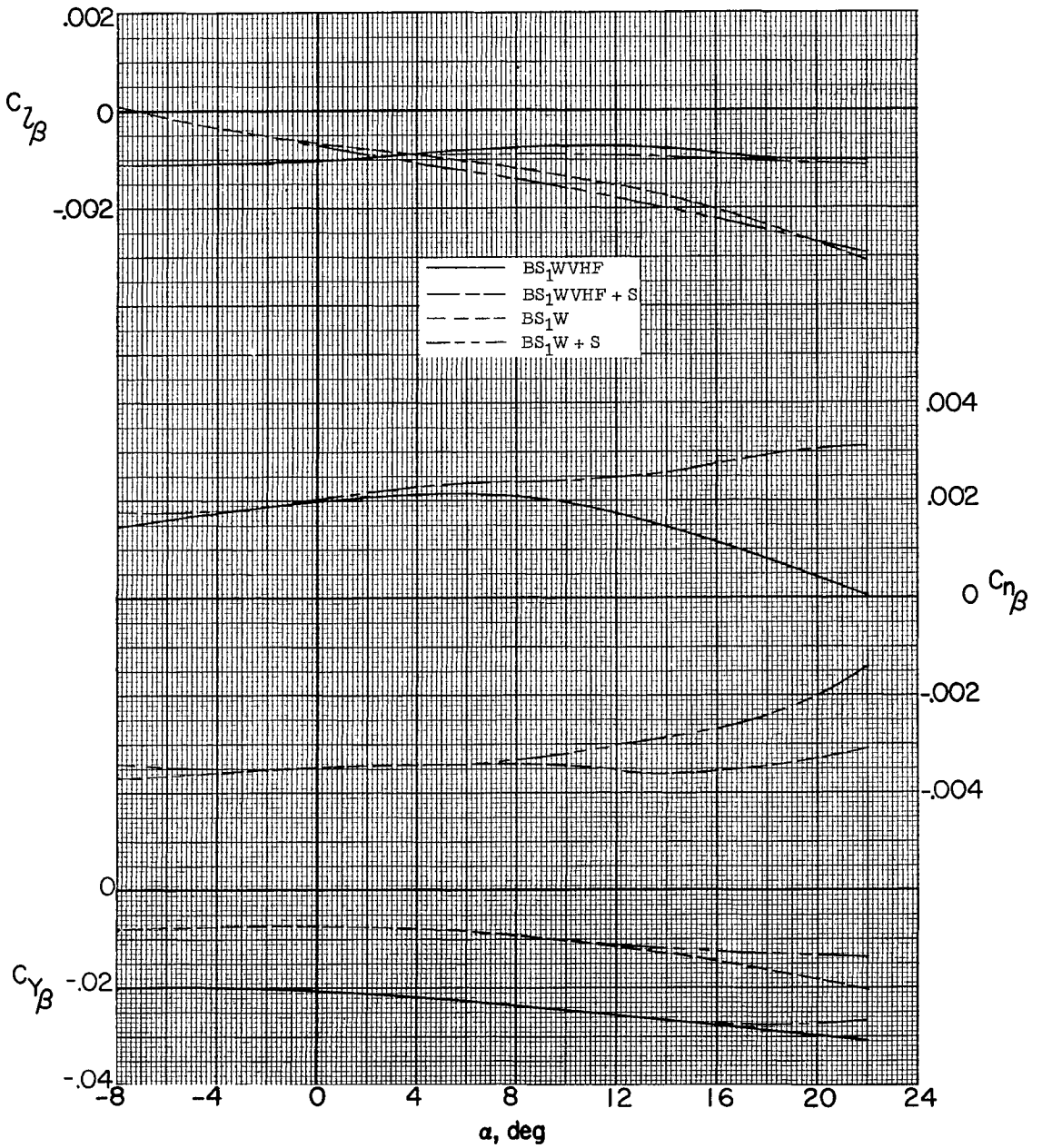

(b) M = 1.90.

Figure 24.- Continued.

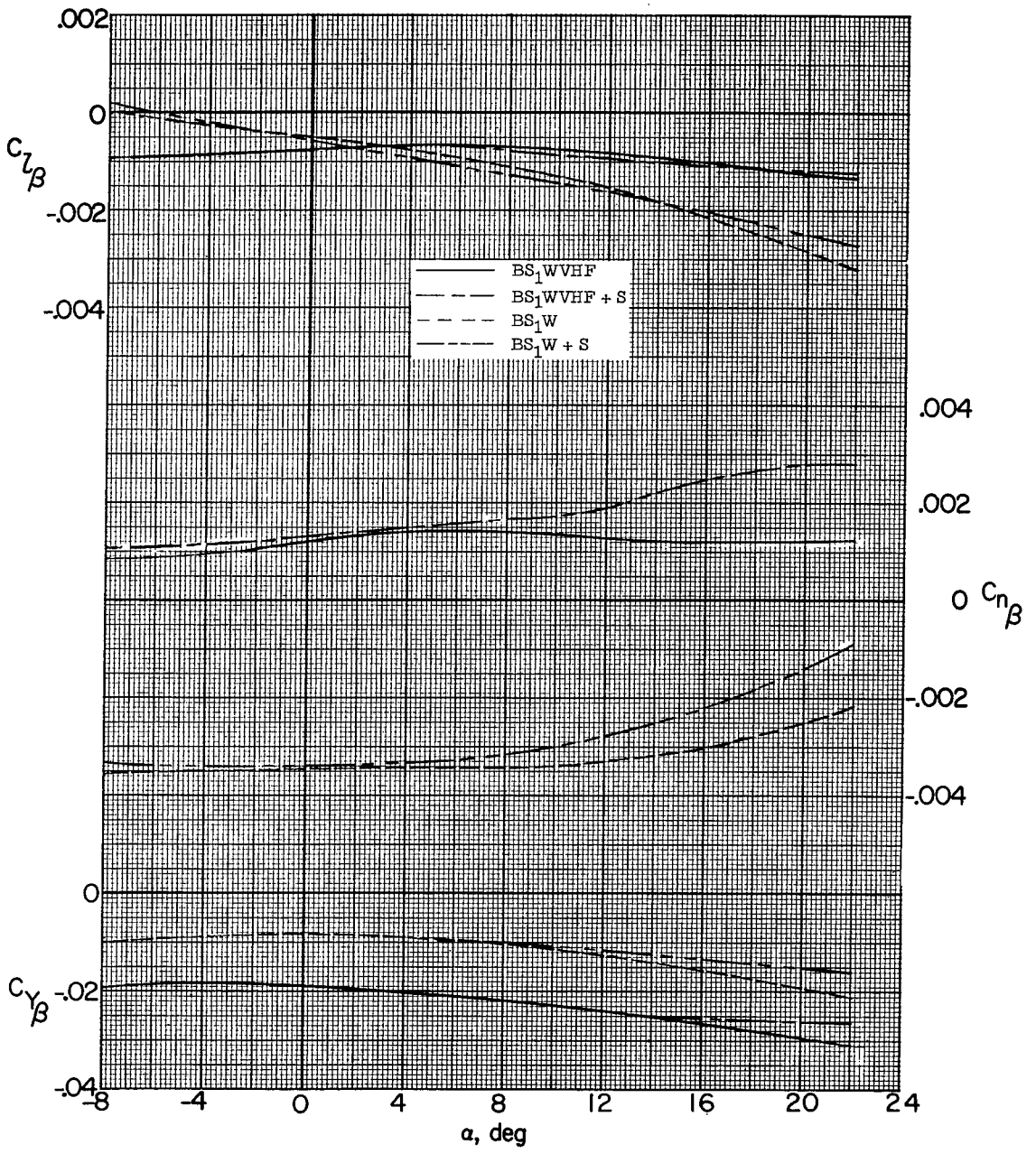

(c) M = 2.20.

Figure 24.- Concluded.

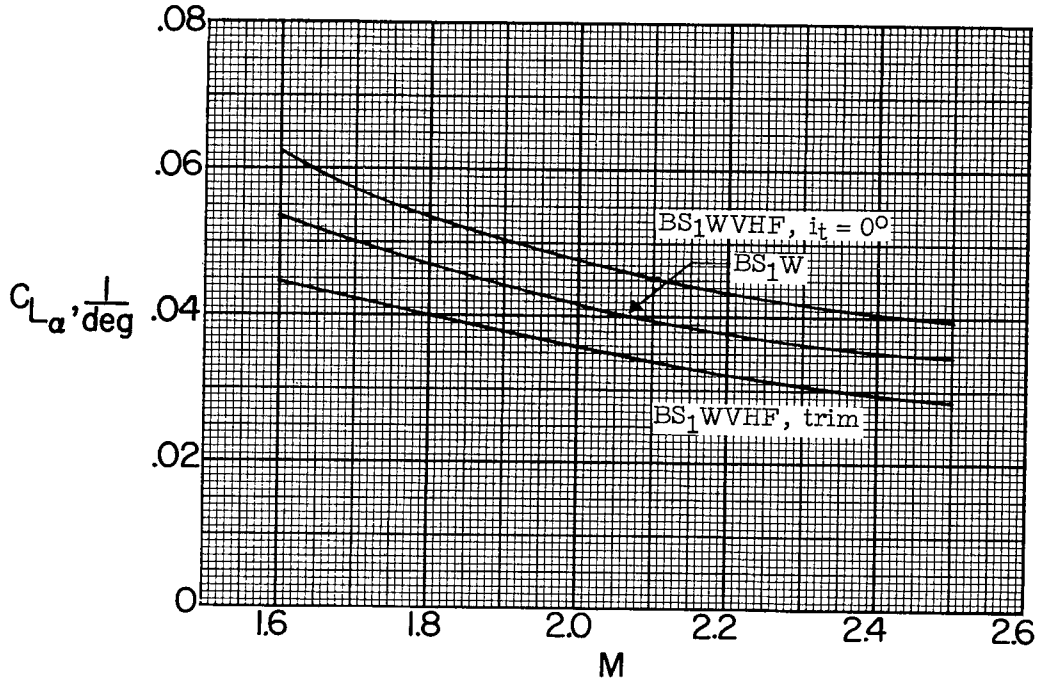

(a) Lift-curve slope.

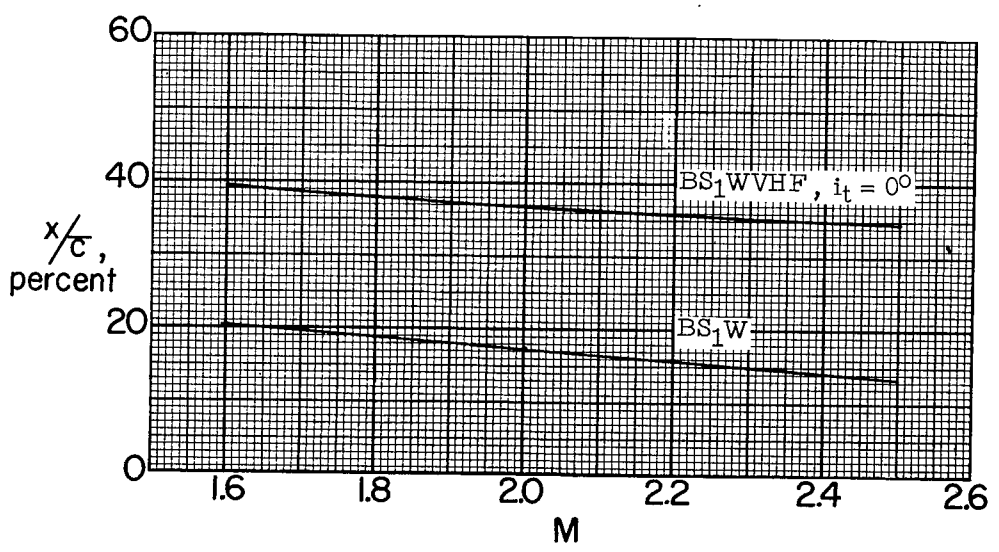

(b) Static margin.

Figure 25.- Variation of lift-curve slope and static margin with Mach number. $\beta = 0^\circ$.

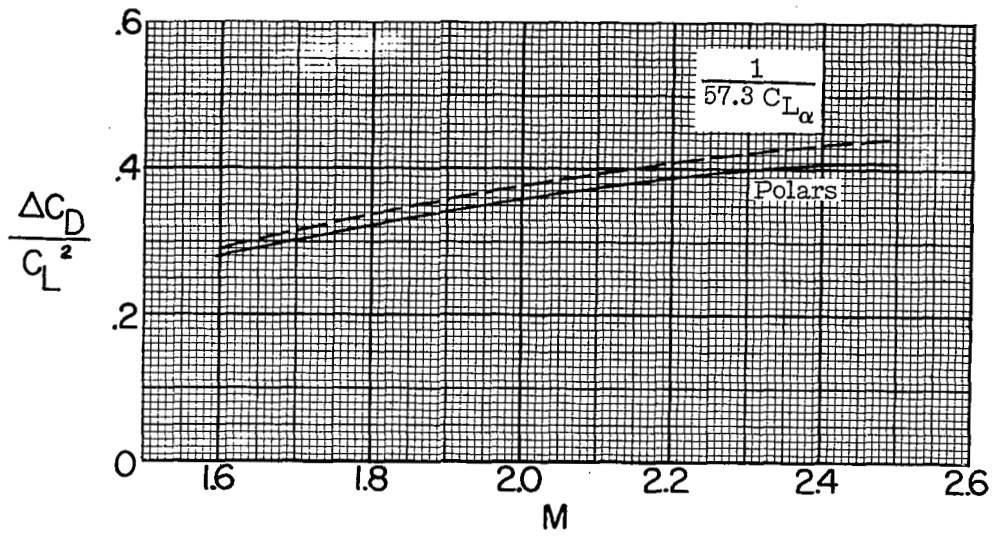

(a) Drag due to lift; BS_1WVHF; $i_t = 0^\circ$.

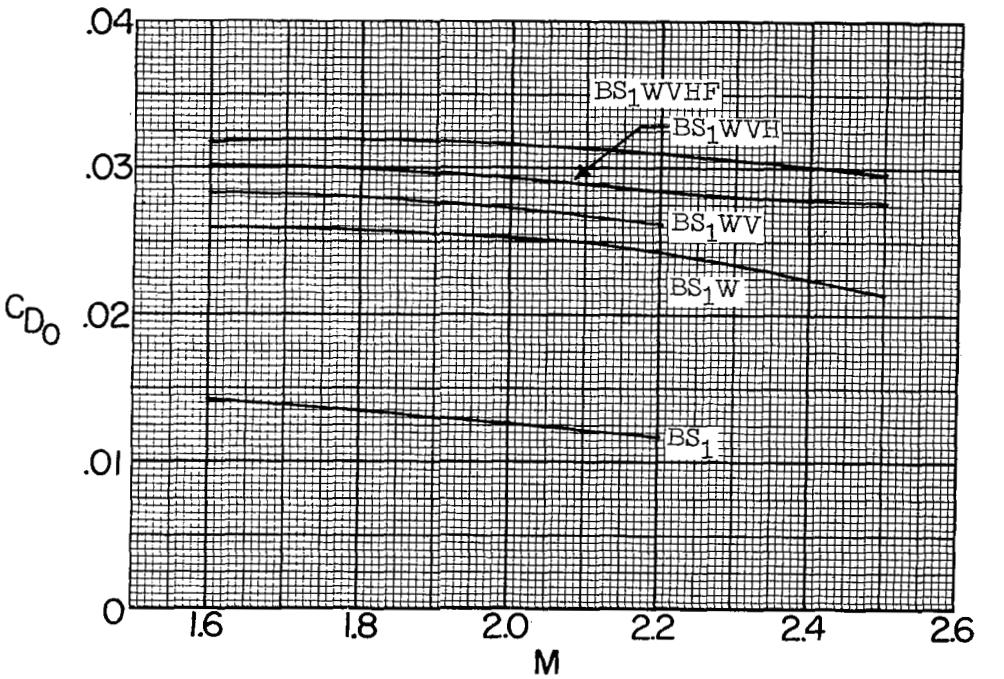

(b) Drag at zero lift.

Figure 26.- Variation of drag due to lift and drag at zero lift with Mach number. $\beta = 0^\circ$.

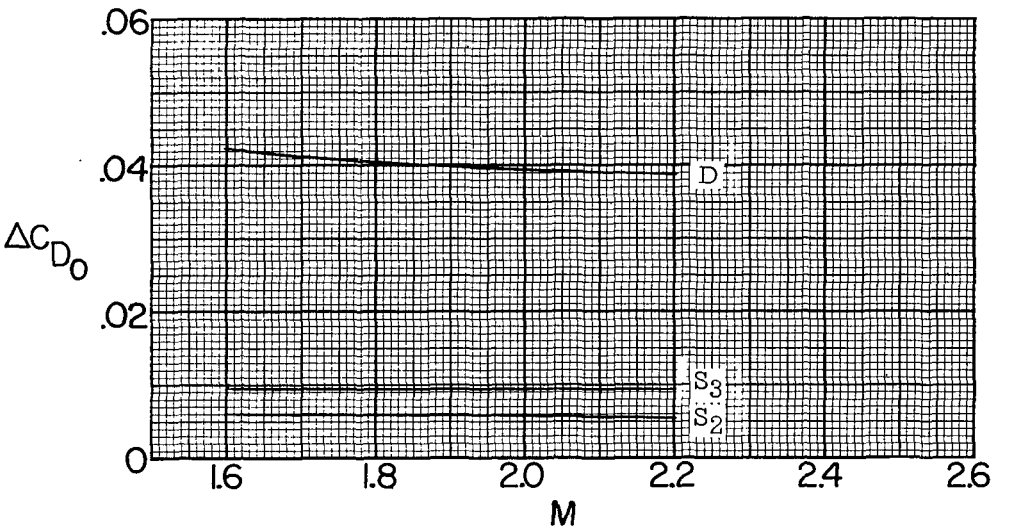

(a) Increment in zero-lift drag from BS_1WVHF.

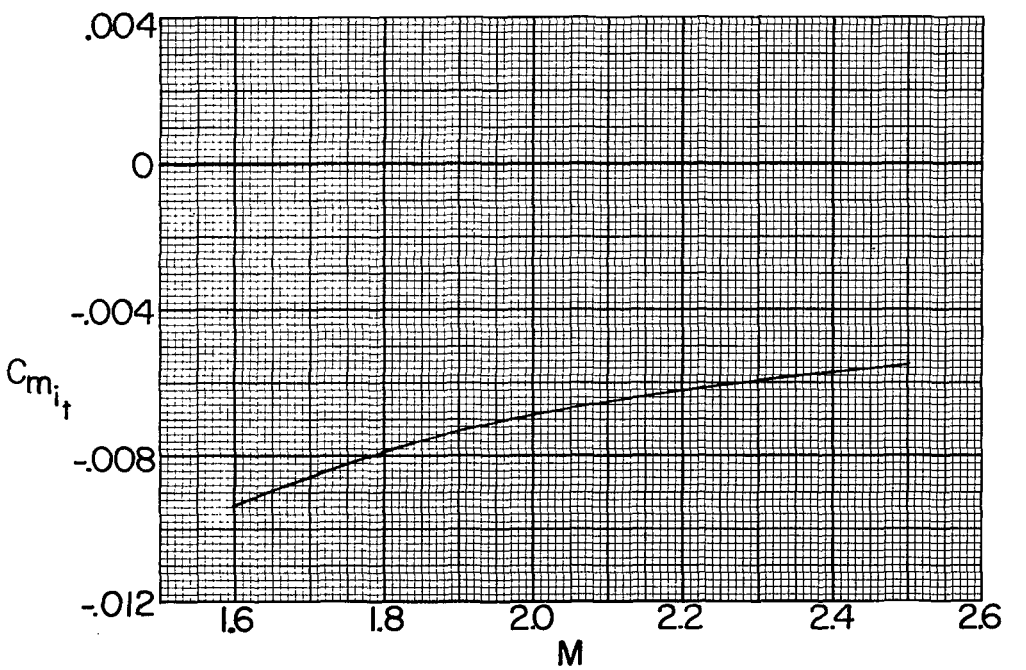

(b) Stabilizer effectiveness at zero lift.

Figure 27.- Variation of zero-lift drag increment and stabilizer effectiveness with Mach number. $\beta = 0^\circ$.

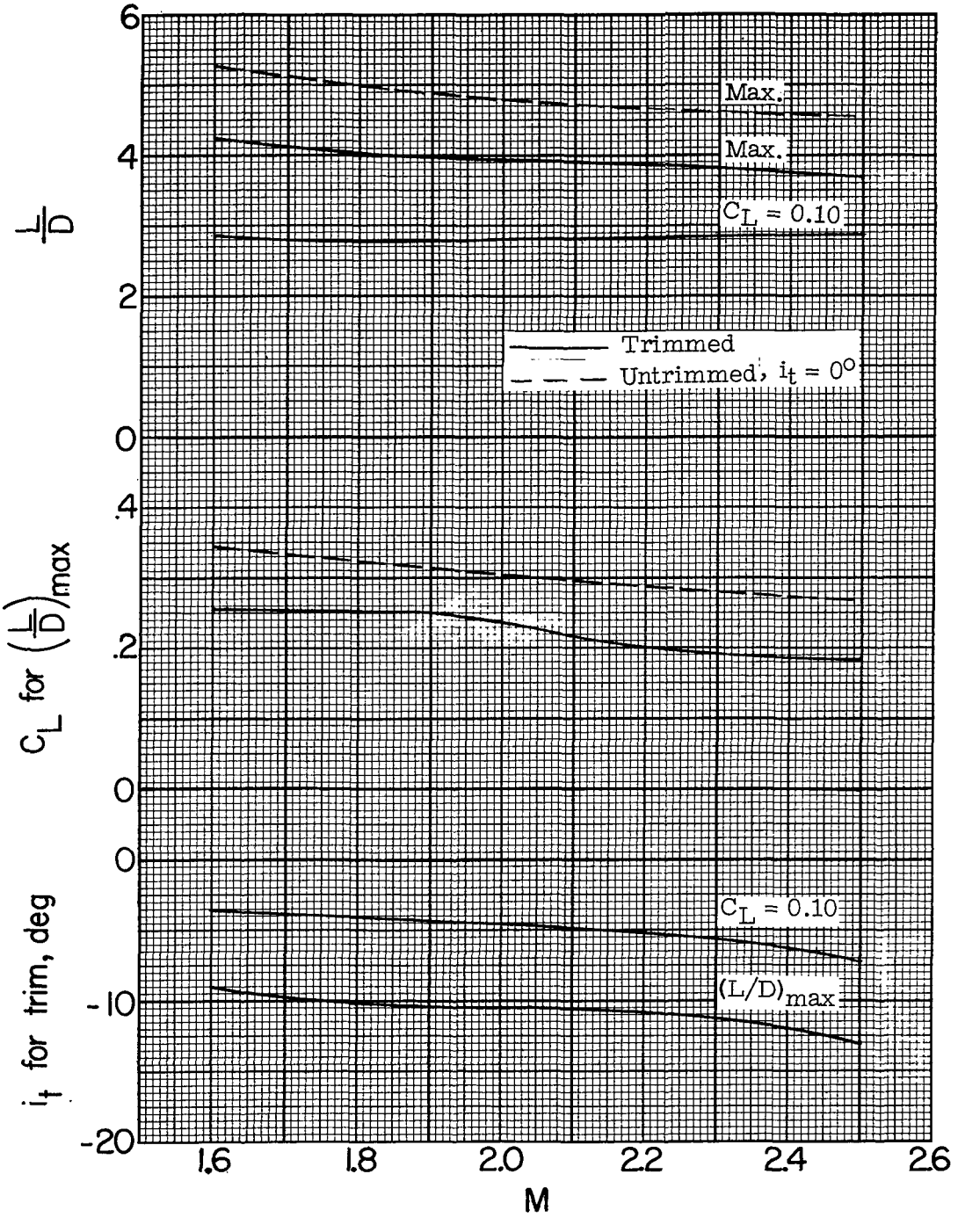

Figure 28.- Variation of trim lift-drag ratio, lift coefficient, and stabilizer incidence angle for trim with Mach number. BS_1WVHF; $\beta = 0^\circ$.

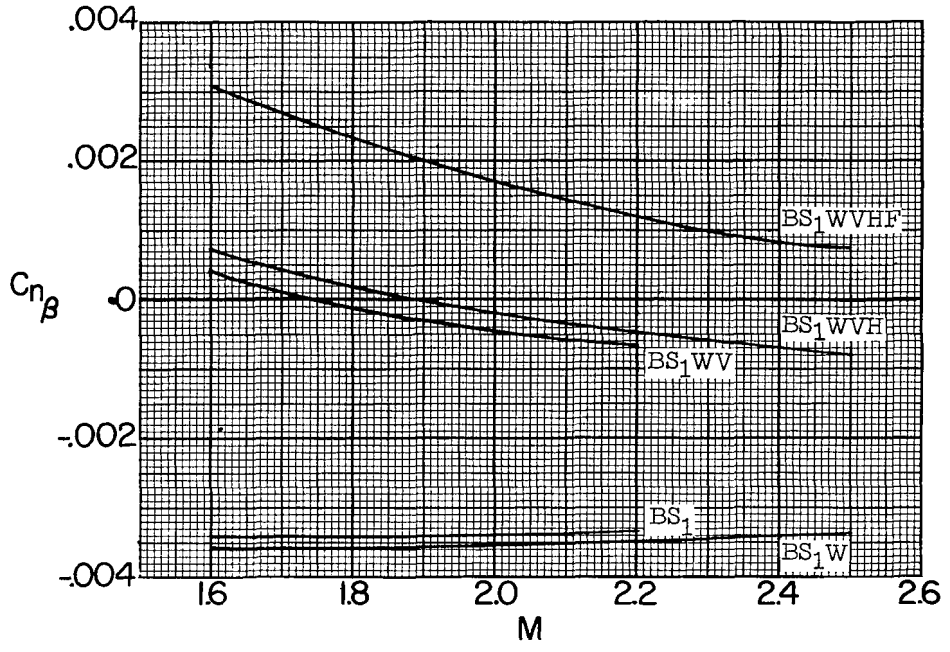

(a) $\alpha = 0^\circ$.

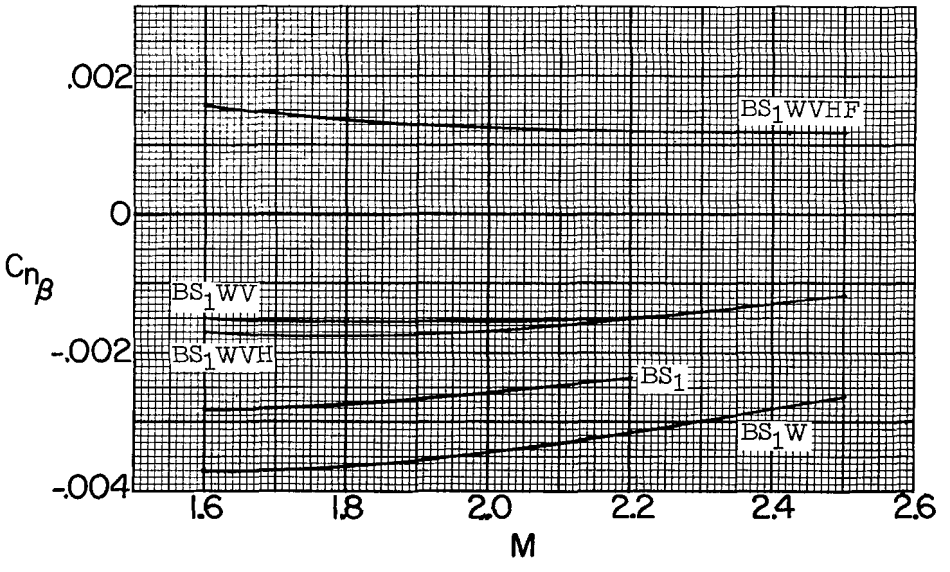

(b) $\alpha = 15^\circ$.

Figure 29.- Effect of model-component breakdown on the variation of the directional stability parameter with Mach number.

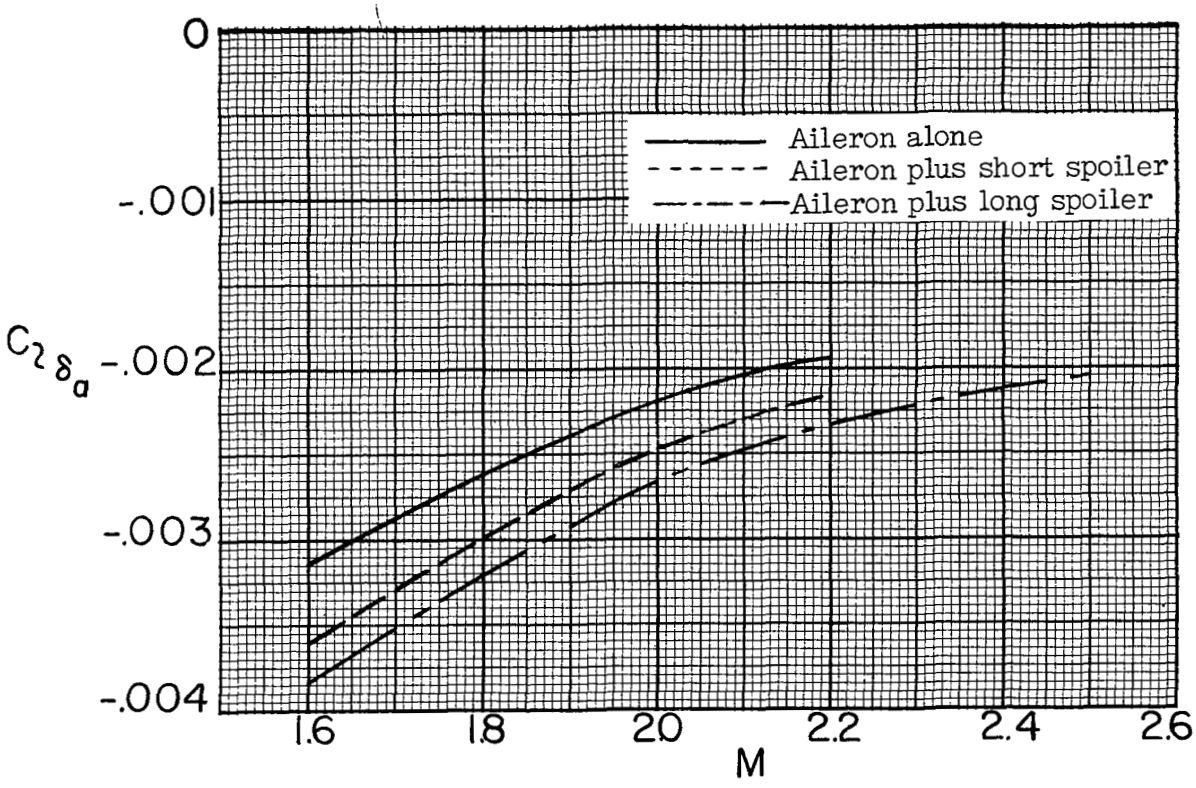

Figure 30.- Variation of lateral control effectiveness with Mach number. BS_1WVHF.